

## ABSTRACT

Title of Document: THEORETICAL AND EXPERIMENTAL  
INVESTIGATIONS OF HIGH SPIN IONIC  
INTERMEDIATES

Arthur Henry Winter, Doctor of Philosophy,  
2007

Directed By: Professor Daniel E. Falvey,  
Department of Chemistry & Biochemistry

In order to identify high-spin organic intermediates that could potentially be used as building blocks for the construction of high-spin organic ferromagnets, density functional theory (DFT) computations were performed to assess the singlet-triplet state energy gaps for a number of substituted aryl ionic intermediates. The quantitative accuracy of these DFT computations was benchmarked by high-level multireference second order perturbation theory (CASPT2) computations for representative species. These computations led to the discovery of a novel meta pi donor effect, wherein substituting the meta positions of aryl cationic species such as arylnitrenium ions (Ar-N-H<sup>+</sup>), arylsilylenium ions (Ar-SiH<sub>2</sub><sup>+</sup>), aryloxenium ions (Ar-O<sup>+</sup>), and benzyl cations (Ar-CH<sub>2</sub><sup>+</sup>), with pi donors stabilizes a  $\pi, \pi^*$  triplet state analogous to the electronic state of the m-xylylene diradical. Two of these benzylic cations were generated experimentally through photochemical methods and analyzed

by laser flash photolysis, chemical trapping studies, and product analysis. The experimental results were consistent with the existence of low-energy triplet states.

Additionally, species with an inverted connectivity (e.g. an anionic donor with two pi electron withdrawing groups) were also found to have low-energy triplet states by density functional theory computations. These anions were generated chemically and studied by NMR and EPR spectroscopy as well as quenching studies. The preliminary results of the experimental studies are consistent with the intermediacy of triplet ground state benzyl anions, in line with the theoretical predictions.

Vinyl cations substituted with  $\beta$  pi donors were also found to have triplet ground states, as computed by DFT and CBS-QB3 methods. In many cases, the singlet vinyl cations are anticipated to have facile rearrangement pathways, but incorporating the pi donors into rings appears to discourage obvious rearrangement pathways.

To permit the photogeneration of congested arylnitrenium ions, a new method for photochemically generating these species was developed through photolysis of protonated 1,1-diarylhydrazines. Additionally, the carbazolyl nitrenium ion was generated photochemically and studied by laser flash photolysis, chemical trapping studies, product analysis and computational studies. This nitrenium ion is found to be more short-lived and reactive than similar diarylnitrenium ions as a likely result of destabilizing antiaromatic character.

THEORETICAL AND EXPERIMENTAL INVESTIGATIONS OF HIGH SPIN  
IONIC INTERMEDIATES

By

Arthur Henry Winter

Dissertation submitted to the Faculty of the Graduate School of the  
University of Maryland, College Park, in partial fulfillment  
of the requirements for the degree of  
Doctor of Philosophy  
2007

Advisory Committee:  
Professor Daniel E. Falvey, Chair  
Professor Jeff Davis  
Professor Steven Rokita  
Professor Philip DeShong  
Professor Ted Einstein

© Copyright by  
Arthur Henry Winter  
2007

## Acknowledgements

Foremost, I thank my advisor, Dr. Dan Falvey, for his support. He has been a fantastic mentor for the better part of seven years, and I've benefited immensely from his encouragement and seemingly encyclopedic knowledge of chemistry. I am particularly grateful for his patience and humor in the times when the experiments were going poorly, and for his flexibility in allowing the project to change directions when doing so would put the project on a more interesting course. I've also appreciated his open-door office policy, allowing me to crow or vent about the day's results.

I also thank the members of the Falvey lab, past and present, for making a fun and interesting work environment. In particular, I thank Dr. Selina Thomas for her friendship, and Drs. Sean McIlroy, Peter Vath, Andy Kung, and Chitra Sundararajan for showing me the ropes when I joined the lab. I thank Brian Borak, Becky Veiera, Susanna Lopez, Zhiyun Chen, Serpil Gonen-Williams, and Connie Jin for making the lab time fun, and Eugene Khaskin for helping me with the glove-box chemistry. I'm also appreciative of our collaborators, Prof. Christopher Cramer and Prof. Ben Gherman, and Dr. Harry Gibson who visited us on sabbatical from Austin College.

I thank Dr. Jeff Davis, Dr. Steven Rokita, and Dr. Ted Einstein for taking the time to serve on my committee. I particularly thank Dr. Philip DeShong for demonstrating the importance of becoming a professional scientist and for critically reviewing my candidacy paper and NIH proposal.

Finally, I thank my friends and family, Jon, Katie, Julian, and Suzanne Winter, Alex Tzannes, Owen McDonough, Kostas Gerasopoulos, Mike Taye, Justin Calabrese, Albert Epshteyn, and Mike Hughes (who was particularly helpful in showing me how to compile some Fortran codes in Unix). Without your support I couldn't have done it.

## Table of Contents

Acknowledgements .....	ii
List of Figures .....	vi
List of Schemes .....	x
1. Chapter 1: Introduction .....	1
1.1. <u>Background</u> .....	1
1.2. <u>Magnetic states</u> .....	2
1.3. <u>Entropic barrier to ferromagnetism</u> .....	3
1.4. <u>An alternative strategy to increase <math>T_C</math> for magnetic organic assemblies</u> .....	4
1.5. <u>Step 1: Finding stable high-spin organic molecules</u> .....	6
1.5.1. Molecules with a single unpaired electron: free radicals .....	7
1.5.2. Molecules with multiple unpaired electrons: di- and tri-radicals .....	7
1.5.3. Space-separated diradicals: The non-Kekule diradicals .....	10
1.5.4. Triplet non-Kekule structures: Disjoint and non-disjoint diradicals ..	11
1.5.5. Atom-centered diradicals .....	13
1.6. <u>Forays to Waypoint 1: Exploiting ferromagnetic coupling units</u> .....	19
1.6.1. Spin defects .....	21
1.6.2. Reducing detrimental spin defects by incorporation of spins into macrocycles .....	23
1.6.3. Stabilizing high-spin building blocks .....	25
1.7. <u>Electronic structure theory</u> .....	27
1.7.1. The Schrodinger Equation .....	27
1.7.2. The Born-Oppenheimer approximation .....	29
1.7.3. Independent electron approximation and spin orbitals .....	30
1.7.4. Slater determinants and the Pauli principle .....	31
1.7.5. Restricted and unrestricted wavefunctions .....	32
1.7.6. Hartree-Fock theory .....	33
1.7.7. Linear combination of atomic orbitals approximation and basis sets ..	35
1.7.8. Self-consistent field (SCF) theory .....	39
1.7.9. Electron correlation methods: Configuration interaction (CI) .....	40
1.7.10. Complete active space (CAS) methods .....	43
1.7.11. Density functional theory .....	45
1.7.12. Modern exchange-correlation methods .....	47
2. Chapter 2: Development of a New Photochemical Method for Generating Nitrenium Ions .....	51
2.1. <u>Introduction</u> .....	51
2.2. <u>Photolysis of 1,1-diarylhydrazinium ions</u> .....	53
2.3. <u>Product studies</u> .....	54
2.4. <u>Laser flash photolysis studies</u> .....	55
2.5. <u>Chemical trapping studies</u> .....	59
2.6. <u>Formation of the cation radical</u> .....	61
2.7. <u>Conclusions</u> .....	62
3. Chapter 3: Theoretical Investigations of Meta-substituted Arylnitrenium Ions ...	63
3.1. <u>Introduction</u> .....	63

3.2.	<u>Theoretical methods</u> .....	66
3.3.	<u>Computed singlet-triplet gaps</u> .....	67
3.4.	<u>Electronic structure of the stabilized triplet state</u> .....	74
3.5.	<u>Basis set effects</u> .....	84
3.6.	<u>Conclusions</u> .....	85
4.	Chapter 4: Application of Meta Effect to other Cationic Reactive Intermediates.....	87
4.1.	<u>Introduction</u> .....	87
4.2.	<u>Triplet benzylic cations</u> .....	89
4.3.	<u>Computational methods</u> .....	90
4.4.	<u>Molecular geometries</u> .....	92
4.5.	<u>Singlet-triplet splittings</u> .....	94
4.6.	<u>Substituted naphthalenes</u> .....	99
4.7.	<u>Geometric effects</u> .....	102
4.8.	<u>Conclusions</u> .....	105
5.	Chapter 5: Experimental Studies of Triplet Aryl Cationic Species and Preliminary Studies of Triplet Benzylic Anions .....	107
5.1.	<u>Introduction</u> .....	107
5.2.	<u>The 3,5-bis(dimethylamino) benzyl cation</u> .....	108
5.2.1.	Generation of the cation .....	108
5.2.2.	Product analysis.....	110
5.2.3.	Effect of the leaving group .....	111
5.2.4.	Kinetics of decomposition.....	111
5.2.5.	Mechanism of product formation.....	112
5.2.6.	Triplet-sensitized photolysis.....	116
5.2.7.	Direct laser flash photolysis studies.....	116
5.2.8.	Triplet-sensitized laser flash photolysis studies.....	118
5.2.9.	Proposed mechanism for benzophenone photolysis.....	121
5.3.	<u>The 3',5'-bis(dimethylamino)-1-bis(trifluoromethyl) benzyl cation</u> .....	124
5.4.	<u>Theoretical studies of benzyl anions</u> .....	126
5.4.1.	Effect of $\alpha$ heteroatoms on $\Delta E_{ST}$ .....	128
5.4.2.	Dramatic effect of counter ion on $\Delta E_{ST}$ of benzyl anions.....	129
5.4.3.	Attenuation of counter ion effect by solvent consideration.....	131
5.5.	<u>Experimental studies of benzyl anions</u> .....	133
5.5.1.	Evidence for a paramagnetic species in solution .....	139
5.5.2.	Further NMR evidence for a paramagnetic intermediate .....	141
5.5.3.	EPR studies of the benzyl anions.....	142
6.	Chapter 6: Vinyl Cations Substituted with $\beta$ Pi Donors Have Triplet Ground States.....	145
6.1.	<u>Introduction</u> .....	145
6.2.	<u>Computational methods</u> .....	147
6.3.	<u>Computed singlet-triplet splittings</u> .....	149
6.4.	<u>Structure of the parent vinyl cation</u> .....	150
6.5.	<u><math>\beta</math>-pi donor substituted vinyl cations</u> .....	151
6.6.	<u>Molecular geometries and rearrangements</u> .....	152
6.7.	<u>Incorporation of the pi donors into rings</u> .....	157
6.8.	<u>The nature of the stabilized triplet state</u> .....	160

6.9. <u>Computational methods</u> .....	164
7. Chapter 7: Carbazolyl Nitrenium Ion: Electron Configuration and Antiaromaticity.....	166
7.1. <u>Introduction</u> .....	166
7.2. <u>Generation of the nitrenium ion</u> .....	170
7.3. <u>Evidence for a nitrenium ion intermediate</u> .....	171
7.4. <u>Product studies</u> .....	175
7.5. <u>Trapping rate constants</u> .....	177
7.6. <u>Computed singlet-triplet state energy gaps</u> .....	179
7.7. <u>Electron configuration of the observed nitrenium ion</u> .....	180
7.8. <u>Computational studies of antiaromaticity</u> .....	185
7.9. <u>Computational methods</u> .....	192
8. Chapter 8: Experimental .....	195
8.1. <u>Materials and methods</u> .....	195
8.2. <u>Solvents</u> .....	195
8.3. <u>Laser flash photolysis studies</u> .....	196
8.4. <u>Synthesis of photoprecursors</u> .....	199
Bibliography .....	219



# List of Figures

## Chapter 1 Figures.

Figure 1.1. Schematic diagram of possible magnetic states .....	3
Figure 1.2. Persistent organic radicals.....	7
Figure 1.3. A molecular orbital extension of Hund's rule.....	9
Figure 1.4. A non-Kekule diradical (TMM) and a standard closed-shell Kekule structure (butadiene).....	10
Figure 1.5. Approximate SOMO representations of TME (disjoint) and TMM (non-disjoint) diradicals.....	11
Figure 1.6. Examples of disjoint and non-disjoint diradicals.....	13
Figure 1.7. Diradical reactive intermediates.....	13
Figure 1.8. Possible carbene electronic states.....	14
Figure 1.9. Singlet vs triplet ground state for nitrenium ions.....	15
Figure 1.10. Walsh diagrams for linear and bent $\text{NH}_2^+$ .....	16
Figure 1.11. Singlet and triplet energies as a function of bond angle for $\text{NH}_2^+$ (B3LYP/6-31G*)......	17
Figure 1.12. A triplet aryl nitrenium ion.....	19
Figure 1.13. Coupling units.....	20
Figure 1.14. Ferromagnetic coupling units.....	20
Figure 1.15. High-spin oligomers.....	21
Figure 1.16. Disruptive spin defect in a hypothetical one-dimensional polymer.....	22
Figure 1.17. Spin defects introduced by bond twisting.....	22
Figure 1.18. Incorporation of spin centers into macrocycles prevents a single defect from causing significant spin annihilation.....	24
Figure 1.19. Rajca's magnetic polymer.....	25
Figure 1.20. Stabilized triplet carbenes.....	26
Figure 1.21. Approximating a Slater orbital using Gaussian functions.....	37
Figure 1.22. Schematic of CI wavefunction for a four-electron molecule.....	41

## Chapter 2 Figures.

Figure 2.1 Singlet and triplet $\text{NH}_2^+$ .....	52
Figure 2.2. Transient UV-vis spectra derived from LFP (266 nm excitation) of 2.1a (top), 2.1b (middle), and 2.1c (bottom) in $\text{CH}_3\text{CN}$ solutions. The spectra at early times (filled circles) are assigned to the corresponding diarylnitrenium ions 2.2; those at later times (open circles) are assigned to the corresponding cation radicals 2.5 <sup>+</sup> .....	57
Figure 2.3 Transient spectra derived from LFP (355 nm excitation) of a mixture of 2.6c and 1,4-dicyanobenzene (50 mM) in $\text{CH}_3\text{CN}$ .....	60

### Chaper 3 Figures.

Figure 3. 1. Aryl and heteroarylnitrenium ions.....	64
Figure 3. 2. A stable nitrenium ion.....	66
Figure 3. 3. Rotational isomers of substituted phenylnitrenium ions.....	69
Figure 3.4. Geometries of the singlet (triplet) states of nitrenium ions 3.7 and 3.17 (bond lengths in Å).....	71
Figure 3.5. Geometry of 4-methyl-3,3'bis(dimethylamino)phenylnitrenium ion 3.24 in the triplet state (left) and the singlet state (right). ....	72
Figure 3.6. The non-Kekulé diradical <i>meta</i> -xylylene.....	73
Figure 3.7. Models of the electronic states of <i>meta</i> -substituted phenylnitrenium ion. .....	75
Figure 3. 8. SOMO densities (top and side views) for the UB3LYP computed triplet states of nitrenium ions 3.7 (below) and 3.16 (above).....	77
Figure 3. 9. Mulliken spin densities on substituent heavy atoms on <i>meta</i> -substituted phenylnitrenium ions derived from UB3LYP/6-31G(d,p) calculations. ....	78
Figure 3.10. Geometry and SOMO densities for nitrenium ion 3.15.....	81

### Chaper 4 Figures.

Figure 4.1 General schematic representations of a typical singlet state and a $\pi,\pi^*$ triplet state.....	88
Figure 4. 2 Kohn-Sham SOMOs for representative triplet phenyl oxenium ions and benzyl cations. ....	105

### Chaper 5 Figures.

Figure 5.1. The 3,5-bis(dimethylamino)benzyl cation .....	108
Figure 5.2. Products of 254 nm photolysis of 5.4 (5 mM) in TFE as a function of photolysis time.....	112
Figure 5.3. LFP (266 nm, 10 $\mu$ s after pulse) from direct irradiation of 5.4 in TFE. ....	117
Figure 5. 4. Exponential dependance of the signal ( $\Delta$ OD) of direct 266 nm photolysis of 5.4 (monitored at 470 nm) as a function of laser output power. ....	118
Figure 5. 5. Transient spectrum from LFP of benzophenone and benzyl trifluoroacetate 5.8 in TFE (355 nm) under air. Insert shows waveforms at 400 nm (blue) and 540 nm (red).....	119
Figure 5. 6. Transient LFP spectrum from 355 nm laser photolysis of benzophenone plus dimethylaniline in trifluoroethanol.....	120
Figure 5. 7. Transient LFP spectrum from 355 nm photolysis of benzophenone and benzyl trifluoroacetate 5.8 in CH <sub>3</sub> CN.....	121
Figure 5.8. The 3',5'-bis(dimethylamino)-1,1-bis(trifluoromethyl) benzyl cation 5.9: A computed triplet benzyl cation. ....	124
Figure 5. 9 Effect of counterion on $\Delta E_{ST}$ .....	129

Figure 5. 10. Computed geometries (B3LYP/6-31+G(d,p)) for 5.13 singlet (left hand structures) and 5.13 triplet (right hand structures) with potassium (top structures) and lithium (bottom structures) counter ions. ....	130
Figure 5. 11. Major resonance contributors to the singlet and triplet benzyl anion 5.13. ....	131
Figure 5. 12. Effect of solvent on singlet-triplet splittings on 5.13 Li <sup>+</sup> .....	132
Figure 5.13. DFT geometries (B3LYP/6-31+G(d,p)) of the singlet (left-hand structures) and triplet states (right hand structures) from the dinitrobenzyl anion 5.13 Li <sup>+</sup> with 2 explicit dimethylether molecules (top) and three dimethylether molecules (bottom). ....	132
Figure 5. 14. <sup>1</sup> H NMR of starting material 5.16 aromatic and benzylic protons (left), and product quenched after 1 hr, with 88% <sup>2</sup> H incorporation (right). ....	135
Figure 5.15 Deprotonation kinetics of 5.16 using KH in mineral oil.....	136
Figure 5. 16. <sup>1</sup> H NMR spectrum of dithiane 5.16 and NaH in THF-d <sub>8</sub> at -70°C (left) and 20°C (right). ....	138
Figure 5.17. Evans' NMR method. ....	140
Figure 5. 18. Evans' <sup>1</sup> H NMR method. ....	141
Figure 5. 19. <sup>1</sup> H NMR spectra of 5.16 and KH in DMSO.....	142
Figure 5. 20. EPR spectrum of dithiane 5.16 and KH in THF.....	144

## Chaper 6 Figures.

Figure 6. 1. A ground-state triplet phenyl cation. ....	146
Figure 6.2. Two forms of the singlet vinyl cation.....	151
Figure 6. 3. APT charges for 2-aminovinyl cation (BL3YP/6-31G(d,p)) singlet (top) and triplet (bottom). Fixed charges range from +1 (bright green) to -1 (bright red). ....	161
Figure 6.4. Effect of an $\alpha$ anisyl group on $\Delta E_{ST}$ .....	164

## Chaper 7 Figures.

Figure 7.1 Endocyclic nitrenium ions. ....	167
Figure 7.2. Possible electronic configurations for carbazolyl nitrenium ion.....	169
Figure 7. 3. LFP of 7.4a in CH <sub>3</sub> CN. Timescale in $\mu$ s. Inset shows waveform at 620 nm. ....	171
Figure 7. 4. LFP of 7.4a in the presence of DMA Timescale in $\mu$ s. ....	172
Figure 7. 5. LFP of 7.4a in the presence of carbazole. Timescale in $\mu$ s.....	174
Figure 7. 6. LFP of 7.4a in the presence of TMB. Timescale in $\mu$ s. ....	179
Figure 7.7. Bond lengths ( $\text{\AA}$ ) and APT charges for singlet states of 7.1, 7.2, and 7.3. Fixed charges range from -1 (bright red) to +1 (bright green). ....	187
Figure 7. 8. 7.1 (top), 7.2 (middle), and 7.3 (bottom). Triangles represent the out of plane component of the NICS value, squares the in-plane components, and diamonds the isotropic values. All values were obtained at the center of the five-membered rings. ....	189

Figure 7. 9. Potentially aromatic endocyclic nitrenium ions .....	192
Figure 7. 10. Determination of trapping rate constant for trimethoxybenzene of the carbazoylyl nitrenium ion. ....	197
Figure 7. 11. GC response factor for 3,5-bis(dimethylamino)benzyl alcohol. ....	198

## List of Schemes

### Chapter 2 Schemes.

Scheme 2.1 Methods for generating nitrenium ions.....	53
Scheme 2.2. Proposed photogeneration of nitrenium ions. ....	54
Scheme 2.3. Photochemical generation of nitrenium ions.....	55
Scheme 2.4. Previous method to generate diarylnitrenium ions.....	56
Scheme 2.5. Photogeneration of amine radical cations.....	61
Scheme 2. 6. Generation of amine radical cation.....	62

### Chapter 5 Schemes.

Scheme 5. 1. Demonstration of the meta effect by Zimmerman, et al. ....	109
Scheme 5. 2. Products from photolysis (254 nm) of solutions of benzyl alcohol in alcoholic solvents. ....	110
Scheme 5. 3. Proposed mechanism for formation of TFE adduct and Friedel-Crafts heterodimer.....	113
Scheme 5. 4 Possible mechanisms leading to the reduced product 5.6.....	114
Scheme 5.5. Photolysis of 5.4 in t-BuOH.....	115
Scheme 5.6. Product studies from 355 nm irradiation of Ph <sub>2</sub> CO in the presence of 5.8 under air and N <sub>2</sub> atmosphere. ....	116
Scheme 5. 7. Proposed mechanism of reaction in presence of oxygen.....	122
Scheme 5. 8. Proposed mechanism of reaction of benzophenone and substrate in the presence of nitrogen.....	123
Scheme 5.9. Method for formation of benzyl cation 5.9.....	125
Scheme 5.10. Photolysis of 5.10 in TFE. ....	125
Scheme 5. 11. Photolysis of 5.10 in EtOH or tBuOH. ....	126
Scheme 5.12. Synthesis of benzyl anion precursors. ....	133
Scheme 5. 13. Decomposition of five-membered dithianes. ....	133
Scheme 5. 14. Alpha oxygens lead to ring deprotonation. ....	134
Scheme 5.15. Possible mechanism for peak broadening.....	139

### Chapter 6 Schemes.

Scheme 6. 1. Examples of singlet rearrangements at the DFT (B3LYP/6-31G(d,p)) level.....	156
Scheme 6. 2 Spontaneous C-H insertion .....	157
Scheme 6. 3. DFT rearrangement energies.....	158
Scheme 6. 4. Important canonical forms for the $\beta$ -substituted vinyl cations .....	161

## Chapter 7 Schemes.

Scheme 7. 1. Generation of the carbazolyl nitrenium ion. ....	170
Scheme 7.2. Electron transfer between 7.3 and electron donors. ....	171
Scheme 7. 3. Trapping product studies of 7.4a.....	176
Scheme 7. 4. Addition of TMB to the nitrenium ion. ....	179
Scheme 7. 5. Isodesmic reactions for hydrogen (H <sub>2</sub> ) transfer (B3LYP/6-31G(d,p)). .....	190
Scheme 7.6. An alternative isodesmic reaction. ....	191

# 1. Chapter 1: Introduction

## *1.1. Background*

One of the long-standing unsolved problems in physical organic chemistry is the design and synthesis of stable ferromagnetic organic materials.<sup>1,2</sup> Such organomagnetic materials hold the promise of combining the flexible properties and diversity of organic molecules with the property of ferromagnetism commonly found in transition metal-derived materials. Although the possible applications of organomagnetic materials are limited only by the imagination, practical applications may include the creation of magnetic materials with greater flexibility in material properties, such as lightweight magnetic materials that can be made with less energy consumption, materials for high-density information storage systems exploiting the change in magnetic properties upon exposure to light, or magnetic organic plastics and polymers, which could find use in a number of household appliances and electronic devices. The primary goal of the work in this dissertation was to contribute to that effort by finding novel organic building blocks that could potentially be used to construct such stable organomagnets.

This chapter outlines the origins of the property of magnetism and reviews current strategies for preparing room temperature stable organic ferromagnets. Additionally, since the search for these building blocks can most conveniently be carried out using computational methods, this chapter concludes with a discussion of modern

computational methods including Hartree-Fock and post-Hartree-Fock *ab initio* methods, as well as density functional theory.

### 1.2. Magnetic states.

Magnetism is generally not a property inherent to a molecule, but rather is a macroscopic property of a large number of interacting atoms or molecules, such as a bulk solid. However, in general only materials made from atoms or molecules that possess a net spin (that is, atoms that have unpaired electrons) have the possibility of having this macroscopic property of magnetism. In most organic molecules, all spins are paired and the bulk is diamagnetic (Figure 1.1). If an atom or molecule has a net spin, a number of different alignments of these spins are possible depending on the nature of the interaction between the spins. If the spins between the individual atoms or molecules are non-interacting, the spins orient randomly, leading to paramagnetism (the spins will align only in the presence of a large external magnetic field). If the spins interact, they can adopt an antiparallel orientation leading to the bulk property of anti-ferromagnetism. In mixed spin systems, it is also possible to have two spins with magnetic moments of different magnitudes. In a mixed spin system containing two spins of different magnitudes, if the two kinds of spins align antiparallel there is still a net magnetic moment in the direction of the spins aligned with the larger magnetic moment, a state called ferrimagnetism. Alternatively, all spins can adopt a uni-directional orientation, leading to the bulk property of ferromagnetism. It is this ferromagnetic orientation that is most desirable since it leads to the strong magnetism found in common household magnets such as iron oxide refrigerator magnets.



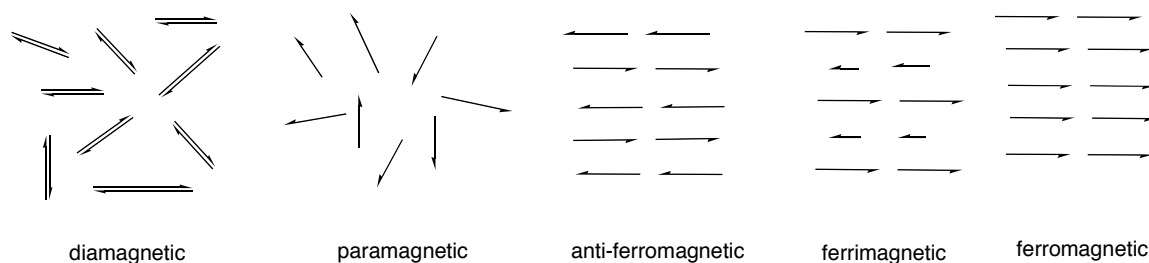
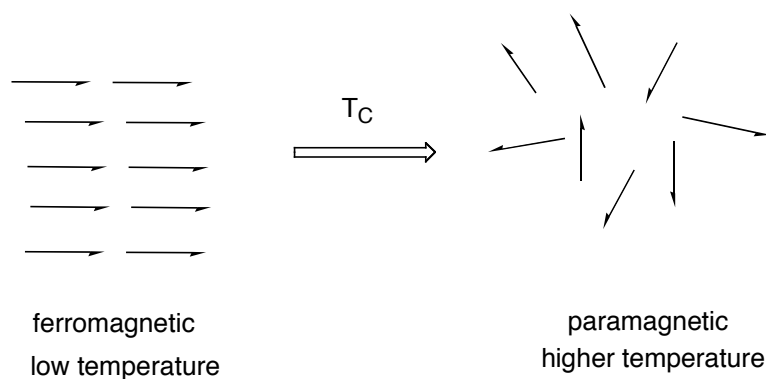


**Figure 1.1. Schematic diagram of possible magnetic states**

*1.3. Entropic barrier to ferromagnetism.*

While the search for ferromagnetic organic materials has been underway for many decades, this remains a challenging problem, and progress has been limited. Part of the problem is that while organic molecules with net spin (such as stable radicals) are known, the coupling between the individual spins in a packed solid or crystal is usually very weak. Since entropy disfavors a ferromagnetic assembly (because of entropy loss following spin ordering), weak spin coupling leads to molecules that are ferromagnetic at low temperatures, but paramagnetic at higher temperatures.

Consequently, all ferromagnets must lose their magnetism at some temperature. The temperature at which the magnetism is lost and the material becomes paramagnetic is called the Curie temperature ( $T_C$ ). For most high-spin organic molecules that form ferromagnetic assemblies, the through-space spin coupling is small enough that the Curie temperature is usually  $< 2$  K, although a derivative of  $C_{60}$  has been synthesized with a Curie temperature as high as 16 K.<sup>3,4</sup>



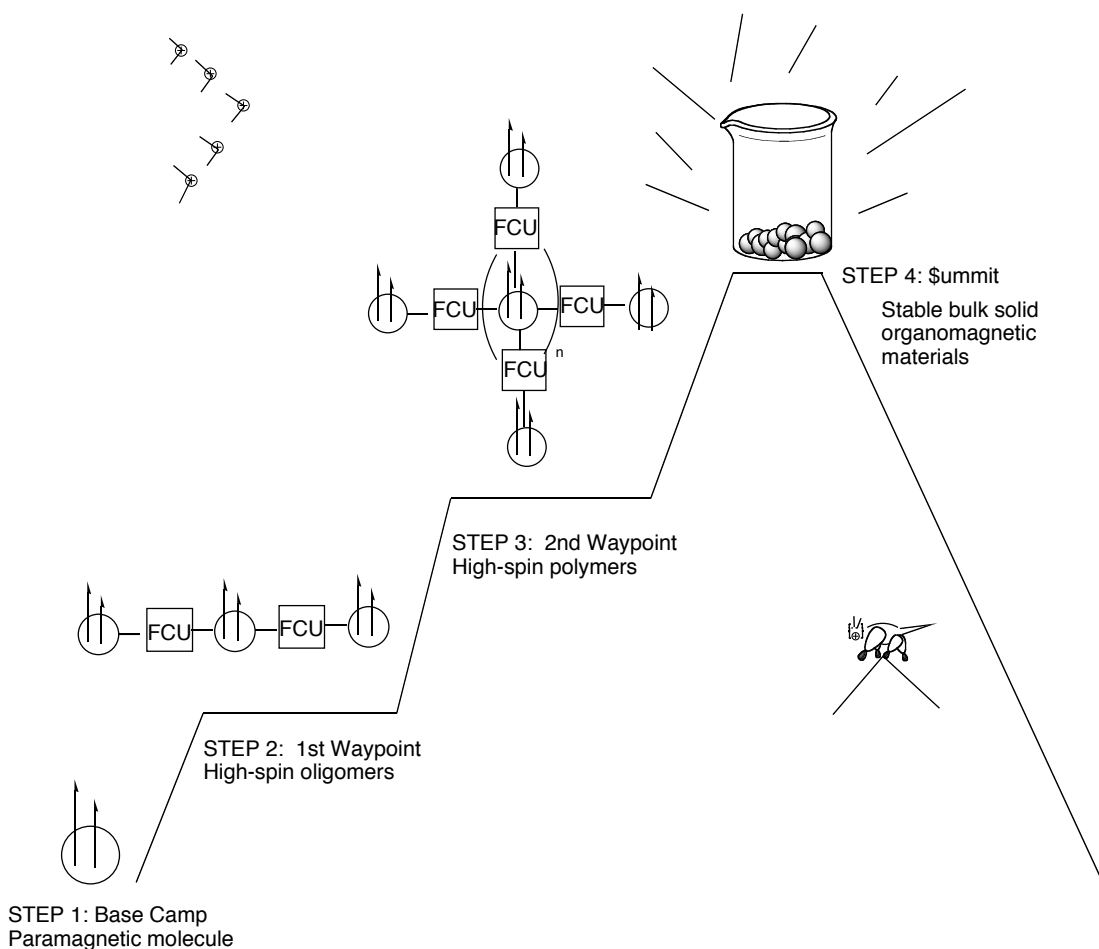
**Scheme 1.1. The Curie temperature ( $T_C$ ).**

*1.4. An alternative strategy to increase  $T_C$  for magnetic organic assemblies.*

These Curie temperatures are far from the range of being practical, since a desirable  $T_C$  for a working material would be 300 K or higher. An alternative strategy for strongly coupling the individual spins in order to obtain a molecule with higher  $T_C$  has been proposed.<sup>5-7</sup> Rather than relying on the weak “through-space” exchange interaction between the spins of individual molecules in a solid or crystal to form a ferromagnetic assembly, it has been proposed that the spins might be more strongly coupled via “through-bond” conjugated linkages on the *same* molecule. That is, pi linkages could be used to conjugate high-spin organic monomeric units. In this way, the spins on individual units would strongly “feel” the presence of the spins on adjacent units, which would result in much stronger spin-coupling, and, presumably, higher  $T_C$  values as a consequence.

The basic roadmap<sup>2,7</sup> for the successful creation of an organic ferromagnetic system exploiting this strategy is shown in Scheme 1.2, and consists of four discrete steps:

(1) discovery and characterization of a stable organic molecule with one or more net spins (such as a radical or polyradical); (2) Synthesis and characterization of an oligomer containing several of these radical units with large net spin; (3) Transformation of the simple high-spin oligomeric unit into a mesoscopic material with magnetism; (4) Synthesis of an assembly or bulk solid with the property of ferromagnetism. Because of some very difficult challenges encountered at each stage (discussed below), it should be noted that chemists remain far from step (4) with regard to completion of the roadmap.



**Scheme 1.2.** Roadmap for climbing the mountain of organic magnetism (summit), shown here for a triplet diradical monomeric unit. FCU = Ferromagnetic Coupling Unit.

### 1.5. Step 1: Finding stable high-spin organic molecules

The base-camp on the climb to the successful creation of organic ferromagnets is a stable high-spin organic molecule. While stable high-spin molecules are common in inorganic molecules containing transition metals, they remain the exception to the rule in organic molecules containing only first and second-row atoms. Organic molecules with high-spin are typically unstable reactive intermediates. The most common strategy is to find persistent reactive intermediates that have high spin.<sup>1,2,8-16</sup>

Common high-spin organic molecules include free radicals, and both free and atom-centered di- and polyradicals.<sup>17,18</sup> The next section discusses the different types of known high-spin organic molecules.

#### 1.5.1. Molecules with a single unpaired electron: free radicals

Free radicals are molecules that contain one unpaired electron and are paramagnetic. Radicals are common reactive intermediates in organic transformations, but few are persistent (kinetically stable). The first stable organic radical discovered was the triphenylmethyl radical, found by Gomberg<sup>11</sup> at the turn of the twentieth century. Generally, persistent organic radicals are stabilized by both steric (kinetic) and electronic (thermodynamic) structural elements. Some persistent organic free radicals are shown in Figure 1.2.<sup>19,20</sup>

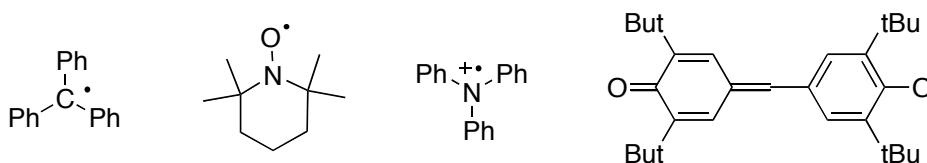


**Figure 1.2.** Persistent organic radicals.

#### 1.5.2. Molecules with multiple unpaired electrons: di- and tri-radicals

A more attractive building block than simple free radicals is high-spin di- and tri-radicals (triplet and pentet states, respectively), because these units pack a higher spin density into a single structure than monoradical units, and thus have the potential to lead to molecules with stronger magnetism.

In general, triplet states are favored over singlets in polyradicals because of the so-called exchange interaction of parallel spins, discovered by Heisenberg and Dirac in 1926. It is instructive to examine the origin of the preference for a high spin state triplet or quartet (spin unpaired) state over a singlet (spin-paired) state. The exchange energy arises in quantum mechanics from the antisymmetrized nature of the one-electron wavefunctions (that is, interchange of any two electrons reverses the sign of the wavefunction). Mathematically, the antisymmetrized nature of the one-electron wavefunctions leads to a lower electronic energy when two electrons have the same spin function (the origins of this quantum mechanical exchange is derived below). From a molecular view, the motions of two electrons of the same spin are said to be correlated—that is, their motions are highly coupled so that the two electrons are never found adjacent to each other, creating a region of zero electron density around them called the Fermi hole, which reduces their electron-electron repulsion.

For diradicals, this exchange energy leads to a triplet state in preference to the singlet state whenever the frontier orbitals are degenerate. In such a case, the electrons prefer to occupy separate orbitals with the same spin—a molecular orbital extension of Hund's Rule for atomic electron configurations (see Figure 1.3).

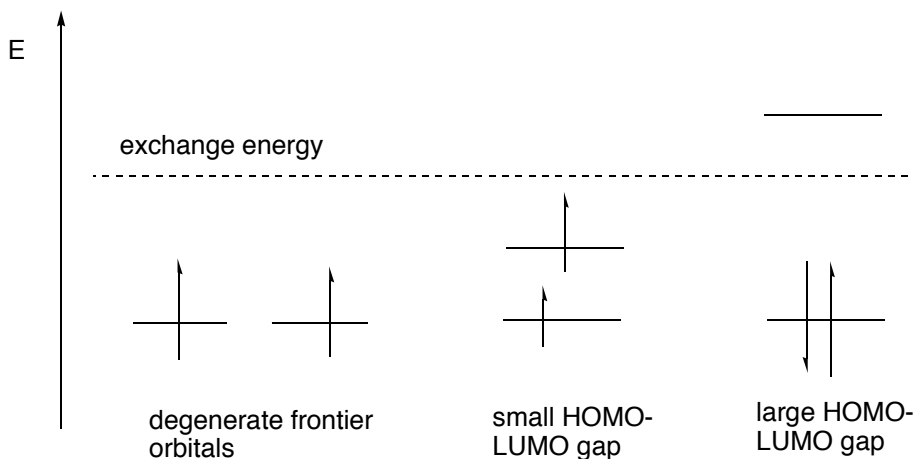


**Figure 1.3.** A molecular orbital extension of Hund's rule.

In cases where the frontier orbitals (HOMO and LUMO) are non-degenerate, the expected spin state is less clear. To a first approximation, molecules with exchange energies larger than the HOMO-LUMO gap still prefer a triplet state (that is, when a molecule has a small HOMO-LUMO gap). On the other hand, when the magnitude of the HOMO-LUMO separation is larger than the magnitude of the exchange energy, the singlet state is preferred. Although this analysis does not offer a specific prescription for finding molecules with high spin, it provides a general criterion for finding high-spin organic molecules: find a molecule with degenerate frontier orbitals, or orbitals with small separation between the HOMO and LUMO orbitals. In these cases, the exchange energy will make the triplet state favored over the closed-shell singlet state.

Triplet diradicals can be classified into space-separated diradicals and atom-centered diradicals. The essential feature of these high-spin diradicals is that the two spins

interact strongly with each other so that the exchange energy makes the high-spin form (triplet diradical favored over the low-spin form (singlet diradical)).

### 1.5.3. Space-separated diradicals: The non-Kekule diradicals.

The non-Kekule diradicals are molecules that cannot be described by a classical Kekule structure (that is, it's impossible to draw a closed shell Kekule structure for that molecule consistent with the valence bond rules). An example of a non-Kekule structure is trimethylenemethane (Figure 1.4).<sup>21</sup> This molecule cannot be described by a closed-shell Kekule structure, but rather must be described using a diradical formalism. Conversely, an isomer of TMM, butadiene, does have a resonance structure that can be described by a closed-shell Kekule structure. Molecules that can be described by a closed-shell Kekule structure (most organic molecules), often have large HOMO-LUMO separations and are therefore ground-state singlets. Conversely, non-Kekule diradicals can exist as either singlet diradicals or as triplet diradicals depending on whether the radicals are disjoint or non-disjoint.

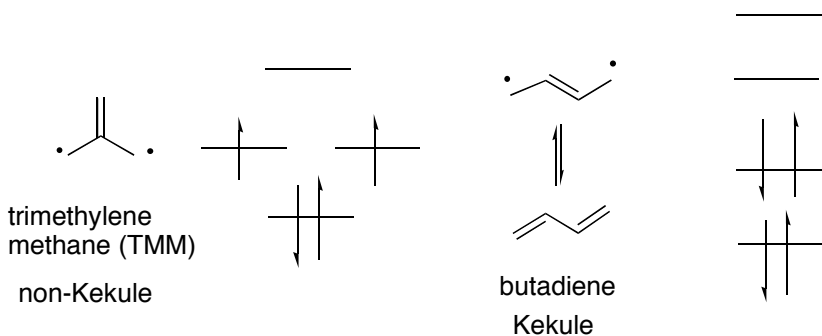


**Figure 1.4.** A non-Kekule diradical (TMM) and a standard closed-shell Kekule structure (butadiene).



1.5.4. Triplet non-Kekule structures: Disjoint and non-disjoint diradicals.

Diradicals by definition have two singly occupied molecular orbitals (SOMOs). If both of the two SOMOs have wavefunction amplitude on one or more of the same atoms, the diradical is said to be non-disjoint. If the SOMOs occupy separate atoms, the diradical is said to be disjoint. Translating this to the valence-bond model represented by Lewis structures, to a first approximation if a resonance structure exists for both radicals that place the radical on the same atom, the radical is said to be *non-disjoint*. If all resonance structures place the radical on different atoms, the diradical is said to be *disjoint*. TMM is an example of a non-disjoint diradical.<sup>21</sup> Both SOMOs have amplitude on the same atoms (Figure 1.5). Tetramethylenethane (TME) is an example of a disjoint diradical.<sup>22</sup> To a first approximation, the wavefunctions for both SOMOs occupy separate atoms.

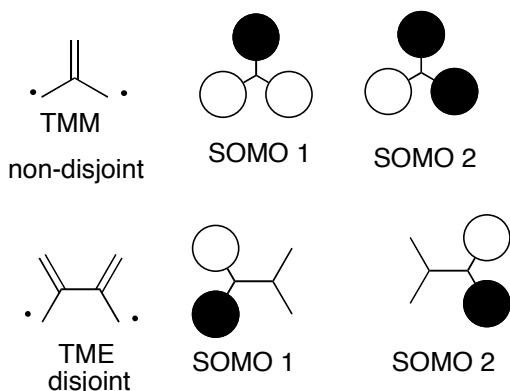


**Figure 1.5.** Approximate SOMO representations of TME (disjoint) and TMM (non-disjoint) diradicals.

Non-disjoint diradicals in general have triplet ground states. As a consequence of having finite wavefunction amplitude on one or more shared atoms, the two radical electrons “feel” the presence of each other, and so the stabilizing exchange energy (exchange integral) is large for the triplet state, making this high-spin configuration preferred over a singlet diradical configuration that does not have this exchange stabilization.

Conversely, disjoint diradicals have only small exchange energies. Since the radicals occupy separate spaces, for disjoint diradicals the exchange energy is non-existent (or very small) for the triplet state. Consequently, the singlet and triplet energies are predicted to be very nearly degenerate for disjoint diradicals, and the singlet state may be the ground state as a result of higher-level correlation effects that stabilize the singlet state in preference to the triplet. The TME diradical discussed in the example above is thought to have essentially degenerate singlet and triplet state energies, but with the triplet state slightly lower in energy than the singlet.<sup>17</sup> Figure 1.6 gives some examples of disjoint and non-disjoint diradicals. All of the non-disjoint diradicals shown have been experimentally confirmed to have triplet ground states, in line with the predictions from the simple theories described above. For the disjoint diradicals, some debate still surrounds the ground-state spin assignment, but in most cases these are thought to be ground state triplet species with nearly degenerate singlet states.

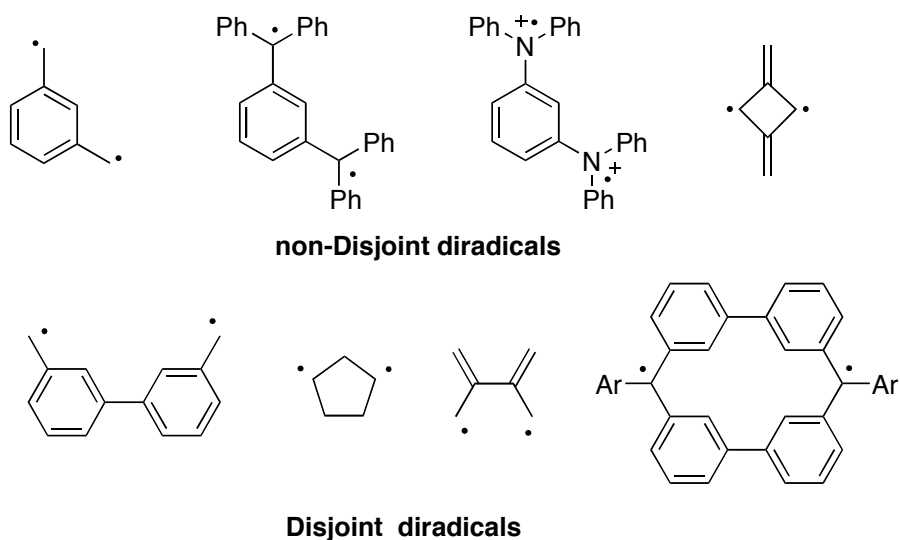


**Figure 1.6.** Examples of disjoint and non-disjoint diradicals.

#### 1.5.5. Atom-centered diradicals.

Another class of diradicals that have the possibility of having triplet ground states is atom-centered diradicals. Atom-centered diradicals are generally reactive intermediates, and include neutral reactive species such as carbenes, nitrenes, and silylenes, and positively-charged species such as oxenium ions and nitrenium ions (Figure 1.7).

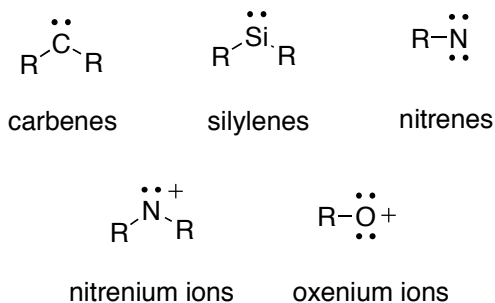


**Figure 1.7.** Diradical reactive intermediates.

The possible electron configurations for a nitrenium ion are shown in Figure 1.8. Similar electronic states exist for the other atom-centered diradical reactive intermediates (they all have a second-row atom with six valence electrons). Three singlet states are possible: a closed-shell  $n^2$  singlet state, an open-shell  $n,p$  singlet state, and a closed shell  $p^2$  singlet state. In general, the  $n,p$  and  $p^2$  singlet states are higher in energy than the  $n^2$  singlet state because of the energy cost of placing an electron in a higher-energy orbital.<sup>23</sup> In simple systems, the only accessible triplet state is an  $n,p$  triplet state (in arylnitrenium ions, a  $\pi,\pi^*$  triplet state is also possible).<sup>24-26</sup>

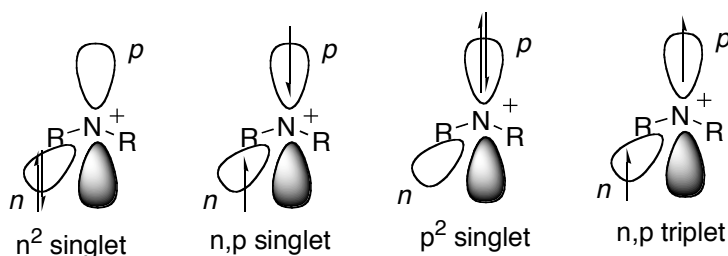


**Figure 1.8.** Possible carbene electronic states.

Whether a nitrenium ion exists as a singlet ground state or a triplet ground state depends on both steric and electronic factors.<sup>23</sup> On a most basic level, the exchange energy favors the triplet state, following Hund's rule. Acting antagonistically to the favorable exchange energy is the cost of putting an electron into a higher energy  $p$  orbital rather than the lower lying  $n$  orbital. A large energy gap between the  $n$  and  $p$  orbitals, therefore, favors the singlet spin state, whereas a small gap favors the triplet. To phrase it another way, for ground-state singlets the cost of putting an electron into the higher energy  $p$  orbital is greater than the exchange term.

Therefore, the singlet state is favored by substituents that increase the orbital energy gap either by lowering the energy of the n orbital or by raising the energy of the p orbital. For triplets just the reverse is true, and this spin state is favored when there is a small orbital energy gap, with substituents that either raise the n orbital in energy or lower the p orbital in energy (Figure 1.9).

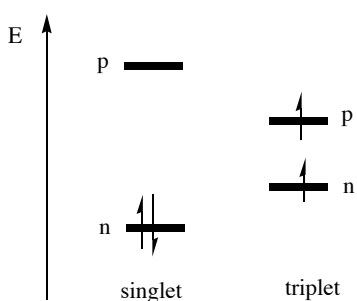


**Figure 1.9.** Singlet vs triplet ground state for nitrenium ions

To the extent that substituents can influence the bond angle, the electronic states can also be altered by steric factors. Qualitative MO theory (QMOT) in the form of a Walsh diagram can be used to show that the triplet and singlet states should prefer different bond angles. The Walsh diagram for the valence orbitals and valence electrons for  $\text{NH}_2^+$  are shown in Figure 1.10 for a linear (left) and bent (right) geometry. In the linear geometry the two p orbitals are necessarily degenerate by symmetry, and degenerate frontier orbitals favor a triplet state following Hund's rule. In the bent geometry, the degeneracy is broken, and the in-plane p orbital is significantly stabilized as a result of mixing with the highest-energy orbital shown (which stabilizes the p orbital and destabilizes the anti-bonding orbital); the out-of-

plane p orbital remains unperturbed. This breaks the frontier orbital degeneracy, which favors the singlet state in preference to the triplet.

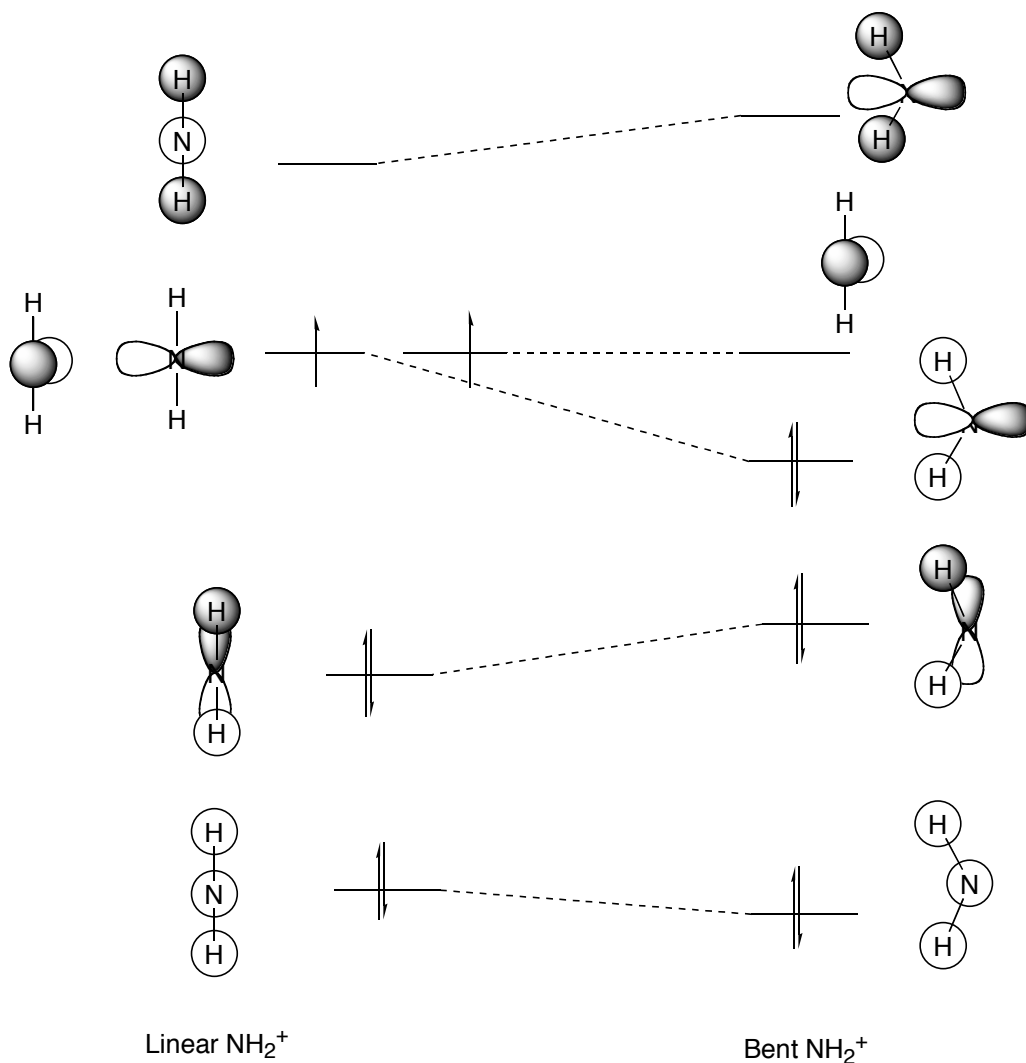


**Figure 1.10. Walsh diagrams for linear and bent  $\text{NH}_2^+$ .**

Of course, this analysis only suggests that the triplet should favor a more linear geometry and that the singlet should favor a bent geometry; this model is not sophisticated enough to predict the ground state of  $\text{NH}_2^+$  (except to say that at the linear geometry where the frontier orbitals are degenerate the triplet state should be

the lower-energy state following Hund's rule). These qualitative conclusions from QMOT are supported by theoretical calculations. Figure 1.11 shows a plot that we computed of the singlet and triplet energies of  $\text{NH}_2^+$  as a function of bond angle at the DFT (B3LYP/6-31G\*) level of theory. At wide bond angles, the triplet state is the predicted ground state for  $\text{NH}_2^+$ ; at more acute bond angles, the singlet state is the predicted ground state. High level *ab initio* calculations show that the H-N-H bond angle is 108 deg for the singlet, whereas the triplet is found to be nearly linear, with a bond angle of 153 deg and a barrier to inversion smaller than the zero-point vibrational energy.<sup>27</sup>

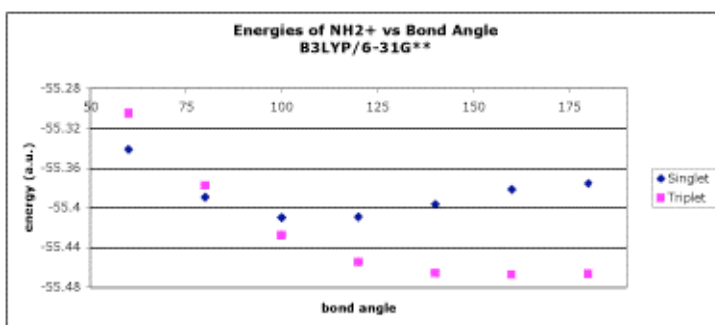


**Figure 1.11.** Singlet and triplet energies as a function of bond angle for  $\text{NH}_2^+$  (B3LYP/6-31G\*).

Theoretical and experimental studies derived from photoelectron spectroscopy experiments definitively assign the ground state for  $\text{NH}_2^+$  to the triplet state. The singlet-triplet gap ( $\Delta E_{ST}$ ) for nitrogen ions, which is defined as the energy difference between the lowest energy singlet state and the lowest energy triplet state, appears to be subject to large swings upon changing the nature of the substituents. Parent nitrogen ion,  $\text{NH}_2^+$ , is a triplet by 29.9 kcal/mol, as determined by photoelectron

spectroscopy experiments.<sup>28,29</sup> Replacing one of the hydrogens on  $\text{NH}_2^+$  with a phenyl ring shifts the energy gap in favor of the singlet by 50 kcal/mol, going from a triplet ground state species by roughly 30 kcal/mol to a singlet ground state species by 20 kcal/mol.<sup>30,31</sup> This swing in the  $\Delta E_{\text{ST}}$  is readily explained by the pi-donating ability of the aromatic ring, which acts to raise the energy of the p orbital on the nitrenium center, increasing the energy gap between the n and p orbitals, favoring the singlet. For all but a few select cases, aryl nitrenium ions have been found to have singlet ground states, whereas alkyl nitrenium ions, in which the nitrenium center is substituted with much poorer pi donors, are likely to have triplet ground states.<sup>23,25,32</sup>

These geometrical preferences found for  $\text{NH}_2^+$  appear to be generally true for other nitrenium ions. Singlet states, being approximately  $\text{sp}^2$  hybridized, prefer smaller bond angles than do the roughly sp-hybridized triplets. This geometric preference of the singlet state for more acute bond angles can be exploited to alter the singlet-triplet energy gap. Forcing a wider bond angle at the nitrenium center by substituting the R groups with large, sterically-demanding substituents destabilizes the singlet state more than the triplet, increasing the energy gap in favor of the triplet.

The N-t-butyl-N-(2-acetyl-4-nitrophenyl) nitrenium ion (Figure 1.12) is an example of a nitrenium ion with a spin state manipulated by both steric and electronic factors.<sup>33</sup> While most aryl nitrenium ions are ground-state singlets because of the pi-donating ability of the aromatic rings, this aryl nitrenium ion is a ground state triplet. Two factors contribute to making the triplet state the ground electronic state. First,



the pi-donating ability of the phenyl ring is decreased because of the pi-withdrawing effect of both the nitro group and the acetyl group. This acts to lower the energy of the *p* orbital on the nitrenium center relative to unsubstituted phenylnitrenium ion. Second, the bulky tertiary butyl group forces the wider bond angle preferred by the triplet. While this nitrenium ion has not been observed directly, trapping studies and other experiments as well as DFT theoretical studies leave little doubt that this nitrenium is a ground state triplet.

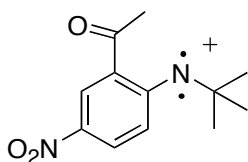


**Figure 1.12.** A triplet aryl nitrenium ion.

Similar electronic state arguments can be made for carbenes. In general, carbenes<sup>34</sup> have triplet ground states except those substituted with strong pi donors such as halogen substituents (like Cl, F), amino or alkoxy groups, or electron-rich aromatic rings (unsubstituted phenyl carbene is a ground-state triplet).

#### *1.6. Forays to Waypoint 1: Exploiting ferromagnetic coupling units*

Once high-spin organic molecules have been made and characterized (such as triplet diradicals), in principle they can be linked to make oligomers with very high spin values. Of course, there is no guarantee that coupling two high-spin molecules will lead to a new molecule with increased spin. If the two monomeric units are linked so that the spins on the monomeric units are not strongly coupled to each other (that is,

the spins on one monomeric unit do not “feel” the presence of the spins on the other unit), the spins will orient randomly and paramagnetism will result. However, if a linker that strongly couples the spins between the two monomeric is used to attach the two monomeric units, the spins may orient in the same direction and create a new molecule with very high spin values (Figure 1.13).

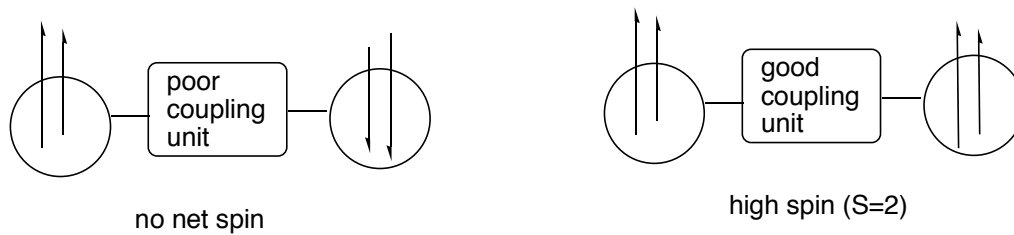


**Figure 1.13.** Coupling units.

Fortunately, a number of ferromagnetic coupling units have been identified that can be used to link two high spin monomers to create oligomers with very high spin values. These are shown in Figure 1.14. These linkers allow the spins from the two joining units to couple. In the case of the meta-disubstituted benzene linker, the spins from the joining units can both occupy the same carbon atoms in the ring; in the case of the vinyl linker, spins from the joining units can both delocalize onto the primary double bond carbon. The cyclobutane linker relies on a “through-space” interaction of the two spins.

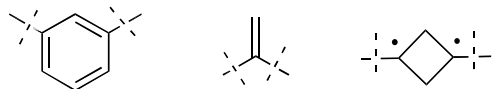


**Figure 1.14.** Ferromagnetic coupling units.

A few examples of very high-spin oligomers that use known high-spin units with these ferromagnetic coupling units are shown in Figure 1.15.<sup>8,9,16,35</sup> These species have been experimentally generated and studied by EPR spectroscopy to determine the ground spin state. Unfortunately, while these species can be generated and characterized in frozen matrices, they are unstable at room temperature.

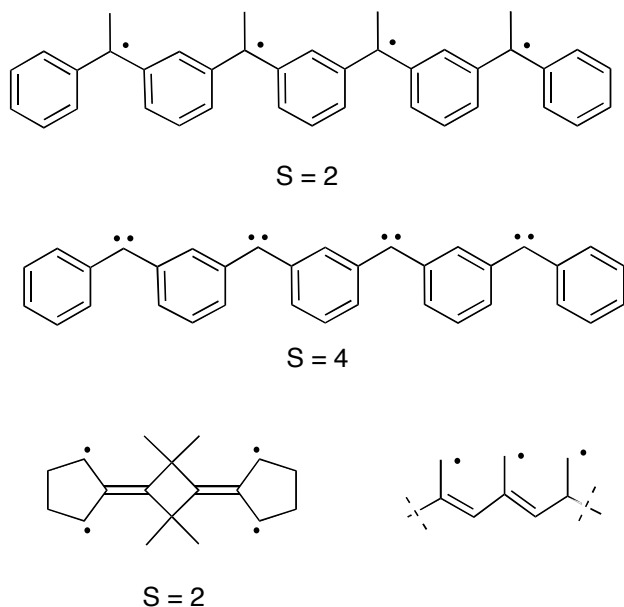


**Figure 1.15.** High-spin oligomers.

#### 1.6.1. Spin defects.

In addition to the kinetic instability of many high-spin organic building blocks, another problem that can plague the formation of very high-spin oligomers is disruptive spin defects in oligo(poly)meric spin systems. Figure 1.16 shows a hypothetical one-dimensional polymer consisting of radical monomeric units. A spin defect is introduced in the middle. Given that the spin coupling is linear, this spin

defect can disrupt the oligomer into two strands with smaller spin, significantly reducing the magnetic moment of the oligomer.

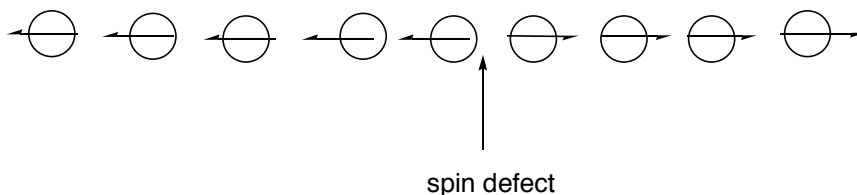


**Figure 1.16.** Disruptive spin defect in a hypothetical one-dimensional polymer.

Spin defects can arise from a number of different sources. One source of these defects is twisting of a conjugated bond out of planarity (See Figure 1.17). The effect of such a bond twist is to remove the conjugation, and, consequently, the spin coupling. Often, this causes the oligomer to break into two segments with smaller  $S$  values.

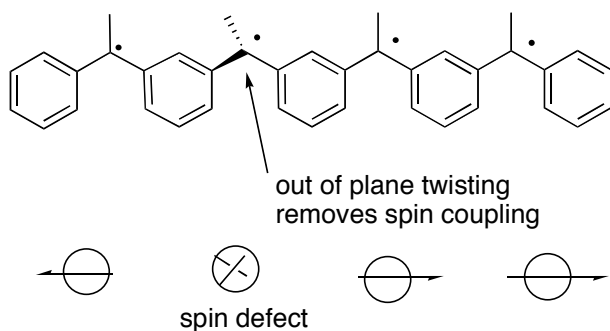
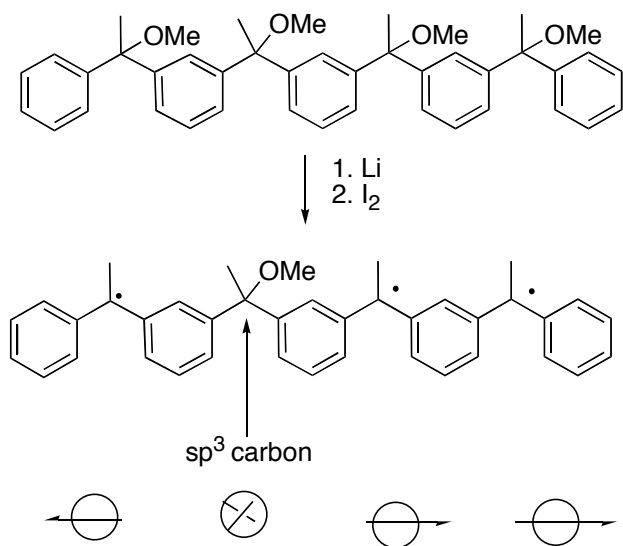


**Figure 1.17.** Spin defects introduced by bond twisting.

A second source of spin defects arises from incomplete generation of the radical centers. Incomplete generation by chemical or photochemical methods can result in an  $sp^3$  atom in the core, which decouples the joining branches as a result of this spin

defect. An example is shown in Scheme 1.3. Additionally, if photochemical means are used to generate the spin center (radical, carbene, etc), the radical may not be photostable. For example, polycarbenes generated by photolysis of polydiazole compounds often crosslink to form spin defects.<sup>16</sup>



**Scheme 1.3. Hypothetical incomplete generation of radical centers.**

1.6.2. Reducing detrimental spin defects by incorporation of spins into macrocycles.

Perhaps the best solution to prevent problems associated with introducing defects is to incorporate spins into macrocyclic polymers. In this way, should a spin defect be introduced into the macrocycle, a second ferromagnetic coupling unit exists to keep the two ends of the polymer spin coupled. Two spin defects would need to be

introduced to break the ferromagnetic coupling, a lower probability event. An example of a system created by Rajca is shown in Figure 1.18.<sup>36</sup>

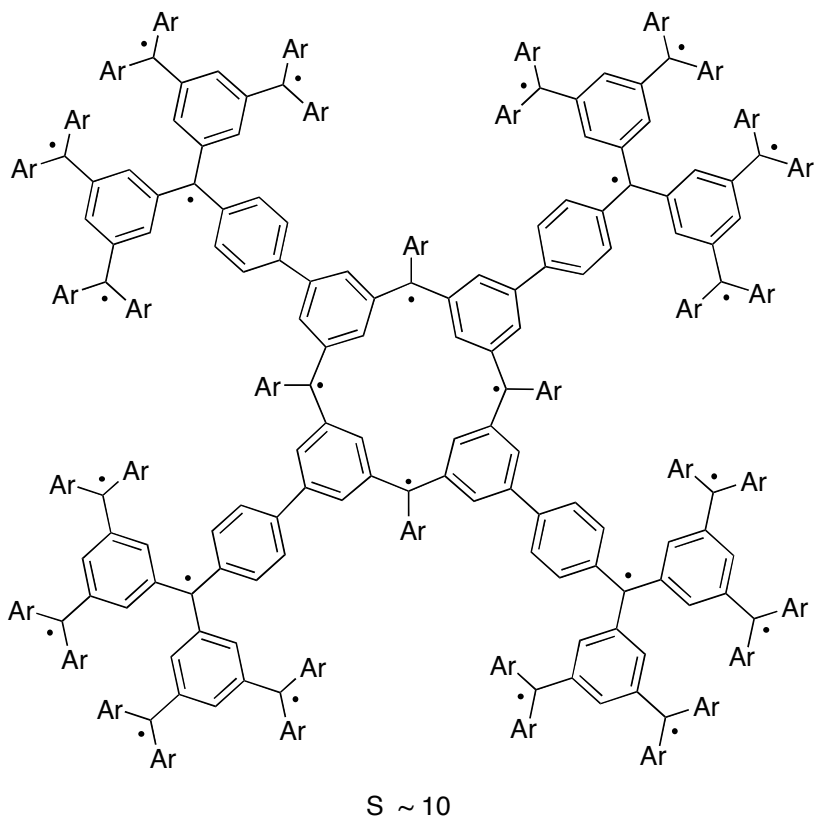
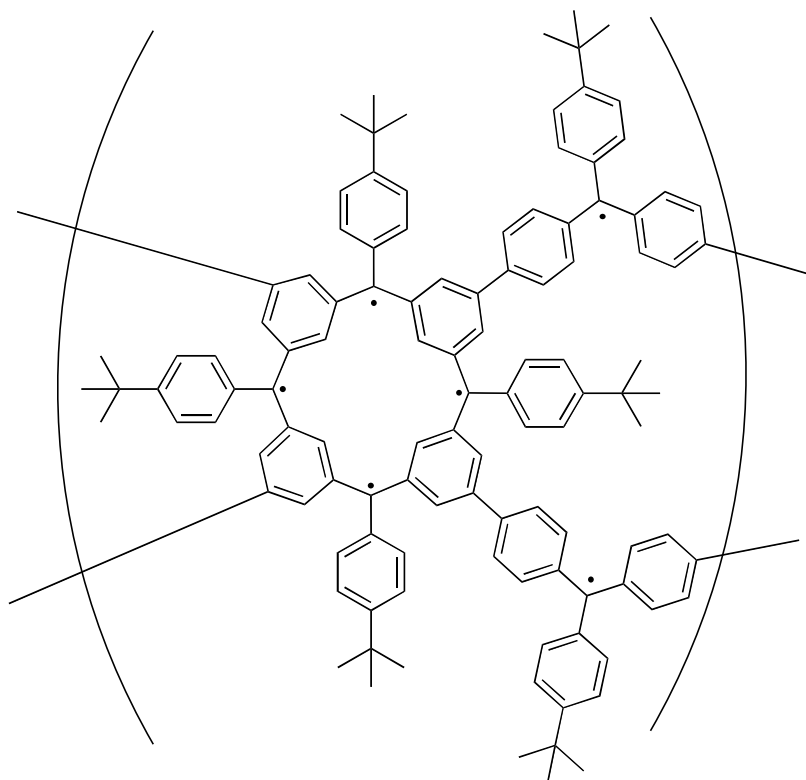


**Figure 1.18.** Incorporation of spin centers into macrocycles prevents a single defect from causing significant spin annihilation.

The organic molecule with the highest-known magnetic moment is the polymeric system of Rajca (Figure 1.19). This system consists of a macrocyclic tetradical core with triphenylmethyl radical linkers. At 3.5 K, it has the highest known spin value for an organic system ( $S \sim 5000$ ). Additionally, it has a higher Curie temperature ( $T_C$ ) of 10 K, better than the 2 K value for  $T_C$  seen for most organic ferromagnetic systems, but still far from becoming a practical organic ferromagnet.<sup>37,38</sup>



$S = 5000, 3.5 \text{ K}; T_C = 10 \text{ K}$

**Figure 1.19.** Rajca's magnetic polymer.

### 1.6.3. Stabilizing high-spin building blocks.

In addition to the low Curie temperatures of the known high-spin oligomeric systems shown in Figure 1.15, one of the principal problems associated with these structures and related species is that these high-spin building blocks are generally kinetically unstable. These high-spin oligomers can be made in low-temperature glassy matrixes and studied, for example, with Electron Spin Resonance spectroscopy (ESR), but they decompose once brought to room temperature. Therefore, to reach the ultimate

goal of a room-temperature organic ferromagnet, there is a need for stabilized high-spin (e.g. triplet) building blocks that can be linked into stable oligomeric structures.

Tomioka has carried out one of the most comprehensive and elegant studies designed to stabilize high-spin intermediates on triplet carbenes.<sup>8,12,39</sup> This decades-long effort has resulted in the identification of stabilized triplet carbenes that have the potential to be used as building blocks for constructing stable oligomeric assemblies. As a result of numerous mechanistic studies, Tomioka found that diarylcarbenes with bulky substituents in the ortho and para positions, led to persistent triplet carbenes in solution. The bulky ortho groups prevent reactions at the carbene center due to steric blocking (ortho alkyl groups such as t-butyl have little value because the carbene can undergo C-H insertion into the alkyl groups). The blocked para position prevents reactions at the para position resulting from spin density leakage at the para position. These stabilized triplet diarylcarbenes have lifetimes of days or weeks in de-aerated solution (Figure 1.20).

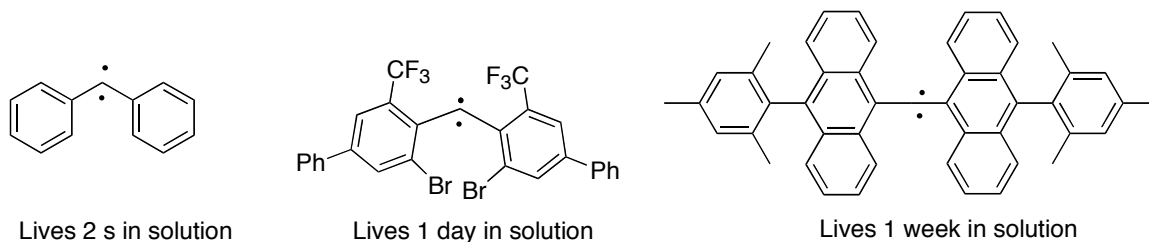


**Figure 1.20.** Stabilized triplet carbenes.



### 1.7. Electronic structure theory.

While significant strides have been made towards obtaining practical organomagnets, the two most challenging fundamental problems remain: 1) Stabilization of high-spin monomeric units, and 2) Increasing the  $T_C$  of the resulting ferromagnetic polymers to room temperature or higher. New paramagnetic building blocks with large spin coupling (often represented by molecules with large singlet-triplet state energy differences), that are either stable or can be made stable, are needed. Given the advances in theoretical methods, identifying new paramagnetic species with large singlet-triplet splittings is most easily accomplished using computational modeling. This chapter outlines the electronic structure theory and evaluates the methods with regard to their use for describing open-shell structures such as radicals.

#### 1.7.1. The Schrodinger Equation

The foundation of modern quantum mechanical methods is the Schrödinger equation:

$$\hat{H}\Psi = E\Psi$$

where  $\hat{H}$  represents the Hamiltonian operator,  $E$  represents the system energy, and  $\Psi$  represents the wavefunction. The square of a wavefunction gives a function with units of electron probability density. The wavefunction is an eigenfunction, and so the application of quantum mechanical operators (such as operators describing kinetic energy, potential energy, position, momentum, dipole moment, magnetic

susceptibility, etc) returns the eigenvalue (a scalar) of the operator multiplied by the unperturbed wavefunction.

The full Hamiltonian operator for the energy of a molecule (ignoring relativistic effects) is given by the equation:

$$\hat{H} = -\frac{\hbar^2}{2} \sum_A^N M_A^{-1} \nabla_A^2 + \sum_{A<B} e^2 Z_A Z_B r_{AB}^{-1} - \frac{\hbar^2}{2m} \sum_i^n \nabla^2 - \sum_A \sum_i e^2 Z_A r_{Ai}^{-1} + \sum_{i<j} e^2 r_{ij}^{-1}$$

where  $Z$  is the nuclear charge,  $e$  is the electron charge (in some notations labeled  $-e$ ),  $r_{ij}$  is the distance between electrons  $i$  and  $j$ , and  $r_{Ai}$  is the distance between nucleus  $A$  and electron  $i$ , and  $\nabla^2$  is the kinetic energy operator given by the following differential equation for a three-dimensional system:

$$\nabla^2 = \frac{\partial^2}{\partial x^2} + \frac{\partial^2}{\partial y^2} + \frac{\partial^2}{\partial z^2}$$

The full Hamiltonian consists of five terms: The first term of the Hamiltonian represents the kinetic energy of the nuclei; the second term represents the nuclear-nuclear repulsion; the third term represents the kinetic energy of the electrons; the fourth term represents the nuclear-electron attraction; and the fifth (and most troubling) term represents the electron-electron repulsion.

Solving the Schrodinger equation for the energy can be accomplished by the following equation (where  $\tau$  represents all space):

$$\int \Psi^* \hat{H} \Psi d\tau = E \int \Psi^* \Psi d\tau$$

Rearranged to solve for the energy, in bracket notation this equation becomes:

$$E = \frac{\langle \Psi | \hat{H} | \Psi \rangle}{\langle \Psi | \Psi \rangle}$$

Unfortunately, the Schrödinger equation cannot be solved exactly for all but the smallest systems containing a single electron. Consequently, approximations to this equation are necessary to make the equation tractable to systems of interest.

#### 1.7.2. The Born-Oppenheimer approximation.

The most benign approximation to the Schrodinger equation is the Born-Oppenheimer approximation, which relies on a simplification of the Hamiltonian operator. Virtually all modern theoretical methods rely on this approximation. Under the Born-Oppenheimer approximation, it is assumed that because electrons are so much smaller in mass than nuclei, the motions of the nuclei and the electrons can be

decoupled without significant loss of accuracy. That is, because electrons are more than 2000 times less massive than protons, any motion of the nuclei is compensated by a rapid redistribution of electrons. As a result of this approximation, the nuclei are not treated as wavefunctions but rather are represented by stationary point charges. This approximation eliminates the first term of the full Hamiltonian (nuclear kinetic energy term) and simplifies the Hamiltonian to the following:

$$\hat{H} = \sum_{A<B} e^2 Z_A Z_B r_{AB}^{-1} - \frac{\hbar^2}{2m} \sum_i^n \nabla^2 - \sum_A \sum_i e^2 Z_A r_{Ai}^{-1} + \sum_{i<j} e^2 r_{ij}^{-1}$$

This results in a simple expression for the nuclear-nuclear repulsion, and a complicated expression for the electronic energy:

$$E_{TOTAL} = E_{ELECTRONIC} + \sum_{A<B} Z_A Z_B r_{AB}^{-1}$$

Thus, once the electronic energy is computed, it is a simple task to find the total energy by adding the nuclear-nuclear repulsion term. The rest of this discussion concerns the more difficult treatment of the electronic energy.

### 1.7.3. Independent electron approximation and spin orbitals

A second commonly employed approximation is the assumption that the total wavefunction,  $\Psi$ , for a molecule can be approximated as the product of single-electron wavefunctions,  $\psi$ . Additionally, to account for a further degree of angular

momentum inherent to electrons—spin—the one-electron wavefunctions (orbitals) are multiplied by the spin function, of which two values are possible, designated  $\alpha$  and  $\beta$ ; the product of the spin function and the one-electron wavefunctions results in a spin orbital. Notationally, this approximation can be given by the following:

$$\Psi = \psi_a(1)\alpha(1)\psi_b(2)\beta(2)\psi_c(3)\alpha(3)\dots$$

where  $\psi_a(1)\alpha(1)$  represents the spin orbital for the first electron,  $\psi_b(2)\beta(2)$  represents the spin orbital of the second electron, and so forth. This approximation assumes that the one-electron wavefunctions are independent of all the other electrons.

#### 1.7.4. Slater determinants and the Pauli principle

A consequence of the Pauli principle is that the total wavefunction must be antisymmetric with respect to changing the coordinates of any two electrons. That is, changing any two electrons should lead to a sign change in the overall wavefunction. For example, switching electrons 1 and 2 on a molecule by using a permutation operator (notated  $P_{1,2}$ ) must lead to a new wavefunction with opposite sign, e.g.:

$$P_{1,2}\Psi = -\Psi$$

Note, though, that switching any two electrons does not change any physical observables (electrons are indistinguishable particles since they are fermions), because physical observables relate to  $\Psi^2$ , which is the same as  $(-\Psi)^2$ .

A convenient notation of a total electronic wavefunction that retains the antisymmetry of the one-electron wavefunctions is through the use of a determinant (often called a Slater determinant), since exchange of any two rows in a determinant flips the sign of the resulting wavefunction, in keeping with the Pauli principle. Additionally, if two columns are identical (suggesting that two electrons with the same spin occupy the same orbital) the resulting determinant is 0. This is a manifestation of the Pauli exclusion principle. For a system with  $n$  electrons, the total wavefunction represented by the product of all the anti-symmetrized one-electron wavefunctions is given by the following determinant:

$$\Psi = \begin{vmatrix} \psi_a(1) & \psi_b(1) & \psi_c(1) & \cdots & \psi_n(1) \\ \psi_a(2) & \psi_b(2) & \psi_c(2) & \cdots & \psi_n(2) \\ \vdots & \vdots & \vdots & \ddots & \\ \psi_a(n) & \psi_b(n) & \psi_c(n) & \cdots & \psi_n(n) \end{vmatrix}$$

#### 1.7.5. Restricted and unrestricted wavefunctions.

As shown in the Slater determinant above, each electron can be represented by a spin orbital consisting of a spatial component and a spin component. This is called the unrestricted formalism because it allows each one-electron orbital to have a different spatial component. A common approximation, called the restricted formalism, permits two electrons of opposite spin to occupy every spatial wavefunction (the resulting  $\alpha$  and  $\beta$  spin orbitals are still orthogonal because  $\alpha$  and  $\beta$  spin functions are orthogonal). In this way, the wavefunction is simplified because only half the

number of spatial single-electron wavefunctions is required to approximate the total wavefunction.

#### 1.7.6. Hartree-Fock theory

One of the most conceptually elegant approximations to the Schrodinger equation is given by the Hartree-Fock formalism. In this method, the repulsion between electrons is considered in an average way. That is, each electron sees an average electric field created by all the other electrons in the system. The approximation inherent to this theory is that electron correlation, or the instantaneous movement of an electron in response to nearby electrons, is ignored. Since the ability of an electron to move out of the way of an approaching electron is a stabilizing feature, the energies obtained by the Hartree-Fock theory will always be greater than the exact energy. In other words:

$$E_{HF} > E_{Exact}$$

Because the Hartree-Fock theory always provides an energy that is higher than the true energy, the variational method can be employed to find the Hartree-Fock wavefunction. That is, any change to a trial wavefunction that lowers the energy results in a value for the energy (and presumably, equations for the wavefunction) that more closely resemble the true energy (and wavefunction).

For a one-electron wavefunction (an orbital), the Fock operator ( $\hat{F}$ ) can be used to find the approximate energy of that one-electron wavefunction. The sum of the Fock

energies for each of the occupied one-electron orbitals for a system with  $n$  electrons gives the total Hartree-Fock energy. This can be described by:

$$E_{HF}\Psi = \hat{F}_1\psi_1 + \hat{F}_2\psi_2 + \hat{F}_3\psi_3 + \dots\hat{F}_n\psi_n$$

The form of the one-electron Fock operator is given by the equation:

$$\hat{F} = [H_{ii} + \sum_j(2J_{ij} - K_{ij})]$$

The  $H_{ii}$  term of the Fock operator is the so-called core integral. This term represents the kinetic energy of the electron (term 3 in the complete Hamiltonian) and the electron-nuclear attraction terms (term 4 in the complete Hamiltonian).

$$H_{ii} = \int \psi_i(1)[-\frac{1}{2} \nabla_i^2 - \sum_A Z_A r_{Ai}^{-1}]\Psi_i(1)d\tau$$

The  $J_{ij}$  term, or the Coulomb integral, approximates the electron-electron repulsion term in the exact Hamiltonian (term 5). This Coulomb integral represents a double integral between each one-electron wavefunction and every other one-electron wavefunction; Coulombic repulsion is also dependent on the distance between the two electrons (the  $r$  term in the operator). The molecular interpretation of this double integral is that it represents the repulsion between the electron and the average electron cloud of another electron, and this calculation is repeated between each electron in the molecule.



$$J_{ij} = \int \int \psi_i^*(1)\psi_j^*(2)r_{1,2}^{-1}\psi_i(1)\psi_j(2)d\tau_1d\tau_2$$

The final term of the Fock operator is the exchange integral,  $K_{ij}$ . This term arises from the antisymmetrized nature of the wavefunction required by the Pauli principle. This term takes into account the correlation between electrons with the same spin, following:

$$K_{ij} = \int \int \psi_i^*(1)\psi_j^*(2)r_{1,2}^{-1}\psi_j(1)\psi_i(2)d\tau_1d\tau_2$$

If two electrons have opposite spins, the  $K_{ij}$  integral becomes zero, because the spin functions  $\alpha$  and  $\beta$  are orthogonal (integration of the product of two orthogonal functions gives a value of zero). However, this integral has magnitude if the spins are identical. This stabilization of electrons having the same spin is called the exchange energy, and is the quantum mechanical foundation for Hund's rule. At the molecular level, this suggests that electrons of the same spin have correlated motions that allow them to avoid each other, which helps minimize electron-electron repulsion.

#### 1.7.7. Linear combination of atomic orbitals approximation and basis sets.

A convenient way of computing the energy of a molecule is to represent wavefunctions as a linear combination of other functions. Chemical intuition suggests that atomic orbital functions will be useful for making molecular orbitals.

That is, molecular orbitals can be conveniently formed from a linear combination of atomic orbitals following:

$$\Psi_i = \sum_k c_{ik} \phi_k$$

where  $c$  is the atomic orbital coefficient and  $\phi_k$  represents an atomic orbital.

The atomic functions that are used to approximate the molecular orbitals make up the so-called *basis set*. However, one inconvenient feature associated with this method is that standard Slater-type atomic hydrogen-like orbitals cannot be integrated analytically. For example, the Slater type orbital for the s orbital is shown in Figure 1.21. This function has a cusp at the nucleus, making it impossible to integrate analytically, following the equation:

$$\phi = r^{n-1} e^{-\frac{Z}{n}r}$$

Much slower numerical methods would be needed to integrate this function. The most common solution is to represent the Slater-type orbitals themselves using functions that are integrable—most commonly, Gaussian type functions. Gaussian type functions are represented by:

$$\phi = e^{-\frac{Z}{n}r^2}$$

for which analytical integrals are available. Although a single Gaussian function poorly represents a Slater-type orbital, the linear combination of several Gaussian functions can be made to mimic the STO reasonably closely. Even though more functions are required in order to use Gaussian functions, a significant savings in computational cost is achieved because the integrals can be computed analytically. Thus, in most cases molecular orbitals are made from a linear combination of atomic functions, and the atomic functions are made in turn from a linear combination of Gaussian functions (Figure 1.21).

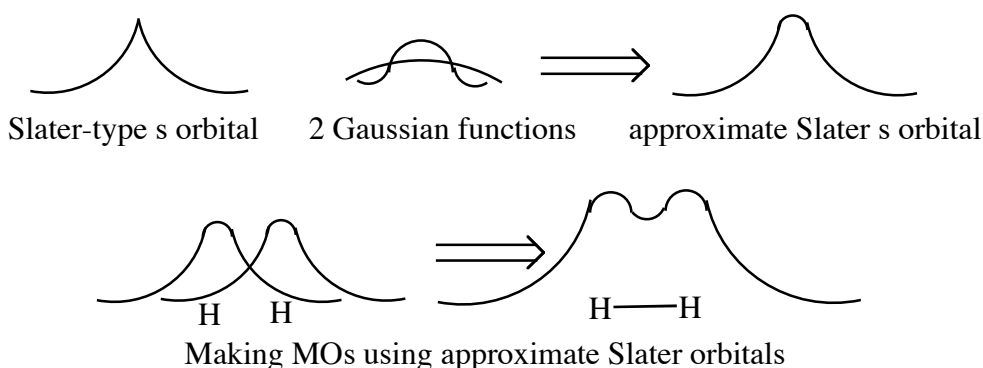


**Figure 1.21.** Approximating a Slater orbital using Gaussian functions

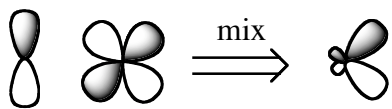
Thus, the atomic Slater orbital ( $\phi_i$ ) can be represented by two or more Gaussian type functions. For two Gaussian functions, this follows the equation:

$$\phi_i = a_1 G_1 + a_2 G_2$$

where the coefficients  $a_1$  and  $a_2$  are optimized to best mimic the Slater type function (usually these coefficients are optimized beforehand over some test set). A common

small basis set is the STO-3G basis set, where 3 Gaussian functions are used to represent each Slater type orbital (STO). More sophisticated basis sets such as the popular 6-31G basis set of Pople can be used. These basis sets are called split-valence basis sets, because they give more basis-set flexibility to valence orbitals, while core orbitals are treated more crudely. For example, a 6-31G basis set informs that 6 Gaussian functions will be used to approximate the core orbitals. The 31 suggests that the valence will be made up of two basis functions, the first of which is formed from a linear combination of 3 gaussian functions and the second from a single gaussian function. Since the valence is made up of two functions, this basis set is called a double  $\zeta$  basis set. If the valence orbitals are made from three basis functions, such as in the 6-311G basis set, the basis set is called triple  $\zeta$ , and so forth.

Polarization functions can also increase the flexibility of a basis set. For example, allowing some d orbital character to mix with p functions generates a new asymmetric orbital with larger amplitude on one side. For example, such “leaning” p functions often better approximate pi orbitals than do lone p orbitals. Of course, it’s important to note that the LCAO method is an approximation and any additional mathematical flexibility that can be permitted for obtaining the proper wavefunction is always welcome; chemical intuition should not get in the way of increased mathematical flexibility for describing the overall wavefunction.



Adding d orbital polarization functions to a basis set is designated with a (d) or a \*, such as in the popular 6-31G(d) (also represented as 6-31G\*) basis set. Additionally, *p* polarization functions can be mixed into hydrogen functions, such as in the 6-31G(d,p) basis set (or, commonly, 6-31G\*\*) to give more basis set flexibility for treating X-H bonds.

#### 1.7.8. Self-consistent field (SCF) theory

One problem with solving the Hartree-Fock equations is that to determine the molecular orbitals, the Fock equations for J and K need to be solved for every pairwise interaction between each electron in the molecule. In addition to the computational expense involved in such a calculation, this is a chicken and egg problem because to determine the wavefunction of a one-electron orbital you need to already know the wavefunction of all the other one-electron orbitals. In practice, then, the first one-electron wavefunction is found by guessing all the other one-electron MOs, and then using those guessed functions to find the approximate one-electron wavefunction at hand. This approximate one-electron wavefunction is then stored and then the next one-electron wavefunction is computed using this improved one-electron wavefunction to give a better guess of the second one-electron wavefunction. After each iteration, the improved one-electron MOs are plugged back into the Fock equations, and this process is repeated until the change in the energy has reached below some pre-defined threshold, and the wavefunction is said to have reached self-consistency.

### 1.7.9. Electron correlation methods: Configuration interaction (CI).

Since the Hartree-Fock theory ignores the correlation energy, the correlation energy can be found by the equation:

$$E_{Exact} = E_{HF} + E_{Correlation}$$

Hartree-Fock theory, as described above, overestimates the system energy because it ignores the instantaneous interaction of electrons, or the electron correlation energy. While Hartree-Fock theory is often adequate for obtaining energy differences for molecules that have roughly equal electron correlation (and thus cancel each other out reasonably well), electron correlation becomes very important for modeling more difficult systems that have electron correlation such as transition states, radical species, heats of formation, etc. In these cases, the Hartree-Fock method performs poorly, and better methods that take into account electron correlation are needed. Methods that take into account this electron correlation take a number of different forms. The most conceptually simple method is called configuration interaction (CI). In a complete CI, the total wavefunction is found as the sum of all the possible electronic configurations (or Slater determinants) for a molecule with coefficients representing the weight of each determinant in the expansion (typically, the largest coefficient precedes  $\Psi_1$ , the ground-state HF wavefunction).

$$\Psi_{CI} = c_1\Psi_1 + c_2\Psi_2 + c_3\Psi_3 + \dots c_n\Psi_n$$

where  $\Psi_1$  represents the ground-state Hartree-Fock wavefunction and the other wavefunctions represent excited-state Slater determinant wavefunctions. Visually, this can be represented for a four-electron molecule by the diagram shown in Figure 1.22.

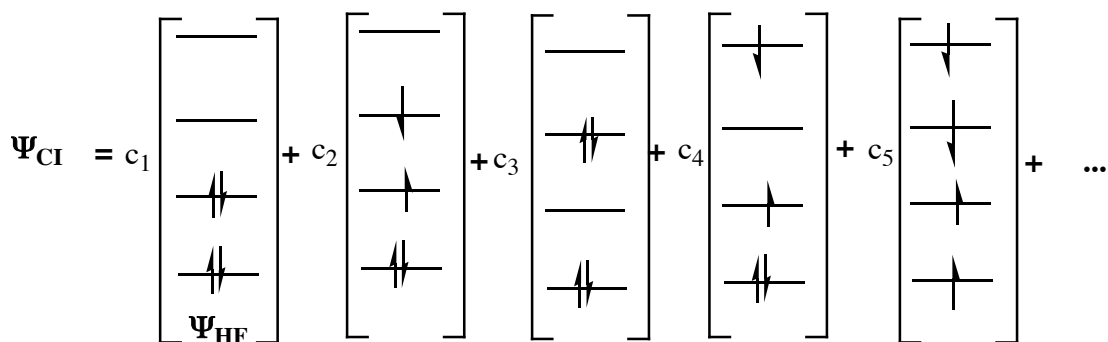


**Figure 1.22.** Schematic of CI wavefunction for a four-electron molecule.

Conceptually, mixing excited state wavefunctions into the ground-state wavefunction allows the electrons to avoid each other because it increases the size and flexibility of the wavefunction. Ignoring relativistic effects (usually negligible for organic molecules), a full CI calculation with an infinite basis set represents the exact solution to the Born-Oppenheimer-approximated Schrodinger equation. Of course, a full CI calculation quickly becomes intractable as the system size increases, because of the computational expense associated with finding all the coefficients and Slater determinants. Shown in the equation below is the computational route to a full CI computation of  $\text{H}_2$ . First, the Slater-type orbitals are approximated using Gaussian functions, and then combined to make the one-electron wavefunctions (shown here

using the restricted formalism). Then the CI expansion is made as the sum of all possible configurations (Slater determinants) of the one-electron wavefunctions. Finally, the coefficients of each Slater determinant are optimized to minimize the system energy. For a molecule made with two molecular orbitals, under the restricted formalism the total CI wavefunction could be written:

$$\Psi_{\text{CI}} = c_1 \psi_1^2 + c_2 \psi_1 \psi_2 + c_3 \psi_2 \psi_1 + c_4 \psi_2^2$$

where the coefficients ( $c_n$ ) are scalar values optimized to minimize the energy of the CI wavefunction. The problem with CI is that this method quickly becomes computationally impractical as the number of atoms and basis functions increase, simply because of the sheer number of possible determinants for which expansion coefficients and wavefunctions will need to be optimized, which increases exponentially with the number of basis functions. Thus, to expand the practical application of computational methods that include electron correlation, simplifications must be made.

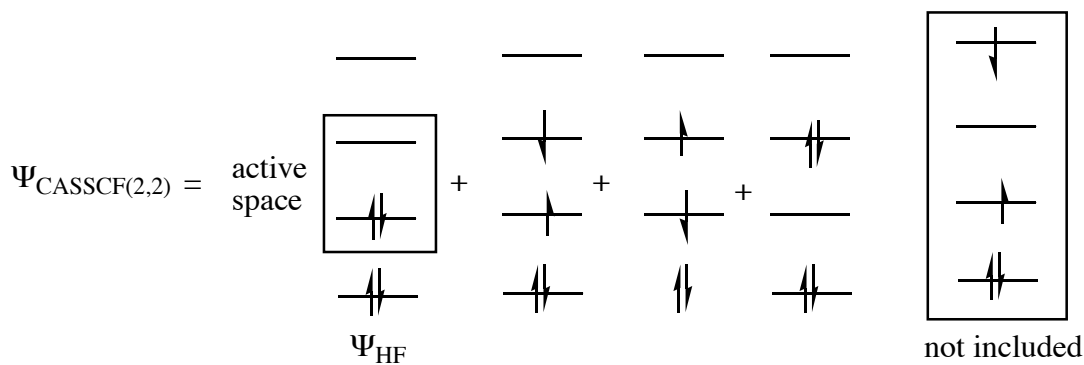
A common simplification of the Full CI wavefunction is to allow only a certain number of excitations to mix into the ground-state wavefunction. For example, under the CISD method, only single and double-excitation Slater determinants are allowed to mix into the ground-state wavefunction (in Figure 1.22 above, for example, the last Slater determinant would not be included since it represents a triple excitation). With



the CISDT method, single, double, and triple excitation wavefunctions are permitted, but at a significant increase in computational expense.

#### 1.7.10. Complete active space (CAS) methods.

Alternatively, a complete active space method can be employed (often annotated CASSCF). In this method, certain orbitals are designated as active orbitals from which all excitations are allowed. Shown in Scheme 1.4 is a diagram representing a CASSCF(2,2) wavefunction. In this case, the active space is confined to 2 orbitals and 2 electrons and all excitations with those electrons and those orbitals are considered. All other excitations outside the active space are not considered. The larger the active space, the more the electron correlation energy is captured, but at considerable additional computational expense. Typically the active space is chosen to consist of the largest number of frontier orbitals that are computationally tractable. However, selection of an active space is not always chemically intuitive. In some cases, such as with extended pi systems, the active space is reasonably obvious, and should probably include at least all pi electrons and pi orbitals, but in saturated molecules, the best orbitals to include are not always apparent. In these cases, chemical intuition and experience are good guides, but in inscrutable systems simply testing a number of different active orbitals with small basis sets in trial CASSCF calculation to see which contribute significantly to a CAS expansion is the best way out of this dilemma.



**Scheme 1.4.** Schematic of a CASSCF(2,2) wavefunction.

A modern flavor of the CASSCF method is the so-called CASPT2 method, which uses a complete active space calculation to capture any major non-dynamical correlation (correlation from contributions of higher excited state wavefunctions to the ground-state), and then uses second order perturbation theory to capture dynamical correlation outside of the active space. This CASPT2 method has been shown to be particularly robust for excited states and “problem” molecules that often are treated poorly by other methods (such as non-Kekule diradicals, hypovalent reactive intermediates, strained systems, etc). However, analytical gradients of the CASPT2 energy are not widely available, so geometry optimizations must be computed numerically (as a result, CASPT2 optimizations can only be performed on the smallest of systems). Often a CASPT2 single point calculation is performed at a geometry computed at a lower level of theory (often CASSCF). It should be noted, though, that these CASPT2 computations are often incredibly computationally expensive.

### 1.7.11. Density functional theory

Density functional theory (DFT) has become one of the most popular computational methods. This method is not based on building wavefunctions as a product of one-electron orbitals, such as in the Hartree-Fock theory, but rather computes the energy of a system as a function of the electron density. The basic idea for DFT is that, rather than computing a multidimensional function ( $\Psi$ ) that is a function of the three spatial coordinates and the spin for every electron in the system (number of dimensions =  $4n$ , where  $n$  is the number of electrons), the problem would be much simpler if one could work with a function that consists of only four-dimensions: the total molecular electron density as a function of the spatial coordinates and the spin.

*Kohn-Sham orbital approximations.* Unfortunately, while an operator that directly computes the exact system energy from the electron density must exist (as proven by Hohenberg and Kohn), the form of this operator is still unknown. Kohn and Sham realized that solving for the energy would be simpler if the total density could be built as the sum of one-electron density functions that did not interact (similar to Hartree orbitals), but coincidentally had an overall density that was the same as a system that *did* have interacting electrons. The density function is built essentially in the same way as the Hartree-Fock wavefunction as the product of one-electron density functions. The resulting density functions are called the Kohn-Sham orbitals.

Within the Born-Oppenheimer approximation, the DFT energy can then be computed computed as follows:

$$E = E^T + E^V + E^J + E^{XC}$$

The first three terms are classical and are similar to the terms in the wavefunction Hamiltonian, where  $E^T$  is the electron kinetic energy term, similar to the single kinetic energy integral seen in HF theory ( $\Psi$  represents density orbitals under the Kohn-Sham approximation and  $\rho$  represents the electron density):

$$E^T = -\frac{\hbar^2}{2} \sum_i^N \int \psi^*(r_1) \nabla^2 \Psi(r_1) dr$$

$E^V$  defines the potential energy involving the nuclear-nuclear repulsions and the nuclear-electron attraction:

$$E^V = \sum_k^N \int \frac{Z_K}{r_1 - r_2} \rho(r) dr$$

And  $E^J$  is the Coulombic electron repulsion term:

$$E^J = \frac{1}{2} \int \int \frac{\rho(r_1)\rho(r_2)}{r_1 - r_2} dr_1 dr_2$$

The final and most interesting term,  $E^{XC}$ , represents (among other things) the non-classical terms arising from exchange and electron correlation and corrections to the

kinetic energy term. The exact operator for computing this term is unknown (although a form must exist), so this term must be approximated.

#### 1.7.12. Modern exchange-correlation methods.

The basis of Kohn-Sham DFT is that it results in three reasonably simple classical terms ( $E^T$ ,  $E^V$ , and  $E^J$ ), with all the unpleasant non-classical operators and the electron correlation lumped into the  $E^{XC}$  term (ie. it puts all the rotten eggs into one basket). The operator that gives the exact  $E^{XC}$  energy is unknown (although Hohenberg and Kohn proved that such an operator must exist), so modern density functionals must make approximations to this term.

The most common approximation to the exchange-correlation functional is through assuming that the correlation of electrons in a molecule has similar correlation to a hypothetical substance called the uniform electron gas (or “jellium” as it is sometimes called). The uniform electron gas is a number of electrons interacting with a uniform potential (such that the potential plus the electronic charge is zero). The correlation energy has been computed for these hypothetical systems to a high level of accuracy. Consequently, the electron correlation for a given density can be computed by comparison to the correlation found for that density in a uniform electron gas. In practice, this is carried out by placing a grid over a molecule and for each point on the grid the correlation energy at each of the points is computed. The grid size is a tradeoff between accuracy and computational cost. Density functionals that derive

the correlation energy from such a method are called local density functionals (or LDA functionals, representing the Local Density Approximation).

Inherent to the local density DFT method is the implicit assumption that the correlation energy for a molecule doesn't change significantly as a result of a gradient in the electron density (there is no density gradient in the uniform electron gas). A better method for computing the correlation over a grid is to also consider the gradient in the electron density at each of the points on the grid when computing the energy, viz:

$$\epsilon_{x/c}^{Gradient}[\rho(r)] = \epsilon_{x/c}^{Local}[\rho(r)] + \Delta\epsilon_{x/c}\left[\frac{|\nabla\rho(r)|}{\rho^{4/3}(r)}\right]$$

where the first term represents the corresponding energy corresponding to the local density and the second term provides the correction to the correlation energy as a result of the density gradient.

A variety of gradient-corrected exchange and correlation functionals have been developed. Becke developed the most popular exchange functional. This method includes a single empirical parameter derived from the exact known exchange energy seen in the noble gases (thus functionals exploiting the Becke exchange functional are not strictly "ab initio"). Another popular exchange functional incorporating three empirical parameters into the exchange functional of Becke is termed the Becke3 (or B3) exchange functional. Popular correlation functionals include those of Lee, Yang,

and Parr (abbreviated LYP) and Perdew and Wang (PW91, for the correlation functional developed in 1991). Thus the acronym Becke3LYP or simply B3LYP suggests that the three-parameter exchange functional of Becke and the correlation functional of Lee, Yang, and Parr was used to find the DFT energy. BPW91 informs that the calculation used the exchange functional of Becke and the correlation function of Perdew and Wang. While these gradient-corrected functionals are more computationally expensive than local density DFT methods, they offer such an improved performance that local density functionals that the local density functionals are seldom seen outside of specialized computational studies.

In conclusion, we have described two popular computational methodologies that include explicit incorporation of the electron correlation energy—the configuration interaction method and the density functional theory method. The complete configuration interaction method is essentially intractable for most interesting systems and so approximations to this method such as CISD and CASSCF are made. The disadvantage of these *ab initio* wavefunction methods is that, within a given basis set, these methods tend to be more computationally expensive than DFT methods. They offer the advantage, however, over DFT in that there is a clear path to the complete solution of the Schrodinger equation by adding more of the possible configurations (Slater determinants) and increasing the basis set—at an exponential increase in the computational cost. For DFT, since the form of the operator that connects the ground state density to the system energy is currently unknown, there is no set path to complete solution of the Schrodinger equation within Kohn-Sham DFT.

However, comparison of DFT results to experimental or high-level *ab initio* methods leads to the conclusion that DFT can offer good computational accuracy at a fraction of the computational cost of comparably accurate wavefunction methodologies.



## 2. Chapter 2: Development of a New Photochemical Method for Generating Nitrenium Ions <sup>1</sup>

### 2.1. Introduction

The idea of adapting high-spin nitrenium ions to make building blocks for high-spin oligomers was of particular interest, in large part because nitrenium ions often have very high spin couplings (as evidenced by large singlet-triplet gaps) that could lead to building blocks with improved magnetic properties (for example, large spin couplings are anticipated to lead to higher Curie temperatures). As part of our initial efforts to find stable high-spin nitrenium ion building blocks, we first looked to find a more facile and convenient method for generating nitrenium ions with bulky adjacent substituents.

Nitrenium ions are reactive intermediates characterized by a dicoordinate, positively charged nitrogen atom.<sup>23-26</sup> The simplest example is  $\text{NH}_2^+$ . Like the isolectronic carbenes, nitrenium ions have two low-energy electronic configurations, which are depicted schematically in Figure 2.1. For  $\text{NH}_2^+$ , the lowest energy state is the  $np$  triplet state, with the  $n^2$  singlet state being +29.9 kcal/mol higher in energy.<sup>23,28</sup> The  $p^2$  and  $np$  singlets are higher in energy and are generally not considered to be chemically significant. For substituted nitrenium ions, the singlet-triplet state energy difference ( $\Delta E_{ST}$ ) has been the subject of numerous theoretical<sup>23-25,30,40,41</sup> and experimental studies.<sup>26,40-51</sup> Aromatic nitrenium ions, in particular, have received the

---

<sup>1</sup> Taken in part from Winter, A. H.; Thomas, S. I.; Kung, A. C.; Falvey, D. E. *Org. Lett.* **2004**; 6(25); 4671-4674.

most experimental attention due to their suspected roles in carcinogenesis<sup>50,52</sup> and in the synthesis of conducting polymers.<sup>51,53</sup>

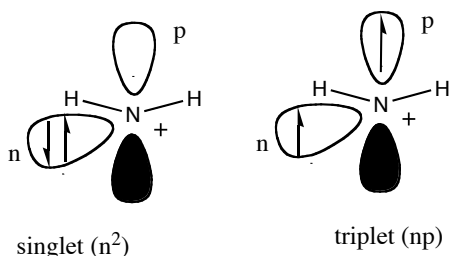
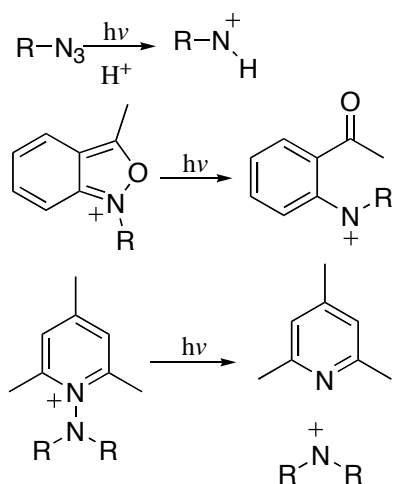


**Figure 2.1** Singlet and triplet  $\text{NH}_2^+$ .

While carbenes have been explored as possible building blocks for construction of high-spin assemblies (refer to Ch. 1), to our knowledge there have been no attempts to adapt triplet nitrenium ions towards such an effort. One of the lessons learned by Tomioka in his studies directed towards finding stable triplet carbene species was that imparting kinetic stability to the triplet carbene in the form of large sterically-demanding substituents most successfully led to persistent carbenes in solution than other efforts. Unfortunately, we felt that the current methods for generating nitrenium ions were sufficiently limited that they would not permit the formation of nitrenium ions with very bulky substituents.

Three primary methods have been used for making nitrenium ions photochemically, and each has limitations. The first involves photolysis of azides in the presence of acids (Scheme 2.1). Excitation of the azide results in loss of nitrogen gas and formation of a nitrene intermediate, which is then protonated by acid to make the nitrenium ion. Unfortunately, this method is limited to formation of primary

nitrenium ions (e.g. nitrenium ions with only one substituent). A second method is photolysis of anthranilium salts. This method is inherently limited to formation of nitrenium ions having an acetyl group in the ortho position. The most general method, however, is photolysis of N-amino pyridinium salts. Upon photolysis, these compounds undergo heterolytic N-N bond scission to generate the nitrenium ion and a pyridine derivative. This method is currently the most general and popular precursor for studying nitrenium ions; however, the collidine leaving group is large and bulky and thus is not expected to permit the formation of much steric bulk around the nitrogens.

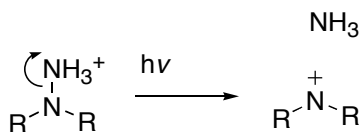


**Scheme 2.1 Methods for generating nitrenium ions.**

### 2.2. Photolysis of 1,1-diarylhydrazinium ions.

Therefore, we sought to find a new method for photochemically generating nitrenium ions that had a smaller leaving group so that steric bulk could be built around the resulting nitrenium ion. We considered that an ammonia leaving group would be

small enough to permit bulky substituents to be attached to the nitrenium ion, but still retain the good leaving group quality (Scheme 2.2).



**Scheme 2.2. Proposed photogeneration of nitrenium ions.**

Thus, in order to expand the available routes to nitrenium ions, we examined the photochemistry of protonated 1,1-diarylhazines. Through a combination of LFP experiments, product analysis, and time-dependent density functional theory (TD-DFT) calculations, it is demonstrated that photolysis of protonated 1,1-diarylhazines generates the corresponding nitrenium ions in high yields.

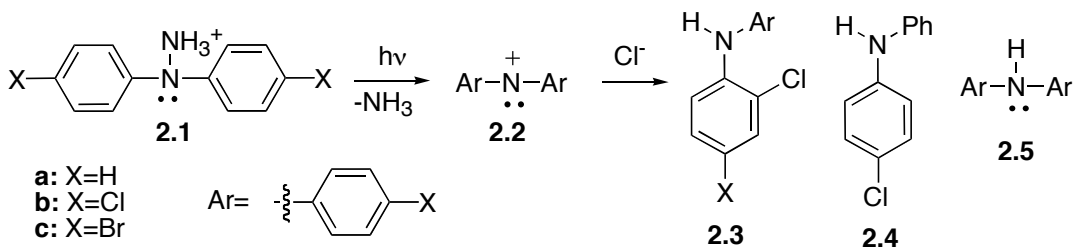
*2.3. Product studies.*

Three 1,1-diarylhazine derivatives were studied: 1,1-diphenylhazine **2.1a**, 1,1-di(4-chlorophenyl)hazine **2.1b** and 1,1-di(4-bromophenyl)hazine **2.1c**.

Protonation of the hazines using  $\text{HBF}_4$  to make the hazinium ions was followed by UV spectroscopy. In each case the free bases have strong absorption bands with maxima in the 295-305 nm region. Upon addition of a stoichiometric amount of  $\text{HBF}_4$ , this highest wavelength absorption band is replaced with a long absorption tail that extends from 240 to ca. 300 nm. Consequently, compounds **2.1a**, **2.1b**, and **2.1c** require lower wavelength light for excitation than do the corresponding N-aminopyridinium salts. The latter can generally be excited with wavelengths as high

as 400 nm. The protonated hydrazines show only weak fluorescence ( $\Phi_{fl} < 0.03$ ) in  $\text{CH}_3\text{CN}$ .

Photolysis of the pyridinium ions **2.6** ( $\text{BF}_4^-$  salts) in  $\text{CH}_3\text{CN}$  produces stable products that are characteristic of the nitrenium ions **2.2** (Scheme 2.3). The product mixtures were analyzed by GC, and the products identified by co-injection with authentic samples. Photolysis of diphenylhydrazinium ion (**2.1a**) in  $\text{CH}_3\text{CN}$  with added  $\text{Cl}^-$  (as  $n\text{Bu}_4\text{N}^+\text{Cl}^-$ ) gives a mixture of 4-chloro-N-phenylaniline **2.4** and diphenylamine **2.5**. Likewise, the para-substituted examples **2.1b** and **2.1c** each give a mixture of chloride adduct **2.3** and the reduction product **2.5**.

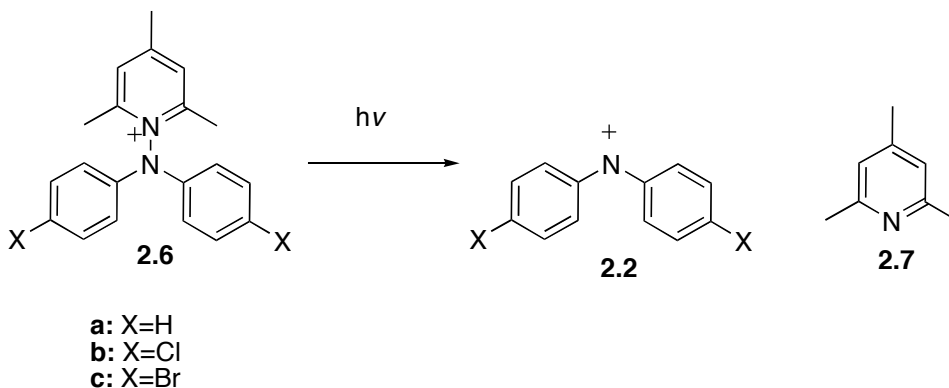


**Scheme 2.3.** Photochemical generation of nitrenium ions.

#### 2.4. Laser flash photolysis studies.

Laser flash photolysis (266 nm, 4 ns, 10-25 mJ/pulse) shows that the corresponding nitrenium ions **2.2** are formed following photolysis. Figure 1 shows the transient UV-Vis spectra generated from pulsed laser photolysis of protonated 1,1-diphenylhydrazine **2.1a** in  $\text{CH}_3\text{CN}$ . The spectrum immediately following the laser pulse, having bands at 650 nm and 410 nm, is experimentally indistinguishable from

the spectrum generated from the corresponding N-aminopyridinium salt **2.6** (Scheme 2.4). In a previous work the identity of this intermediate was established as the diarylnitrenium ion **2.2** by a variety of experiments, including trapping studies and time-resolved infrared as well as resonance Raman spectroscopy.



**Scheme 2.4.** Previous method to generate diarylnitrenium ions.

The other two hydrazinium ions **2.1b** and **2.1c** give similar transient spectra upon laser flash photolysis (Figure 2.2). Both of these initial intermediates decay within 5-7 ms to give a second, longer-lived intermediate. For reasons discussed below, this secondary transient is attributed to the radical cation, deriving from an electron transfer reaction between **2.2** and **2.1**.

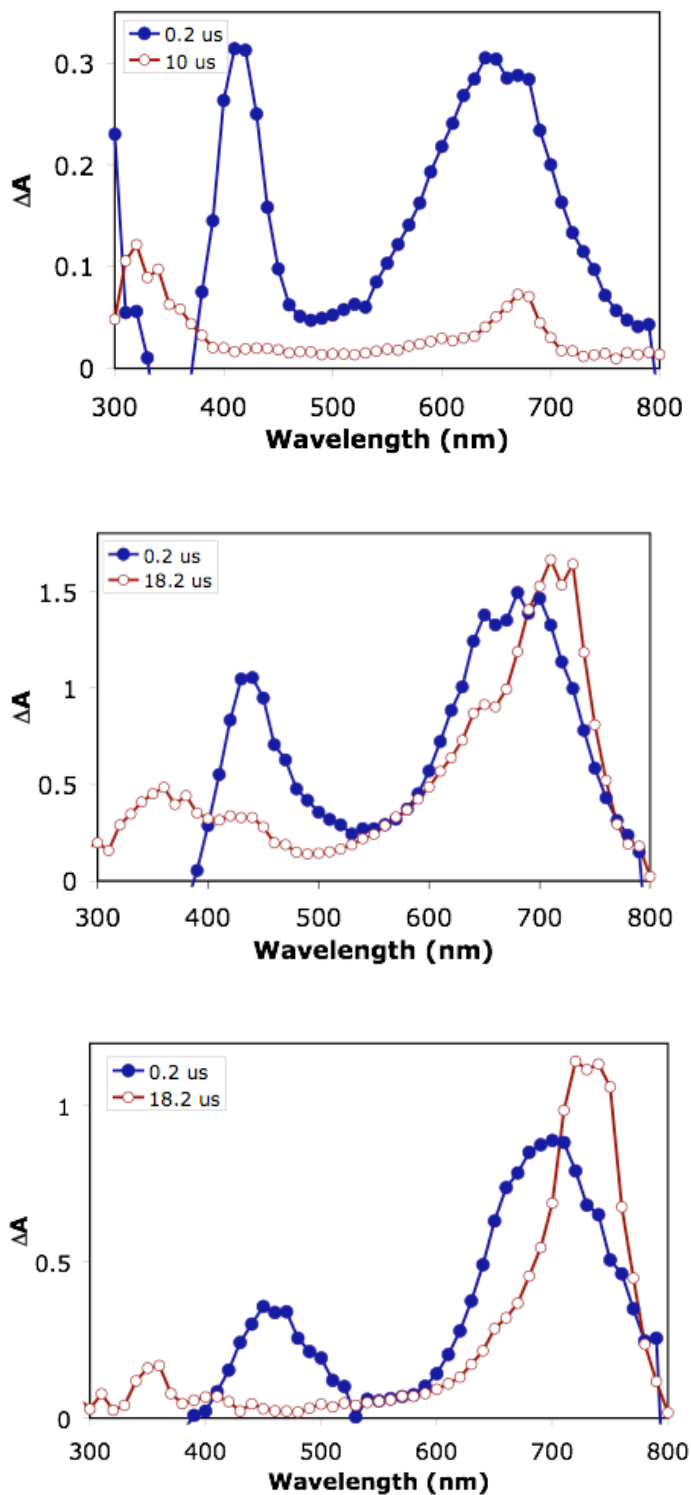


**Figure 2. 2.** Transient UV-vis spectra derived from LFP (266 nm excitation) of **2.1a** (top), **2.1b** (middle), and **2.1c** (bottom) in  $\text{CH}_3\text{CN}$  solutions. The spectra at early times (filled circles) are assigned to the corresponding diarylnitrenium ions **2.2**; those at later times (open circles) are assigned to the corresponding cation radicals **2.5<sup>++</sup>**.

**Table 2.1.** Rate Constants for Reaction of **2.1** and **2.6** with Chloride Ion.

Precursor	$k_{Cl}$ ( $M^{-1}s^{-1}$ ) <sup>a</sup>
<b>2.6a</b>	$1.0 \times 10^{10}$
<b>2.1a</b>	$5 \times 10^9$
<b>2.6b</b>	$1.1 \times 10^{10}$
<b>2.1b</b>	$4.7 \times 10^9$
<b>2.6c</b>	$9.8 \times 10^9$
<b>2.1c</b>	$5.5 \times 10^9$

a. Derived from one trial

Two experiments confirm that the absorptions seen immediately after the laser pulse correspond to the nitrenium ions. First, laser flash photolysis (355 nm, 20-30 mJ, 6 ns) of the corresponding NAPs (**2.6**) give transient absorption peaks at the same maxima as those observed for the corresponding hydrazinium ions (Table 2.1). With the NAP-generated transients, however, no long-lived intermediate was detected following the decay of the arylnitrenium ion. In fact, the lifetimes of the NAP-generated transients were significantly longer (>100 ms) than the initial intermediates generated from **2.1b** and **2.1c**.

**Table 2.1.** Calculated and Experimental Absorption Maxima (nm) [Lifetimes ( $\mu s$ )] of **2.2 a, b, c**. Derived from LFP of **2.1a, 2.1b, and 2.1c**.

Precursor	<b>2.2a</b>	<b>2.2b</b>	<b>2.2c</b>
<b>2.1</b>	420, 640 [1.3]	440, 680 [6.1]	450, 690 [4.5]
<b>2.6</b>	420, 640 [1.2] <sup>a</sup>	440, 670 [159]	440, 690 [125]
DFT	645	637	647



### 2.5. Chemical trapping studies.

The assignment of **2.2** was further verified by kinetic quenching studies. In each case, addition of Cl<sup>-</sup> was found to diminish the lifetime of the initially formed transient species. A pseudo first-order analysis of the decay rates with varying concentrations of the trap provides second-order rate constants that are near the diffusion limit. In these experiments, we note that the trapping rate constants are slightly smaller when the nitrenium ions are generated from **2.1** than those from the NAPs **2.6**. This difference can be traced to the acid (HBF<sub>4</sub>) that is added to the solutions of **2.1** in order to protonate the hydrazine. It is likely that the acid protonates some of the Cl<sup>-</sup> ions as well (which are much more basic in CH<sub>3</sub>CN than in H<sub>2</sub>O), reducing their reactivity. This was supported by repeating the experiment with **2.1a** in the presence of a 40-fold excess of HBF<sub>4</sub>, which reduced the trapping rate constant by a factor of ten.

As a final confirmation of the assignments, TD-DFT calculations were performed to predict the absorption spectra for nitrenium ions **2.2a-c**. TD-DFT calculations have been shown to reasonably predict the UV spectra of organic compounds including organic free radicals. Structures for the singlet states of each example were optimized at the RB3LYP/6-31G level. Analytical force field calculations verified that the optimized structures corresponded to minima on their respective potential energy surface. In each example, the TD-DFT calculations predict a strong absorption band in the 600-700 nm region. As shown in Table 1, theoretical-experimental agreement is excellent for the unsubstituted system **2.1a**, and

reasonable for the cases of **2.1b** and **2.1c**, given the approximations inherent in the formalism.

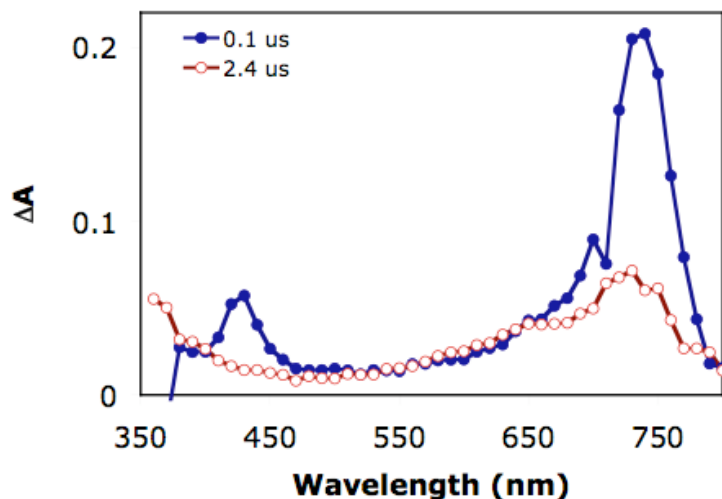


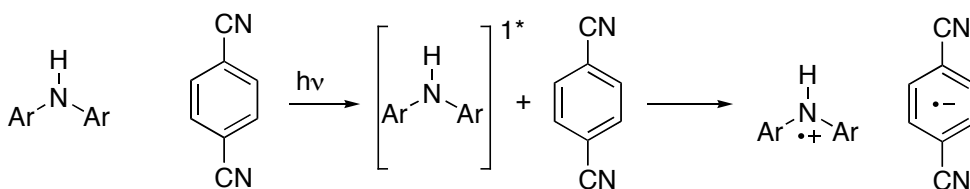
**Figure 2.3** Transient spectra derived from LFP (355 nm excitation) of a mixture of **2.6c** and 1,4-dicyanobenzene (50 mM) in  $\text{CH}_3\text{CN}$ .

The long-lived intermediates detected in the LFP experiments on **2.1b** and **2.1c** are assigned to the cation radicals of the corresponding amines **2.5**. Two experiments confirm this assignment. First, we generated the same cation radicals by LFP using an alternative route. Specifically, both **2.5b** and **2.5c** were photolyzed in the presence of an electron acceptor, 1,4-dicyanobenzene (DCB). It was expected that the excited singlet states of these amines would transfer an electron to DCB, following Scheme 3. The resulting radical ion pair can then be detected by LFP. The results from this experiment with **2.1c** are illustrated in Figure 2.3. The two other

amines, **2.5b** and **2.5b**, both give very similar results. A sharp absorption band is seen at 720 nm for **2.5b** and at 730 nm for **2.5c**.

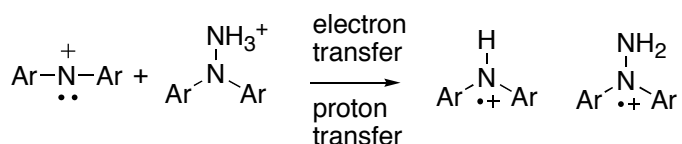
### 2.6. Formation of the cation radical

The mechanism by which **2.5<sup>+</sup>** is formed is shown in Scheme 2.5. It is postulated that nitrenium ion **2.2** abstracts an electron from unreacted hydrazinium ion **2.1**. Under the acidic conditions required to protonate the hydrazine, the resulting aminyl radical is also protonated to give **2.5<sup>+</sup>**. This mechanism is supported by additional LFP experiments. In this case, the NAPs **2.6b** and **2.6c** were excited in the presence of the corresponding hydrazinium ions using 355 nm excitation. At this wavelength, the NAPs but not the hydrazinium ions absorb light. In both cases long-lived absorption bands at 720 nm and 730 nm, attributed to **2.2b** and **2.2c** respectively were detected following the laser pulse. This result confirms that the postulated electron transfer reaction occurs rapidly. It should be noted that the same intermediates could also form from a direct H atom abstraction; further experiments would be necessary to rigorously distinguish these pathways.



**Scheme 2.5.** Photogeneration of amine radical cations

The unsubstituted system, **2.1a**, shows only a very weak signal for the cation radical **2.5a<sup>++</sup>** following the decay of the nitrenium ion **2.2a**. This can be traced to the short lifetime of the latter intermediate in the absence of hydrazine. Previous studies have shown that this diarylnitrenium ion undergoes a unimolecular cyclization reaction, eventually forming carbazole. This apparently competes with the reaction shown in Scheme 2.6.



**Scheme 2. 6.** Generation of amine radical cation

### 2.7. Conclusions

In conclusion, photolysis of 1,1-diarylhydrazinium ions generates diarylnitrenium ions via N-N bond heterolysis. The chief advantage to this method is these photolytic precursors are easier to obtain than the NAPs **2.6** that have been used previously. On the other hand, protonated hydrazines **2.1** require the use of lower wavelength UV light (<300 nm) than NAPs. An additional limitation is the rapid reaction of the photogenerated nitrenium ion intermediate with unconverted hydrazinium ion.

### 3. Chapter 3: Theoretical Investigations of Meta-substituted Arylnitrenium Ions<sup>1</sup>

#### 3.1. Introduction.

In this chapter we describe computational studies aimed at identifying novel triplet nitrenium ions with the potential of being stabilized by chemical substitutions. In order to find such high-spin nitrenium ion species, we turned to computational studies to assess the singlet and triplet state energies for substituted aryl nitrenium ions.

For substituted nitrenium ions, the prevailing view is that the singlet-triplet state energy gap (abbreviated  $\Delta E_{ST}$ ) is determined by both steric and electronic factors. For the parent system ( $\text{NH}_2^+$ ), the singlet state has a bent geometry with a bond angle of 107 deg, whereas the triplet is quasilinear, having an equilibrium bond angle of 150 deg and a very low barrier to inversion. Thus, increasing the RNR bond angle with large, sterically-demanding substituents is predicted to destabilize the singlet state more than the triplet.<sup>31</sup> Non-symmetric substituents that interact differentially with the two nonbonding orbitals will tend to stabilize the singlet state. For example, the filled  $\pi$ -orbitals on an aromatic ring act to raise the energy of the p orbital and thus stabilize the singlet.<sup>19,41,42</sup> In fact, calculations at various levels of theory predict phenylnitrenium ion to be a ground state singlet with  $\Delta E_{ST} \approx -20$  kcal/mol (a positive value of  $\Delta E_{ST}$  indicates a triplet ground state).<sup>19,41,43</sup> Although an experimental measurement of this value is not available, the sum of the indirect evidence on phenylnitrenium ion and similar systems is consistent with this prediction.<sup>3,22,25,44,45</sup>

---

<sup>1</sup> Taken in part from: Winter, A. H.; Falvey, D. E.; Cramer, C. J. *J. Am. Chem. Soc.* **2004**; 126(31); 9661-9668

The trend predicted from this simple picture is supported by a variety of experimental and computational studies. For example, Sullivan et al.<sup>43</sup> calculated  $\Delta E_{ST}$  values for a series of *para*-substituted phenylnitrenium ions (**3.1**). It was found that  $\pi$ -donor substituents (e.g. OCH<sub>3</sub>, NH<sub>2</sub>, NMe<sub>2</sub>) favor the singlet state and that  $\pi$ -acceptor substituents (CHO, NO<sub>2</sub>, etc) favor the triplet state. In fact,  $\Delta E_{ST}$  in this series shows a reasonable Hammett linear free energy correlation with the  $\sigma^+$  parameter, which represents the resonance electron-withdrawing effect of *para* substituents. In a related study<sup>46</sup> it was demonstrated that replacing the benzene ring carbons with nitrogens (e.g. 2-triazolylnitrenium ions **3.2**) also favors the triplet state. Such heteroaromatic rings are expected to be less effective  $\pi$  donors due to the electronegative nitrogen atoms.

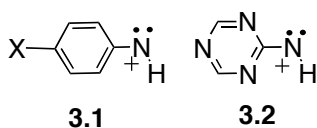


**Figure 3. 1.** Aryl and heteroarylnitrenium ions.

Organic molecules with stabilized triplet states have attracted interest due to the long-term promise of designing materials with interesting magnetic and electronic properties.<sup>47,48</sup> As a rule, however, paramagnetic organic entities such as free radicals and triplet carbenes are kinetically unstable. Thus, there is interest in identifying novel organic groups that are both paramagnetic and capable of being stabilized through appropriate substitution. To our knowledge, there has been no effort to

exploit triplet nitrenium ions to this purpose. This is understandable given the short lifetimes of these species in condensed media,<sup>49,50</sup> and that simple structural modifications of  $\text{NH}_2^+$  tend to stabilize the singlet in preference to the triplet.

We anticipated that a computational study would show how various substitution patterns affected  $\Delta E_{ST}$  values in phenylnitrenium ions. In particular, we hoped to identify triplet species having sufficient structural complexity that stabilizing elements could be incorporated into the structures without compromising the electronic state. Secondly, it was hoped that analysis of several such structures would lead to some simple qualitative generalizations that would be useful in guiding future computational and experimental efforts. While the earlier study had addressed the effects of *para* substitution on  $\Delta E_{ST}$  for phenylnitrenium ion derivatives, we set out to examine the effects of *meta* substituents.

The qualitative picture developed from the previous studies led us to expect only modest effects of *meta* substituents. Surprisingly, it was found that *meta* donors dramatically stabilize the triplet states in arylnitrenium ions. It is argued that such nitrenium ions have a triplet state that is not well described by Fig 3.1. Rather, the *meta* donor systems have  $\pi, \pi^*$  orbital character and are better described as *meta*-xylylene analogs.

### 3.2. Theoretical methods

Several earlier studies have demonstrated the utility of density functional theory (DFT) calculations in quantitatively predicting various nitrenium ion properties. For example McIlroy et al.<sup>51</sup> compared the theoretical and experimental  $\Delta E_{ST}$  for a stable nitrenium ion **3.3**. Because this species is stable, it was possible to measure  $\Delta E_{ST}$  experimentally using standard photophysical techniques. The value derived from BPW91/cc-PVDZ computations (-64.7 kcal/mol) agrees well with the experimentally-derived value (-66±3 kcal/mol). Similar DFT computations successfully predict experimental IR frequencies (measured by time-resolved techniques) for diphenylnitrenium ion<sup>52</sup> and *N*-(4-substituted)phenyl-*N*-methylnitrenium ions.<sup>45</sup> More recently Phillips et al.<sup>53-55</sup> have successfully computed nitrenium ion Raman frequencies using this approach. Also relevant to this work is the application of DFT methods to the study of  $\Delta E_{ST}$  values in arylcarbenes.<sup>19,39,56-61</sup>

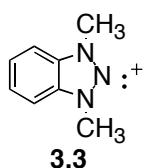


**Figure 3. 2. A stable nitrenium ion.**

Structures for all of the nitrenium ions in the present study were determined using density functional theory (DFT) at the UB3LYP/6-31G(d,p) level. Both the geometry optimizations and the vibrational modes were calculated at this level. Energy differences ( $\Delta E_{ST}$ ) include zero point vibrational energy corrections, which were

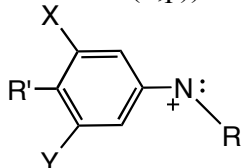


unscaled. All singlet and triplet states were found to be local minima with no imaginary vibrational frequencies. As discussed in a subsequent section of this chapter, several alternative basis sets were examined. The trends described below are robust irrespective of the size of the basis set or the absence or presence of polarization functions.

### 3.3. Computed singlet-triplet gaps

Table 3.1 lists all of the substituted phenylnitrenium ions examined along with their corresponding  $\Delta E_{ST}$  values. Also included in that table are some key geometric data including the ArN bond length ( $r_1$ ), the ArNR bond angle ( $\theta$ ), and the torsional angle ( $\omega$ ) between the N-R bond and the phenyl ring. The first two examples, phenylnitrenium ion **3.4** and *N*-methyl-*N*-phenylnitrenium ion **3.21**, have been studied previously. These are computed at the present level of theory to be ground state singlets by  $-19.5$  and  $-14.3$  kcal/mol, respectively. The smaller  $\Delta E_{ST}$  value predicted for the *N*-methyl system has been attributed to the steric effect of the *N*-methyl group, where the methyl group forces a wider bond angle preferred by the triplet state. We note that for the triplet states of these two nitrenium ions, the N-R bond (R=H, Me) is approximately perpendicular to the phenyl ring. This was also predicted by the previous study.<sup>19,40,62</sup>

**Table 1.** Singlet-Triplet Gaps and Selected Geometric Parameters for Substituted Phenylnitrenium Ions (UB3LYP/6-31G(d,p)).



No.	R	R'	X	Y	$\Delta E_{ST}$ (kcal/mol)	Spin State	$\theta$ (deg)	$R_1$ (ang)	$\omega$ (deg)
3.4	H	H	H	H	-19.2	Singlet Triplet	112.5 131.8	1.294 1.326	0.00 92.63
3.5	H	H	CH <sub>3</sub>	H	-18.9	Singlet Triplet	112.3 129.8	1.295 1.330	0.00 92.36
3.6	H	H	(CH <sub>3</sub> ) <sub>3</sub> Si	H	-19.2	Singlet Triplet	112.2 130.2	1.294 1.326	0.07 97.31
3.7	H	H	F	H	-17.1	Singlet Triplet	112.5 130.2	1.295 1.331	0.00 92.81
3.8	H	H	CN	H	-17.4	Singlet Triplet	112.8 132.4	1.295 1.327	0.01 92.74
3.9	H	H	OH	H	-13.6	Singlet Triplet	112.2 122.7	1.297 1.349	0.00 91.53
3.10	H	H	CH=CH <sub>2</sub>	H	-10.7	Singlet Triplet	112.2 110.9	1.296 1.339	0.00 0.00
3.11	H	H	PH <sub>2</sub>	H	-9.8	Singlet Triplet	112.4 110.9	1.295 1.336	0.23 0.48
3.12	H	H	SH	H	-6.4	Singlet Triplet	112.3 111.1	1.296 1.336	0.02 0.00
3.13	H	H	OCH <sub>3</sub>	H	-6.9	Singlet Triplet	112.1 111.1	1.296 1.335	0.00 0.00
3.14	H	H	NH <sub>2</sub>	H	+0.4	Singlet Triplet	112.0 111.0	1.298 1.336	0.00 0.00
3.15	H	H	N=O	H	+2.3	Singlet Triplet	112.6 111.1	1.295 1.346	-0.17 0.00
3.16	H	H	P(CH <sub>3</sub> ) <sub>2</sub>	H	+5.7	Singlet Triplet	112.1 110.4	1.294 1.337	0.24 -0.38
3.17	H	H	NH <sub>2</sub>	NH <sub>2</sub>	+7.7	Singlet Triplet	111.6 111.0	1.303 1.334	0.00 0.00
3.18	H	H	(CH <sub>3</sub> ) <sub>2</sub> N	(CH <sub>3</sub> ) <sub>2</sub> N	+11.8	Singlet Triplet	111.2 110.6	1.305 1.335	0.00 0.00
3.19	H	H	1-aziriny	H	+11.0	Singlet Triplet	112.0 110.4	1.300 1.335	1.03 -0.27
3.20	H	H	C <sub>4</sub> H <sub>3</sub>	H	+21.2	Singlet Triplet	111.7 110.5	1.310 1.343	-0.15 0.00
3.21	CH <sub>3</sub>	H	H	H	-14.3	Singlet Triplet	124.4 144.0	1.310 1.324	0.00 92.39
3.22	CH <sub>3</sub>	H	NH <sub>2</sub>	NH <sub>2</sub>	+3.0	Singlet Triplet	123.6 122.0	1.317 1.341	0.00 0.00
3.23	<i>t</i> -Bu	H	NH <sub>2</sub>	NH <sub>2</sub>	-4.7	Singlet Triplet	131.7 135.6	1.321 1.342	0.00 93.19
3.24	H	CH <sub>3</sub>	Me <sub>2</sub> N	Me <sub>2</sub> N	+3.6	Singlet Triplet	111.4 110.7	1.300 1.331	-2.15 -1.10

For several of the mono-substituted systems (3.5-3.16, 3.19, 3.20) there exists the possibility for two rotational isomers. The first isomer, which we label “anti,” has the nitrenium center NH bond directed away from the substituent. The second isomer, which we label “syn” has the NH bond directed toward the substituent. Likewise, some substituents themselves can isomerize through rotation about their bond to the phenyl ring. For the mono-substituted systems, this results in 4 isomers for each state: anti-anti’, anti-syn’, syn-anti’, and syn-syn’. These are shown in Fig 3.3. The relative stabilities of these isomers were compared at the semi-empirical level (AM1). In most cases, the anti-anti’ isomers were found to be the more stable. The differences were not large, in most cases being less than 1 kcal/mol within a given spin state. Therefore, the detailed DFT calculations were carried out only for the anti and the anti-anti’ isomers.

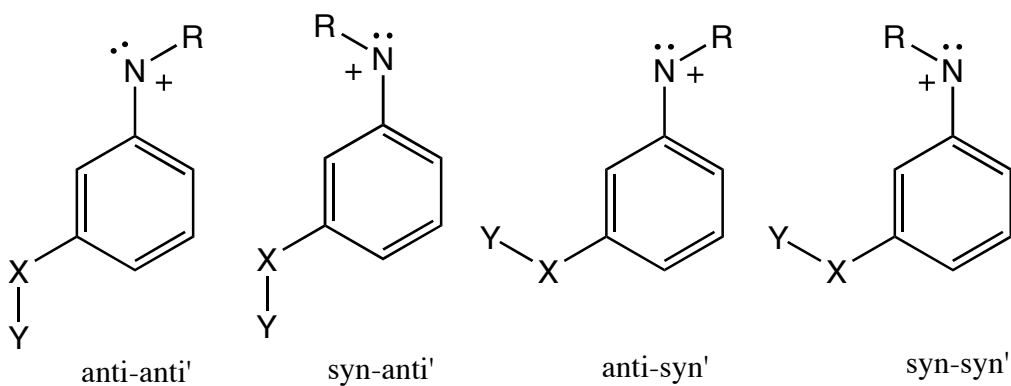


**Figure 3. 3.** Rotational isomers of substituted phenylnitrenium ions.

Extrapolation of the earlier Hammett correlation<sup>43</sup> predicts that *meta* substituents will have only a very modest effect on  $\Delta E_{ST}$ . Indeed, calculations on the systems with *m*-

Me (**3.5**), *m*-SiMe<sub>3</sub> (**3.6**), *m*-F (**3.7**), and *m*-CN (**3.8**), support this prediction. None of these substituents alters  $\Delta E_{ST}$  by more than 2.1 kcal/mol relative to the unsubstituted system **4**. It is also noteworthy that these arylnitrenium ions show singlet and triplet geometries that are not greatly altered from PhNH<sup>+</sup>. That is, the singlets all have ArNR bond angles in the range of 112-113 deg and the N-H bond is essentially coplanar with the ring ( $\omega \sim 0$  deg). In the case of the triplets, the NH bonds are perpendicular to the plane of the phenyl ring ( $\omega \sim 90$ ) and the ArNH bond angles fall in the range of 129-132 deg.

Substitution with *meta*-donor substituents, however, dramatically alters the nature of the triplet state. First, *m*-NH<sub>2</sub> (**3.14**), *m,m'*-diNH<sub>2</sub> (**3.17**), *m,m'*-diNMe<sub>2</sub> (**3.18**), *m*-PMe<sub>2</sub> (**3.16**), *m*-cyclobutadienyl (**3.20**), *m*-azirinyll (**3.19**), and *m*-nitroso groups (**3.15**) substantially alter  $\Delta E_{ST}$  increasing it by over 19 kcal/mol. In fact, all of these derivatives are predicted to be ground state triplets. Second, in each case the triplets show planar geometries ( $\omega \sim 0$  deg). Third, and more remarkably, the triplet states of these derivatives all have ArNR bond angles ( $\theta$ ) that are ca. 20 deg smaller than the bond angle for the triplet states of the non *meta*-donor systems (**3.5-3.8**). Indeed, the *meta*-donor triplets all have bond angles that are smaller than the corresponding singlets. Finally, the C-N bond lengths (where C refers to the ipso carbon in the phenyl ring) are ca. 0.005 Å longer than the non *meta*-donor triplets. Figure 3.4 shows the geometries of the 3-amino-phenylnitrenium ion and the 3-fluoro-phenylnitrenium ion, which are typical examples of the non *meta*-donor and *meta*-donor series.

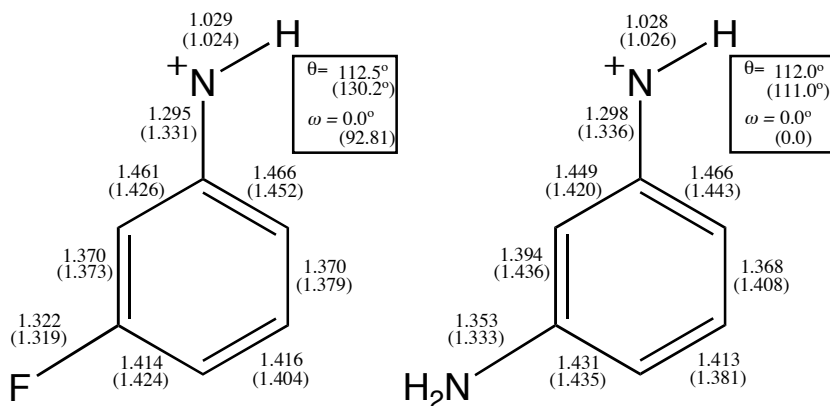


**Figure 3.4.** Geometries of the singlet (triplet) states of nitrenium ions **3.7** and **3.17** (bond lengths in Å)

In contrast, *meta*-donor substitution seems to have only a modest effect on the singlet states of the corresponding nitrenium ions. The singlet ArNH bond angles are relatively insensitive to the presence of *meta*-donor substituents. Likewise, the singlets in every case we have examined are planar ( $\omega \sim 0$  deg). The only parameter showing any significant effect is the Ar-N bond distance  $rI$ . This is consistently shorter in the *meta*-donor systems than it is in the non-*meta* donor derivatives.

The significance of the conjugation by the meta-donor groups is further emphasized by nitrenium ion **3.24**, shown in Fig 3.5. In this species the two dimethylamino groups flank an additional *para*-methyl substituent. The steric effect of this methyl group requires that the dimethylamino groups rotate out of the phenyl ring plane by 58 deg in the singlet and 23 deg in the triplet. This appears to destabilize the triplet

more significantly than the singlet as  $\Delta E_{ST}$  decreases by over 8 kcal/mol compared with **3.18**, where this group is not present.

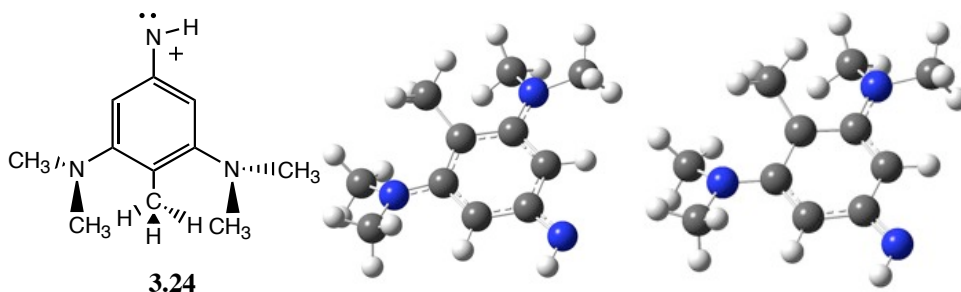


**Figure 3.5.** Geometry of 4-methyl-3,3'-bis(dimethylamino)phenylnitrenium ion **3.24** in the triplet state (left) and the singlet state (right).

The *meta*  $\pi$ -donor systems also differ in how  $\Delta E_{ST}$  responds to *N*-alkylation. The current study (see examples 1 and 2), as well as previous reports, indicates that *N*-alkylation of phenylnitrenium ions destabilizes the singlet relative to the triplet state. This is generally attributed to a steric effect wherein the singlet state, preferring the smaller ArNR bond angle, is destabilized more than the triplet. By our computations, *N*-methylation of phenylnitrenium ion shifts  $\Delta E_{ST}$  by ca. 5 kcal/mol in favor of the triplet. In contrast, consider examples **3.22**, and **3.23**. Here the methyl and *tert*-butyl group shifts  $\Delta E_{ST}$  in favor of the *singlet* by 5 and 9 kcal/mol, respectively. Of special note is that the *tert*-butyl group in the triplet of **3.23** is actually out of plane in the same way that the N-R bonds in the *meta* non- $\pi$ -donor triplets. As might be expected, *N*-alkylation increases the bond angle for both the singlet and the triplet state.

Nitrenium ions **3.14-3.20** all differ in rather substantial ways from phenylnitrenium ion, and its simple *para* derivatives. First, these species all have triplet, rather than singlet, ground states. Second, they respond in the opposite way to *N*-alkylation. Finally, the triplet state geometries of these species are qualitatively different from the geometries of the parent system. These rather substantial differences suggest that the effect of the *meta* donors goes beyond a simple quantitative perturbation of the electronic structure depicted in Fig 3.2.

The diradical, *meta*-xylylene (also known as *meta*-benzoquinodimethane or MBQDM), shown in Fig. 3.6, has a triplet ground state with  $^3A'$  state symmetry, and  $\Delta E_{ST}$  of +9.6 kcal/mol.<sup>63-69</sup> This species has been the subject of numerous computational and experimental studies, as have many of its simple derivatives. In contrast to the carbenes and simple nitrenium ions, where the two SOMOs are orthogonal, *meta*-xylylene's triplet ground state is attributed to degenerate but non-disjoint SOMOs.<sup>70-72</sup>

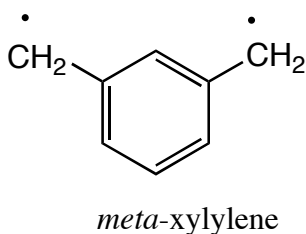


**Figure 3.6.** The non-Kekulé diradical *meta*-xylylene.

### 3.4. Electronic structure of the stabilized triplet state

We considered the possibility that the *meta*-donor phenylnitrenium ions might adopt an electronic structure analogous to *meta*-xylylene. This can be visualized in a schematic way by starting with the aryl nitrenium ion's singlet state, and then transferring an electron from a non-bonding orbital on the donor substituent(s) to the out-of-plane non-bonding orbital on the nitrenium ion center. This would create a species that would have aminyl radical character at the original nitrenium ion center and a cation radical site on the *meta* substituent(s).

Figure 3.7 illustrates simple models for the lowest electronic states of *meta*-donor substituted nitrenium ions. The lowest singlet state is designated " $n^2$ ", referring to the occupancy of the HOMO. The lowest triplet state typical of non *meta*-donor aryl nitrenium ions is designated " $n,\pi^*$ ." This state is derived from promotion of an electron from the  $n$  orbital on the nitrenium center to a  $\pi^*$  orbital which results from the mixing of the non-bonding orbital on the N and the  $\pi^*$  orbitals of the phenyl ring. Finally, the lowest triplet state of the *meta*  $\pi$ -donors is designated " $\pi,\pi^*$ " indicating that this state is derived from promotion of an electron on a substituent non-bonding orbital of  $\pi$  symmetry to the  $\pi^*$  level.

One potential source of confusion in Fig 3.7 is the nature of the non-bonding orbitals. In our studies, every  $n,\pi^*$  triplet has the N-R bond nearly perpendicular ( $\omega=90$  deg) to the plane of the aromatic ring. Thus, the relevant N-localized nonbonding orbital that is antisymmetric with respect to the plane of the phenyl ring is approximately  $sp^2$



hybridized. Likewise, the N-localized nonbonding orbital that is symmetric with respect to the phenyl ring plane is unhybridized. In contrast, the  $n^2$  singlet and  $\pi,\pi^*$  triplet both have an unhybridized  $p$  nonbonding orbital, which interacts with the phenyl  $\pi$ -orbitals, and an  $sp^2$ -like orbital which is designated “ $n$ ”.

This qualitative picture leads to three specific predictions. (1) The two SOMOs in the  $\pi,\pi^*$  triplet state should have  $\pi$ -symmetry. That is, they should both have a nodal plane that coincides with the phenyl ring's plane. (2) Such a  $\pi,\pi^*$  triplet state should exhibit substantial spin delocalization onto the substituent(s). (3) The nitrenium ion center, having a doubly occupied n-orbital, should be approximately  $sp^2$  hybridized and thus have geometric characteristics similar to that of the anilino radical (PhNH•). More specifically the doubly-occupied n-type orbital on nitrogen should lead to a  $sp^2$ -like geometry and a CNH angle  $<120$  deg due to the in plane lone pair.

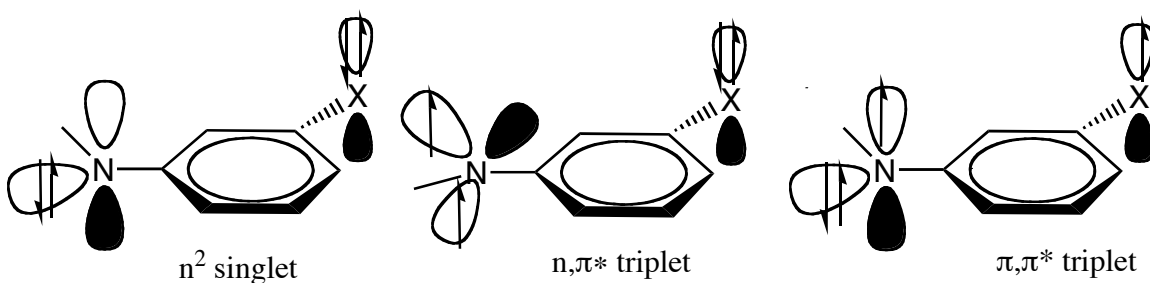


**Figure 3.7.** Models of the electronic states of *meta*-substituted phenylnitrenium ion.

The first prediction, regarding the nodal properties of the SOMOs, is illustrated in Fig 7, which shows visualizations of the Kohn-Sham SOMOs derived from the DFT calculations for triplet *m*-fluorophenylnitrenium ion 3.7 along with the those

calculated for *m,m'*-bis(diamino)phenylnitrenium ion **3.17**. The former is representative of the non *meta*-donor series and the latter of the *meta*-donors.

As the simple model predicts, the triplet state of ion **7** has the characteristics of a  $n,\pi^*$  state. One SOMO is symmetric and the other is antisymmetric with respect to the phenyl ring's plane. Similar SOMOs are observed for **3.4-3.6**, **3.8**, **3.9** (data not shown). In contrast, the triplet state of ion **3.17** has the characteristics of a  $\pi,\pi^*$  state. The two SOMOs are anti-symmetric with respect to the phenyl ring plane. Similar pictures are derived from the triplet states of the other *meta*-pi donor systems: **3.10-3.14** and **3.16-3.20**. The *meta* nitroso derivative, **3.15**, is considered below.

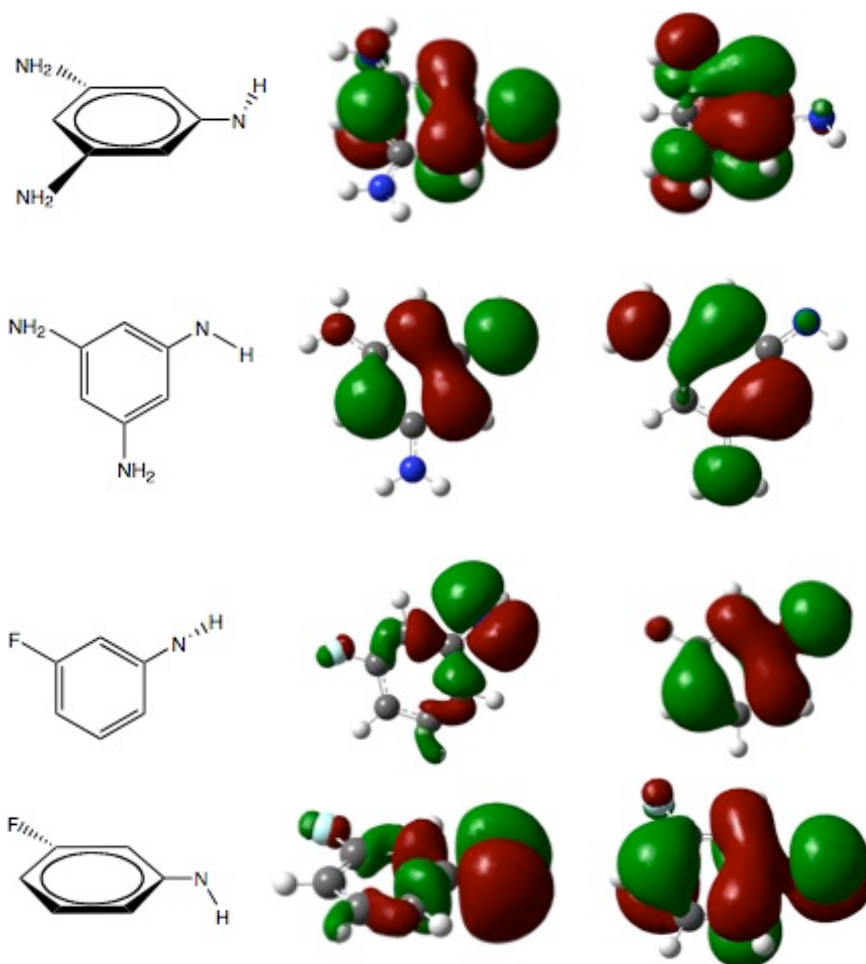


**Figure 3. 8.** SOMO densities (top and side views) for the UB3LYP computed triplet states of nitrenium ions **3.7** (below) and **3.16** (above).

The second prediction is illustrated by the Mulliken spin densities shown in Fig 3.9. The numbers in the figure represent the Mulliken spin densities on the non-hydrogen atoms in the substituent. It is clear that the non *meta*-donor systems (e.g. **3.5-3.8**) show very little ( $<0.08$ ) spin delocalization onto the *meta* substituents. In contrast, the *meta*-donor species (**3.11-3.20**) all show significant ( $>0.3$ ) spin density on the substituents. Structures **3.22** and **3.23** are interesting because, as noted above, *N*-alkylation actually acts to *destabilize* the  $\pi,\pi^*$  triplet state relative to the singlet and

the  $n,\pi^*$  triplet. This is seen in the reduced spin delocalization in these structures. In the case of the *N-tert*-butyl derivative (**3.23**) the perpendicular (ie.  $\omega \sim 90$  deg) geometry of N-substituent as well as the nodal properties of the SOMO indicate that the lowest triplet for this species is  $n,\pi^*$ .

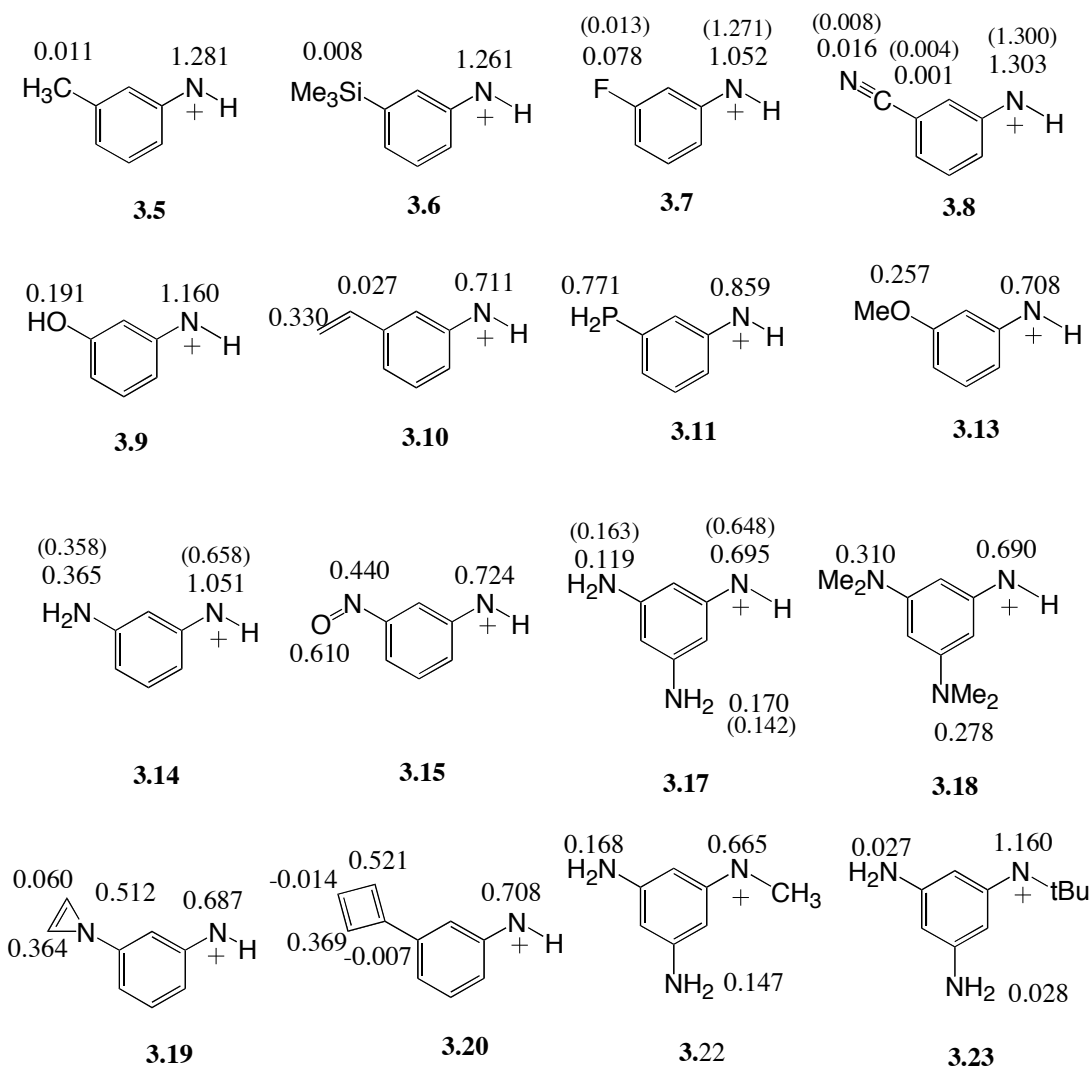


**Figure 3. 9.** Mulliken spin densities on substituent heavy atoms on meta-substituted phenylnitrenium ions derived from UB3LYP/6-31G(d,p) calculations.

Finally, the geometry of the anilino radical ( $\text{PhNH}\cdot$ ) was computed using the same methodology as was applied to the nitrenium ions. This species shows an NH bond that is coplanar with the phenyl ring and has an equilibrium PHNH bond angle of 111.0 deg. This small bond angle is readily attributed to a filled  $n$  orbital on the nitrogen that is in the plane of the ring. This bond angle resembles the triplet meta-donor nitrenium ion bond angles (110-111 deg) far more than the non *meta*-donor aryl nitrenium ions, whose bond angles are  $>130$  deg.

Nitrenium ions **3.10-3.13** having vinyl, phosphino, sulfhydryl, and methoxy substituents illustrate intermediate cases. Each of these species is predicted to be a ground-state singlet. However their lowest triplet states are apparently  $\pi,\pi^*$ . All of these have CNH bond angles closer to the ideal of the anilino radical, in the range of 110-111 deg. Visualization of the SOMOs also verifies that these are  $\pi,\pi^*$  in nature. Apparently these substituents interact sufficiently with the phenyl  $\pi$ -system to make  $\pi,\pi^*$  the lowest triplet state, but not so sufficiently as to make that state more stable than the singlet. Thus we concluded that *meta* substituents have their strongest effect on the  $\pi,\pi^*$  triplet states. This is illustrated in Figure 9. In some cases, the computations identified two geometrically and energetically distinct triplet states. For example initial calculations on **3.7** showed a  $\pi,\pi^*$  triplet state, with  $\omega = 0.02$  deg, 3.84 kcal/mol higher in energy than the  $n,\pi^*$  triplet ( $\omega = 92.81$  deg) reported in Table 3.1. We hope to undertake a more systematic study of these higher energy triplet states in the future.

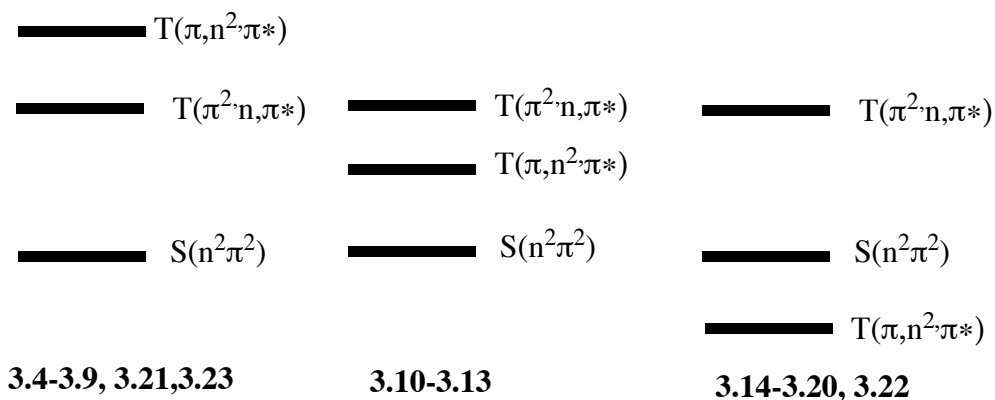


**Figure 3.9.** Proposed qualitative state orderings for substituted phenylnitrenium ions, illustrating the effect of increasingly effective meta pi donation from left to right

The nitroso derivative **15** is an interesting exception to the trends described above. This ion is predicted to be a ground state triplet and its triplet state has the small bond angle characteristic of the  $\pi, \pi^*$  states. However, calculations constrained to  $C_s$  symmetry show that the triplet state has  ${}^3A''$  orbital symmetry. Visualization of the Kohn-Sham SOMOs for the triplet is given in Figure 3.10. Note the conspicuous *lack* of n-SOMO density on the formal nitrenium center. It is clear that this triplet state can be approximated as being derived from promotion of an electron from the *nitroso* lone pair to the  $\pi^*$  orbital. Thus we term **3.15** and similar systems  $n', \pi^*$  triplets. Here the prime indicates that the electron is derived from an orbital primarily on the substituent, rather than the formal nitrenium ion center. A similar, albeit less pronounced, effect has been proposed for the triplet states of certain heteroarylnitrenium ions<sup>46</sup>.

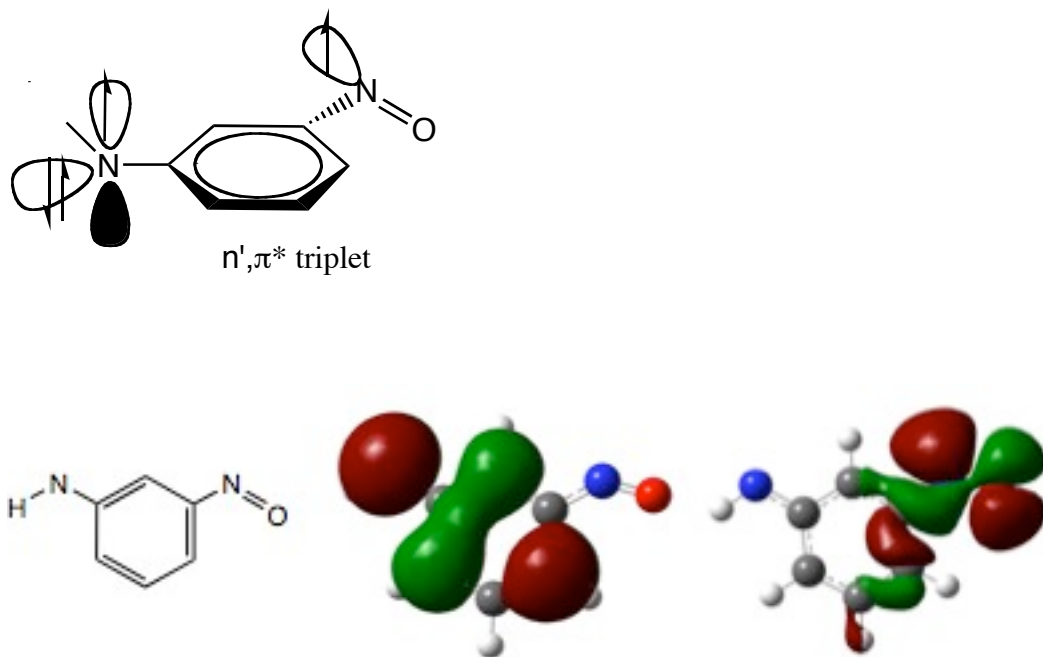


**Figure 3.10.** Geometry and SOMO densities for nitrenium ion **3.15**.

All geometry optimizations and vibrational frequency calculations were carried out using the Gaussian03 suite of programs.<sup>73</sup> The values in Table 3.1 were calculated using density functional theory, and in particular the hybrid B3LYP functional, comprised of Becke's B3 three-parameter gradient-corrected exchange functional<sup>74,75</sup> with the LYP correlation functional of Lee, Yang, and Parr<sup>76</sup> as originally described by Stevens et al.<sup>77</sup> For these calculations, the 6-31G(d,p) basis set<sup>78</sup> was employed. We note that  $\langle S^2 \rangle$  for all triplet states was computed to range from 2.0002 to 2.0021, implying negligible spin contamination.

For the singlet spin states, the values in Table 3.1 were computed using restricted DFT. We examined in several instances whether the restricted Kohn-Sham solutions were stable with respect to symmetry breaking, since broken-symmetry solutions

more accurately account for non-dynamical correlation effects that are often present in singlet biradicals.<sup>54,55</sup> In the case of **3.7**, which is a typical member of the set of nitrenium ions having the singlet state much more stable than the triplet, the restricted solution was found to be stable. In the case of **15**, the restricted singlet was also found to be stable. In the case of **3.14**, on the other hand, symmetry-breaking was found to lower the energy of the singlet state by 1.9 kcal/mol (thereby inverting the ordering of the singlet and triplet states). Finally, for **3.17**, symmetry breaking also was observed to lower the energy of the singlet state by a similar margin as for **3.14**, which was therefore not enough to invert the state ordering in this system. As we were here concerned more with the qualitatively novel aspects of *meta* substitution than we were with obtaining quantitatively accurate gas-phase predictions, we did not examine the propensity to break symmetry in additional cases, judging that **3.7**, **3.14**, **3.15**, and **3.17** were sufficiently representative. We note that  $\langle S^2 \rangle$  values for the broken-symmetry non-interacting Kohn-Sham wave functions of **3.14** and **3.17** were 0.0246 and 0.0606, respectively, indicating that the restricted solutions are very *nearly* stable.

Although the 6-31G(d,p) basis set was chosen on the basis of size and balance, it is conceivable that one might wish to employ more economical (but less well balanced) basis sets in much larger systems. In order to evaluate the likely success of such an approach, Table 3.2 compares the performance of other basis sets for several examples from this series, including phenylnitrenium ion **3.4**, and *m*-fluorophenylnitrenium ion **3.7**. These species are taken to be representative of the



nitrenium ions that show no *meta*-donor effect. Likewise 3-aminophenylnitrenium ion **3.14** and 3,3'-diamino-phenylnitrenium ion **3.17** were also studied. These latter two species are taken to be representative of species that show the *meta*-donor effect.

Several generalizations can be made. All of the methods predict very similar geometries. For example the triplet states of **3.4** and **3.7** are predicted to give out-of-plane NH bonds ( $\omega \sim 90$  deg) regardless of the basis set or method applied. In contrast, the triplet states of **3.14** and **3.17** are predicted to have in-plane NH bonds ( $\omega \sim 0$  deg). Likewise, the singlets are all predicted to have in-plane NH bonds ( $\omega=0$  deg) with much more acute bond angles. Arylnitrenium geometries are well converged with the unpolarized 6-31G basis set.

For the *meta* pi-donor systems (**3.14** and **3.17**) discrepancies in  $\Delta E_{ST}$  values are small, being  $<2$  kcal/mol when 6-31G is compared with 6-311G and 6-31G(d,p). On the other hand, the H-atom polarized basis sets show systematically smaller ArNH bond angles, differing by  $<4$  deg for the singlets and as much as 9 deg for the triplets. Likewise, the polarized basis sets show smaller Ar-N bond distances for the singlets by  $0.011\text{\AA}$ . Thus for these systems, we conclude that 6-31G is overall adequate for calculating  $\Delta E_{st}$  and predicting general trends in this value as the structures are modified.

In contrast,  $\Delta E_{ST}$  values in the non *meta*-donor systems **3.4** and **3.7** show a much stronger dependence on the inclusion of H-atom polarization functions. In both cases,

use of the 6-311G and 6-31G basis sets consistently overestimated the stability of the triplet state by 3-6 kcal/mol compared to the polarized, cc-pVDZ and 6-31G(d,p) basis sets. We note that the triplet state *meta* fluoro compound shows two local minima. One is at the  $\omega=90$  deg dihedral. There is another minimum ca. 3.5 kcal/mol higher in energy at the planar geometry.

### 3.5. Basis set effects

Finally, to gauge how well converged  $\Delta E_{ST}$  values may be considered to be with the 6-31G(d,p) basis set, we carried out calculations with the cc-pVTZ basis set of Dunning<sup>56</sup> for **3.7** and **3.14**. As can be seen in Table 2, the significant increase in basis set size has fairly little effect on the predicted splittings and geometrical parameters. The most noteworthy effect is the systematic shortening of the CN bonds in both states with the larger basis set. As noted above, when symmetry breaking was allowed for the singlet state of **3.14** with the larger basis set, the energy lowering effect was small and reoptimization of the restricted geometry afforded less than 0.1 kcal/mol additional energy lowering.

**Table 3.2.** The effect of basis set on predicted singlet-triplet gaps  $\Delta E_{ST}$  (kcal/mol) and various geometric parameters of selected *meta*-substituted phenylnitrenium ions.

Nitrenium ion	Basis set	$\Delta E_{ST}$	$\theta$ (deg) singlet / triplet	$rI$ (Å) singlet / triplet	$\omega$ triplet
<b>3.4</b>	6-31G	-15.4	115.4 / 139.4	1.306 / 1.330	92.4
	6-311G	-15.5	115.2 / 139.7	1.305 / 1.330	92.2
	6-31G (d,p)	-19.2	112.5 / 131.8	1.294 / 1.326	92.6
<b>3.7</b>	6-31G	-13.5	115.6 / 139.1	1.306 / 1.332	92.1
	6-311G	-13.7	115.3 / 139.5	1.306 / 1.332	92.6
	6-31G (d,p)	-17.1 (-17.1)**	112.5 / 130.2	1.295 / 1.331	92.8
	cc-pVDZ	-21.9	112.3 / 111.2	1.297 / 1.337	93.3
	cc-pVTZ	-17.3*	112.9 / 130.4	1.289 / 1.325	92.0
<b>3.14</b>	6-31G	+1.3	114.9 / 113.5	1.310 / 1.351	0.0
	6-311G	-1.2	114.6 / 113.2	1.310 / 1.353	0.0
	6-31G (d,p)	+0.4 (-1.4)	112.0 / 111.0	1.336 / 1.335	0.0
	cc-pVDZ	-1.4	111.6 / 110.8	1.303 / 1.339	0.0
	cc-pVTZ	-0.1* (-1.9)**	112.3 / 111.5	1.293 / 1.331	0.0
<b>3.17</b>	6-31G	+8.8	114.4 / 113.4	1.315 / 1.350	0.0
	6-311G	+8.7	114.1 / 113.2	1.315 / 1.351	0.0
	6-31G (d,p)	+7.7	111.6 / 111.0	1.303 / 1.334	0.0
	cc-pVDZ	+7.7	111.2 / 110.6	1.304 / 1.335	0.0

\*\*Numbers in parentheses derived from broken-symmetry calculations. Geometry reoptimization lowers the energy by less than 0.1 kcal/mol, so different geometric data for the broken-symmetry solution are not reported. *b* Zero-point vibrational corrections added from cc-pVDZ calculations.

### 3.6. *Conclusions*

These computations identify a novel class of triplet organic species: arylnitrenium ions having electron-donating *meta* substituents. Analysis of the structures of these species suggests that the effect of these substituents is to stabilize a  $\pi, \pi^*$  triplet state that is qualitatively similar to the well-characterized non-Kekulé *meta* xylylene

diradicals. The generalizations derived from this study suggest that triplet diradical ions of this nature are not confined to the phenylnitrenium ion series. Any species with a strong electron acceptor and a strong donor that are conjugated with non-disjoint  $\pi$ -orbitals could, in principle, have a triplet ground state. While this generalization has been appreciated for many years with respect to neutral diradicals, to our knowledge there have been few, if any, studies of ionic species having this connectivity. We note that preliminary calculations on  $m,m'$ -bis(dimethylamino)benzyl cation suggest that this species is also a ground state triplet with  $\Delta E_{ST} = +2.0$  kcal/mol ( in contrast to unsubstituted benzyl cation, which is predicted to have  $\Delta E_{ST} = -40$  kcal/mol (B3LYP/6-31G(d,p)). Attempts to generate and characterize these triplet nitrenium ions experimentally are discussed in Chapter 5.

## 4. Chapter 4: Application of Meta Effect to other Cationic Reactive Intermediates.<sup>1</sup>

### 4.1. *Introduction*

In this chapter, the meta effect described in the previous chapter is extended to species other than arylnitrenium ions, including aryloxygenium ions, arylsilylenium ions, and arylcarbenium ions. DFT (B3LYP/6-31G(d,p)) calculations are used to compute the singlet-triplet energy splittings, and multireference second order perturbation theory (CASPT2) calculations are used to benchmark the quantitative accuracy of the DFT calculations for representative systems.

As reported in the previous chapter, we were surprised to find that *meta* substitution of phenylnitrenium ions with  $\pi$  donors stabilizes a  $\pi,\pi^*$  triplet diradical state with an electronic configuration similar to meta-xylylene. Meta-xylylene is a well-known triplet diradical that has been the subject of extensive theoretical<sup>17,57</sup> and experimental studies.<sup>2,57-63</sup> This change in the electron configuration of phenylnitrenium ions to a meta-xylylene-like triplet state upon meta donor substitution can be pictured by promoting an electron from the lone pair associated with the meta donor substituent (D, e.g. NMe<sub>2</sub>) into the LUMO formally associated with the nitrenium based *p* orbital (see Figure 4.1).

---

<sup>1</sup> Taken in part from: Winter, A. H.; Falvey, D. E.; Cramer, C. J.; Gherman, B. F. *J. Am. Chem. Soc.* **2007**; 129(33); 10113-10119.

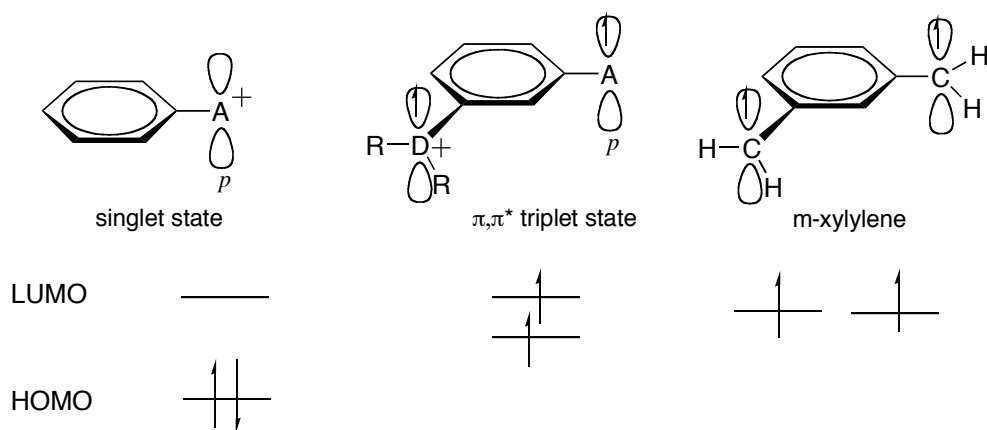


**Figure 4.1** General schematic representations of a typical singlet state and a  $\pi, \pi^*$  triplet state.

Thus, while the unsubstituted phenylnitrenium ion ( $PhNH^+$ ) is predicted to be a ground state singlet by 19 kcal/mol, adding sufficiently strong  $\pi$  electron donors (such as two *N,N*-dimethylamino substituents,  $NMe_2$ ) to the *meta* positions stabilizes the triplet state sufficiently to make the  $\pi, \pi^*$  triplet state the predicted ground state by DFT.

We considered that this same ‘*meta* effect’ might translate to other cationic species. In particular, we were interested if this triplet stabilization by *meta*  $\pi$  donors would occur with benzylic cations, since these intermediates hold a central place in the historical development of physical organic chemistry in general, and the understanding of electronic effects of substituents in particular. For example, historically the first experimental observation of cationic carbon has been accredited to Baeyer and others for the discovery of the triply-benzylic triphenylmethyl cation using conductivity measurements at the beginning of the 20<sup>th</sup> century.<sup>64-66</sup> These types of benzylic cations were further characterized by NMR in the mid 1960s under

stable ion conditions.<sup>67,68</sup> There are also several linear free energy relationships in use based on the quantitative effects of substituents on the reactivity of benzylic cations, including the Hammett  $\sigma^+$  substituent parameters.<sup>69,70</sup> Despite this intense activity over many decades, there are to our knowledge no investigations of the effects of extremely strong *meta*- $\pi$ -donors (e.g. 3,5-bis(*N,N*-dimethylamino) substitution) on the behavior of benzylic cations.

#### 4.2. Triplet benzylic cations.

The prospect that such an important species could have a stabilized triplet state caused us to turn our attention towards these intermediates. In fact, the DFT calculations described below predict low-energy or ground-state triplet states for benzyl cations substituted with strong  $\pi$  donors in the *meta* positions. Moreover, the current computational investigation suggests that the previously reported *meta*-substituted triplet arylnitrenium ions<sup>71</sup> are just one member of a broad class of ion diradicals exhibiting the connectivity of a  $\pi$  donor linked through non-disjoint  $\pi$  orbitals to a  $\pi$  acceptor.

The cationic species calculated in this study include aryloxenium ions ( $\text{Ar-O}^+$ ), arylnitrenium ions ( $\text{Ar-NH}^+$ ), arylsilylenium ions ( $\text{Ar-SiH}_2^+$ ), and benzyl cations ( $\text{Ar-CH}_2^+$ ). As with the previously reported phenylnitrenium ions,<sup>71</sup> all of these species show a stabilization of a  $\pi, \pi^*$  diradical state when substituted with *meta*  $\pi$  donors, as shown by a marked change in the singlet-triplet state energy gaps ( $\Delta E_{\text{ST}}$ ) with strong

donors. Here the symbol  $\Delta E_{ST}$  is used to refer to the 0 K adiabatic energy differences (plus zero point vibrational energies) between the singlet and triplet states. In nearly all cases the triplet state is stabilized sufficiently to make it the predicted ground state when the cationic intermediates are substituted with the strongest *meta*  $\pi$  donors.

#### 4.3. Computational methods

*State-energy calculations.* In order to model the cations, we chose two different levels of electronic structure theory. The first, multireference second-order perturbation theory (CASPT2),<sup>72</sup> provides a rigorous method for constructing singlet and triplet states and comparing their relative energies. It is a particularly appropriate method for describing singlet states with small frontier orbital separations (which is typical for molecules having nearly degenerate singlet and triplet states) because it incorporates non-dynamical electron correlation directly into its multireference complete active space self-consistent field formulation.<sup>73</sup> Moreover, a recent level-shift modification to the CASPT2 model has corrected for a small bias in earlier formulations that favored high-spin states over low-spin analogs by 1–5 kcal/mol.<sup>74</sup>

While the CASPT2 model is rigorous, as a highly correlated wave-function theory (WFT) model it imposes high demands on computational resources, in part because good convergence in relative energies typically requires reasonably complete one-electron basis sets, e.g., polarized valence-triple- $\zeta$  or better. Given the size of some of the molecules in which we are interested, we also explored the utility of density functional theory (DFT) calculations, noting that we can benchmark DFT against



CASPT2 in smaller instances in order to gauge its effectiveness for the problem at hand. In prior studies, DFT models have been shown to predict singlet-triplet state energy gaps to within 2–4 kcal/mol of experiment (or converged quantum chemical calculations) at a fraction of the cost of high-level WFT methodologies for hypovalent species like nitrenium ions and carbenes,<sup>40,75-78</sup> and somewhat more delocalized diradical species like vinylidenes.<sup>79</sup> For example, DFT accurately predicts the singlet-triplet energy gap of the two nitrenium ions for which experimental values are available for comparison: the parent nitrenium ion,  $\text{NH}_2^+$ , for which the DFT (BLYP/cc-pVTZ) value of 30.6 kcal/mol agrees closely with the 30.1 kcal/mol gap found by photoelectron spectroscopy;<sup>80</sup> and the triazolium cation, a stable nitrenium ion for which the DFT value of -64.7 kcal/mol (BPW91/cc-pVDZ) is within the experimental error of the value determined by traditional photophysical methods (-66±3 kcal/mol).<sup>40</sup> However, in cases where two configurations for a singlet state have nearly equal weight in a multireference expansion, Kohn-Sham DFT has been shown to be less robust, e.g., for cases like arylnitrenes<sup>81</sup> and trimethylenemethane (TMM).<sup>82,83</sup> Given the similarity of the  $\pi,\pi$  triplets considered here to, say, TMM, a careful calibration of DFT against CASPT2 seems particularly important.

Using unrestricted broken-symmetry formulations for the singlet state can improve the accuracy of Kohn-Sham DFT predictions in the event of narrow frontier orbital separations.<sup>73</sup> Thus, the restricted Kohn-Sham determinants for all singlets were tested for instability to breaking spin-state symmetry (i.e., a restricted --> unrestricted instability). For those singlets that were found to have such an instability, single-

point broken symmetry calculations were performed at the restricted geometries. As expected, most singlet wavefunctions were stable, but instabilities were found in cases where the triplet state was either very close to or lower in energy than the singlet. In such cases, the energy of the singlet state was computed using the equation.<sup>84-87</sup>

$$E_{\text{singlet}} = \frac{2E_{\langle S_z \rangle=0} - \langle S^2 \rangle E_{\langle S_z \rangle=1}}{2 - \langle S^2 \rangle}$$

where  $E_{\text{singlet}}$  is the desired singlet energy,  $E_{\langle S_z \rangle=0}$  is the broken-symmetry energy,  $\langle S^2 \rangle$  is the expectation value of the total-spin operator for the broken-symmetry calculation (anywhere from about 0.2 to 1.0), and  $E_{\langle S_z \rangle=1}$  is the energy of the triplet at the singlet geometry. The largest effect of R/U instability was observed for aryloxonium ion **4.17** where the projected broken-symmetry singlet energy relative to the triplet was 3 kcal/mol lower than that for the restricted singlet.

#### 4.4. Molecular geometries.

Although we expect the CASPT2 model to provide the most accurate description of the molecular energetics examined here, this level of theory is not particularly convenient for the determination of molecular structures because analytic gradients of the energy are not available for use in geometry optimization. DFT, on the other hand, is well established to provide excellent molecular geometries, particularly when hybrid functionals (incorporating exact Hartree-Fock (HF) exchange) are used;

B3LYP is particularly accurate based on many benchmark studies.<sup>73</sup> Thus, we began by optimizing the molecular geometries for all of the molecules listed in Table 1 at the B3LYP/6-31G(d,p) level of theory, using the restricted and unrestricted Kohn-Sham formalism for the singlets and triplets, respectively. However, for the particular case of **4.9**, which was chosen because it falls roughly in the middle of the predicted spectrum of S-T splittings for the arylnitrenium ions, we examined the sensitivity of the geometries to choice of functional. Thus, we optimized the more difficult singlet state not only with the B3LYP functional, but also the BLYP, *mPWPW*,<sup>88-90</sup> *mPW1PW*,<sup>88-90</sup> and TPSSh<sup>91,92</sup> functionals employing the 6-31G(d,p) basis set. We then assessed the variation in energy at the B3LYP/6-31G(d,p) level: over all 5 structures the total variation in energy was less than 0.8 kcal/mol. On that basis, we elected to continue to use B3LYP geometries for all purposes, noting that any error introduced by this choice is likely to be no more than 1 kcal/mol.

A separate question, in cases where the singlet state is subject to breaking spin-symmetry, is whether one should ideally use the restricted singlet or unrestricted mixed-spin-state geometry. Restricted singlet geometries are sometimes found to be superior to broken-symmetry geometries after spin purification,<sup>93</sup> since the broken-symmetry formalism introduces spin contamination. In the case of **4.17**, which exhibits the largest value of  $\langle S^2 \rangle$  for the broken-symmetry Kohn-Sham determinant, allowing the broken-symmetry geometry to reoptimize at the unrestricted B3LYP level led to a change in the spin-projected singlet energy of 3.6 kcal/mol. As this value is reasonably small, and is moreover likely to be considerably reduced in the

other molecules because of their smaller values of  $\langle S^2 \rangle$ , we adopted restricted singlet geometries throughout.

#### 4.5. Singlet-triplet splittings.

Meta *disubstituted* cations were chosen to enhance the meta effect described above and also to take computational advantage of the molecular symmetry of the disubstituted systems. Table 1 provides the computed singlet-triplet energy gaps ( $\Delta E_{ST}$ ) for these species and the Ar-X bond length predicted for the triplet state. Because of their smaller size, it proved possible to compute S-T splittings at the CASPT2/pVTZ level for **4.4**, **4.7**, **4.9**, **4.16**, and **4.19**. Repeating the calculation with a smaller pVDZ basis set led to a systematic stabilization of the triplet state relative to the singlet in all of these cases except for **4.19**, by 1.3 to 2.4 kcal/mol. This trend is in the expected direction, since electron correlation is more important for the singlet than the triplet (owing to its additional set of paired electrons) and reducing the size of the basis set degrades the CASPT2 model's ability to capture this correlation energy. However, the effect is small and systematic, suggesting that it should be transferrable to the remaining systems, where molecular size restricts the CASPT2 calculations to use of the pVDZ basis set. Such calculations were completed for **4.8**, **4.10**, **4.11**, and **4.13**.

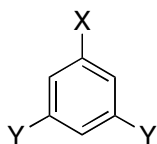


**Table 1.**  $\Delta E_{ST}$  (kcal/mol) and triplet Ar-X bond distances (ang).<sup>a</sup>

Structure Number	X	Y	$\Delta E_{ST}$			Triplet Ar-X bond distance
			CASPT2/ pVTZ	CASPT2/ pVDZ	B3LYP/ 6-31G(d,p)	
4.4	CH <sub>2</sub> <sup>+</sup>	H	-44.6	-43.2	-39.7	1.403
4.5		F			-26.8	1.401
4.7		CH=CH <sub>2</sub>	-27.7	-26.5	-17.4	1.403
4.9		NH <sub>2</sub>	-10.1	-7.7	-4.4 <sup>b</sup>	1.402
4.10		NMe <sub>2</sub>		-0.1	+1.9 <sup>b</sup> (+1.4)	1.403
4.11	CHCF <sub>3</sub> <sup>+</sup>	NMe <sub>2</sub>		+2.0	+5.1 <sup>b</sup>	1.410
4.12	C(CF <sub>3</sub> ) <sub>2</sub> <sup>+</sup>	H			-29.8	1.433
4.13		NMe <sub>2</sub>		+8.7	+12.2 <sup>b</sup>	1.430
4.14	CF <sub>2</sub> <sup>+</sup>	NMe <sub>2</sub>			-7.8 <sup>b</sup>	1.391
4.15	O <sup>+</sup>	H			-13.5	1.263
4.16		NH <sub>2</sub>	+4.5	+5.9	+11.4 <sup>b</sup> (+8.8)	1.250
4.17		NMe <sub>2</sub>			+15.4 <sup>b</sup> (+11.8)	1.252
4.18	SiH <sub>2</sub> <sup>+</sup>	H			-47.7	1.880
4.19		NH <sub>2</sub>	-19.1	-20.4	-9.7	1.875
4.20		NMe <sub>2</sub>			-4.6	1.874
4.21	Si(CF <sub>3</sub> ) <sub>2</sub> <sup>+</sup>	NMe <sub>2</sub>			+5.1 <sup>b</sup>	1.878

<sup>a</sup> All S-T splittings include differential zero-point vibrational energy computed at the B3LYP level. A negative value for  $\Delta E_{ST}$  indicates a singlet ground state. <sup>b</sup> Indicates a spin-projected broken symmetry calculation on the singlet state (energies in parentheses refer to a singlet geometry reoptimized using UB3LYP)

Comparing the CASPT2 calculations to the B3LYP calculations, we see that the DFT model predicts the triplet state to be too stable relative to the singlet. Comparing to the CASPT2/pVTZ values, or to the value derived from adding -2 kcal/mol to the CASPT2/pVDZ value (this being a conservative estimate of the transferrable basis set effect), we see that the B3LYP model's error is a fairly consistent 5-10 kcal/mol.

Turning to specific substitutions, as shown in Table 1, the unsubstituted benzyl cation **4.4** is predicted at this level of theory to be a ground-state singlet by 39.7 kcal/mol (a negative value for  $\Delta E_{ST}$  indicates a singlet ground state). Substituting the meta position with weak  $\pi$  donors (like fluoro **4.5**) has a modest effect on the singlet-triplet energy gap. However, substituting with moderate to strong  $\pi$  donors significantly stabilizes the triplet state and dramatically increases the  $\Delta E_{ST}$ . In all cases, increasing the strength of the pi donor (e.g. going from  $\text{NH}_2$  to  $\text{NMe}_2$ ) or making the cationic acceptor more electron deficient (such as by adding  $\text{CF}_3$  groups) favors the triplet state as a result of decreasing the gap between the frontier molecular orbitals. With the 3,5-bis(dimethylamino) benzyl cation **4.10** the meta substituents are sufficiently strong  $\pi$  donors to make the triplet state the predicted ground state by 1.9 kcal/mol at the B3LYP level. However, the systematic error in the DFT model and the CASPT2/pVDZ prediction suggest that the correct ground state will still be the singlet for **4.10**, albeit by only a small margin. Adding one or two trifluoromethyl ( $\text{CF}_3$ ) substituents to make the cationic center even more electron-deficient (and thus a better electron receptor) enhances the importance of the meta effect, and cations **4.11** and **4.13** are predicted to have still more stable triplet states relative to their

singlet states. In the case of **4.11**, uncertainty in the theory does not allow a firm prediction of the ground state: the singlet and triplet are likely to be nearly degenerate. In the case of **4.13**, on the other hand, the preference for a triplet ground state is sufficiently large that remaining quantitative uncertainty in the theory is unlikely to affect this prediction.

It is a significant finding from this study that the benzylic carbocation **4.13** has a triplet ground state, and triplet reactivity from carbocations **4.10** and **4.11** may be thermally accessible if intersystem crossing is facile. Virtually all previous studies on simple substituted carbenium ions have assumed that these species have singlet ground states. Moreover, the extant chemical and spectroscopic behavior of typical carbenium ions is consistent with strongly electrophilic singlet states. Exceptions to this are limited to the antiaromatic cyclopentadienyl cation<sup>94</sup> and some substituted phenyl cations ( $X\text{-Ph}^+$ ).<sup>95,96</sup> The current study is to our knowledge the first to identify a new class of carbocations with triplet ground states.

Similarly, phenylsilylenium cations and phenyloxenium cations show an increase in the  $\Delta E_{\text{ST}}$  by substituting the meta position with  $\pi$  donors.<sup>97</sup> Substituting the phenylsilylenium cation **4.18** with two bis(*N,N*-dimethylamino) groups, **4.20**, stabilizes the triplet state by approximately 41 kcal/mol relative to the singlet, but not sufficiently enough to overcome the 47 kcal/mol required to make the triplet the ground state; **4.20** is predicted to be a singlet by about 5 kcal/mol at the B3LYP level.<sup>98</sup> By making the silylenium center more electron-deficient (and thus a better

acceptor) by substituting the silicon with two electron-withdrawing trifluoromethyl ( $\text{CF}_3$ ) substituents, **4.21**, the triplet is predicted to be the ground state by 5.1 kcal/mol at the B3LYP level. Given the magnitude of the systematic error in B3LYP, this suggests that the two spin states will be nearly degenerate, but with the singlet being more likely to be lower. With phenyloxenium ion **4.15**, which is predicted to be a singlet by approximately 14 kcal/mol at the B3LYP level, adding either two amino groups (**4.16**) or two bis(dimethylamino) groups (**4.17**) is enough to make the triplet the ground state by margins sufficiently large that they exceed likely uncertainty in the theory; we expect these species to be ground state triplets.

We close our discussion of the substituted phenyl systems with a brief assessment of the more general utility of DFT in this context. As B3LYP incorporates exact HF exchange, which stabilizes systems having a larger number of unpaired electrons, it is consistent that the model appears biased in favor of the triplet state in **4.4-4.21**. In Table **4.1a**, we compare a variety of functionals and broken-symmetry protocols with respect to their ability to predict  $\Delta E_{\text{ST}}$  for **4.9**. The CASPT2/pVTZ value of -10.1 kcal/mol is likely to be reasonably converged and serves as a benchmark against which to judge the DFT models. The conclusions to be drawn from Table 4.1a are that spin-purified broken-symmetry singlet energies (i.e., computed using eq. 1 above) are to be preferred over either raw broken-symmetry energies or restricted singlet energies, and that pure functionals (i.e., those not incorporating any HF exchange) are superior to hybrid functionals, but in the latter instance by a margin that is moderate in magnitude. Thus, comparing BLYP to B3LYP, the spin-projected



broken-symmetry S-T splitting predicted by the former is -7.2 kcal/mol, which represents a 2.9 kcal/mol improvement over the B3LYP result; the B3LYP functional incorporates 20% exact HF exchange. Similarly, the *m*PWPW prediction of -6.1 kcal/mol improves on the hybrid *m*PW1PW prediction by 4.4 kcal/mol; the latter functional incorporates 25% HF exchange. We note that for **4.9** *all* functionals predict a singlet Kohn-Sham determinant that is unstable to symmetry breaking, although the pure functionals deliver smaller values of  $\langle S^2 \rangle$  for the converged unrestricted solution.

**Table 4.1a.** Singlet-triplet state energy gaps (kcal/mol) from various DFT protocols for **4.9**.

Functional	Restricted singlet	BS singlet	Spin-purified BS singlet
BLYP	-6.0	-6.2	-7.2
B3LYP	-2.5	-3.0	-4.3
<i>m</i> PWPW	-4.7	-5.0	-6.1
<i>m</i> PW1PW	0.7	-0.2	-1.7
TPSSh	-0.7	-1.4	-2.8

#### 4.6. Substituted naphthalenes.

We also chose to explore if this same triplet-stabilizing effect would be found in systems that were analogous to non-Kekule diradicals other than *m*-xylylene. 1,8-naphthaquinodimethane (1,8-NQM), **4.22**, is a well-known non-Kekule triplet

diradical with a recorded ESR spectrum. The 1,3- and 1,6-naphthaquinodimethane diradicals (**4.23** and **4.24**) are also thought to have low energy triplet states as predicted by the Borden-Davidson method<sup>17</sup> (Figure 2). Therefore, we examined the effect of applying this electron-donor electron-acceptor motif to select naphthyl systems containing a positively charged center (nitrenium ion or oxenium ion) at the 1 position, and  $\pi$ -donating amino substituents at the 3, 6, and 8 position. The B3LYP/6-31G(d,p) results are given in Table 2; the size of the naphthyl systems, with typically 16 electrons in 14 active  $\pi$  orbitals, just exceeds the current practical limit for CASPT2, so we do not present any results from this level of theory, but bear in mind that the B3LYP model is likely to retain a systematic bias in favor of the triplet state.

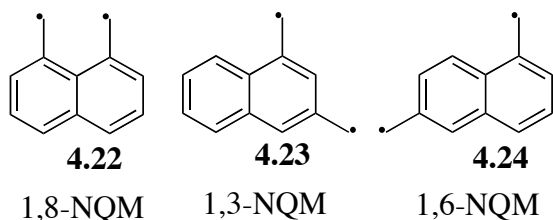


**Figure 2.** Naphthaquinodimethanes.

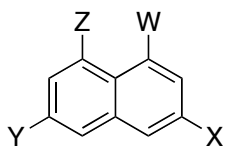


**Table 2.** Singlet-triplet energy gaps ( $\Delta E_{ST}$ ) for select naphthyl systems.

Structure Number	W	X	Y	Z	$\Delta E_{ST}$ (kcal/mol)	Ar-W bond length
<b>4.25</b>	NH <sup>+</sup>	H	H	H	-23.0	1.352
<b>4.26</b>		NH <sub>2</sub>	H	H	-8.5	1.333
<b>4.27</b>		H	NH <sub>2</sub>	H	-4.3	1.328
<b>4.28</b>		H	H	NH <sub>2</sub>	-4.8	1.337
<b>4.29</b>		NH <sub>2</sub>	NH <sub>2</sub>	NH <sub>2</sub>	+0.6 <sup>a</sup>	1.334
<b>4.30</b>	O <sup>+</sup>	H	H	H	-23.1	1.263
<b>4.31</b>		NH <sub>2</sub>	H	H	-6.8	1.242
<b>4.32</b>		H	NH <sub>2</sub>	H	-3.2	1.247
<b>4.33</b>		H	H	NH <sub>2</sub>	-7.5	1.257
<b>4.34</b>		NH <sub>2</sub>	NH <sub>2</sub>	NH <sub>2</sub>	-2.9 <sup>a</sup>	1.254

a. Indicates a spin-projected broken-symmetry (UB3LYP) calculation on the singlet state

As the results in Table 2 show, both parent naphthylnitrenium ion **4.25** and naphthylloxenium ion **4.30** are ground state singlets with singlet-triplet energy gaps of ca. -23 kcal/mol. In all cases, substituting the 3, 6, or 8 position with amino groups stabilizes the triplet state relative to the singlet, although only in the case of the tri-substituted naphthylnitrenium ion **4.29** is the triplet stabilized sufficiently to make it the predicted ground state at the B3LYP level. Given the likely bias in this calculation, even **4.29** is probably a ground state singlet, although not by a very large

margin. The lack of state switching in these cases may be due to the extended  $\pi$  system of the naphthyl system as compared to the phenyl system. Extended conjugated systems tend to favor the singlet state because of their  $\pi$ -donating ability, which acts to raise the energy of the  $p$  orbital on nitrogen. Indeed, the singlet-triplet energy splitting in phenylnitrenium ion is predicted to be -19 kcal/mol at this level of theory, 4 kcal/mol smaller than the naphthyl nitrenium ion (-23 kcal/mol).

#### 4.7. Geometric effects.

In the previous report on phenylnitrenium ions,<sup>71</sup> geometrical changes were observed for the triplet states upon changing the character of the substituent attached to the meta position. These geometrical changes are consistent with the change in the nature of the triplet electronic state from  $n,\pi^*$  to  $\pi,\pi^*$ . For example, upon changing the character of the meta substituent from electron-withdrawing (or weakly donating) to strongly donating, a systematic increase in the Ar-N bond distances and a decrease in the Ar-N-H bond angles was observed. Moreover, while the N-H bond for the non-meta donor systems was found to be orthogonal to the aromatic ring, it was typically found to be coplanar to the aromatic ring for those systems substituted with  $\pi$  donors.

In agreement with the previous report,<sup>71</sup> the naphthyl nitrenium ions included in this study show a decrease in the bond angle for the triplets upon substitution with  $\pi$  donors. For example, the unsubstituted naphthyl nitrenium ion **4.25** has an Ar-N-H bond angle of  $120^\circ$ , whereas all the amino-substituted analogs have bond angles between  $110$ - $111^\circ$ . Also consistent with the previous report, the NH bond is

orthogonal to the ring in the unsubstituted naphthyl nitrenium ion **4.25**, but coplanar in all others substituted with  $\pi$  donors **4.26-4.29**. On the other hand, all meta donor-substituted naphthyl nitrenium ions show an increase in the Ar-N bond of between 0.018 Å and 0.024 Å for the triplets. For the aryl oxenium ions included in this study, a decrease in the triplet Ar-O bond length was observed upon appropriate substitution with  $\pi$  donors. Conversely, for the phenyl silylenium ions and benzyl carbenium ions, no major geometrical changes were observed between the non-meta- $\pi$ -donor systems and those substituted with  $\pi$  donors (the aryl silylenium ions show a slight shortening of the Ar-Si bond).

This lack of systematic geometrical change in the triplet states upon meta-donor substitution of the benzyl carbenium ions and benzyl silylenium cations may be explained by observing the nature of the starting electronic states between the oxenium ions and nitrenium ions as compared to the silylenium ions and carbenium ions. That is, for the nitrenium ions and oxenium ions, the triplet electronic states for most of the non-meta donor systems adopt electron configurations that are  $n,\pi^*$  in nature, and change to  $\pi,\pi^*$  upon meta substitution with  $\pi$  donors. Observing the Kohn-Sham SOMOs for these molecules shown in Figure 4.2 demonstrates this change. The unsubstituted phenyloxenium ion **4.14** is taken as representative of the former case, and the diamino oxenium ion **4.16** is taken as representative of the latter. Conversely, because aryl silylenium ions and benzyl cations lack a lone pair on the positively-charged atom, the triplet states begin as  $\pi,\pi^*$  in the unsubstituted system and do not change upon adding the *meta*-donating substituent. Figure 4.2 shows the

Kohn-Sham orbitals of the unsubstituted benzyl cation **4.4** which is taken as representative of the former case as well as the diamino substituted benzyl cation **4.9** which is taken as representative of the latter. Thus, it appears that large systematic geometrical changes between the non-*meta*  $\pi$  donors and those substituted with *meta*  $\pi$  donors are observed primarily for those systems undergoing a change in the electron configuration of the triplet state.

One interesting exception to this trend is found with the unsubstituted naphthyloxenium ion **4.30**. In this case, the lowest energy triplet state is found to be  $\pi,\pi^*$  in nature rather than  $n,\pi^*$  like the phenyloxenium ion **4.15**. Apparently, the additional conjugation of the naphthyl system relative to the phenyl system stabilizes the  $\pi,\pi^*$  triplet state sufficiently to make it lower in energy than the  $n,\pi^*$  triplet state. For all species, however, significant Mulliken spin density was found to be located on all  $\pi$ -donating substituents, but little or none was observed on weak donors (like F) or electron-withdrawing groups (like CN).

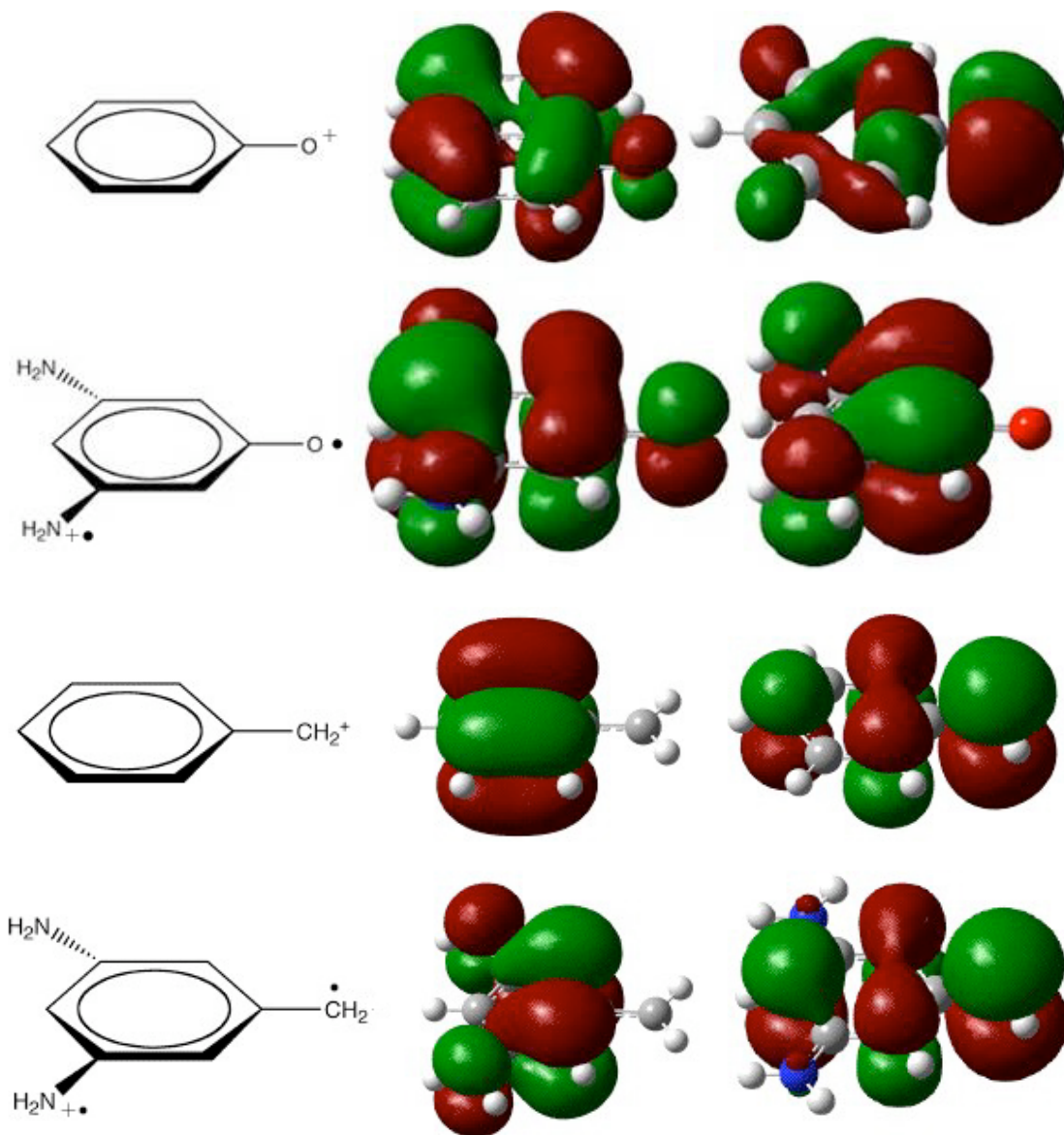


**Figure 4. 2** Kohn-Sham SOMOs for representative triplet phenyl oxenium ions and benzyl cations.

#### 4.8. *Conclusions.*

In conclusion, these calculations predict that substituting the meta position (or the 3, 6, and 8 positions for the naphthyl series) of aryl cationic species with  $\pi$  donors stabilizes a  $\pi, \pi^*$  triplet state analogous to non-Kekule diradicals. While we have only

demonstrated this effect for phenyl and select naphthyl systems, in principle this  $\pi$ -donor –  $\pi$ -acceptor connectivity should hold for alternative ionic species analogous to other non-Kekule diradicals conjugated with non-disjoint SOMOs, such as other variants of the naphthoquinodimethane system (e.g. those with the cationic center at the 3, 6 and 8 position), the biphenylquinodimethanes, and the trimethylenemethane diradical. Theoretically, any system with a strong  $\pi$  donor coupled to a strong electron acceptor with non-disjoint SOMOs could see a stabilization of a  $\pi, \pi^*$  triplet (or at least diradical) state similar to the ones described in this paper. Such benzylic cations can be generated and characterized using a variety of well-known methods, such as photolysis of meta-substituted esters or alcohols. In fact, preliminary experiments show that benzylic cations **4.10** and **4.12** can be generated photochemically in protic solvents from appropriate precursors. An initial product study shows that the corresponding toluene derivative is the minor product of **4.10** but is the major product for **4.12**, suggestive of the intermediacy of a triplet cationic species, but by no means definitive evidence (the major product of **4.10** and the minor product of **4.12** are typical solvent alcohol addition products). Additionally, preliminary DFT investigations suggest that the reverse connectivity also stabilizes a  $\pi, \pi^*$  triplet state in analogous fashion (e.g. a  $\pi$  electron-donating group conjugated through non-disjoint  $\pi$  orbitals to  $\pi$ -withdrawing groups). Thus, the 3,5-dinitrobenzyl anion is predicted to have a  $\Delta E_{ST}$  of ca. -1 kcal/mol at the B3LYP/6-31+G(d,p) level, in contrast to the unsubstituted benzyl anion which has a predicted  $\Delta E_{ST}$  of roughly -40 kcal/mol. These further computational studies and experimental investigations aimed at characterizing these ion diradicals will be reported in due course.



## 5. Chapter 5: Experimental Studies of Triplet Aryl Cationic Species and Preliminary Studies of Triplet Benzylic Anions

### 5.1. *Introduction.*

In Chapters 3 and 4, we examined the effects of meta substitution on the singlet-triplet energy gaps ( $\Delta E_{ST}$ ) of substituted aryl cationic species using density functional theory (DFT) and multireference second order perturbation theory (CASPT2). The overall conclusion from this computational study was that while unsubstituted aryl cationic species ( $Ar-X^+$ ) are ground state singlet species with a very large gap to the lowest-energy triplet state, substituting the meta positions of these cations with pi donors stabilizes a  $\pi, \pi^*$  triplet state similar to the electronic state of the m-xylylene diradical. In cases where the meta positions are substituted with very strong pi donors, this  $\pi, \pi^*$  triplet state is stabilized sufficiently to make this high-spin electronic state the computed ground state. To confirm these computational predictions, this chapter describes our efforts to generate two of these computed triplet cations experimentally. Additionally, computational studies of the singlet-triplet gaps of ionic species with an inverted connectivity (ie. anionic electron donors with two meta electron acceptors) are discussed, as well as preliminary attempts to generate and characterize these triplet anionic species experimentally.

## 5.2. The 3,5-bis(dimethylamino) benzyl cation.

On the basis of our previously described computations (Chapter 4), the 3,5-bis(dimethylamino) substituted benzyl cation **5.1** is computed to have essentially degenerate singlet and triplet state energies (Figure 5.1). In order to test this computational prediction, the substituted benzylic cation **5.1** was generated photochemically and the stable product distributions from its decay reactions were analyzed.

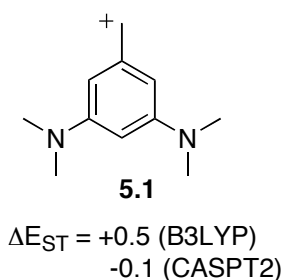


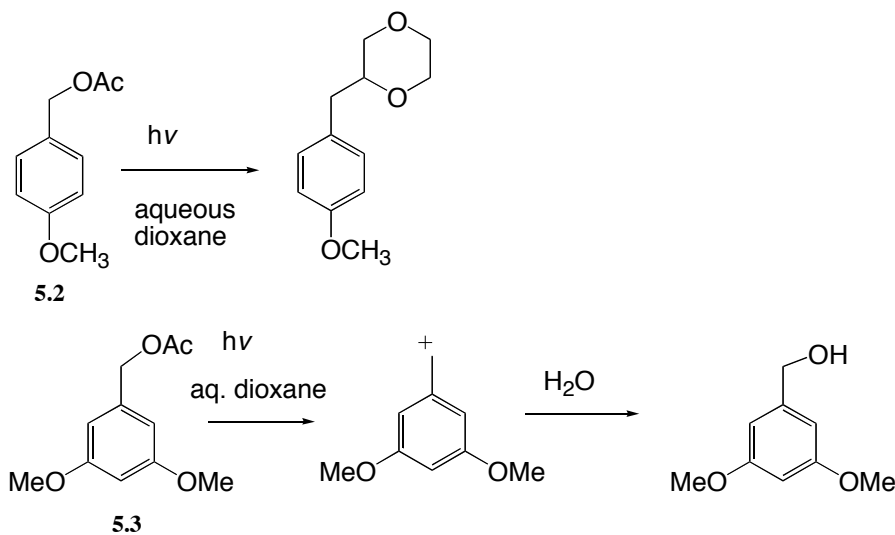
**Figure 5.1.** The 3,5-bis(dimethylamino)benzyl cation

### 5.2.1. Generation of the cation

While the most common method for generating benzylic cations is thermal heterolysis of leaving-group-substituted benzyl systems under acidic conditions (such as benzyl alcohols or benzyl halides), this method was deemed unsatisfactory for our purposes as even moderately strong acids would protonate the amine groups.

Therefore we chose a photochemical route that could be employed under less acidic conditions. Specifically we exploited the so-called meta-effect wherein meta-electron donors are known to promote photoheterolysis of benzylic C-O bonds. For example,

Zimmerman showed that while photolysis of para-methoxy benzyl acetate **5.2** gives predominantly radical-derived photoproducts (Scheme 5.1), benzyl acetates with meta methoxy substituents yield a water-addition solvolysis product resulting from benzylic cation intermediates. In fact, with the 3,5-dimethoxy benzyl acetate **5.3**, only a single product resulting from photoheterolysis was observed. To our knowledge, the effect of meta amino groups have not been examined to test the ability of these donating groups to facilitate photoheterolysis. However, the meta effect is well established for methoxy and hydroxy groups, and amino groups are anticipated to be better pi donors than methoxy or hydroxy groups. Consequently, we expected these groups to be even better facilitators of this C-O heterolytic scission upon photolysis than previously described donors such as OH or OMe.



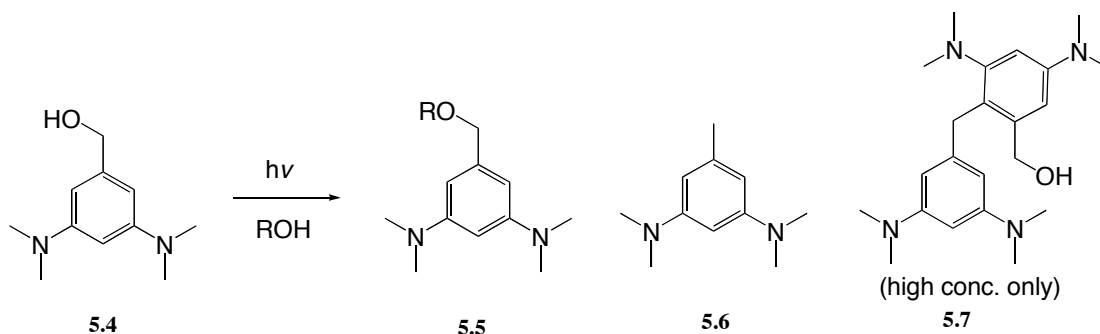
**Scheme 5. 1. Demonstration of the meta effect by Zimmerman, et al.**

Consistent with the general predictions of the meta-effect, we find that the precursor alcohol **5.4** photolyzes rapidly in polar protic solvents (Scheme 5.2). For example 254 nm irradiation of 4 mg of the benzyl alcohol **5.4** in 2,2,2-trifluoroethanol (3.0 mL) for

60 min results in 80% conversion of the reactants. Good conversion was also observed in 1,1,1,3,3,3-hexafluoro-2-propanol (HFIP) (44% in 60 min) and in ethanol (>99% in 60 min). In contrast, photolysis in nonpolar solvents is less efficient if it occurs at all. For example photolysis of **5.4** in diethyl ether and dichloromethane shows no observable photoproducts by GC after 18 hours of photolysis.

### 5.2.2. Product analysis.

Typically benzylic cations decay through addition of nucleophiles to the exocyclic carbon. On the other hand, triplet diradicals often react via sequential H atom abstraction reactions. The latter pathway would be expected to produce 3,5-bis(dimethylamino) toluene **5.6**. Under low concentration conditions (ca. 5 mM), photolysis of the benzylic alcohol **5.4** in TFE provides two main products: the ether adduct **5.5** and the reduction product **5.6** (Scheme 1), in a 12:1 ratio (after 1 hr of photolysis). Under high-concentration preparative conditions (ca. 0.1M) a Friedel-Crafts heterodimer **5.7** was also isolated and characterized by  $^1\text{H}$  and  $^{13}\text{C}$  NMR and mass spectrometry. Photolysis of the benzyl alcohol **5.4** (5 mM) in ethanol and HFIP also gave similar ratios of the solvent-derived ether **5.5** and the reduction product **5.6**.



**Scheme 5. 2.** Products from photolysis (254 nm) of solutions of benzyl alcohol in alcoholic solvents.

### 5.2.3. Effect of the leaving group

We note that switching the leaving group from OH to OAc or OCOCF<sub>3</sub> gives identical products in essentially the same ratio. However, the benzyl alcohol proved to be a more convenient photoprecursor since it was bench stable. On the other hand, the acetate and trifluoroacetate derivatives hydrolyzed slowly over several days even when stored at below 0°C to give the benzyl alcohol, although the trifluoroacetate derivative could be conveniently stored as its stable trifluoroacetic acid salt and free-based with saturated bicarbonate when needed. However, because of the bench stability of the benzyl alcohol precursor, except where noted all subsequent discussions refer to the benzyl alcohol **5.4** as the photoprecursor.

### 5.2.4. Kinetics of decomposition.

In trifluoroethanol (TFE), the product distributions from photolysis of **5.4** (5 mM) were determined. Yields were determined using gas chromatography using the peak area percent corrected for the GC response factors. The results are shown in Figure 5.2. As the plot in Figure 5.2 demonstrates, the TFE adduct **5.5** and the reduction product **5.6** grow in at roughly a 12:1 ratio as the benzyl alcohol was photolyzed. Significant mass balance begins to be lost after 60 minutes of photolysis, presumably because of the formation of secondary photoproducts. After 24 hours of photolysis, the major product by GC is the reduction product **5.6**. Interestingly, photolysis of the benzyl alcohol in an ethanol glass at 77K occurs very slowly to give exclusively the reduced product **5.6**.

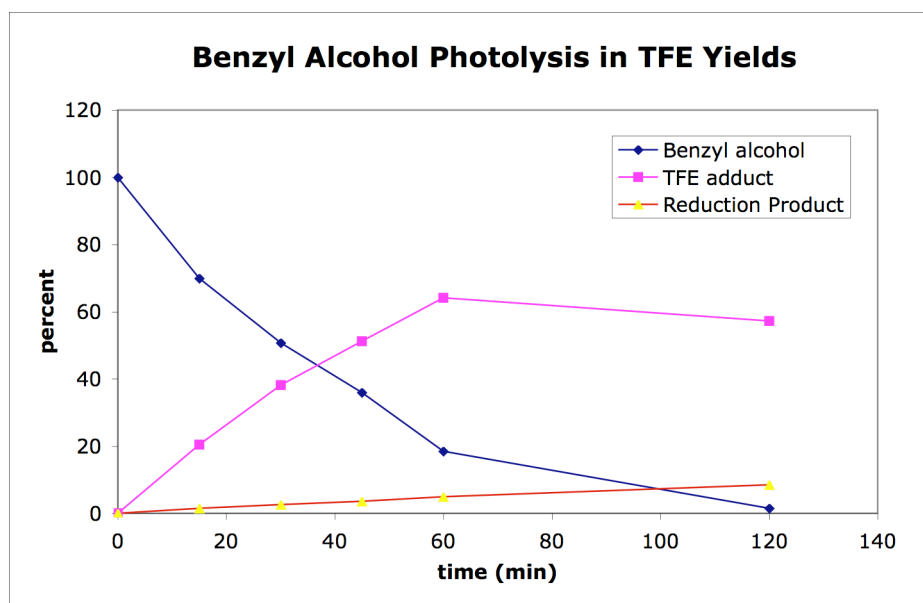
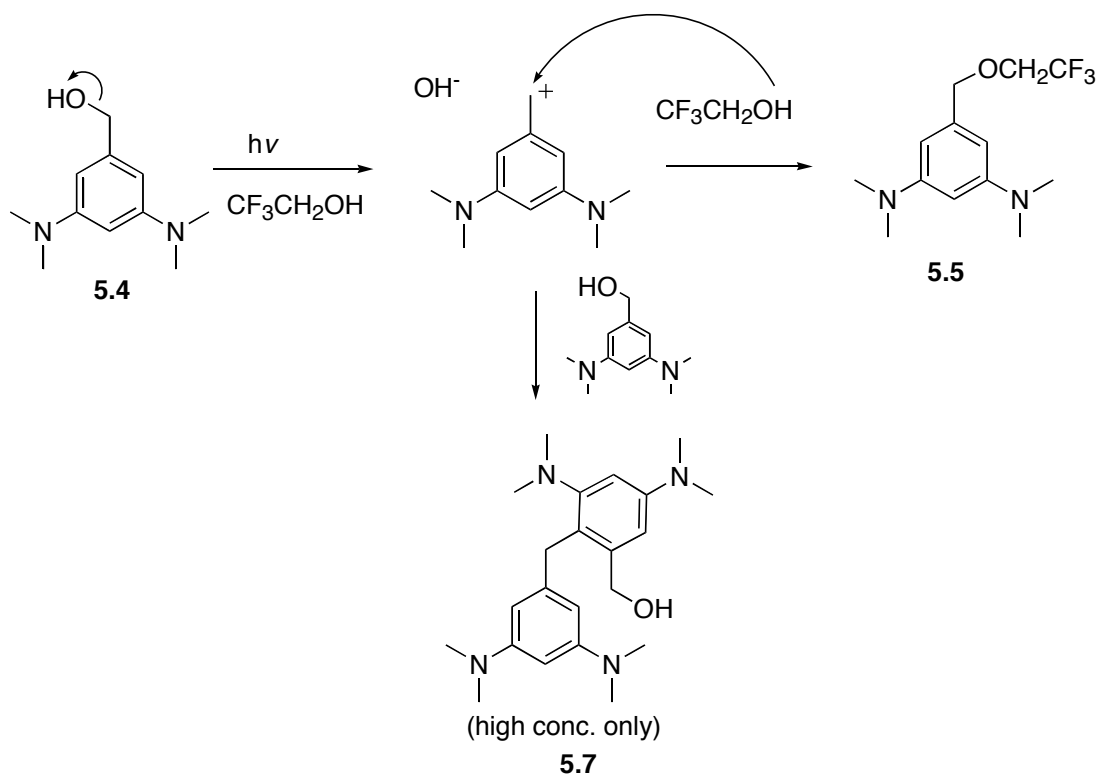


**Figure 5.2.** Products of 254 nm photolysis of **5.4** (5 mM) in TFE as a function of photolysis time.

#### 5.2.5. Mechanism of product formation.

Upon photolysis, the benzyl alcohol is presumed to undergo C-O heterolytic bond cleavage to generate the benzyl cation. The cation is expected to be generated initially in the singlet state, irrespective of whether this is the ground electronic state. Solvent addition to the intermediate singlet cation then generates the major ether adduct. This ether adduct **5.5** is assumed to arise from reactions of the predominantly closed-shell singlet benzylic cation, as it reflects typical decay reaction of simple benzylic cations. Moreover, the Friedel-Crafts heterodimer is presumed to arise from reaction of the intermediate singlet benzylic cation with an unreacted molecule of the benzyl alcohol **5.4**.

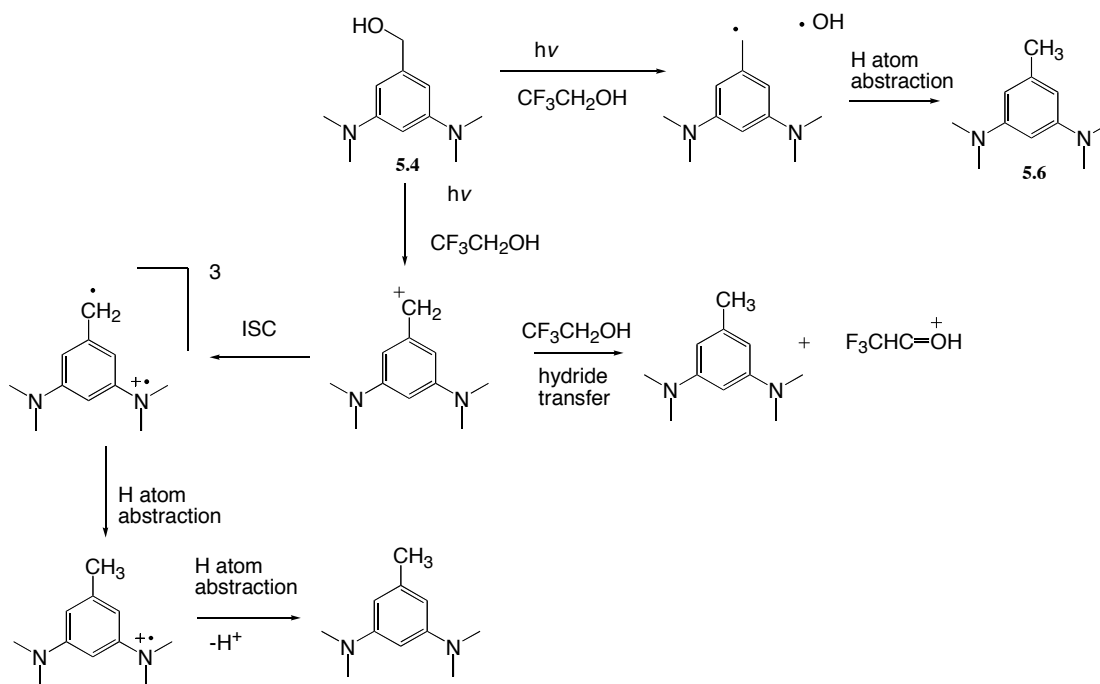


**Scheme 5. 3.** Proposed mechanism for formation of TFE adduct and Friedel-Crafts heterodimer.

While the solvent-addition product **5.5** and the Friedel-Crafts heterodimer **5.7** are the expected products of a typical singlet carbocation, the toluene derivative **5.6** does not derive from typical cation chemistry. This product is particularly unusual because Zimmerman et al. reported only solvolysis products from photolysis of the similar 3,5-dimethoxybenzyl acetate. Mechanistic possibilities that account for its formation are shown in Scheme 5.4.

We considered the possibility that **5.6** might originate from a parallel homolytic pathway. Two experiments suggest that this pathway is unlikely. First, such a homolytic pathway is expected to be reasonably insensitive to the polarity of the

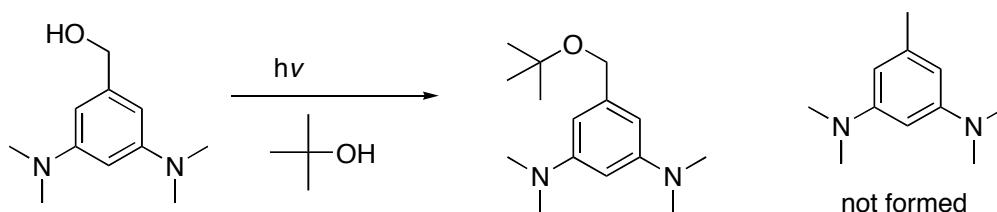
solvent since no ionic intermediates are formed. The lack of formation of any observable products by GC following exhaustive photolysis of **5.4** in diethyl ether and dichloromethane argues against this alternative. Additionally, switching the leaving group from hydroxide to acetate or trifluoroacetate does not increase the amount of reduction product **5.6** observed after initial photolysis, despite the change in the nature of the leaving group and the decreased C-O bond strength of acetate as compared to hydroxide. The fact that the product distributions do not change upon switching the leaving group is strongly suggestive of a common intermediate. It should be noted that upon photolysis of the acetate derivative the amount of reduction product increases exponentially over time in contrast to the rough linear dependence as seen for the benzyl alcohol, presumably as a result of secondary photolysis or reactions with accumulated byproducts.



**Scheme 5. 4** Possible mechanisms leading to the reduced product **5.6**.



Another possibility for formation of the reduced product is through a hydride transfer mechanism from the solvent to the benzyl cation. Some evidence for this mechanism is provided by photolysis of **5.4** in t-butyl alcohol solvent, since t-butyl alcohol is a poor hydride donor. The lack of any observable reduced product in this solvent appears to support this mechanism.

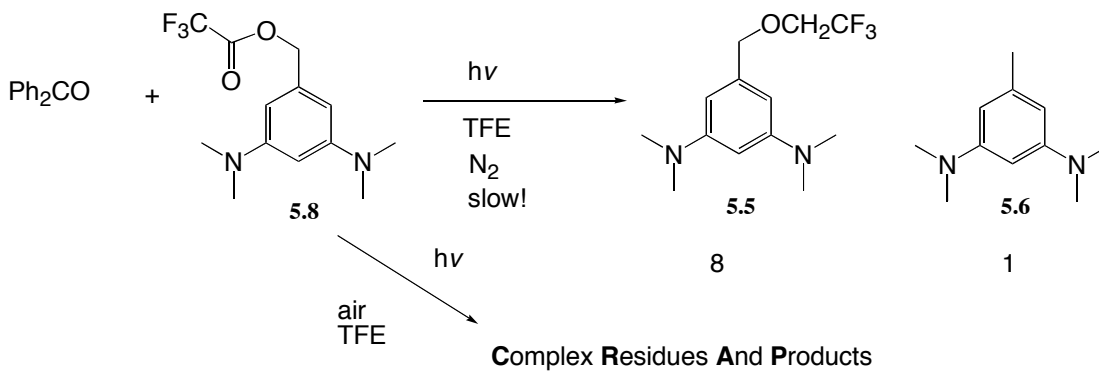


**Scheme 5.5.** Photolysis of **5.4** in t-BuOH.

The final possibility is that the initially formed singlet carbocation undergoes intersystem crossing to give the triplet, which then decays via hydrogen atom abstractions to the toluene derivative. However, at this time we have no further evidence to distinguish these possibilities, except to note that the dimethoxybenzyl cation as observed by Zimmerman, et al, gives exclusively solvent adducts. It is unexpected that switching from meta methoxy groups to meta dimethylamino groups would alter the hydride affinity of the intermediate cation significantly. Irrespective of whether the reduced product **5.6** derives from a hydride transfer mechanism or a triplet diradical mechanism, it seems clear that the major products from photolysis of the alcohol **5.4** are singlet-derived products. Therefore, we tentatively assign the ground state of this cation to predominantly closed shell singlet state.

### 5.2.6. Triplet-sensitized photolysis.

Attempts were made to generate the triplet benzyl cation via triplet sensitization experiments. Triplet sensitized photolysis with benzophenone as the triplet sensitizer was carried out in TFE using 355 nm excitation. No products were observed when the benzyl alcohol was used as the precursor, but switching the leaving group from OH **5.4** to  $\text{OCOCF}_3$  **5.8** gave the same stable products as seen from direct photolysis and in nearly the same ratio after extended photolysis under  $\text{N}_2$  (slightly more reduced product was observed). Presumably, the meta effect dominates only from the singlet excited state and not from the triplet excited state, which is why a better leaving group is required for triplet-sensitized photolysis. Under air atmosphere, a complex mixture of products was obtained, which were not characterized. The mechanism for the formation of these products is discussed below.



**Scheme 5.6.** Product studies from 355 nm irradiation of  $\text{Ph}_2\text{CO}$  in the presence of **5.8** under air and  $\text{N}_2$  atmosphere.

### 5.2.7. Direct laser flash photolysis studies

Since the product studies following photolysis of the benzyl alcohol **5.4** in protic solvents are suggestive of the intermediacy of a benzylic cation, laser flash photolysis

(LFP) studies were performed in an attempt to directly observe the intermediate cation. Direct laser flash photolysis of the benzyl alcohol **5.4** in TFE gave the transient spectrum shown in Figure 5.3. Similar spectra were seen in TFE/H<sub>2</sub>O and EtOH. A large long-lived peak at 470 nm was observed. This absorption was not trapped by 1,4-cyclohexadiene, oxygen, or chloride, suggesting this peak absorption does not correspond to an intermediate carbenium ion.

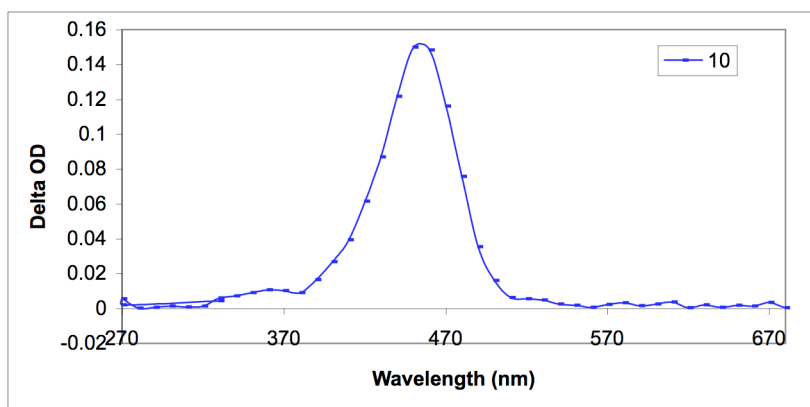


**Figure 5.3.** LFP (266 nm, 10  $\mu$ s after pulse) from direct irradiation of **5.4** in TFE.

Additionally, an identical transient was observed from LFP of 1,3-bis(dimethylamino)benzene, suggesting the transient derives from photochemistry of the aromatic ring and not from heterolytic cleavage of the exocyclic alcohol moiety. Moreover, the signal amplitude was found to depend exponentially on the laser power output (Figure 5.4), suggesting that the transient derived from two-photon absorption chemistry, a reasonably common event with very electron-rich aromatics. No transients were observed by LFP when the benzyl alcohol **5.4** was photolyzed in non-polar solvents such as CH<sub>3</sub>CN and CH<sub>2</sub>Cl<sub>2</sub>. The obvious candidate, the radical cation resulting from photoionization of **5.4**, is shown later in this chapter to have an

absorption at 560 nm in TFE. However, once the transient was found to be derived from photochemistry of the aromatic ring, its identity was not explored further.

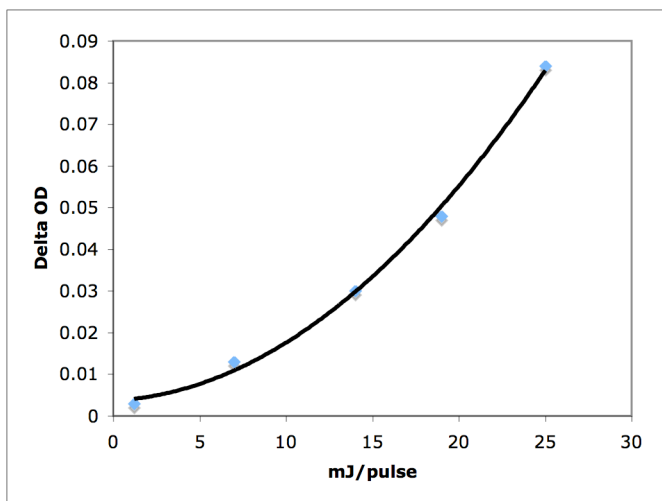


**Figure 5. 4.** Exponential dependance of the signal ( $\Delta OD$ ) of direct 266 nm photolysis of **5.4** (monitored at 470 nm) as a function of laser output power.

#### 5.2.8. Triplet-sensitized laser flash photolysis studies.

Since the carbenium ion was not observed by direct photolysis, laser flash photolysis experiments were also carried out using triplet sensitization. Benzophenone was used as the triplet sensitizer since this molecule has a reasonably large triplet energy, and this sensitizer was excited using 355 nm laser light. The expectation was that the triplet benzophenone would sensitize the substrate and lead to formation of the triplet benzyl cation. The observed LFP spectrum is shown in Figure 5.5. Based on a number of further LFP experiments described below, the peak(s) at 540 nm at the 0.1  $\mu s$  time interval is assigned to the initial triplet excited state of benzophenone. This decays to another peak, which is found to be two overlapping absorptions of the benzophenone anion radical and the cation radical of the benzyl trifluoroacetate **5.8**.

The peak at 400 nm has not been further characterized but is presumed to arise from decay of the cation radical.

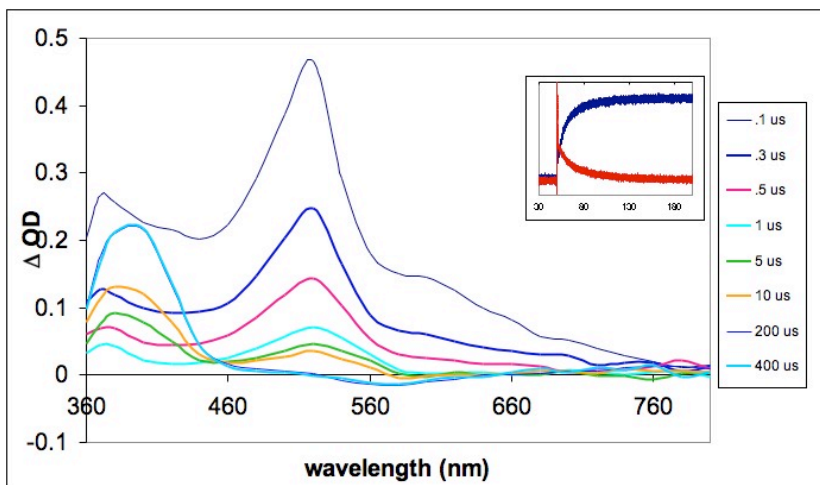


**Figure 5. 5.** Transient spectrum from LFP of benzophenone and benzyl trifluoroacetate **5.8** in TFE (355 nm) under air. Insert shows waveforms at 400 nm (blue) and 540 nm (red).

Rather than observing a triplet sensitization reaction, the observed transients are consistent instead with an electron transfer reaction from the substrate to the excited state of benzophenone. The next section describes how the absorption bands were assigned.

The location of the anion radical signal of benzophenone was found by LFP of N,N-dimethylaniline and benzophenone in TFE (Figure 5.6). Transients were observed for the known absorption of the dimethylaniline cation radical signal at 470 nm and the benzophenone radical anion signal at 540 nm. The anion radical signal was

confirmed by oxygen quenching experiments wherein purging the solution with oxygen was observed to quench the signal.

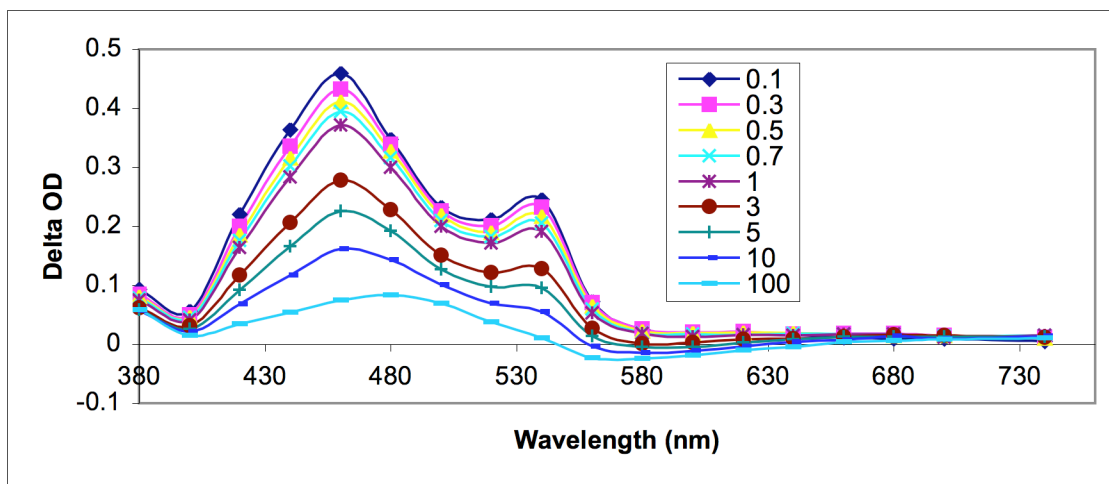
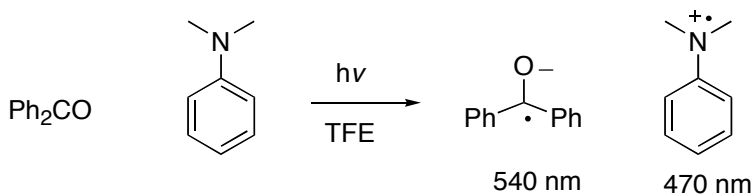


**Figure 5. 6.** Transient LFP spectrum from 355 nm laser photolysis of benzophenone plus dimethylaniline in trifluoroethanol.

Secondly, the location of the cation radical signal of the benzyl trifluoroacetate **5.8** was obtained by LFP of benzophenone plus the alcohol in  $\text{CH}_3\text{CN}$  (Figure 5.7). The aprotic nature of the  $\text{CH}_3\text{CN}$  red shifts the benzophenone anion radical signal to ca. 700 nm, and leaves the cation radical signal of the benzyl alcohol at 560 nm.

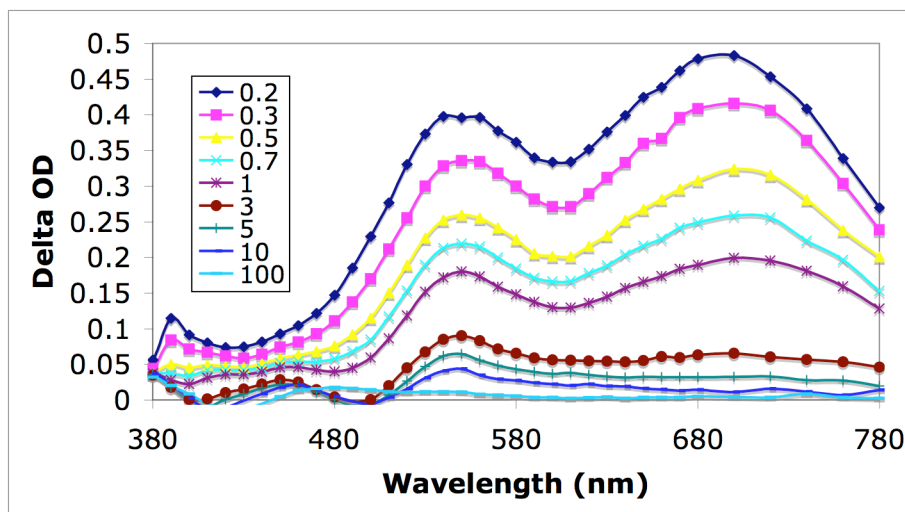
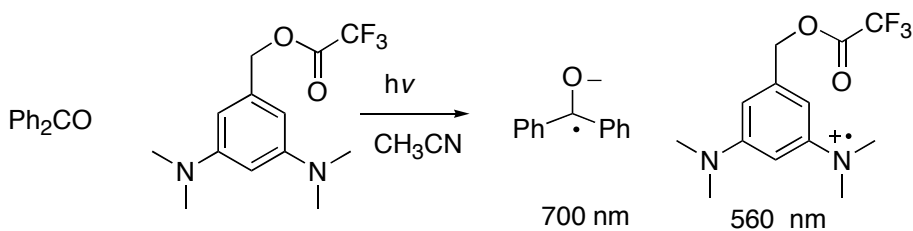
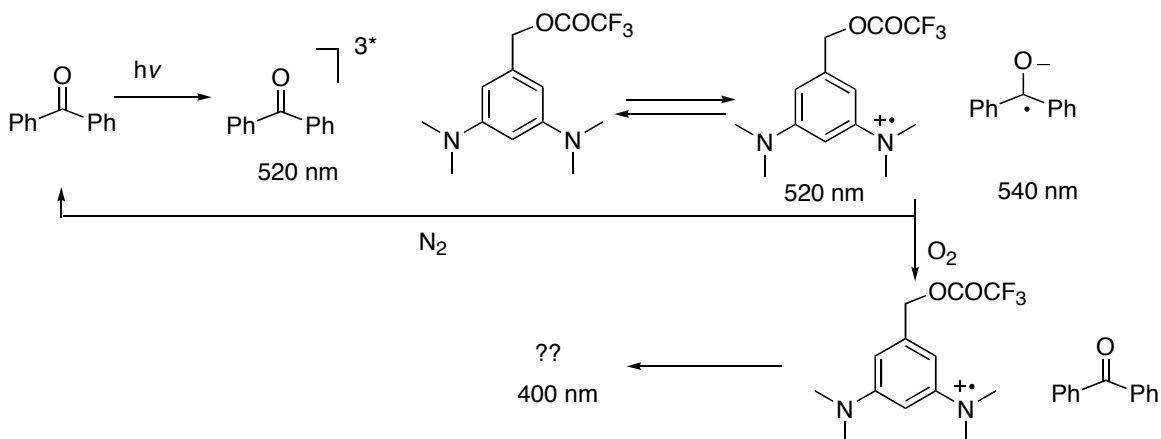


**Figure 5. 7.** Transient LFP spectrum from 355 nm photolysis of benzophenone and benzyl trifluoroacetate **5.8** in  $\text{CH}_3\text{CN}$ .

#### 5.2.9. Proposed mechanism for benzophenone photolysis.

It is interesting to note that the products of these studies using benzophenone show that triplet sensitization appears to be successful under nitrogen, whereas complex uncharacterized product mixtures result from ambient air (or  $\text{O}_2$  purged) photolysis. On the other hand, all LFP spectra show exclusively electron transfer intermediates. We believe that these seemingly discordant results can be explained by the mechanism shown in Scheme 5.7, wherein electron transfer is the predominant pathway. Under nitrogen, the major pathway following electron transfer is a non-destructive back electron transfer to return the unchanged starting materials. Under oxygen (or ambient air) conditions, some of the anion radical is quenched by oxygen,

preventing a back electron transfer pathway, leading to complex products resulting from decomposition of the cation radical of the benzyl trifluoroacetate **5.8**.

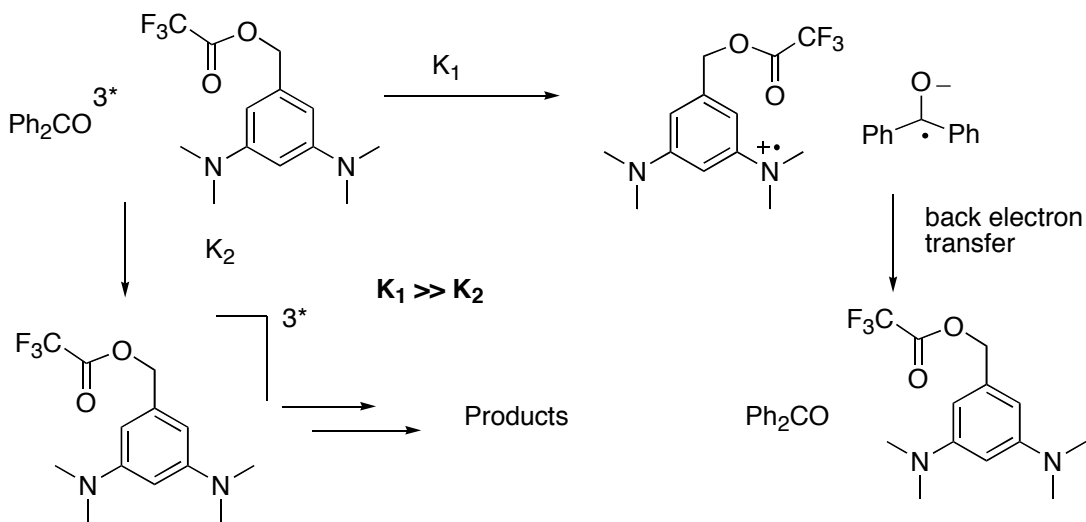


**Scheme 5. 7.** Proposed mechanism of reaction in presence of oxygen.

While the electron transfer is the major pathway, the triplet sensitization is proposed to be a minor concomitant pathway so that it is not observed by LFP. The basic proposed mechanism for the triplet sensitization experiments is given in Scheme 5.8. We hypothesize, that the major pathway under nitrogen is a non-destructive electron-transfer – back electron transfer pathway, but that the minor pathway is triplet sensitization to yield the TFE-adduct and the reduced product. Given that even this triplet sensitization experiment results in products that could be characterized as predominantly singlet-derived products, this mechanism suggests that the singlet state of the benzyl cation is the ground state. An alternative explanation is that the triplet state is in dynamic equilibrium with the singlet state but that reactions occur faster from the singlet state than the triplet. However, the fact that triplet sensitization occurs at all provides evidence that the triplet benzyl cation is a reasonably low-



energy species, since triplet-sensitized photolysis to give an unstable triplet cation (such as in the case of the triplet benzyl cation where the triplet state is ca. 45 kcal/mol higher in energy than the singlet) would be anticipated to be unsuccessful.



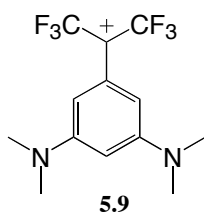
**Scheme 5. 8.** Proposed mechanism of reaction of benzophenone and substrate in the presence of nitrogen.

In conclusion, the products of the photolysis of both the 3,5-bis(dimethylamino)benzyl alcohol **5.4** and triplet-sensitized photolysis of the trifluoroacetyl derivative **5.8** are indicative of the intermediacy of the expected benzyl cations. Although direct and triplet-sensitized laser flash photolysis (LFP) do not give any additional clues to the identity of the intermediate because of undesirable artifacts associated with the electron rich nature of the ring, product studies from direct photolysis of the precursor are indicative of the intermediacy of the singlet benzyl cation. Photolysis of **5.4** gives primarily singlet-derived products, although a small quantity of reduced product can be attributed either to a hydride transfer from the solvent or to a product derived from the triplet benzyl cation. On the basis of

these studies, we believe that the singlet state is likely the ground state for this cation, but that the triplet state is low in energy.

### 5.3. The 3',5'-bis(dimethylamino)-1-bis(trifluoromethyl) benzyl cation.

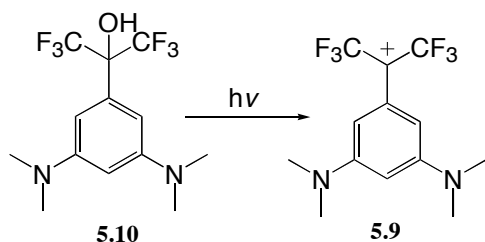
While the 3,5-bis(dimethylamino)benzyl cation is computed to have nearly degenerate singlet-triplet state energies (and the early experimental studies are consistent with this prediction, but with a singlet state lower in energy than the triplet), a derivative with two exocyclic CF<sub>3</sub> groups **5.9** (shown in Figure 5.8) is computed to be a ground state triplet species with a gap to the lowest energy singlet state that is larger than the likely error inherent in the computational methods.



$$\Delta E_{\text{ST}} = + 12 \text{ kcal/mol (B3LYP)} \\ + 9 \text{ kcal/mol (CASPT2)}$$

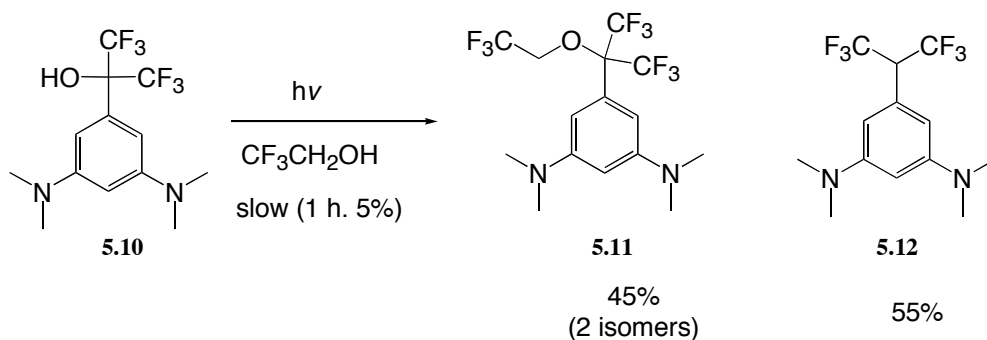
**Figure 5.8.** The 3',5'-bis(dimethylamino)-1,1-bis(trifluoromethyl) benzyl cation **5.9**: A computed triplet benzyl cation.

The method to generate this cation was photolysis of the benzyl alcohol **5.10**, as shown in Scheme 5.9, in analogous fashion as employed with the unsubstituted derivative.



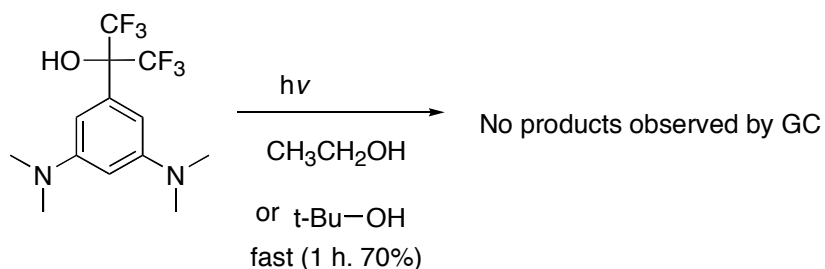
**Scheme 5.9.** Method for formation of benzyl cation **5.9**.

Photolysis of the benzyl alcohol **5.10** in TFE occurred slowly, with 5% decomposition after 1 h. The major product was the reduced toluene derivative **5.12** (55% by GC area percent) and two isomeric TFE adducts **5.11** were also observed.



**Scheme 5.10.** Photolysis of **5.10** in TFE.

In ethanol or t-butyl alcohol solvent, consumption of the benzyl alcohol **5.10** through photolysis occurred quickly, but no significant products were observed by GC. Most likely, non-volatile products were formed, making them invisible by GC. While this is simply a preliminary study, we note that this appears to represent significantly different chemistry than that observed for the unsubstituted benzyl alcohol, suggestive of a fundamentally different intermediate. However, further experiments are required to confirm this prediction.



**Scheme 5. 11.** Photolysis of **5.10** in EtOH or tBuOH.

#### 5.4. Theoretical studies of benzyl anions.

We considered the possibility that a reverse connectivity might also stabilize a triplet state. That is, rather than having two meta electron donors (amino groups) attached to an acceptor (cation), we considered that a similar triplet state might be stabilized by an anionic donor with two meta electron accepting groups. To test this hypothesis, we computed the singlet-triplet energy gaps for a number of benzyl anions using density functional theory (B3LYP/6-31+G(d,p)). Acceptors included cyano and nitro groups, and donors included phenyl silyl anions, aniline anions, benzyl anions, and phenolates. The results of these computations are shown in Table 5.1.

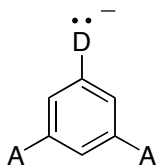


Table 5.1.  $\Delta E_{ST}$  of meta disubstituted anionic species. A negative value indicates a singlet ground state.

<b>D</b>	<b>A</b>	<b><math>\Delta E_{ST}</math> (Kcal/mol)</b>
CH <sub>2</sub> <sup>-</sup>	H	-41.9
	CN	-21.5
	NO <sub>2</sub>	-1.3
SiH <sub>2</sub> <sup>-</sup>	H	-50.5
	CN	-26.0
	NO <sub>2</sub>	-6.0
NH <sup>-</sup>	H	-50.8
	CN	-32.8
	NO <sub>2</sub>	-12.5
O <sup>-</sup>	H	-61.5
	CN	-43.8
	NO <sub>2</sub>	-26.6

As shown in Table 5.1, in all cases the parent anionic species is a singlet ground state with a very large computed energy gap to the lowest-energy triplet state. Moreover, in all cases, substitution of the two meta positions with cyano or nitro groups stabilized the triplet state in preference to the singlet, although in no case was this effect strong enough to make the triplet state the computed ground state. In the case of the 3,5-dinitrobenzyl anion, the singlet-triplet states are computed to be nearly degenerate, with the singlet state computed to be the ground state with a  $\Delta E_{ST}$  of 1.3 kcal/mol to the lowest energy triplet state.

#### 5.4.1. Effect of $\alpha$ heteroatoms on $\Delta E_{ST}$ .

Substituting the alpha positions with heteroatoms on the 3,5-dinitrobenzyl anion shifts the singlet-triplet gap in favor of the triplet. Table 5.2 shows the singlet-triplet gaps of the benzyl anions substituted with oxygen or sulfur constrained in five- or six-membered rings. In all cases, the heteroatoms shifted the singlet-triplet gap in favor of the triplet, but the effect of oxygen is greater than the effect of sulfur.

Qualitatively, this result can be readily explained by a donor-acceptor motif, wherein a better donor (with a higher HOMO) or a better acceptor (stabilized LUMO) favors the triplet state by reducing the frontier orbital separation. Heteroatoms adjacent to the anionic carbon appear to raise the energy of the HOMO, presumably as a result of a destabilizing  $\alpha$  effect of the adjacent lone pairs in the singlet state.

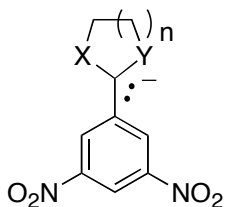


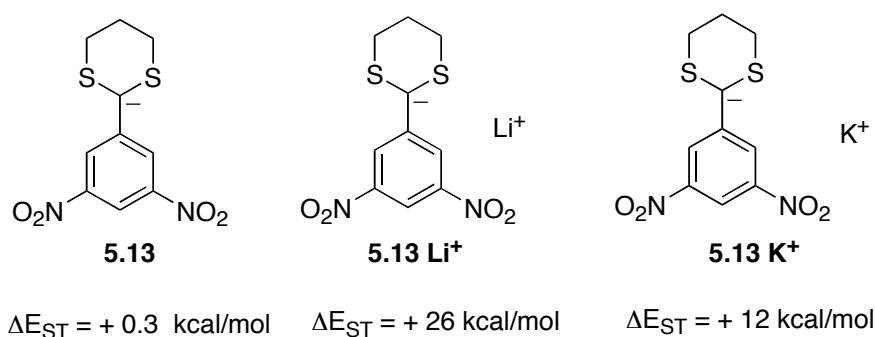
**Table 5.2.** Effect of adjacent heteroatoms on  $\Delta E_{ST}$  of benzyl anions.

X	Y	n	$\Delta E_{ST}$ (Kcal/mol)
S	S	1	0.0
S	S	2	+0.3
S	O	1	+3.5
S	O	2	+1.7
O	O	1	+5.5
O	O	2	+5.8

5.4.2. Dramatic effect of counter ion on  $\Delta E_{ST}$  of benzyl anions.

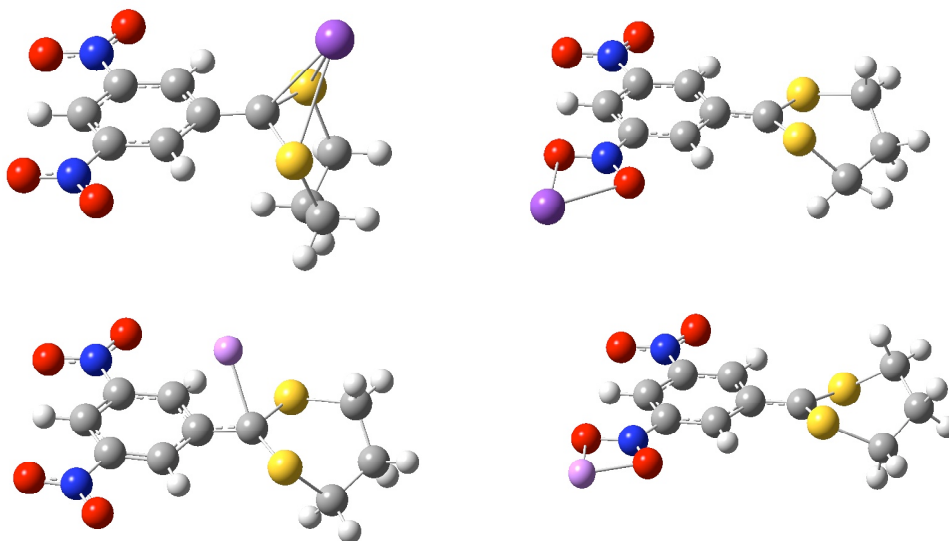
Additionally, the anion counter ion appears to have a significant effect on the  $\Delta E_{ST}$  in the gas phase. Inclusion of the counter ion into the calculation dramatically stabilizes the triplet state in preference to the singlet relative to the naked anion.

Figure 5.9 shows the effect of counter ion on the  $\Delta E_{ST}$ . With a lithium counter ion, the triplet is computed to be the ground state by 26 kcal/mol in the gas phase. With a potassium counter ion, the anion is computed to be a triplet by 12 kcal/mol.



**Figure 5. 9** Effect of counterion on  $\Delta E_{ST}$ .

The computed geometries for the dithiane singlet and triplet states with potassium and lithium counterions are shown in Figure 5.10. We note that a number of minima were found with the counter ions in different locations for the singlet and triplet states; however, in the singlet states, the counterion attaches to the exocyclic carbon in the lowest energy configuration. In the triplet state, the counterion attaches to one of the nitro groups in the lowest-energy configuration.



**Figure 5. 10.** Computed geometries (B3LYP/6-31+G(d,p)) for **5.13** singlet (left hand structures) and **5.13** triplet (right hand structures) with potassium (top structures) and lithium (bottom structures) counter ions.

One explanation for the effect of counter ion on the singlet-triplet gap is that the counter ion preferentially stabilizes the negative charge in the triplet state relative to the singlet state. This explanation is most apparent by observing the resonance contributors in the singlet and triplet state (Figure 5.11). In the singlet state, most of the charge is localized on the exocyclic benzylic carbon; in the triplet state, the charge is found predominantly on the nitro group oxygens. It appears that the counter ion forms the most favorable ionic salt interaction in the triplet state, in which the counter ion bridges the two oxygens on the nitro group holding the negative charge. In the singlet state, the counter ion is more weakly associated to the exocyclic carbon, as shown by the longer distance between the exocyclic carbon and the counter ion.



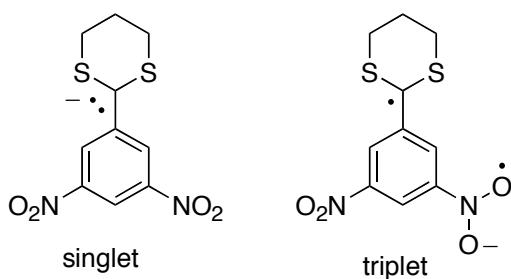


**Figure 5. 11.** Major resonance contributors to the singlet and triplet benzyl anion 5.13.

#### 5.4.3. Attenuation of counter ion effect by solvent consideration.

Incorporation of dimethyl ether (DME) solvent into the lithium-coordinated benzyl anions was performed to test whether solvent can attenuate the effect of counterion on the  $\Delta E_{ST}$ . The prediction is that solvent would weaken the ionic bond between the anion and the counter ion by forming a solvent sphere around the counter ion, reducing its ability to interact with the negative charge. We chose to incorporate solvent explicitly with two dimethylether (DME) solvent molecules and three DME molecules starting with the lowest energy geometries found in the absence of solvent. Consistent with the prediction described above, adding two DME molecules reduces the  $\Delta E_{ST}$  from +26 kcal/mol to +17 kcal/mol, and addition of three DME molecules reduces the gap still further to +14 kcal/mol. The solvent sphere can be seen in the optimized geometries with explicit solvent consideration in Figure 5.12. We note that we were unable to perform frequency calculations on the optimized structures because of the system size, so no corrections for the zero-point vibrational energies were made for the anions with explicit solvent incorporation.

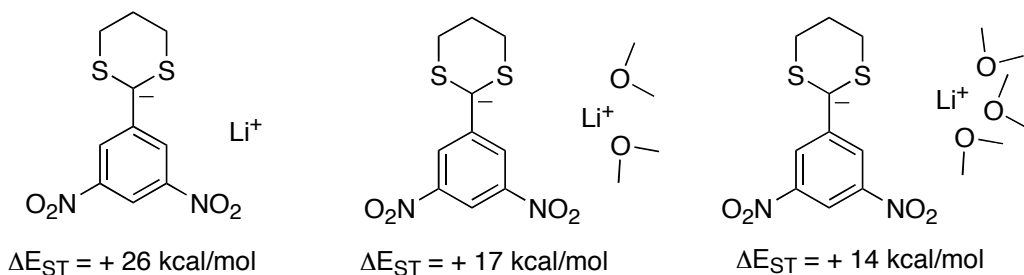


**Figure 5. 12.** Effect of solvent on singlet-triplet splittings on **5.13**  $\text{Li}^+$ .

The computed geometries for the singlet and triplet states with explicit solvent inclusion are shown in Figure 5.13.

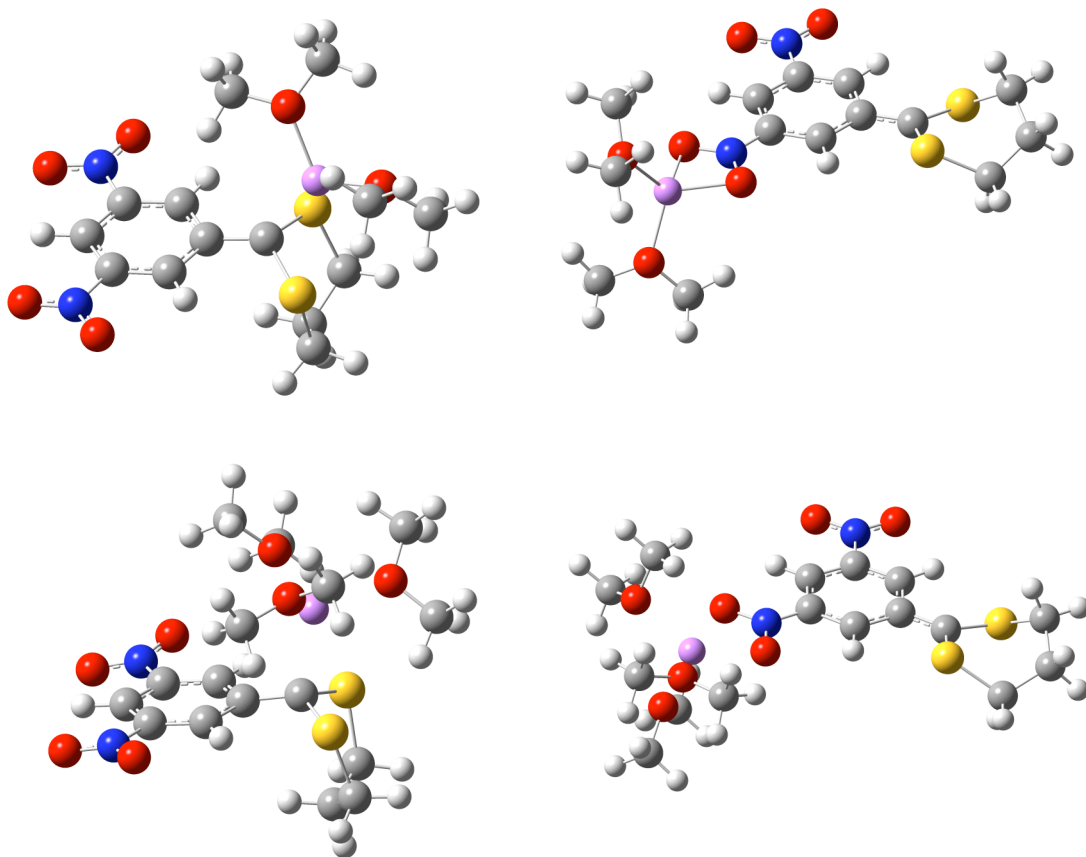
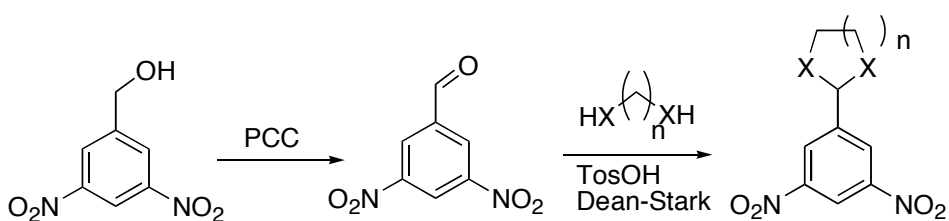


**Figure 5.13.** DFT geometries (B3LYP/6-31+G(d,p)) of the singlet (left-hand structures) and triplet states (right hand structures) from the dinitrobenzyl anion **5.13**  $\text{Li}^+$  with 2 explicit dimethylether molecules (top) and three dimethylether molecules (bottom).

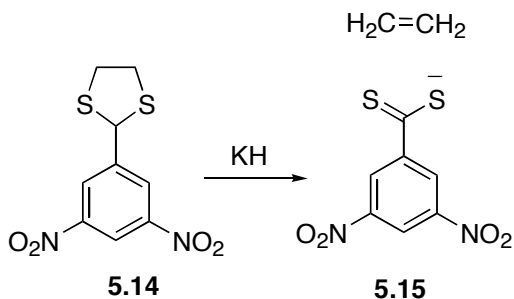
5.5. Experimental studies of benzyl anions.

We were interested to see whether we could make and observe a triplet benzyl anion. To our knowledge, no benzyl anion with a triplet ground state has been observed previously. The synthetic scheme for making the precursors is shown in Scheme 5.12.



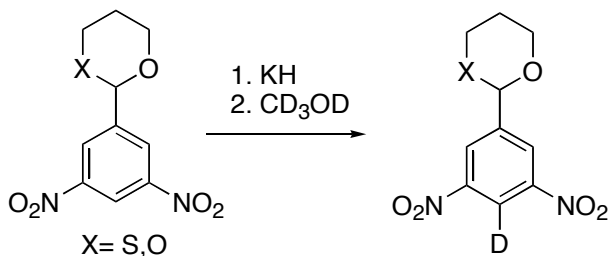
**Scheme 5.12.** Synthesis of benzyl anion precursors.

We started with the dinitrodithiane **5.14** shown in Scheme 5.13. Unfortunately, reaction with potassium hydride appeared to lead to loss of ethylene and formation of a dithioic acid **5.15**.



**Scheme 5. 13.** Decomposition of five-membered dithianes.

To eliminate this pathway, we synthesized analogs with one additional carbon in the ring. However, rings containing one or two oxygens did not lead to benzylic deprotonation, but rather to ring deprotonation. This ring deprotonation was observed by quenching studies with CD<sub>3</sub>OD which returned the starting material with ring-substituted deuterium rather than benzylic-substituted deuterium (Scheme 5.14).



**Scheme 5.14. Alpha oxygens lead to ring deprotonation.**

However, with the dithiane **5.16**, deprotonation occurs cleanly as hoped in the benzylic position. Deprotonation was followed by reaction with potassium hydride, followed by quenching with deuterated methanol. The incorporation of deuterium could be followed by <sup>1</sup>H NMR, observing the decrease in the benzylic C-H signal relative to the aromatic C-H signals. Incorporation of deuterium was confirmed by GC-MS (M<sup>+</sup> peak one unit higher) and <sup>13</sup>C NMR from benzylic C-D coupling (triplet in the proton-decoupled spectrum).

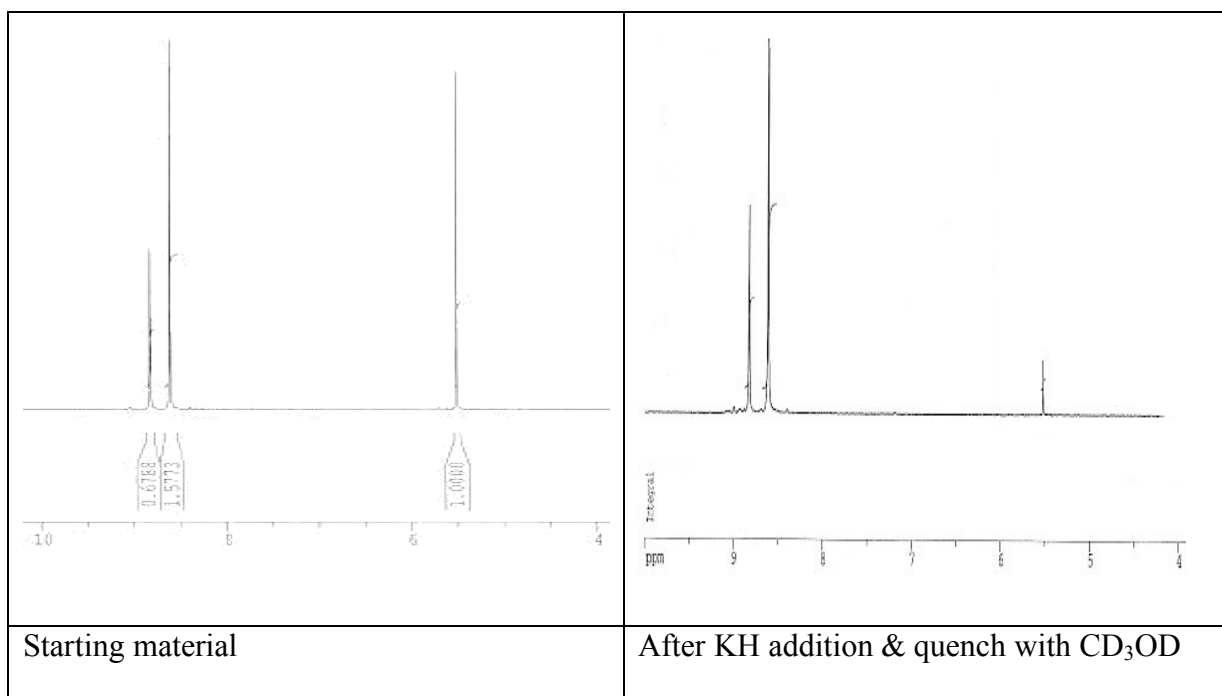
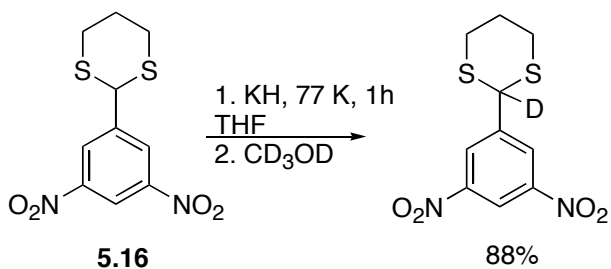


**Figure 5. 14.** <sup>1</sup>H NMR of starting material **5.16** aromatic and benzylic protons (left), and product quenched after 1 hr, with 88% <sup>2</sup>H incorporation (right).

Using potassium hydride suspended in mineral oil, deprotonation of **5.16** at 77 K under nitrogen atmosphere (Schlenk line techniques) does not occur instantaneously. The kinetics of deprotonation were followed by quenching the deprotonation reaction at different times with CD<sub>3</sub>OD and following the decrease in the benzylic C-H signal in the <sup>1</sup>H NMR spectrum. The kinetic plot of the deuterium incorporation over time is shown in Figure 5.15.

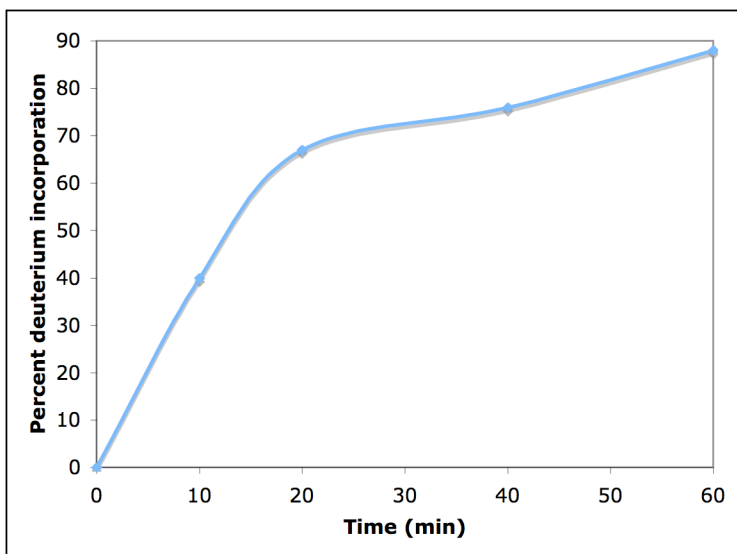


**Figure 5.15** Deprotonation kinetics of **5.16** using KH in mineral oil.

On the other hand, addition of solid potassium hydride at room temperature in a glove box under argon atmosphere led to essentially an instantaneous deprotonation reaction with observable hydrogen gas bubbling ceasing after a few minutes. In these cases, up to 99% deuterium incorporation following quenching with  $\text{CD}_3\text{OD}$  (or  $\text{CH}_3\text{OD}$ ) was observed. Similar results were observed for LDA in THF, t-butyl lithium in THF, and KH in DMSO. Apparently, the KH dispersion in mineral oil slows the deprotonation reaction considerably.

Deuterium incorporation into the benzylic position following quenching provides good evidence of the successful generation of the benzyl anion. Therefore, we attempted to take an NMR spectrum of the anion. A triplet species is expected to have highly broadened (or invisible) peaks due to magnetic relaxation. Conversely,

singlet benzyl cations can be observed by an upfield shift in the aromatic and benzylic carbon signals in the  $^1\text{H}$  and  $^{13}\text{C}$  NMR spectra.

Consistent with the prediction of an NMR-silent triplet anion, upon addition of base in THF at low NMR temperatures (performed in a sealed Young NMR tube under argon), the only observable peaks in the  $^1\text{H}$  NMR spectrum were the starting material

**5.16.** Raising the NMR temperature, however, showed peak broadening of the starting material, particularly of the aromatic peaks and the benzylic C-H peak. Less broadening was observed for the dithiane ring C-H peaks. Cooling the NMR tube back down and retaking the NMR returned the sharp peaks, and allowing the NMR to warm regenerated the broad peaks. Despite the absence of any peaks that could be attributable to the anion, quenching of this solution with  $\text{CD}_3\text{OD}$  or  $\text{CH}_3\text{OD}$  led to >80% deuterated product. Figure 5.16 shows the spectrum with NaH in THF, but identical starting material peak broadening was observed using LDA or KH in THF.

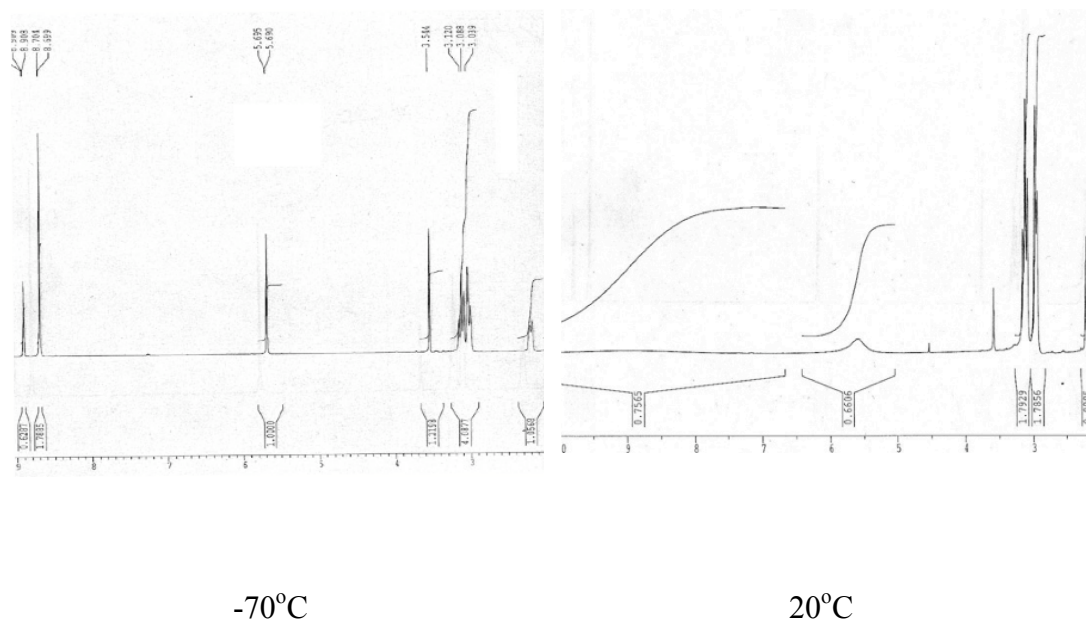
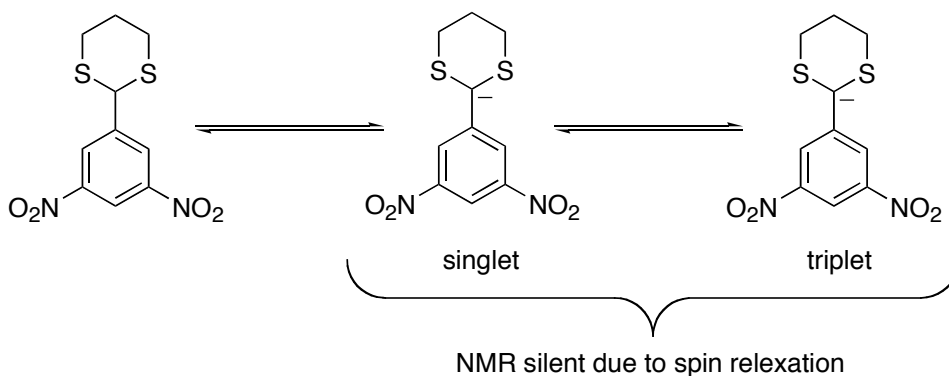


**Figure 5.16.**  $^1\text{H}$  NMR spectrum of dithiane **5.16** and NaH in  $\text{THF-d}_8$  at  $-70^\circ\text{C}$  (left) and  $20^\circ\text{C}$  (right).

The broadening of the starting material peaks as the temperature is raised is difficult to interpret. Often, NMR peak broadening is due to a chemical exchange; however, in those cases, the chemical shifts move to give the average of the chemical shifts of the two species in exchange. Here, the chemical shifts remain the same. Given that it's reasonably clear that the desired benzyl anion is being formed based on the deuterium incorporation following quenching, one possible explanation is a dynamic equilibrium between starting material and an NMR silent anion (shown in Scheme 5.15). At low temperatures, diffusion is slower and so unchanged dithiane may not encounter other molecules of anion on the NMR time scale. At higher temperatures, diffusion becomes quicker and protons can be exchanged between units on the NMR time scale, resulting in peak broadening. This explanation assumes, however, that the benzyl anion exists as a triplet ground state or is in a rapid dynamic equilibrium



between the singlet and triplet states, which would explain why no peaks for the anion are observed.



**Scheme 5.15.** Possible mechanism for peak broadening.

Another possible explanation for the absence of any signals attributable to a benzylic cation may be solubility issues. While the dithiane starting material is completely miscible in THF, the solution becomes deep purple upon addition of base and some purple solid does precipitate. However, it's unexpected that the NMR spectrum shows no peaks for the benzyl anion, as the phenyldithiane (without nitro groups) has previously been observed by  $^1\text{H}$  NMR in THF solution.

#### 5.5.1. Evidence for a paramagnetic species in solution

Further evidence for a paramagnetic species in solution comes from the Evans' NMR method. In this NMR experiment, a thin capillary is placed inside an NMR tube containing only the deuterated solvent ( $\text{THF-d}_8$ ). See Figure 5.17. In the outer NMR tube, the sample is prepared (dithiane plus KH) in deuterated THF. The NMR is locked onto the center solvent capillary containing pure solvent. If the solvent containing the outer sample is interacting with a paramagnetic species, the chemical

shift is expected to be shifted. Conversely, if the solvent interacts only with closed-shell diamagnetic species, the solvent peaks for the inner capillary and the outer tube should be the same.

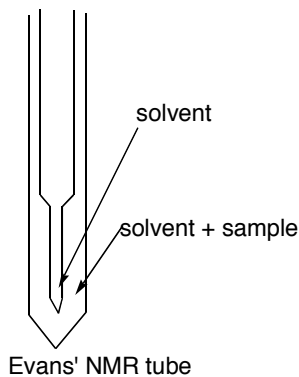


**Figure 5.17.** Evans' NMR method.

Indeed, when pure THF-d8 is placed in the inner capillary and THF-d8 plus the dithiane **5.16** and KH are placed in the outer NMR tube, two signals appear to be observed for the solvent, as two sets of THF signals are observed. We believe this provides good evidence for the formation of a paramagnetic species in solution, although it does not give any evidence for the identity of the paramagnetic species.

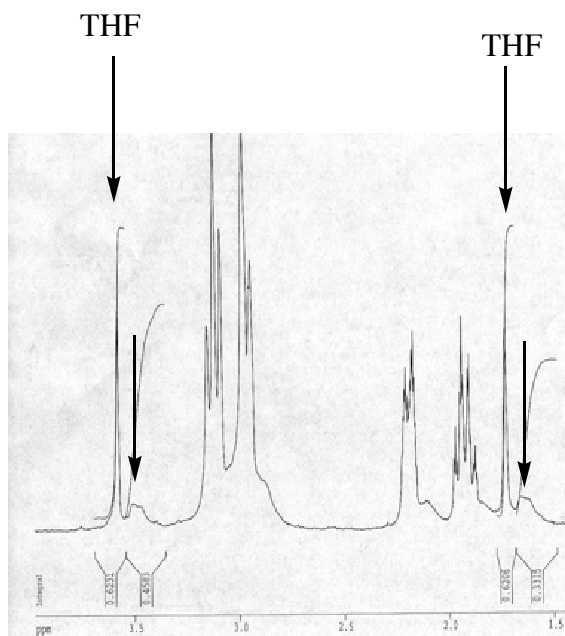


**Figure 5.18.** Evans'  $^1\text{H}$  NMR method.

#### 5.5.2. Further NMR evidence for a paramagnetic intermediate

The anion appears to be more soluble in  $\text{DMSO-d}_6$  than  $\text{THF-d}_8$ , giving a viscous apparently homogeneous, rich purple solution upon addition of 1 equivalent of solid KH with vigorous hydrogen gas evolution. Despite the apparent solubility of the anion in DMSO, taking the  $^1\text{H}$  NMR spectrum in a sealed Young NMR tube under argon showed only the signals of diamagnetic impurities, in spite of the high concentration of substrate **5.16** (15 mg dithiane in ca. 1 mL  $\text{DMSO-d}_6$ ). Note the very large solvent residual peak in spite of the very high concentration of substrate. However, quenching with  $\text{CH}_3\text{OD}$ , followed by neutralization of the solution and extraction with ether returned the starting material with essentially 100% deuterium substitution at the benzylic position. In addition to the deuterated dithiane, some impurities were also evident, possibly from decomposition of the anion. We believe

that this experiment provides good evidence of a paramagnetic species. We hypothesize that the anion itself is a triplet species and is NMR silent, but returns to being NMR active upon protonation to give a diamagnetic species; however, further studies are required to make a definitive case.

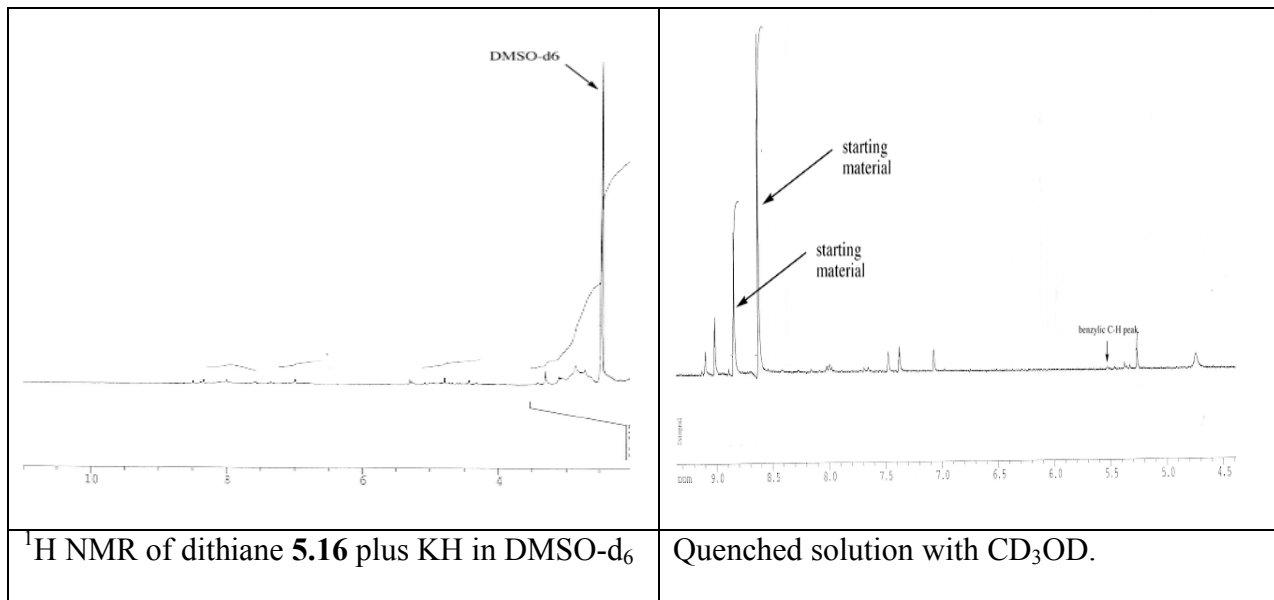


**Figure 5.19.** <sup>1</sup>H NMR spectra of **5.16** and KH in DMSO.

### 5.5.3. EPR studies of the benzyl anions.

Additionally, attempts were made to observe the triplet anion by EPR spectroscopy. Unfortunately, we have so far been unsuccessful in observing the triplet anion by EPR. Triplet diradicals often are distinguishable from doublet monoradicals in an EPR spectrum because of the zero-field splitting of the triplet states. While most organic doublet radicals have peaks in the EPR spectrum between 3200-3400 Gauss, triplet diradicals are often found in different locations of the spectrum or have broader peaks than double radicals. For m-xylene and other non-Kekule species, zero field

splitting appears to be much smaller than atom-centered triplet diradicals such as carbenes, making them somewhat more difficult to distinguish than doublet radicals.

Samples were prepared in a sealed EPR tube in distilled degassed THF under argon. Bases tested included potassium hydride and LDA. In THF, we observed the EPR spectrum shown in Figure 5.20 regardless of base used. No other peaks were seen in the EPR spectrum at different external magnetic field strengths. Temperatures in the EPR cavity were varied from 100K to room temperature using a liquid nitrogen blow-off method. No new peaks were seen at lower or higher temperatures.

We believe that the signal seen in the EPR spectrum is that of the anion radical of the starting material because an identical spectrum was observed on treating the starting material with sodium metal in THF. Part of the difficulty in observing a triplet diradical absorption may be the solubility of the anion. At low temperatures, it is clear that a dark purple solid precipitates from solution; at higher temperatures more of it dissolves. However, at high temperature where more of the sample is dissolved, spin relaxation may broaden the peaks of the EPR sufficiently so that no signals can be observed. The anion appears to be more soluble in DMSO; however, we were unable to lock the solvent signal in a sample dissolved in DMSO due to the polarity of DMSO solvent (which absorbs the microwave irradiation). Thus, the EPR studies are inconclusive at this time as to the ground state of the benzyl anion.

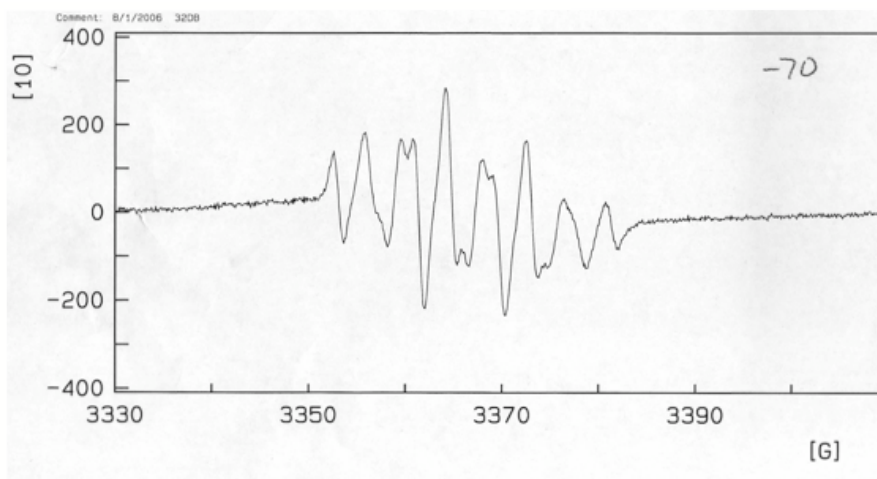


**Figure 5. 20.** EPR spectrum of dithiane **5.16** and KH in THF.

## 6. Chapter 6: Vinyl Cations Substituted with $\beta$ Pi Donors Have Triplet Ground States

### 6.1. Introduction

In this chapter, computations at the CASSCF, CBS-QB3, and B3LYP levels of theory are performed to demonstrate that  $\beta$  substitution of vinyl cations with pi donors stabilizes a carbene-like triplet state similar to the electronic state of triplet phenyl cations. Although the parent vinyl cation is a ground-state singlet species with a seemingly insurmountable energy gap of a computed 48.5 kcal/mol to the lowest energy triplet state, substituting the beta hydrogens with just one strong pi donor (e.g.  $\text{NH}_2$ ,  $\text{NMe}_2$ ,  $\text{OMe}$ ), or two moderate pi donors (eg. F, OH, Ar, vinyl) makes the triplet state the expected ground electronic state. In many cases the singlet states for these  $\beta$  pi donor-substituted vinyl cations are prone to rearrangements, although spontaneous rearrangements can be discouraged through incorporation of the pi donors into rings. In contrast to the singlet states, the triplet states appear to be well behaved and more immune to rearrangements.

Phenyl cations ( $\text{Ph}^+$ ) are a member of the carbenium family of intermediates having an electronic structure similar to vinyl cations.<sup>96,99-102</sup> One of the most interesting features of phenyl cations is that they are one of only a few known classes of carbenium ion that can exist in either a singlet state or a triplet electronic state.<sup>94,103,104</sup> The unsubstituted phenyl cation is a ground-state singlet, but the triplet state becomes the lower-energy state when the ortho or para positions of the phenyl ring are

substituted with pi donors (e.g. OR, NR<sub>2</sub>). The triplet state of a phenyl cation bears some resemblance to a triplet carbene<sup>105</sup> (see Figure 6.1 for an example.).

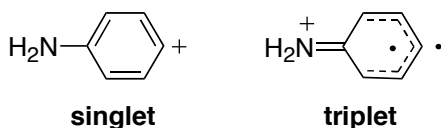


**Figure 6. 1. A ground-state triplet phenyl cation.**

Given that triplet phenyl cations can be exploited to undergo useful synthetic transformations,<sup>106-110</sup> and given the similarity of phenyl cations to vinyl cations, we thought it worthwhile to test whether similar pi-donor group substitutions could stabilize a triplet state in vinyl cations. Vinyl cations are intermediates in many important industrial and commercial reactions, and they are typically formed from the solvolysis of leaving-group-substituted olefins, from the photolysis of vinyl halides, and from electrophilic addition reactions (including protonations) of allenes and alkynes.<sup>99,100,111-114</sup> Vinyl cations have been studied by laser flash photolysis,<sup>115-117</sup> mass spectrometry,<sup>118-120</sup> stable ion media NMR,<sup>121-123</sup> trapping studies and product analyses,<sup>99,100,115,124</sup> and, in one exceptional case, x-ray crystallography.<sup>125</sup> Although numerous theoretical and experimental studies have been published on the effect of substituents on the stabilities of vinyl cations,<sup>99,124,126</sup> to our knowledge none have explored the possibility of a stabilized triplet state. To the extent that the parent vinyl cation is a ground-state singlet with a very large energy gap (48.5 kcal/mol) to the lowest-energy triplet state, this is understandable. However, as discussed below, DFT, CBS-QB3, and CASSCF calculations show that  $\beta$  substitution of vinyl cations with pi donors dramatically stabilizes a carbene-like triplet state with an electronic



structure similar to triplet phenyl cations. When the  $\beta$  position is substituted with a single moderate pi donor (e.g. F, OH, Ar), the singlet is still the ground state but with a small gap to the lowest-energy triplet state. In cases where the  $\beta$  position is substituted with one or two strong pi donor groups (e.g., OMe, NH<sub>2</sub>, NMe<sub>2</sub>) or two moderate pi donor groups (e.g. OH, F, Ar, Vinyl), the triplet state is the predicted ground state.

### *6.2. Computational methods.*

We chose to examine the singlet-triplet state energy gaps ( $\Delta E_{ST}$ ) of the vinyl cations examined in this study by three computational methods: complete active space self-consistent field theory (CASSCF), the complete basis set (CBS-QB3) method of Petersson, and density functional theory (B3LYP). Here, the singlet-triplet energy gap, or  $\Delta E_{ST}$ , refers to the gas phase adiabatic energy difference between the lowest energy singlet and the lowest energy triplet state (including unscaled zero point vibrational energies). A negative value for  $\Delta E_{ST}$  indicates a singlet ground state.

CASPT2 is a particularly appropriate method to model these electron-deficient species because this method explicitly takes into account non-dynamical correlation resulting from any near-degeneracy of the frontier orbitals, and accounts for dynamical correlation outside of the active space using second order perturbation theory. When employed with a large and flexible basis set and a well-chosen active space, this method typically gives quantitative estimates of the  $\Delta E_{ST}$  to within 5 kcal/mol of the actual value for similar hypovalent species, and in favorable cases to

within 2-3 kcal/mol. For all the CASSCF calculations, the active space was chosen to include all pi electrons (including pi lone pairs) and all pi orbitals plus the empty  $\sigma$  orbital on the cationic vinylic carbon. For example, the 2,2-difluorovinyl cation was computed at the CASSCF(6,5) level. We note that in all cases we observe virtually no changes in the molecular geometries on going from CASSCF/cc-pVDZ to CASSCF/cc-pVTZ, indicating that the geometries are well converged with respect to basis set size.

We also used the complete basis set CBS-QB3 method of Petersson, which employs a DFT (B3LYP) optimization, and a coupled cluster single point energy calculation using an extrapolation procedure to find the electronic energy at the basis set limit (along with an empirically determined correction for spin contamination). Since the electronic energy is derived from a coupled cluster calculation, this method tends to perform poorly when an electronic state cannot be well described by a single reference wavefunction. However, the CASSCF calculations show that all the singlet states in this study consist almost entirely of a single closed-shell determinant. While CBS-QB3 is fairly new and has therefore not been benchmarked for a large number of similar systems, we note that this method gives excellent quantitative estimates for the singlet-triplet gaps for hypovalent species with experimentally known  $\Delta E_{ST}$  values or values obtained from converged *ab initio* methods. These include the parent carbene methylene (CBS-QB3 predicted  $\Delta E_{ST} = +8.6$  kcal/mol, experimental = +9 kcal/mol<sup>127</sup>), difluorocarbene (CBS-QB3 predicted  $\Delta E_{ST} = -56.1$  kcal/mol, experimental = -57 kcal/mol<sup>128</sup>), phenyl carbene (CBS-QB3 predicted  $\Delta E_{ST} = +4.5$

kcal/mol, experimental = +2.3 kcal/mol<sup>129</sup>), the parent nitrenium ion  $\text{NH}_2^+$  (CBS-QB3 predicted  $\Delta E_{\text{ST}} = +28.6$  kcal/mol, experimental = +29.9 kcal/mol<sup>29,46</sup>), and the parent phenyl cation  $\text{Ph}^+$  (CBS-QB3 predicted  $\Delta E_{\text{ST}} = -24.9$  kcal/mol, CAS-MP2/6-311+G(3df,2p) = -24.6 kcal/mol<sup>96</sup>). This method has also successfully predicted the ground states of simple nitrenes.<sup>130-132</sup> These benchmarks for related species lead us to anticipate good quantitative accuracy from this method in the current study.

While both the CASSCF and CBS-QB3 models are rigorous computational methods, DFT has also shown to be quite robust for predicting relative energies of many hypovalent species that have wavefunctions consisting of primarily a single closed-shell determinant. Since DFT can be employed at a fraction of the computational cost of the CASSCF and CBS-QB3 methods, this method is applicable to larger systems that are intractable at the higher levels of theory. Thus, we also chose to model these vinyl cations using DFT, employing the hybrid B3LYP functional along with the polarized double-zeta 6-31G(d,p) basis set.

### *6.3. Computed singlet-triplet splittings.*

Except where noted, geometries were optimized at the same level of theory as the single point energy calculation. The results of these computations are summarized in Table 6.1.

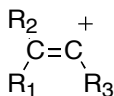


Table 6.1. Predicted singlet-triplet splittings for substituted vinyl cations

Compound Number	R <sub>1</sub>	R <sub>2</sub>	R <sub>3</sub>	$\Delta E_{\text{ST}}$			
				B3LYP/ 6-31G(d,p)	CASSCF/ cc-pVDZ	CASSCF/ cc-pVTZ	CBS-QB3 (CBS-APNO)
6.1	H	H	H	-41.9	-38.7 <sup>a</sup>	-38.1 <sup>a</sup>	-48.5 (-49.0)
6.2	OH	H	H	-2.4 <sup>c</sup>	-6.6	-7.9	S.R.
6.3	OMe	H	H	+3.8 <sup>c</sup>	+13.6	+12.1	S.R.
6.4	NH <sub>2</sub>	H	H	+3.8	+12.7	+10.8	S.R.
6.5	NMe <sub>2</sub>	H	H	+11.1	+13.1	+12.8 <sup>b</sup>	+8.2
6.6	NH <sub>2</sub>	NH <sub>2</sub>	H	+17.1 <sup>d</sup>	+14.4	+13.1	S.R.
6.7	NH <sub>2</sub>	H	F	+5.5	-0.5	-1.0	+2.0
6.8	F	F	H	+4.6	-3.9	-4.1	+0.1
6.9	F	F	F	+2.9			-1.6
6.10	F	H	CH <sub>3</sub>	-19.2			-25.5

S.R. = Singlet Rearranges. A negative value for  $\Delta E_{\text{ST}}$  indicates a singlet ground state. a.  $\Delta E_{\text{ST}}$  using the open form of the vinyl cation. b. ZPVE added at cc-pVDZ level. cA. Single point calculation at CASSCF/cc-pVTZ geometry (singlet rearranges spontaneously by 1,2-hydride shift at DFT level). D. Single point at CASSCF/cc-pVTZ geometry (singlet rearranges spontaneously by formation of a three-membered ring at DFT level; see Scheme 6.1)

#### 6.4. *Structure of the parent vinyl cation.*

In most cases, the computed values of  $\Delta E_{\text{ST}}$  at the CASSCF, CBS-QB3, and B3LYP levels show reasonably good quantitative agreement, although the B3LYP values tend to systematically underestimate the singlet stability by 3-6 kcal/mol as compared to the higher-level methods. Poorer agreement between the methods is observed for the  $\Delta E_{\text{ST}}$  of the unsubstituted vinyl cation **6.1**. This poor agreement results from the non-classical structure of the singlet state of the parent species. The classical open and non-classical (or bridged) forms of the singlet vinyl cation are shown in Figure 6.2. The non-classical structure resembles a proton-coordinated acetylene. Early computational studies suggested that the classical open form was energetically

favored, but the best modern computational methods and even some recent experimental studies suggest that the non-classical bridged form is the preferred structure in the gas phase.<sup>133</sup> The CBS-QB3 method used here predicts the bridged form to be more stable than the classical form by 3.7 kcal/mol. Virtually identical values for the energy difference between these two structures have been reported in previous high-level computational studies.<sup>133,134</sup> The CASSCF values for the  $\Delta E_{ST}$  reported in Table 6.1 represent the difference in energy between the classical open singlet structure and the triplet state (to accurately model the non-classical singlet state using CASSCF, an expensive full valence active space calculation would likely be required). As seen recently,<sup>133</sup> DFT appears to poorly model the non-classical structure, as the two forms are found to have essentially degenerate energies at this level of theory. Consequently, both the CASSCF and DFT values underestimate the singlet stability of the parent vinyl cation. The best estimate for the  $\Delta E_{ST}$  of the parent vinyl cation comes from the CBS-QB3 method that gives a value for  $\Delta E_{ST}$  of -48.5 kcal/mol (-49.0 kcal/mol from CBS-APNO).

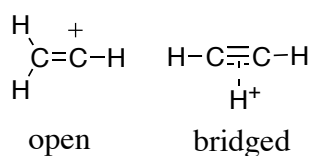


**Figure 6.2.** Two forms of the singlet vinyl cation

### 6.5. *$\beta$ -pi donor substituted vinyl cations.*

Substituting the  $\beta$ -position on the vinyl cations with pi donors clearly leads to a stabilized triplet state. For example, the parent vinyl cation **6.1** is predicted to have a

singlet-triplet gap of 48.5 kcal/mol in favor of the singlet state (CBS-QB3), but substituting just a single dimethylamino substituent in the  $\beta$  position **6.5** causes the triplet state to be the predicted ground state by 8.2 kcal/mol—a swing in the  $\Delta E_{ST}$  of roughly 57 kcal/mol! Even traditionally weak pi donors cause remarkable changes in the singlet-triplet state energy gaps. For example, substituting two fluorines **6.8** in the  $\beta$  position makes the singlet and triplet states have essentially degenerate state energies.

Conversely, CASSCF shows that substituting just a single moderate pi donor such as a hydroxyl group **6.2** or fluorine **6.10** for hydrogen stabilizes the triplet state significantly, but not sufficiently enough to make the triplet state the computed ground state. In these two cases, the singlet state is still the predicted ground state but with a substantially smaller gap to the lowest-energy triplet state. (As discussed below, rearrangements in the singlet states for these species occur spontaneously at the DFT level). Apparently, the methoxy group is a better pi donor than the hydroxy group, as the methoxy-substituted vinyl cation is predicted to be a ground-state triplet at this level of theory.

#### 6.6. Molecular geometries and rearrangements.

Table 2 shows select computed geometrical parameters at the DFT (B3LYP/6-31G(d,p)) and CASSCF/cc-pVTZ levels (CASSCF geometries in parenthesis). The triplet geometries resemble a vinyl radical with a roughly  $sp^2$ -hybridized cationic carbon. From these values, it is clear that the triplet geometries do not change

significantly with substitution. Bond angles of between 135 and 145 degrees are seen in all cases for the triplet states of the primary vinyl cations, and the bond lengths are a consistent 1.4 ( $\pm$  0.015) Å. Moreover, the CASSCF/cc-pVTZ and B3LYP/6-31G(d,p) computed geometries are in generally good agreement for the triplet states, although the C-C-R<sub>3</sub> bond angles computed at the DFT level are systematically 3-9 deg. more acute than the bond angles computed at the CASSCF/cc-pVTZ level. More variation in the geometries is seen in the singlet states upon substitution with pi donors. Substituting the  $\beta$  position with pi donors dramatically increases the vinylic C-C bond length in the singlet state, while simultaneously decreasing the C-C-R<sub>3</sub> bond angle. For instance, substituting the  $\beta$  positions with two amino groups increases the computed C-C bond length from 1.270 Å in the parent system to 1.471 Å (at the CASSCF/cc-pVTZ level), while the bond angle changes from an essentially linear 179.9 degrees in the parent vinyl cation to a more acute 109.0 degrees in the diamino-substituted vinyl cation **6.6**. We attribute these geometrical changes in the singlet states to increasing carbene character and less double bond character in the singlet states as the  $\beta$  positions are substituted with increasingly strong pi donors. The geometries for the singlet states computed at the CASSCF/cc-pVTZ geometries and the level and the B3LYP level show only fair agreement. In particular, the vinylic C-C bond length is consistently longer at the CASSCF level of theory.

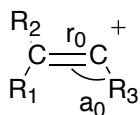


**Table 2.** Select singlet and triplet geometrical parameters for **1-10**:  $r_0$  represents the vinyl CC bond length,  $a_0$  represents the vinyl C-C- $R_3$  bond angle. B3LYP/6-31G(d,p), (CASSCF/cc-pVTZ).

Compound Number	R <sub>1</sub>	R <sub>2</sub>	R <sub>3</sub>	Singlet $r_0$ (Å)	Singlet $a_0$ (deg)	Triplet $r_0$ (Å)	Triplet $a_0$ (deg)
<b>6.1</b>	H	H	H	1.262 (1.270)	180.0 (179.9)	1.400 (1.385)	137.6 (133.8)
<b>6.2</b>	OH	H	H	-- (1.317)	-- (172.0)	1.394 (1.407)	138.3 (131.5)
<b>6.3</b>	OMe	H	H	-- (1.342)	-- (139.4)	1.389 (1.412)	138.3 (131.2)
<b>6.4</b>	NH <sub>2</sub>	H	H	1.309 (1.338)	142.4 (137.1)	1.386 (1.411)	140.0 (132.3)
<b>6.5</b>	NMe <sub>2</sub>	H	H	1.359 (1.438)	126.7 (111.5)	1.371 (1.407)	143.7 (135.3)
<b>6.6</b>	NH <sub>2</sub>	NH <sub>2</sub>	H	-- (1.471)	-- (109.0)	1.422 (1.445)	136.6 (130.0)
<b>6.7</b>	NH <sub>2</sub>	H	F	1.421	123.9	1.392	126.4
<b>6.8</b>	F	F	H	1.338 (1.344)	156.2 (177.5)	1.402 (1.409)	136.9 (129.9)
<b>6.9</b>	F	F	F	1.439	127.4	1.416	125.2
<b>6.10</b>	F	H	CH <sub>3</sub>	1.306	125.3	1.932	119.9

a. classical singlet form. a. B3LYP/6-31G(d,p). b. CASSCF/cc-pVTZ

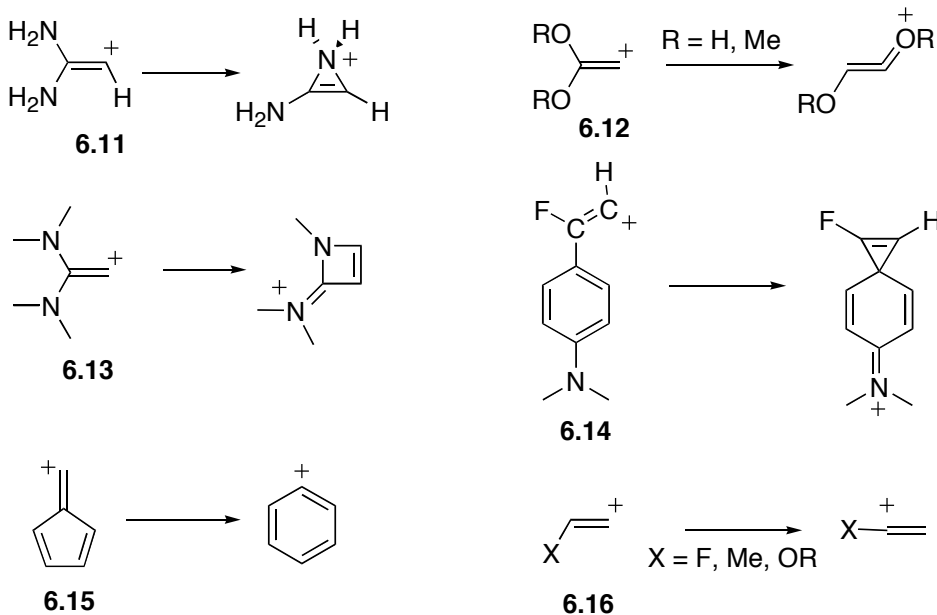
For many of these species, the singlet states are predicted to be prone to rearrangements.<sup>135</sup> In some cases, minima were found for the singlet states at the CASSCF/cc-pVTZ level but rearrangements were found to occur apparently without a barrier at the DFT level of theory (since CBS-QB3 employs a B3LYP optimization, any structures that rearrange at the B3LYP level likewise rearrange when employing CBS-QB3). This was the case for the hydroxy- **6.2**, methoxy- **6.3**, and diamino- **6.6** substituted vinyl cations. Given that CASSCF is a more rigorous model theory than DFT, these structures probably have minima on their singlet potential energy



surfaces, but likely with a barrier for rearrangement that is very small. In other cases, such as with the amino- **6.4** and dimethylamino- **6.5** substituted vinyl cations, minima were found for the singlets at the DFT level, but the barriers for undergoing 1,2-hydride shifts were predicted to be smaller than the zero-point vibrational energy (a barrier of 0.1 kcal/mol for **6.4** and 0.8 kcal/mol for **6.5**). In contrast, the triplet states for **4** and **5** appear less likely to rearrange. The hydride shift rearrangement for triplet **4** and **5** are predicted to be downhill by 0.4 kcal/mol for **4**, but with very large energy barriers of 56.4 kcal/mol. Thus, the triplet states are not anticipated to be prone to rearrangements by hydride shifts. These computations lead to the conclusion that generation of these species in the singlet states will lead to rapid rearrangement prior to intersystem crossing. On the other hand, the triplet states in these substituted vinyl cations may be stabilized sufficiently to permit photochemical generation by triplet sensitization to access reactions from the triplet manifold where rearrangements appear unlikely at ambient temperature.

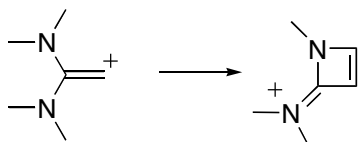
Other “spontaneous” rearrangements seen at the DFT level for various  $\beta$  pi-donor substituted species were observed for the singlet species shown in Scheme 6.1. The left-most structure corresponds to the approximate input geometry and the structure to the right of the arrow indicates the optimized structure. We note that we were unable to locate any minima corresponding to non-classical structures similar to the bridged structure seen in the parent vinyl cation for the singlet substituted species. Inputting geometries for non-classical bridged vinyl cations **6.2-6.10** leads to either the rearranged structure or the classical open singlet structure upon optimization. Of

course, there is always the possibility that other low-energy non-classical structures exist that we have not considered.



**Scheme 6. 1.** Examples of singlet rearrangements at the DFT (B3LYP/6-31G(d,p)) level.

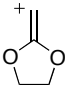
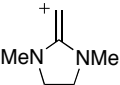
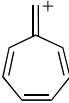
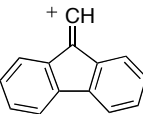
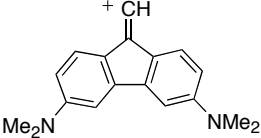
Particularly revealing is the rearrangement observed for the singlet 2,2-bis(dimethylamino)vinyl cation (Scheme 2). No minimum was found for a classic vinyl cation structure; rather, this singlet vinyl cation spontaneously undergoes an insertion at the DFT level of theory to give a four-membered ring. This rearrangement appears to agree with the idea that strong  $\beta$  pi donors make the singlet state resemble a singlet carbene, as this rearrangement appears to be a carbene-like C-H insertion.



**Scheme 6. 2 Spontaneous C-H insertion**

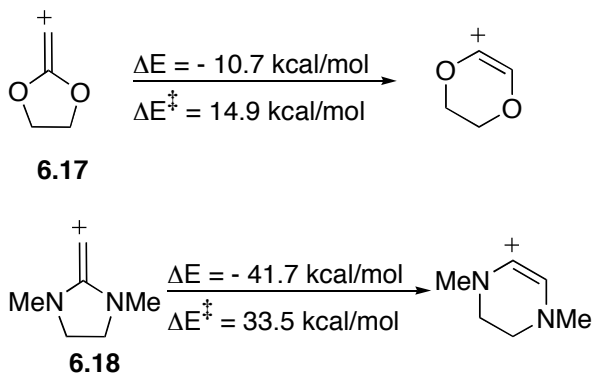
*6.7. Incorporation of the pi donors into rings.*

We close by noting a series of these vinyl cations that are particularly inviting for experimental studies because they appear less likely to rearrange. These are systems where the pi donors have been incorporated into rings (see Figure 3). In all but one case, the magnitudes of the singlet-triplet gaps are large enough to be considered outside the likely error of the calculations. We anticipate **6.11-13**, **6.15** to be ground-state triplet vinyl cations. For **6.14**, **6.15** the system size was sufficiently large to permit only a DFT calculation. Since the DFT results typically underestimate the singlet stability by 3-6 kcal/mol relative to the higher-level methods, no firm predictions can be made for **6.14** on its expected ground state, except to say that the singlet and triplet state energies are likely to be nearly degenerate.

COMPOUND #					
<b>6.17</b>	<b>6.18</b>	<b>6.19</b>	<b>6.20</b>	<b>6.21</b>	
<b>B3LYP/6-31G(d,p)</b>	+13.5	+15.4	+14.3	+ 4.6	+ 17
<b>CBS-QB3</b>	+9.2	+11.2	+10.0		

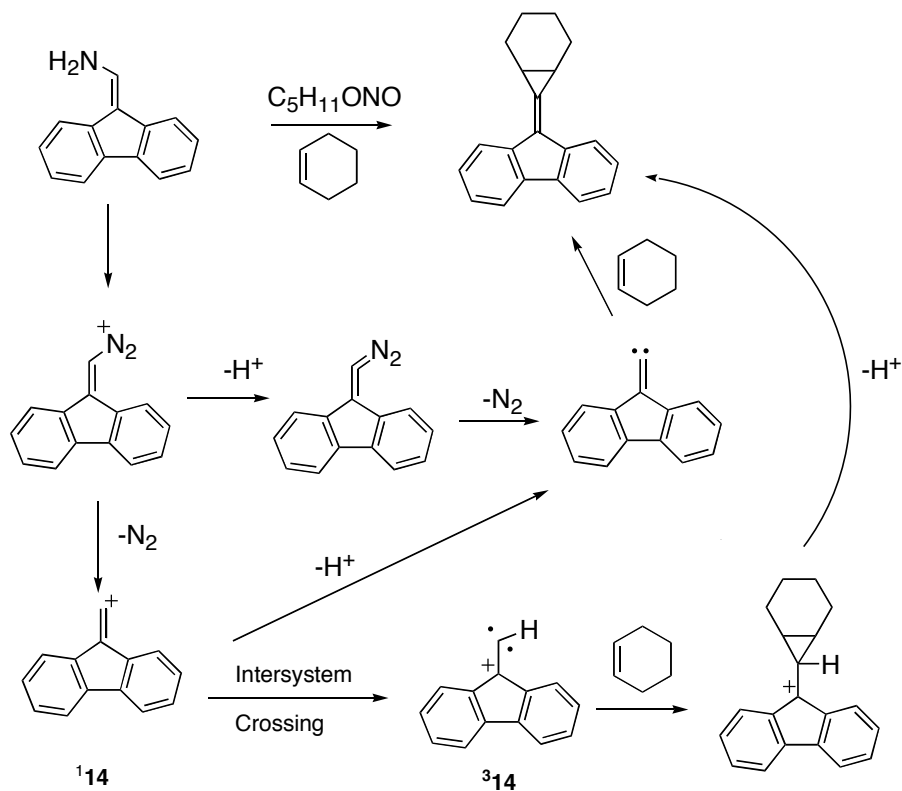
**Figure 3.**  $\Delta E_{ST}$  values for ring-constrained pi donor-substituted vinyl cations.

The only obvious rearrangement pathway for **6.11-15** in the singlet state is a ring expansion, much like the expansion that occurs apparently without a barrier for the cyclopentadienylidene vinyl cation to the phenyl cation. For the dioxane **6.11**, this ring expansion is computed to be a downhill process by 10.7 kcal/mol, but with an energy barrier of 14.9 kcal/mol. For the nitrogen analog **6.12**, this rearrangement is computed to be exergonic by 41.7 kcal/mol, but with a larger barrier of 33.5 kcal/mol. Since most of the methods used to generate carbenium ions generate the cations initially in the singlet state, these barriers to singlet rearrangement may be large enough to permit experimental observation of the singlet state by laser flash photolysis, and potentially large enough to allow the singlet to intersystem cross to the triplet state prior to rearrangement (we note that the ring-expanded vinyl cation is also computed to be a ground-state triplet by 1.8 kcal/mol by B3LYP<sup>136</sup>).



**Scheme 6. 3.** DFT rearrangement energies.

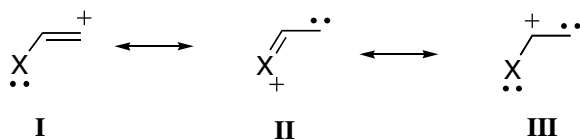
The fluorenylidene vinyl cation **6.14** may have been made previously. The reaction of the amino-substituted compound shown in Scheme 6.2 is with an alkyl nitrite and cyclohexene gives a carbene-like insertion product. Two mechanistic possibilities were considered. The reaction is thought to proceed through a vinyl diazonium ion intermediate. One possibility is loss of a proton from the diazonium intermediate to form a diazo compound, followed by loss of N<sub>2</sub> to give a vinylidene carbene, which undergoes cyclohexene insertion. The other considered mechanism involves loss of N<sub>2</sub> from the diazonium ion to give the vinyl cation, followed by deprotonation to give the vinylidene carbene. In light of this study, we propose a third possibility— involvement of a triplet vinyl cation. That is, formation of <sup>1</sup>**6.14** could be followed by intersystem crossing to give the triplet vinyl cation <sup>3</sup>**6.14**. Insertion into the cyclohexene double bond followed by loss of a proton could give the ultimate product. Even if **6.14** proves to have a singlet ground-state (we anticipate near-degenerate singlet and triplet state energies for this species), a low-energy triplet state may be thermally accessible if intersystem crossing is facile. Zollinger has also studied a system in which **6.14** may be an intermediate, obtaining singlet-like products resulting from a ring expansion in the presence of  $\sigma$  nucleophiles.



Scheme 6.5. An alternative mechanism for C-H insertion.

### 6.8. *The nature of the stabilized triplet state.*

Three canonical forms appear to be important for these pi-donor substituted vinyl cations (Scheme 6.3). Based on the geometrical parameters noted in Table 6.2 and the atomic charges computed at the APT level (Figure 6.3), the singlet states for the unsubstituted system or systems substituted with weak donors consist of primarily canonical structure **I**. When strong pi donors are added to the  $\beta$  position, all three canonical forms appear to be important, with the weights of **II** and **III** appearing to be directly correlated to the strength of the pi donor. All the triplet states appear to consist of **II** and **III**. The APT charges for **6.4** are shown in Figure 6.3. The stabilized triplet states for these  $\beta$ -substituted vinyl cations have significant carbenoid character, and closely resembles the electronic state of triplet phenyl cations.



**Scheme 6.4.** Important canonical forms for the  $\beta$ -substituted vinyl cations

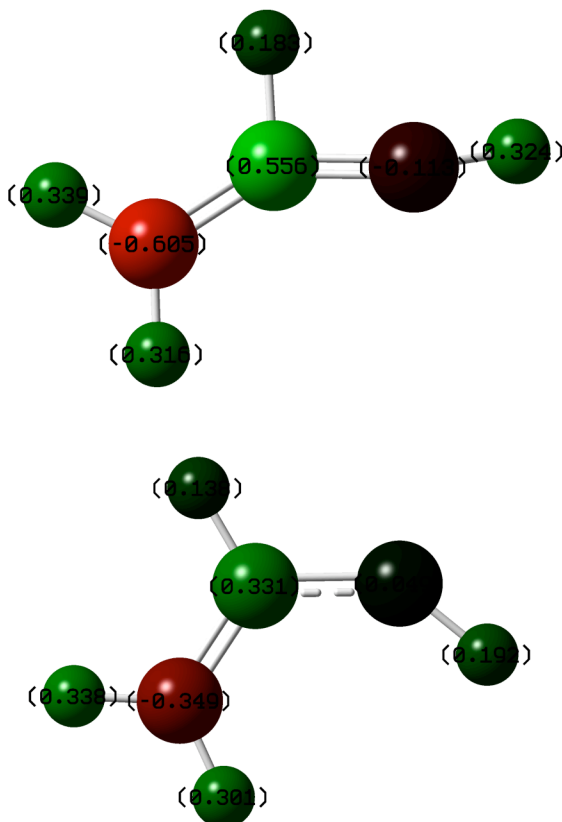


**Figure 6.3.** APT charges for 2-aminovinyl cation (BL3YP/6-31G(d,p)) singlet (top) and triplet (bottom). Fixed charges range from +1 (bright green) to -1 (bright red).

The triplet state of the cycloheptatrienyl vinyl cation **6.13** has a particularly intriguing triplet electronic structure. As shown by computed APT charges, the charge in the singlet state is highly localized on the two vinyl carbons and there is little delocalization throughout the ring. The triplet state, on the other hand, resembles an

aromatic cycloheptadienyl cation-substituted triplet carbene. Representations for the singlet and triplet state of **13** are shown in Figure 5. Significant delocalization of the positive charge is seen throughout the ring in the triplet state (but not in the singlet state), and inspection of the Mulliken atomic spin densities shows that essentially both spins reside on the exocyclic carbon in the triplet state (spin density = 1.68).

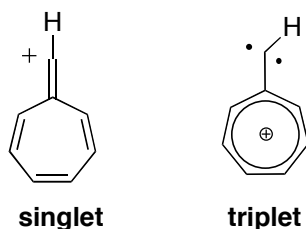


Figure 5. The singlet and triplet states of **6.13**.

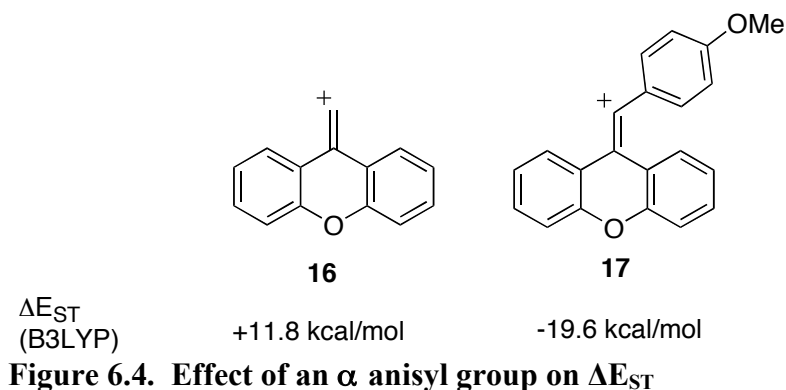
In conclusion, substitution of vinyl cations with  $\beta$  pi donors leads to stabilization of a carbene-like triplet state similar to the electronic state of triplet phenyl cations. Should many of these cations be experimentally generated in the singlet state, spontaneous rearrangements are likely to occur prior to intersystem crossing, although triplet sensitization methods may allow selective generation of the triplet vinyl cations. Vinyl cations with the pi donors incorporated into rings are particularly inviting for experimental studies because these species have no obvious singlet rearrangement pathways; these structures may be less prone to rearrangements from the singlet state prior to intersystem crossing.

Thus, while an implicit assumption in the discussion of most intermediate carbocations is that they adopt closed-shell singlet configurations, recent



computational studies performed in our lab<sup>71,104</sup> and others, however, have caused us to re-examine this assumption, particularly for charged systems where substitutions with pi donors have been shown to cause dramatic swings in the electronic state orderings. For example, recently reported CASPT2 calculations show that the parent benzyl cation ( $\text{Ph-CH}_2^+$ ) adopts a closed-shell singlet state electronic configuration with a large energy gap to the lowest-energy triplet state (45 kcal/mol). Upon substituting the two meta positions with strong pi donors, however, the triplet state is dramatically stabilized. At the CASPT2 level of theory, for instance, the 3,5-bis(dimethylamino)benzyl cation is predicted to have essentially degenerate singlet-triplet state energies!

These studies demonstrate that a very large singlet-triplet energy gap for the parent species is no guarantee that even simple substituted analogs will remain closed-shell singlets. Perhaps part of the reason these triplet vinyl cations may not have been postulated before experimentally is that a large number of the experimentally generated vinyl cations contain an  $\alpha$  donating group, often the anisyl group. This  $\alpha$  anisyl group appears to significantly stabilize the singlet state. To give one example, the unsubstituted xanthyl vinyl cation **6.16** is computed to be a triplet by 11.8 kcal/mol at the DFT level. The cation **6.17** (with the  $\alpha$  anisyl substituent), studied experimentally, is computed to be a singlet by 19.6 kcal/mol. See Figure 6.4. However, some published reports on  $\beta$ -substituted vinyl cations may reward re-examination in light of this finding.



### 6.9. Computational methods.

All DFT calculations were performed using the Gaussian03 software suite employing primarily the B3LYP functional that consists of Becke's three-parameter gradient-corrected exchange functional<sup>137,138</sup> and the LYP correlational functional of Lee, Yang, and Parr<sup>139</sup> along with the 6-31G(d,p) polarized double zeta basis set. Geometries, energies, and analytical frequencies were calculated at this level of theory. In all cases, optimized geometries were found to have zero imaginary frequencies, and corrections for the zero point vibrational energy were added unscaled. CASSCF optimizations were performed using Gaussian03,<sup>140</sup> but CASPT2 calculations were accomplished with the Molcas 7 program. Active spaces were comprised of all  $\pi$  electrons (including the two double bond electrons and any conjugated double bonds or lone pairs of the substituents) and all  $\pi$  orbitals.

Given that the CASSCF calculations show that all the singlet states for these vinyl cations consist almost entirely of a closed-shell determinant (weights greater than 0.9 for the principle closed-shell determinant were observed for all singlet states

computed at the CASSCF level), we elected to use only restricted DFT energies and geometries for the singlet states.

## 7. Chapter 7: Carbazolyl Nitrenium Ion: Electron Configuration and Antiaromaticity<sup>1</sup>

### 7.1. Introduction

In this chapter, we demonstrate that laser flash photolysis of 1-(carbazol-9-yl)-2,4,6-trimethylpyridinium tetrafluoroborate generates the carbazolyl nitrenium ion ( $\tau = 333$  ns,  $k_{\text{obs}} = 3.0 \times 10^6 \text{ M}^{-1}\text{s}^{-1}$ ) having absorption bands at 570 nm and 620 nm in  $\text{CH}_3\text{CN}$ . The nitrenium ion is found to have reactivity comparable to structurally similar closed-shell diarylnitrenium ions, but spectroscopic evidence favors an open-shell singlet diradical assignment for the observed nitrenium ion. The carbazolyl nitrenium ion is also more reactive than diarylnitrenium ions as a likely result of antiaromatic character. *Ab initio* and hybrid DFT calculations were performed to address the degree of antiaromaticity in this and similar nitrenium ions through analysis of optimized geometries, nucleus independent chemical shifts, and isodesmic reactions.

Nitrenium ions are nitrogen-containing reactive intermediates of the formula  $\text{RNR}^{2+}$ ; they are isoelectronic to the more-familiar carbene family of intermediates, and have lifetimes that seldom exceed 100  $\mu\text{s}$ .<sup>23-26</sup> Many of the studies of nitrenium ions have come as a result of evidence that aryl nitrenium ions ( $\text{Ar-N-R}^+$ ) are formed *in vivo* from enzymatic oxidation of arylamines. Due to their extreme electrophilicity, nitrenium ions add to weakly nucleophilic cellular moieties such as proteins and DNA.<sup>45,50,141</sup> The addition of nitrenium ions to DNA has the potential to kill a healthy cell or begin the process to convert it into a cancerous one, and nitrenium ions

---

<sup>1</sup> Taken in part from: Winter, A. H.; Gibson, H. H.; Falvey, D. E. *J. Org. Chem.* **2007**; 72(22); 8186-8195.

have been implicated as the “ultimate carcinogen”<sup>142</sup> of certain anilines and other nitrogen-containing aromatics.<sup>52</sup> On a more positive note, nitrenium ions have also been proposed to be intermediates in the synthesis of the conducting material poly(aniline),<sup>51,53</sup> and have been exploited for useful synthetic purposes, particularly in ring-forming reactions.<sup>43,44,143,144</sup> While most of the recent work on nitrenium ion chemistry has focused on arylnitrenium ions (Ar-N-H<sup>+</sup>), less attention has been given to other kinds of nitrenium ions such as alkylnitrenium ions or nitrenium ions derived from heteroaromatic systems.

To distinguish between nitrenium ions with the formally cationic nitrogen located outside of a ring and those with the cationic nitrogen contained within a ring, we use the term *endocyclic* nitrenium ions to describe nitrenium ions with the formally cationic nitrogen contained within a ring (e.g. all nitrenium ions in Figure 1), and *exocyclic* nitrenium ions for those with the formal nitrenium center outside of a ring (e.g. Ph-N-H<sup>+</sup>).

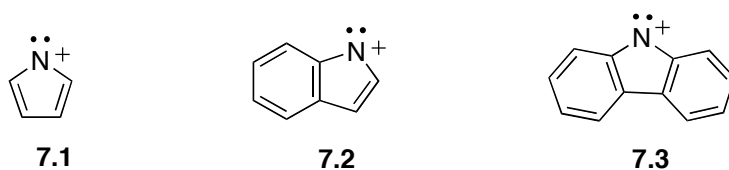


**Figure 7.1** Endocyclic nitrenium ions.

We were particularly interested in the structures of the *endocyclic* nitrenium ions shown in Figure 1 because each possibly has antiaromatic character. The cyclopentadienyl cation is one of the most well known antiaromatic ring systems, and it has a recorded ESR triplet spectrum.<sup>94</sup> The pyrrolyl nitrenium ion **7.1** is its

nitrenium ion analogue, and the indolyl nitrenium ion **7.2** and the carbazolyl nitrenium ion **7.3** both contain this formally antiaromatic core. While the carbocation analogues of **7.1-3** have seen extensive studies and debate regarding the degree of antiaromaticity in these cations,<sup>94,145-150</sup> the nitrenium ions **7.1-3** have received little study.<sup>151-153</sup> Moreover, we were intrigued by the possibility for unusual ground state or low-energy electron configurations in these nitrenium ions that may be favored to avoid any antiaromatic character present in their closed-shell singlet configurations.

For any nitrenium ion, three possibilities for the electronic configuration of the singlet state are typically considered (see Figure 7.2).<sup>23</sup> The only electron configuration of the singlet state that has been observed experimentally is the  $n^2$  singlet state, in which both of the electrons reside in a hybridized non-bonding  $n$  orbital. An open shell  $n,p$  singlet configuration and a closed shell  $p^2$  configuration are usually ruled out on principle because they put electrons into a higher energy  $p$  orbital. In the cases of structures **7.1**, **7.2**, and **7.3**, however, certain energetic advantages can be envisaged for both of these configurations that might compensate for placement of the electrons in higher energy orbitals. For example, in both the  $p^2$  singlet state and the open shell  $n,p$  singlet state any antiaromaticity (if present) is avoided. Moreover, the  $p^2$  singlets may have the added stabilization of additional aromatic character.

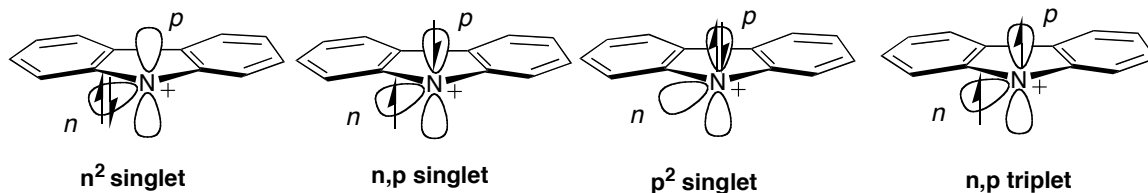


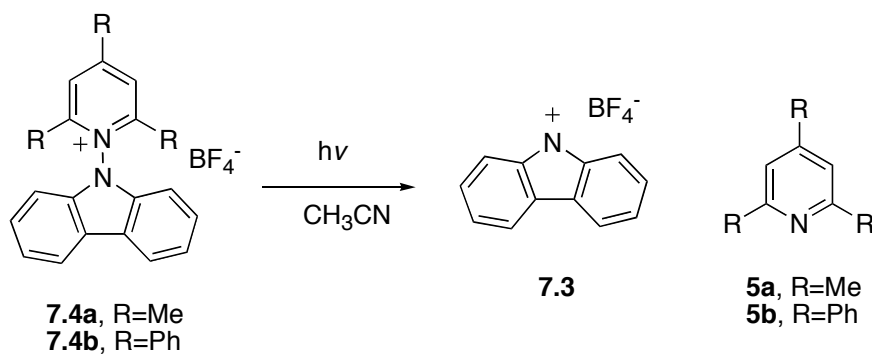
**Figure 7.2.** Possible electronic configurations for carbazolyl nitrenium ion

Additionally, one expects that each of these three configurations for the singlet state should exhibit different reactivity. Typical closed shell  $n^2$  singlet arylnitrenium ions react with nucleophiles at the ortho and para sites of the phenyl rings (addition to nitrogen is sometimes observed with certain pi nucleophiles). Little is known of the reactivity of open-shell  $n,p$  singlet states for carbenes or nitrenium ions, but intuition suggests that they would likely react more like diradicals than typical closed-shell singlet species. Likewise, little is known of  $p^2$  singlet states for carbenes or nitrenium ions (certain palladadiphosphanyl carbenes<sup>154</sup> are thought to be  $p^2$  singlets), but a  $p^2$  singlet nitrenium ion would be anticipated to react like an aryl or vinyl carbenium ion, with exclusive nucleophile addition at the cationic nitrogen (which cannot delocalize the charge through resonance like the  $n^2$  singlet can). All of the known examples of triplet nitrenium ions react by hydrogen atom transfer mechanisms, usually to form the reduced amine as the ultimate photoproduct.

We chose the carbazolyl nitrenium ion **7.3** as the best candidate for experimental studies. As a result of its greater conjugation, we anticipated that it would be longer lived and have more favorable absorption properties than **7.1** and **7.2**, and thus have a greater chance of direct observation using our LFP system.

## 7.2. Generation of the nitrenium ion.

The carbazolyl nitrenium ion was generated by photolysis of 1-(carbazol-9-yl)-2,4,6-trimethylpyridinium tetrafluoroborate **7.4a** as shown in Scheme 1. Upon absorption of ultraviolet light, *N*-aminopyridinium salts are known to undergo heterolytic N-N bond scission to generate the nitrenium ion and the pyridine derivative **7.5**.<sup>42,48,155</sup> Barring rapid intersystem crossing of the excited singlet state of the pyridinium salt precursor **7.4** to its excited triplet state prior to N-N bond scission, nitrenium ions generated from these precursors are initially made in a singlet state, irrespective of whether this configuration is the ground state electron configuration.



**Scheme 7. 1.** Generation of the carbazolyl nitrenium ion.

Upon laser flash photolysis (LFP) of **7.4a**, a short-lived species ( $\tau = 333$  ns,  $k_{\text{obs}} = 3.0 \times 10^6 \text{ M}^{-1}\text{s}^{-1}$ ) having absorption bands at 570 nm and 620 nm was observed (Figure 7.3). Based upon diagnostic LFP studies, chemical trapping experiments, and product analyses discussed below, we assign this transient to the singlet carbazolyl nitrenium ion **7.3**.



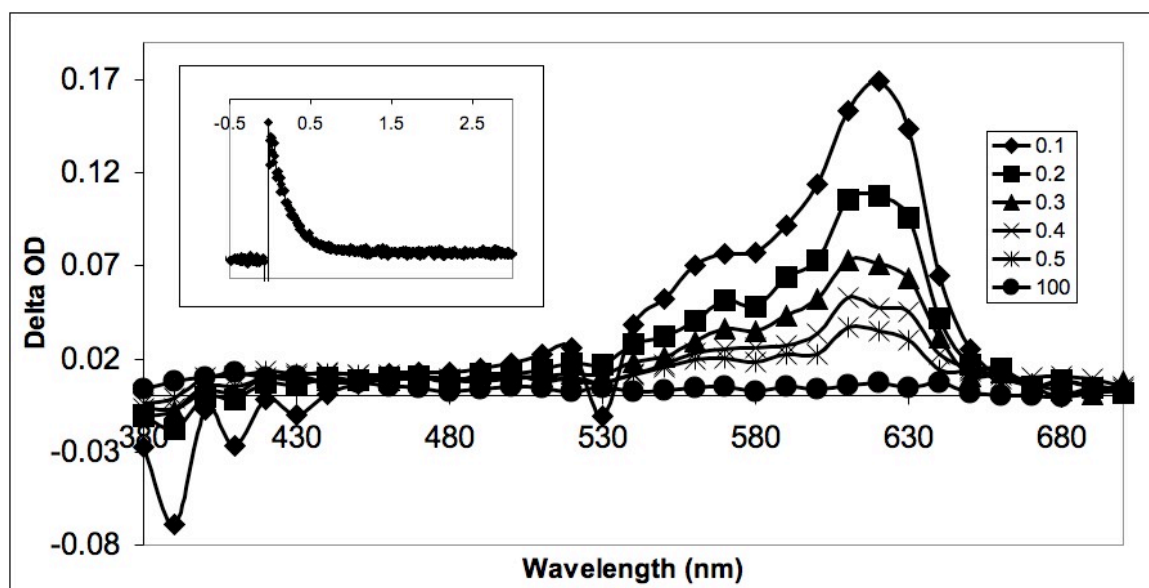
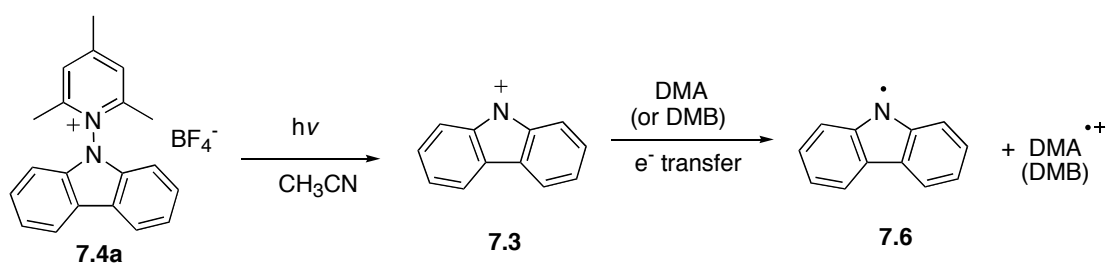


**Figure 7.3.** LFP of **7.4a** in  $\text{CH}_3\text{CN}$ . Timescale in  $\mu\text{s}$ . Inset shows waveform at 620 nm.

### 7.3. Evidence for a nitrenium ion intermediate.

Consistent with the proposed intermediacy of a nitrenium ion intermediate, LFP experiments of **7.4a** in the presence of electron donors show that the observed intermediate undergoes electron transfer reactions. For example, LFP of **7.4a** in the presence of dimethylaniline (DMA) or dimethoxybenzene (DMB) shows transients corresponding to the carbazolyl radical **7.6** and the cation radical of the donor. See Scheme 7.2.



**Scheme 7.2.** Electron transfer between **7.3** and electron donors.

Figure 4 shows the transient spectrum of **7.4a** in the presence of DMA (see Supporting Information for LFP of **7.4a** in the presence of DMB). The peak at 470 nm is readily assigned to the known absorption of the radical cation of DMA and the peaks at 570 and 620 to the carbazolyl radical **7.6**. The reference spectrum of the carbazolyl radical was obtained by LFP of *N*-nitrosocarbazole in CH<sub>3</sub>CN which gave absorption bands at 570 nm and 620 nm that are qualitatively indistinguishable from a previously published spectrum of this radical.<sup>156</sup>

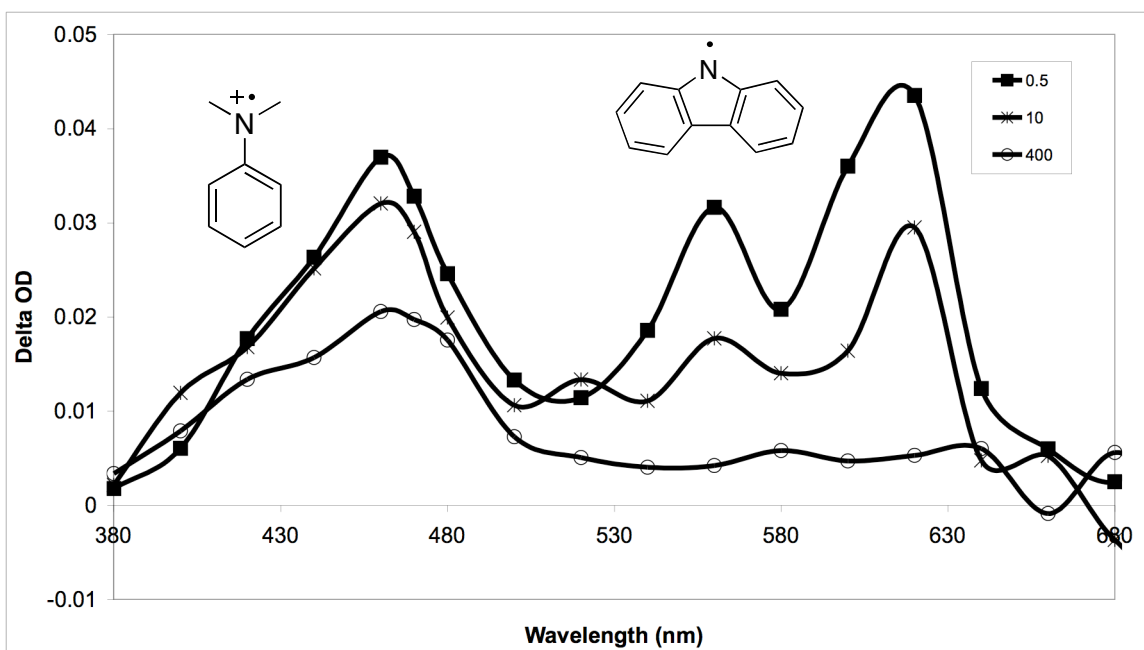


**Figure 7. 4.** LFP of **7.4a** in the presence of DMA Timescale in  $\mu$ s.

Previous studies by Bogdal<sup>152,153</sup> on the photoproducts of the triphenylpyridinium precursor **7.4b** in the presence of mesitylene suggested that the photochemistry of **7.4b** derives from its triplet state because of the formation of products characteristic of radical intermediates. Based on his studies, we considered the possibility that the

trimethylpyridinium salt **7.4a** might follow a similar photochemical pathway. However, we find no evidence that the photochemistry of **7.4a** proceeds through its triplet excited state. On the contrary, as described below, product analyses and trapping rate constants are more consistent with the intermediacy of a singlet nitrenium ion than a triplet. Additionally, attempts to generate the nitrenium ion through triplet sensitization of **7.4a** were unsuccessful. For example, we observed no quenching of the triplet excited states of benzophenone or xanthone upon addition of **7.4a**. Given that benzophenone and xanthone have reasonably large triplet energies of 69 kcal/mol and 74 kcal/mol, respectively, this result suggests that the triplet state of **7.4a** is higher in energy than 74 kcal/mol and is likely not an intermediate in the photochemical pathway from direct photolysis.

One potential hazard of analyzing the photoproducts of **7.3** is that the nitrenium ion reacts with carbazole via electron transfer to give the carbazolyl radical **7.6** and the carbazolyl radical cation (see Figure 4). LFP of **7.4a** in the presence of carbazole gives absorptions that can be assigned to the carbazolyl radical (570 nm and 620 nm) and the carbazolyl radical cation **7.6** (660 nm, 720 nm),<sup>157</sup> derived from electron transfer from carbazole to the nitrenium ion **7.3**.<sup>158</sup> Therefore, any accumulation of carbazole or carbazole addition photoproducts could spuriously give stable products consistent with triplet radical chemistry from electron transfer between the photoproducts and **7.3**. In fact, while we observe no transients in the LFP spectrum of the freshly-prepared triphenylpyridinium salt **7.4b**, after 20 pulses of 355 nm laser light on a solution of **7.4b** in CH<sub>3</sub>CN, a signal corresponding to the carbazolyl radical

is observed that increases in intensity with further laser photolysis. LFP of freshly replenished **7.4b** in the presence of carbazole likewise shows a transient consistent with the carbazolyl radical.

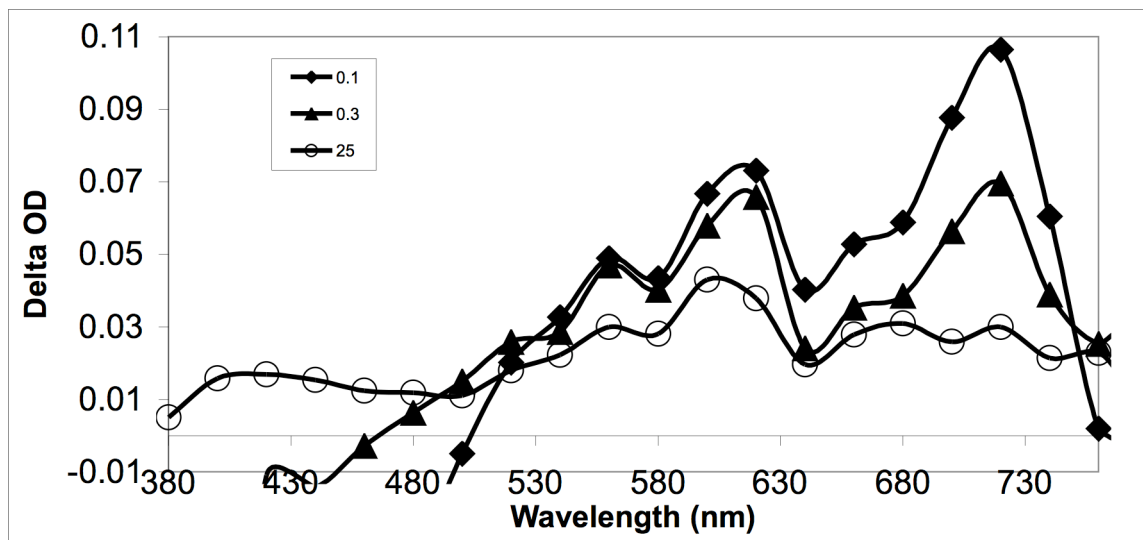
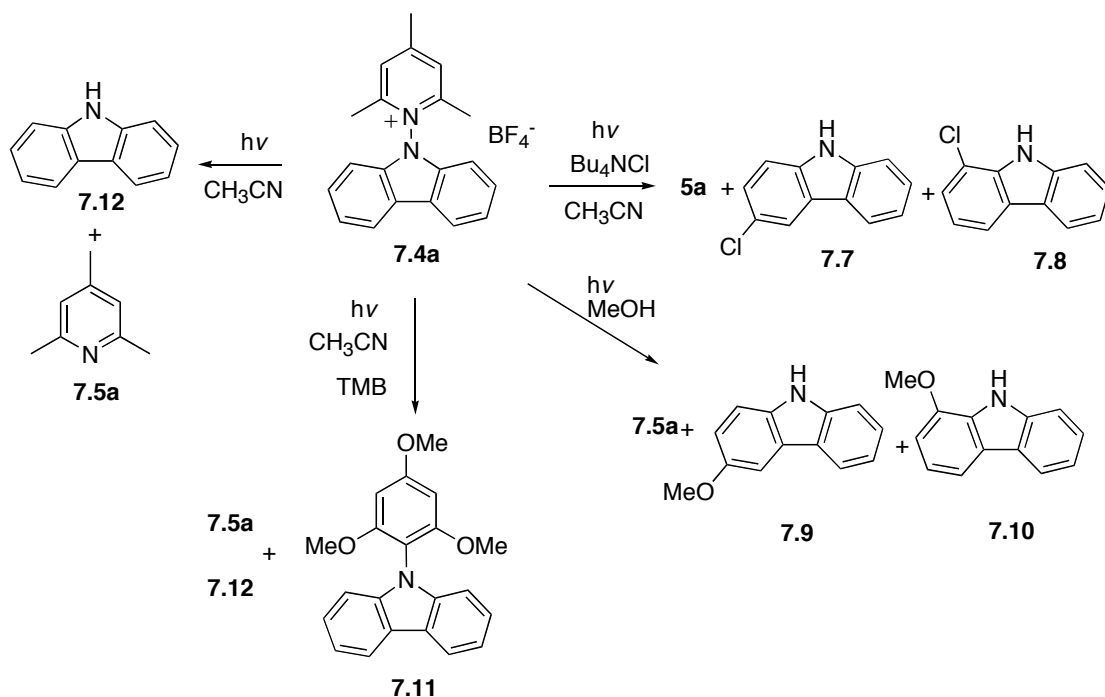


**Figure 7.5.** LFP of **7.4a** in the presence of carbazole. Timescale in  $\mu\text{s}$ .

A simpler explanation of why triplet products are observed from photolysis of **7.4b** while singlet behavior is seen from photolysis of **7.4a** is that **7.4b** may undergo rapid intersystem crossing of the precursor excited singlet state to its triplet excited state before N-N bond scission, while **7.4a** undergoes N-N bond scission from the excited singlet state. That is, excitation of **7.4b** into its excited singlet state is followed rapidly by intersystem crossing to the excited triplet state and subsequent N-N bond scission to make the triplet nitrenium ion. The triplet nitrenium ion could be too short-lived to be detected using our LFP system, or it may have too weak (or unfavorably positioned) absorption bands to be observed. This explanation agrees most closely with the results obtained by Bogdal and the lack of any observable transient species upon LFP of fresh **7.4b** in  $\text{CH}_3\text{CN}$ .

#### 7.4. Product studies.

Analysis of the products obtained from photolysis of **7.4a** in the presence of traps is consistent with the intermediacy of a singlet nitrenium ion (Scheme 3). While triplet nitrenium ions react primarily by hydrogen atom abstraction reactions, the hallmark experiment for closed-shell singlet aryl nitrenium ions is their reaction with nucleophiles in the ortho and para positions of the aromatic ring. Consistent with the chemistry of other closed-shell singlet aryl nitrenium ions, when the photolysis of **7.4a** is carried out in solvent methanol, two methoxy adducts are obtained. These adducts are 3-methoxycarbazole **7.9** and 1-methoxycarbazole **7.10** as identified by comparison (TLC, GC, GC-MS) with authentic samples (in approximately a 64:36 ratio of the 3-chlorocarbazole to 1-chlorocarbazole based on GC area percent). Similarly, two chloro adducts are obtained when **7.4a** is photolyzed in the presence of chloride ion (as *n*-Bu<sub>4</sub>NCl) in CH<sub>3</sub>CN. One of the chloro adducts is definitively identified as 3-chlorocarbazole **7** by comparison (TLC, GC, GC-MS) with an authentic sample; the identity of the other chloro adduct has not been rigorously established but is presumed, by analogy to the reactivity of the carbazolyl nitrenium ion with methanol (and the known reactivity of other singlet aryl nitrenium ions with chloride) to be the 1-adduct **7.8** resulting from addition of chloride to the 1 position of the carbazole (in approximately a 60:40 ratio of the 3-chlorocarbazole to the 1-chlorocarbazole based on GC area percent).



**Scheme 7.3.** Trapping product studies of **7.4a**.

One principal covalent adduct **7.11** is obtained when **7.4a** is photolyzed in the presence of the pi nucleophile 1,3,5-trimethoxybenzene (TMB), resulting from addition of the aromatic ring of TMB to the carbazole nitrogen.<sup>159</sup> This result is surprising in light of the previously-reported finding that diphenylnitrenium ion gives predominantly covalent adducts of TMB to the *ortho* and *para* carbons of the nitrenium ion rather than to nitrogen (30% *N* adduct, 66% *o/p* ring adducts for  $\text{Ph}_2\text{N}^+$ ).<sup>48</sup> The selective *N*-addition of TMB to **7.3** may be due in part to the forced planarity of the carbazole ring that could lead to more favorable rates for *N* addition than with the diphenylnitrenium ion, which opts to twist out of plane to minimize steric repulsion. Additionally, computations predict a high localization of positive charge on the nitrogen in the carbazolyl nitrenium ion (discussed in more detail below).

### 7.5. Trapping rate constants.

For several traps, pseudo first order trapping rate constants were also obtained (see Table 1). The nitrenium ion **7.3** reacts with both  $n$  and  $\pi$  nucleophiles at or near the diffusion limit. For example, the trapping rate constants for methanol, chloride, and 1,3,5-trimethoxybenzene were found to be  $9.8 \times 10^8 \text{ M}^{-1}\text{s}^{-1}$ ,  $3.5 \times 10^{10} \text{ M}^{-1}\text{s}^{-1}$ , and  $9.5 \times 10^9 \text{ M}^{-1}\text{s}^{-1}$ , respectively.<sup>160</sup> Additionally, 1,4-cyclohexadiene (CHD) was found to react near the diffusion limit with a rate constant of  $9.1 \times 10^9 \text{ M}^{-1}\text{s}^{-1}$ . The latter trap can serve as both a hydrogen atom donor (BDE = 74 kcal/mol<sup>161</sup>) or as a hydride donor depending on the reactivity of the nitrenium ion.<sup>162</sup> To distinguish between these two possibilities, a full transient LFP spectrum in the presence of excess CHD was obtained. If CHD were reacting as a hydrogen atom donor one would expect to observe transients corresponding to the carbazolyl radical cation. However, no such transients were observed upon LFP of **7.4a** in the presence of CHD. Given this negative result, it seems more likely that CHD is reacting as a hydride donor rather than a hydrogen atom donor.

**Table 7.1.** Comparison of trapping rate constants between **7.4a** and  $\text{Ph}_2\text{N}^+$ .

Trap	Rate Constant for trapping ( $\text{M}^{-1}\text{s}^{-1}$ )	Rate constant for trapping $\text{Ph}_2\text{N}^+$ ( $\text{M}^{-1}\text{s}^{-1}$ )
MeOH	$9.8 \times 10^8$	$5.2 \times 10^6$
1,3,5-Trimethoxybenzene	$9.5 \times 10^9$	$3.1 \times 10^9$
$\text{Bu}_4\text{NCl}$	$3.5 \times 10^{10}$	$1.0 \times 10^{10}$
1,4-cyclohexadiene	$9.1 \times 10^9$	$6.5 \times 10^6$

Comparison of these trapping rate constants to previously reported rate constants for trapping of the diphenylnitrenium ion in  $\text{CH}_3\text{CN}$  suggests that the carbazolyl nitrenium ion **7.3** is a significantly more reactive species. Particularly noteworthy is

that both methanol and 1,4-cyclohexadiene react with the carbazolyl nitrenium ion roughly three orders of magnitude faster than with the diphenylnitrenium ion. One possible explanation for these faster rates is that the destabilizing antiaromatic character of **7.3** (discussed in more detail below) leads to more favorable rates for nucleophilic attack and hydride transfer than with the diarylnitrenium ions.

Alternatively, the forced planarity of **7.3** might lead to slightly more favorable rates for hydride transfer through less steric crowding of the nitrogen as compared to diphenylnitrenium ion.

As further evidence of the chemical similarity to the diarylnitrenium ions, the carbazolyl nitrenium ion forms observable sigma adducts in the presence of pi nucleophiles. In particular, LFP of **7.4a** in the presence of 1,3,5-trimethoxybenzene (TMB) gives rise to a weakly absorbing long-lived transient at 400 nm in CH<sub>3</sub>CN (Figure 7.6).<sup>163</sup> We assign this transient to the sigma complex resulting from nucleophilic addition of the pi nucleophile to the nitrenium ion. See Scheme 7.4. One might expect that the lifetime of the sigma complex would decrease in more basic media (such as added pyridine) because of an accelerated rate of deprotonation. This is indeed the case, as the lifetime of the 400 nm transient decreases proportionally to the amount of pyridine added to the solution.



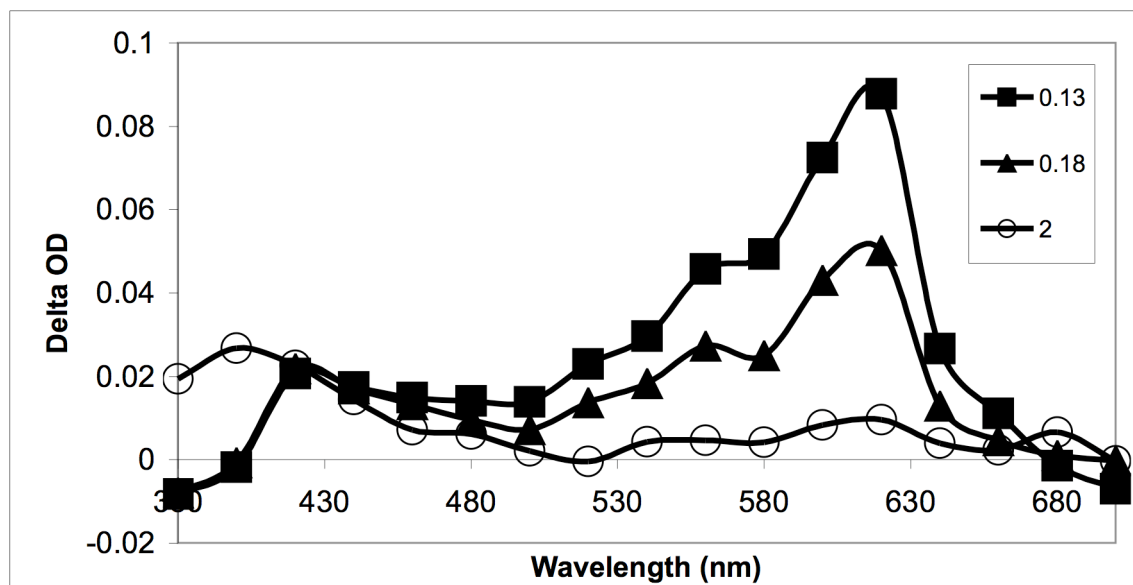
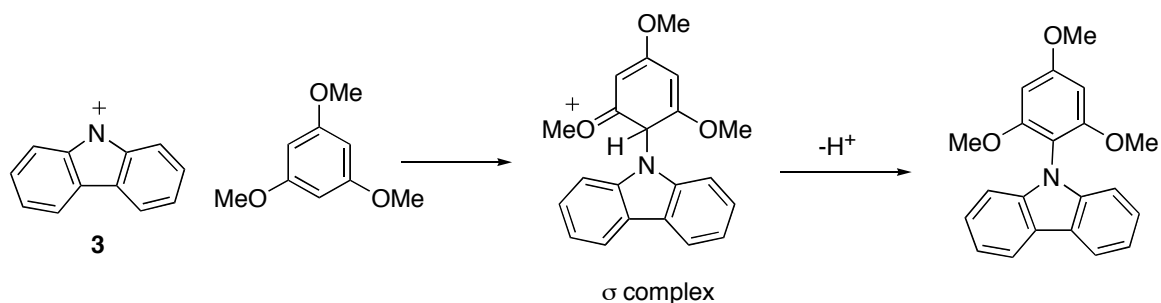


**Figure 7. 6.** LFP of 7.4a in the presence of TMB. Timescale in  $\mu$ s.



**Scheme 7. 4.** Addition of TMB to the nitrenium ion.

### 7.6. Computed singlet-triplet state energy gaps.

The energies of the singlet and triplet states of nitrenium ions **7.1-3** were computed using density functional theory (DFT) to obtain the adiabatic singlet-triplet energy gaps ( $\Delta E_{ST}$ ). The merits of DFT as a method for obtaining good quantitative estimates of the singlet-triplet gaps for nitrenium ions and other hypovalent species have been discussed elsewhere.<sup>40,71,73,76</sup> All three intermediates are predicted to be

ground state singlets, with the pyrrolyl nitrenium ion **7.1** predicted to have the smallest singlet-triplet energy splitting of -2.3 kcal/mol (a negative value indicates a singlet ground state). Benzannulation of the pyrrolyl nitrenium ion **7.1** to obtain **7.2** and **7.3**, as might be expected, alters the singlet-triplet gap in favor of the singlet, giving  $\Delta E_{ST}$  values of -5.8 and -7.8 kcal/mol, respectively.

Table 7.2. Singlet-triplet gaps.

Structure Number	$\Delta E_{ST}$ (B3LYP/6-31G(d,p))
<b>7.1</b>	-2.3, -2.3 <sup>a</sup>
<b>7.2</b>	-5.8
<b>7.3</b>	-7.8

a. B3LYP/6-311G(2d,p)//B3LYP/6-31G(d,p)

### 7.7. Electron configuration of the observed nitrenium ion.

While all of the reactivity of the observed transient is similar to the reactivity seen for previously-characterized closed-shell  $n^2$  nitrenium ions, three observations are suggestive of an  $n,p$  open-shell singlet diradical configuration.

First, the absorption spectrum of the nitrenium ion transient is very similar to that of the carbazoyl radical, with both intermediates having absorption maxima at 570 nm and 620 nm ( $\pm 5$  nm) in CH<sub>3</sub>CN (the two species can be distinguished from each other by the much longer lifetime and more defined 570 nm absorption of the radical). Assuming that the absorption bands derive principally from excitations of pi electrons, one would expect that the closed shell singlet carbazoyl nitrenium ion and the carbazoyl radical would have very different absorption spectra. On the other

hand, this same assumption leads to the prediction that the open-shell *n,p* diradical carbazolyl nitrenium ion would have an absorption spectrum very similar to the carbazolyl radical as a result of having the same electron occupation of the pi orbitals.

Second, the decay of the transient appears to be first order (see Figure 7.3). While the diphenylnitrenium ion ( $\text{Ph}_2\text{NH}^+$ ) has a facile unimolecular decay channel in the form of a Nazarov-like cyclization ( $\tau = 1.5 \mu\text{s}$ ) to ultimately form carbazole,<sup>47</sup> no such decay channel presents itself for the closed-shell singlet carbazolyl nitrenium ion. Despite this lack of an obvious decay channel, the carbazolyl nitrenium ion has a much shorter lifetime ( $\tau = 0.3 \mu\text{s}$ ) than  $\text{Ph}_2\text{N}^+$  in solution. The lifetime of the carbazolyl nitrenium ion transient is the same in  $\text{CH}_3\text{CN}$  and  $\text{CH}_2\text{Cl}_2$  (suggesting that the decay does not involve solvent), is insensitive to the presence of oxygen, laser intensity (and thus the concentration of nitrenium ions), and concentration of the precursor **7.4a**. The isolable photoproducts in the absence of traps were found to be carbazole and collidine (27% yield of carbazole and ca. 100% yield of collidine after 54% decomposition of a 0.01M **7.4a** solution in  $\text{CH}_3\text{CN}$ ). The remaining uncharacterized product(s) is an insoluble residue that is presumably poly(carbazole) oligomers similar to those seen for diphenylnitrenium ion from reaction of the nitrenium ion with accumulated photoproducts.<sup>47,42</sup>

Lastly, while previously-reported time-dependent density functional theory (TD-DFT) calculations of diphenylnitrenium ion and its halogen-substituted analogs give predicted absorption band locations in good agreement with those found from

experiment,<sup>155</sup> the predicted bands for the carbazolyl nitrenium ion do not match well with the observed spectrum of the carbazolyl nitrenium ion. In the previous study, TD-DFT calculations predicted absorptions at 645 nm, 637 nm, and 647 nm for the diphenylnitrenium ion, 4,4'-dichlorodiphenylnitrenium ion, and 4,4'-dibromodiphenylnitrenium ion, respectively, close to the experimentally found absorptions of 640 nm, 670 nm, and 690 nm. Also of relevance, TD-DFT predicts absorption bands for the carbazolyl radical at 643 nm and 525 nm, in reasonable agreement with the observed bands at 620 nm and 570 nm. However, a TD-DFT calculation (B3LYP/6-311G(d,p)) on the closed-shell singlet carbazolyl nitrenium ion gives predicted absorption bands at 249 nm and 488 nm, in poor agreement with the observed absorptions at 570 nm and 620 nm

Few reasonable decay pathways can be proposed that are consistent with these results and the identity of the transient as the closed-shell  $n^2$  singlet nitrenium ion. One possibility is that the nitrenium ion **7.3** decays to give a nitrenium ion of a different electron configuration that has unfavorable absorption properties or absorption bands outside the detection window of our LFP spectrometer. For example, the singlet nitrenium ion could undergo intersystem crossing to give the triplet carbazolyl nitrenium ion. This possibility is unlikely given that DFT predicts the closed-shell singlet to be the ground state with a reasonably large energy gap (7.8 kcal/mol) to the triplet state. (Further, when DFT errs in predicting the singlet-triplet gap, it is almost always by overly favoring the triplet state.) Another possibility is that the closed-shell nitrenium ion decays to give a different singlet state configuration of **7.3**. This

possibility is also not supported by calculations, however, as both DFT (B3LYP) and small basis-set CASSCF(10,10)/3-21G calculations predict the closed-shell singlet state to be the lowest energy singlet electron configuration. The closed-shell singlet DFT wavefunction was found to be stable with respect to breaking orbital symmetry (restricted  $\rightarrow$  unrestricted stability), and CASSCF predicts that the lowest energy singlet configuration consists of primarily the  $n^2$  singlet state (0.82 determinant weight). On the other hand, if the observed transient is the  $n,p$  singlet excited state, an obvious unimolecular decay pathway is relaxation to the  $n^2$  singlet ground state. While a lifetime of  $\sim 0.3 \mu\text{s}$  is unusually long for an excited state, such a configurational change would be expected to be slow for the carbazolyl nitrenium ion because the change in orbital angular momentum resulting from the electron switching from the  $p$  to the  $n$  orbital is not similarly compensated by a change in spin angular momentum. In terms of chemical reactivity, however, the lifetime of the observed transient nitrenium ion is short, and product formation could arise from either the excited  $n,p$  singlet state or from the ground ( $n^2$ ) singlet state depending on the concentration and reactivity of the trap.

Thus, while the product studies, trapping rate constants, and LFP spectra in the presence of traps leave little doubt that the observed transient is a singlet nitrenium ion, the specific electronic configuration of the observed singlet nitrenium ion is less certain. The absorption spectrum and the first-order decay kinetics are most consistent with the detection of an excited  $n,p$  singlet state that relaxes to a lower-energy  $n^2$  state. However, the observed reaction products (which may arise from both

states) are not qualitatively distinct from those products formed from previously characterized  $n^2$  singlet diarylnitrenium ions. Given this consideration, along with our inability to directly detect any intermediates following the decay of the nitrenium ion, the current evidence for this transient being the  $n,p$  singlet carbazolyl nitrenium ion should be considered suggestive rather than definitive.

Part of the difficulty in determining a specific state assignment is that it is currently unclear whether an open-shell singlet  $n,p$  nitrenium ion would give products distinct from a closed-shell  $n^2$  singlet nitrenium ion. While to our knowledge no open-shell singlet nitrenium ion has been reported, certain arylnitrenes (Ar-N) have open-shell singlet states lower in energy than the closed-shell singlet states.<sup>18</sup> Unfortunately, the reactivity of these species offer little insight into the potential reactivity of an open-shell singlet nitrenium ion, as open-shell singlet arylnitrenes typically decay by formation of diazirines, followed by ring expansion to didehydroazepines.<sup>164</sup> The reactivity of open-shell singlet carbenes is likely more relevant to nitrenium ions than the reactivity of nitrenes; unfortunately, there are very few reports of open-shell singlet carbenes.<sup>165</sup> Certain 1,3- and 1,4- open-shell singlet diradicals have been shown to be trapped by nucleophiles such as chloride or alcohols, providing some precedence for an open-shell species with reactivity similar to closed-shell species.<sup>166,167</sup> However, because of the paucity of open-shell diradicals similar to nitrenium ions, the chemical behavior of an open-shell singlet nitrenium ion is unclear at this time. Therefore, further experiments and computations would be

necessary to rigorously identify the electron configuration of the observed singlet nitrenium ion.

### *7.8. Computational studies of antiaromaticity.*

Computational studies were performed to assess the antiaromaticity of the carbazolyl nitrenium ion and its smaller congeners **7.1** and **7.2**. As one of the central ideas of organic chemistry, the concepts of aromaticity and antiaromaticity continue to generate considerable interest and debate for various ring systems.<sup>168-171</sup> Hückel's rules, which are used to predict potentially aromatic and antiaromatic planar ring systems, postulate that ring systems containing  $4n+2$   $\pi$  electrons are aromatic and ring systems with  $4n$   $\pi$  electrons are antiaromatic. While each of the nitrenium ions **7.1**, **7.2**, and **7.3** is predicted to be antiaromatic by Hückel's rules, we turned to computational studies to assess the degree of antiaromaticity (if any) in each of these nitrenium ions.

Three primary measurements related to physical observables have found widespread use for describing the aromaticity or antiaromaticity of a given ring system. These include magnetic measurements such as nucleus independent chemical shifts (NICS)<sup>172</sup> and magnetic susceptibilities,<sup>173</sup> comparison of the thermodynamic stability between a closed ring system and its analogous open ring system,<sup>171</sup> and inspection of the preferred geometries of the ring.<sup>174,175</sup> While each of these criteria has debatable merit for assigning aromaticity/antiaromaticity in the absence of other evidence, there is general agreement that a case for aromaticity or antiaromaticity can be built by looking at the results of several of these measurements in combination. We chose the

following computational measures to assess the antiaromaticity of **7.1**, **7.2**, and **7.3**—the degree of double bond localization (or equalization) in the optimized geometries, the relative energies of the cyclic nitrenium ions versus their open-chain counterparts (as assessed by isodesmic reactions), and the nucleus independent chemical shift (NICS) values.

Typically, double bond localization and deviations from planarity are suggestive of anti-aromatic systems, whereas bond length equalization and planarity are suggestive of aromatic systems. Given these criteria, the pyrrolyl nitrenium ion **7.1** appears to have the most antiaromatic character and **7.3** the least (See Figure 7.7). The geometries for each of the ring systems were optimized with density functional theory (B3LYP/6-31G(d,p)). The optimized geometry of the pyrrolyl nitrenium ion shows slight puckering from planarity and highly localized double bonds, as demonstrated by alternating bond lengths around the ring. Both **7.2** and **7.3** retain double bond localization in the five-membered ring, although it is less pronounced in **7.2** than in **7.1**, and less still in **7.3** than **7.2**. Little, if any, double bond localization is seen in the six-membered rings of **7.2** and **7.3**.



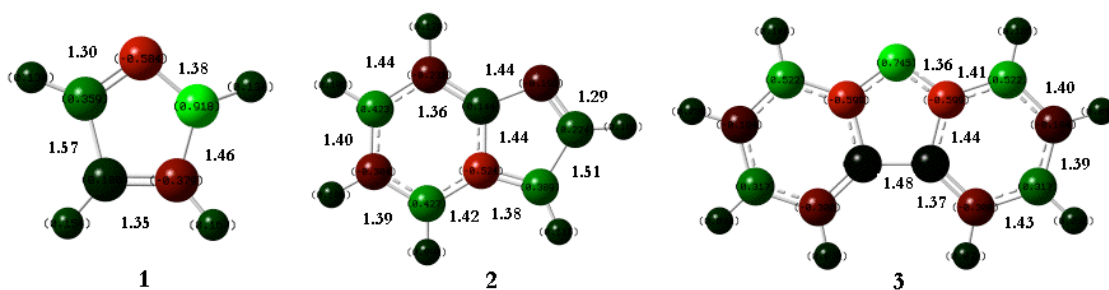
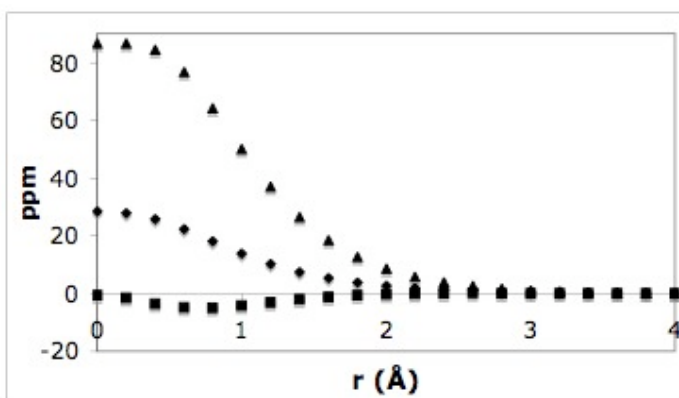
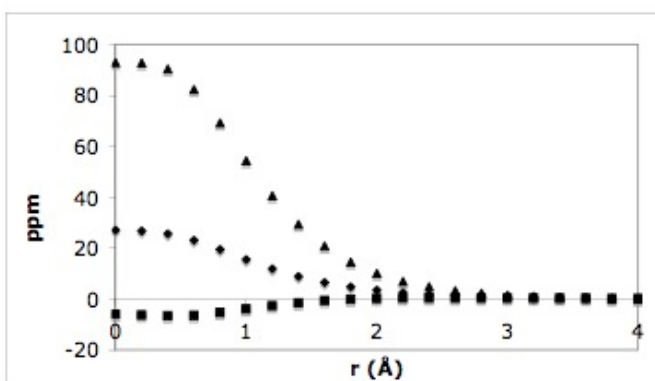


**Figure 7.7.** Bond lengths (Å) and APT charges for singlet states of **7.1**, **7.2**, and **7.3**. Fixed charges range from -1 (bright red) to +1 (bright green).

If the double bonds are localized, it follows that the positive charge should be localized as well. See Figure 7. Indeed, in the pyrrole nitrenium ion **7.1**, most of the positive charge (+0.92), as predicted by the APT method,<sup>176</sup> is assigned to a carbon adjacent to the nitrogen. The indolyl nitrenium ion **7.2** is predicted to have significant charge delocalization off the nitrogen with three carbons carrying significant charge. However, the carbazolyl nitrenium ion **7.3** is predicted to have most of the positive charge (+0.75) reside on the nitrogen, in contrast to **7.1** and **7.2**, with nitrogens predicted to be negatively charged. This charge accumulation on the nitrogen in the carbazolyl nitrenium ion is consistent with the exclusive formation of the N-adduct of 1,3,5-trimethoxybenzene in preference to ring-substituted products.

Nucleus independent chemical shifts are also consistent with significant antiaromatic character in each of the endocyclic nitrenium ions **7.1-3**. For each of the five-membered rings, the NICS values were plotted over a range of distances starting with the probe (Bq) positioned in the plane of the ring ( $r=0$  Å) and moving it to a distance above the ring ( $r = 4$  Å) using the method recently suggested by Stanger,<sup>177</sup> with separation of the in-plane and out-of-plane contributions (Figure 7.8). The

magnitude of the positive values for the out-of-plane components and the shape of the isotropic and out-of-plane curves for all three of these nitrenium ions are indicative of significant antiaromatic character in each of the five-membered rings. While it is tempting to use the magnitude of the NICS values to compare the relative antiaromaticities of **7.1-7.3**, it has been shown that the absolute NICS values cannot be compared for polycyclic ring systems because of the confounding effects of the neighboring rings.<sup>177</sup>



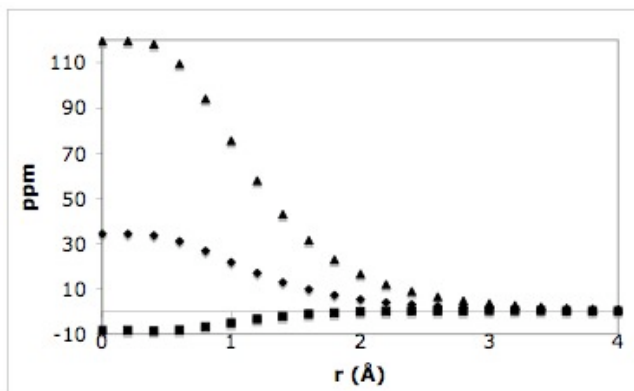
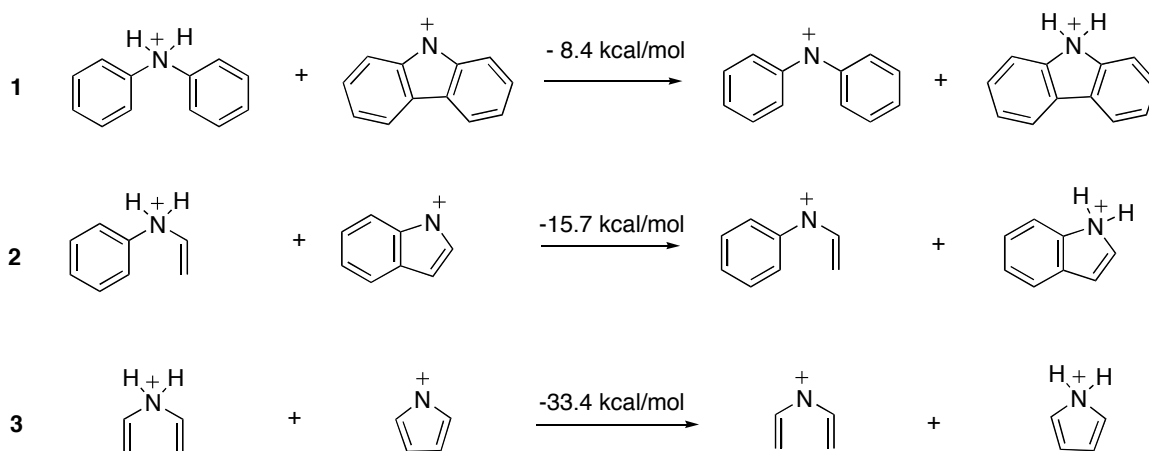


**Figure 7.8.** 7.1 (top), 7.2 (middle), and 7.3 (bottom). Triangles represent the out of plane component of the NICS value, squares the in-plane components, and diamonds the isotropic values. All values were obtained at the center of the five-membered rings.

Isodesmic reactions are consistent with the geometrical predictions of **1** being the most antiaromatic and **3** the least. Ideal isodesmic reactions balance strain, resonance energy, bonds and orbitals,  $\sigma$  (anti)aromaticity, and hyperconjugation between the reactants and products, and provide estimates of the aromatic stabilization energy or antiaromatic destabilization energy for a given ring system.<sup>149,178</sup> While ideal isodesmic systems are rarely available because of difficulties in perfectly balancing these parameters (these difficulties have been appreciated in particular for charged rings<sup>149</sup>), and because of difficulties in defining appropriate reference systems, well-chosen isodesmic reactions can show trends in a series from most (anti)aromatic to least and give estimates of the (anti)aromatic (de)stabilization energy.<sup>179</sup> We chose the three isodesmic reactions for hydrogen ( $H_2$ ) transfer, shown in Scheme 5, to compare the relative thermodynamic stabilities between **7.1**, **7.2**, and **7.3**. Hydrogen ( $H_2$ ) transfer rather than hydride ( $H^-$ ) transfer was chosen for these isodesmic reactions to avoid imbalances between the starting materials and products due to the

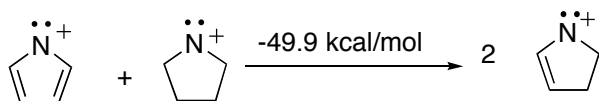
formation of a new aromatic ring. In all cases, H<sub>2</sub> transfer between the ring-opened amines and the nitrenium ions **7.1-3** was significantly favored energetically, suggesting antiaromatic character in each of these *endocyclic* nitrenium ions. Additionally, these reactions suggest that the pyrrolyl nitrenium ion **7.1** is the most destabilized by antiaromatic character (33.4 kcal/mol) and the carbazolyl nitrenium ion **7.3** the least (8.4 kcal/mol).



**Scheme 7.5.** Isodesmic reactions for hydrogen (H<sub>2</sub>) transfer (B3LYP/6-31G(d,p)).

An alternative isodesmic reaction involving H<sub>2</sub> transfer between the pyrrolyl nitrenium ion and pyrrolidenyl nitrenium ion is shown in Scheme 7.6. Similar isodesmic reactions have been used to estimate the antiaromatic destabilization energy of cyclobutadiene.<sup>180</sup> In principle, this isodesmic reaction gives an improved balance of strain energy from starting material to product than the isodesmic reaction in Scheme 7.5 by constraining all structures in five-membered rings. Unfortunately, analogous isodesmic reactions for the indolyl nitrenium ion **7.2** or the carbazolyl nitrenium ion **7.3** are less desirable because of imbalances in resonance energies and

aromaticity between the reactants and products. However, a significant energy difference of 16.5 kcal/mol between the isodesmic reaction shown in Scheme 6 and the isodesmic reaction in Scheme 7.5 suggests imbalances in one (or both) of these equations. Aside from steric imbalances, one possible explanation for the energy difference between these isodesmic reactions is that the reaction shown in Scheme 6, unlike the isodesmic reaction in Scheme 7.5, separates the resonance energy contribution of the two adjacent double bonds. While the differences in the energies for these two isodesmic reactions further emphasize the elusiveness of the concept of the (anti)aromatic (de)stabilization energy, and in particular the difficulty in obtaining appropriate reference systems, the qualitative conclusions that can be made from these reactions are still valid. These conclusions are that all three endocyclic nitrenium ions **7.1-3** are antiaromatic, and that **7.1** is the most destabilized by antiaromaticity and **7.3** the least.



**Scheme 7.6.** An alternative isodesmic reaction.

In conclusion, while the carbazolyl nitrenium ion **7.3** is more reactive than the diphenylnitrenium ion, it shares many of the same chemical behaviors, undergoing nucleophile addition at roughly diffusion-limited rates, accepting electrons from electron-rich species, and forming  $\sigma$  complexes in the presence of the pi nucleophile trimethoxybenzene. The sum of both the computational and experimental evidence presented above suggests that the carbazolyl nitrenium ion **7.3** is destabilized

sufficiently by antiaromatic character to make it more reactive than the diphenylnitrenium ion, but not so sufficiently as to make it favor an unusual ground state electron configuration. For the nitrenium ion observed by laser flash photolysis, spectroscopic evidence is most consistent with the assignment of an  $n,p$  singlet excited state configuration; however, the resulting products are not sufficiently distinct from those seen for previously-studied closed-shell singlet nitrenium ions to permit a definitive assignment. Experimental investigations of *endocyclic* nitrenium ions **7.1** and **7.2**, which are predicted by these computations to have a greater degree of antiaromaticity than the carbazolyl nitrenium ion, would be of considerable interest, as well as related endocyclic nitrenium ions with aromatic character such as those shown in Figure 7.9.

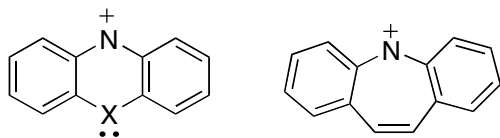


**Figure 7. 9.** Potentially aromatic endocyclic nitrenium ions

### 7.9. Computational methods.

All calculations were performed using the Gaussian03 software package.<sup>140</sup>

Geometries were optimized with density functional theory, in particular the B3LYP functional consisting of Becke's three-parameter correlation functional<sup>137,138</sup> and Lee, Yang, and Parr's exchange functional,<sup>139,181</sup> along with the polarized double-zeta 6-31G(d,p) basis set. All optimized geometries, except where noted, were found to have zero imaginary frequencies, and the singlet states were found to be stable with respect to orbital symmetry breaking. Zero-point vibrational energy corrections were

added unscaled. A preliminary CASSCF(14,13)/STO-3G calculation, which included all pi orbitals (minus the highest antibonding  $a_2$  pi orbital) and the  $n$  orbital on nitrogen in the active space, was performed on the singlet carbazolyl nitrenium ion at the DFT-optimized geometry. From this calculation, orbitals in the active space with occupations greater than 1.96 or less than 0.04 were removed for the larger basis set calculations. These included the highest remaining pi\* orbital ( $b_1$  symmetry), the  $n$  orbital ( $a_1$  symmetry), and the second pi bonding orbital ( $a_2$  symmetry). After removal of these orbitals, the remaining 10,10 active space was used for all larger basis set calculations. NICS values were computed using the GIAO method at the Hartree-Fock level with the 6-31+G(d) basis set at the DFT-optimized geometries.

### Materials and methods.

Laser flash photolysis was carried out using an ND:YAG laser that uses a harmonic generator to create an excitation beam at 355 nm. The probe beam was generated from an 350 W Xe arc lamp. Transient waveforms were digitized by a digital oscilloscope with a bandwidth of 350 MHz at a rate of 1 point per 10 ns.

Samples were prepared in  $\text{CH}_3\text{CN}$  that was distilled from  $\text{CaH}_2$ . Stock solutions of **7.4a** were prepared to have an optical density of between 1.5 and 2.0 at the excitation wavelength (355 nm). The LFP spectra were plotted from waveforms (typically 5 shot signal averaged) obtained every 10 (or 20) nm. To prevent unwanted buildup of photoproducts, the sample was replenished every 10-15 shots.

Pseudo-first order trapping rate constants were acquired by measuring the observed decay rate constant  $k_{\text{obs}}$  for **7.4a** at five different concentrations of the trap. The trapping rate constant is the slope of the line made from plotting the observed rate of decay ( $k_{\text{obs}}$ ) vs. the concentration of trap.

Product analysis was performed using a GC-MS equipped with an SPB-5 column (30 m, 0.25 mm). Carbazole, collidine, 1- and 3-methoxycarbazole, 3-chlorocarbazole, and 1-(carbazol-9-yl)-2,4,6-trimethoxybenzene **7.11** were identified by coinjection with authentic samples. Carbazole, collidine, and 3-methoxycarbazole were obtained commercially. The trimethoxybenzene adduct **7.11** was prepared from thermolysis of **7.3b** in the presence of a large excess of trimethoxybenzene in  $\text{CH}_3\text{CN}$ , followed by component separation using preparatory thin-layer chromatography (15% MeOH, 85% EtOAc). 3-chlorocarbazole was made by reacting carbazole with  $\text{SO}_2\text{Cl}_2$  using a known procedure.<sup>182</sup>



## 8. Chapter 8: Experimental

### 8.1. Materials and methods.

*Computational methodology.* All density functional theory and CBS-QB3 computations were performed using the Gaussian03 software suite. CASPT2 calculations were performed using the MOLCAS software suite. For the benzylic cations, Dr. Ben Gherman and Dr. Chris Cramer performed the CASPT2 calculations at the Minnesota Supercomputer Institute. Unless otherwise indicated all optimized geometries were found to have zero imaginary frequencies, suggesting the optimized structures correspond to minima on their respective potential energy surfaces. Conversely, all transition states were found to have 1 imaginary frequency that converted the starting structure into the product. Singlet-triplet gaps include corrections for the zero-point vibrational energies, which were added unscaled.

### 8.2. Solvents.

Dichloromethane and acetonitrile was distilled over calcium hydride. THF was distilled over Na/benzophenone ketyl. THF-d<sub>8</sub> was distilled over LiAlH<sub>4</sub> using a vacuum transfer technique.

### 8.3. Laser flash photolysis studies.

Laser flash photolysis was carried out using an ND:YAG laser that uses a harmonic generator to create an excitation beam at 355 nm. The probe beam was generated from an 350 W Xe arc lamp. Transient waveforms were digitized by a digital oscilloscope with a bandwidth of 350 MHz at a rate of 1 point per 10 ns.

Samples were prepared in CH<sub>3</sub>CN that was distilled from CaH<sub>2</sub>. Stock solutions were prepared to have an optical density of between 1.5 and 2.0 at the excitation wavelength (355 nm). The LFP spectra were plotted from waveforms (typically 5 shot signal averaged) obtained every 10 (or 20) nm. To prevent unwanted buildup of photoproducts, the sample was replenished every 10-15 shots. Alternatively, a flow cell technique was used to replace photolyzed solution with fresh sample.

Pseudo-first order trapping rate constants were acquired by measuring the observed decay rate constant  $k_{\text{obs}}$  at five different concentrations of the trap. The trapping rate constant is the slope of the line made from plotting the observed rate of decay ( $k_{\text{obs}}$ ) vs. the concentration of trap.

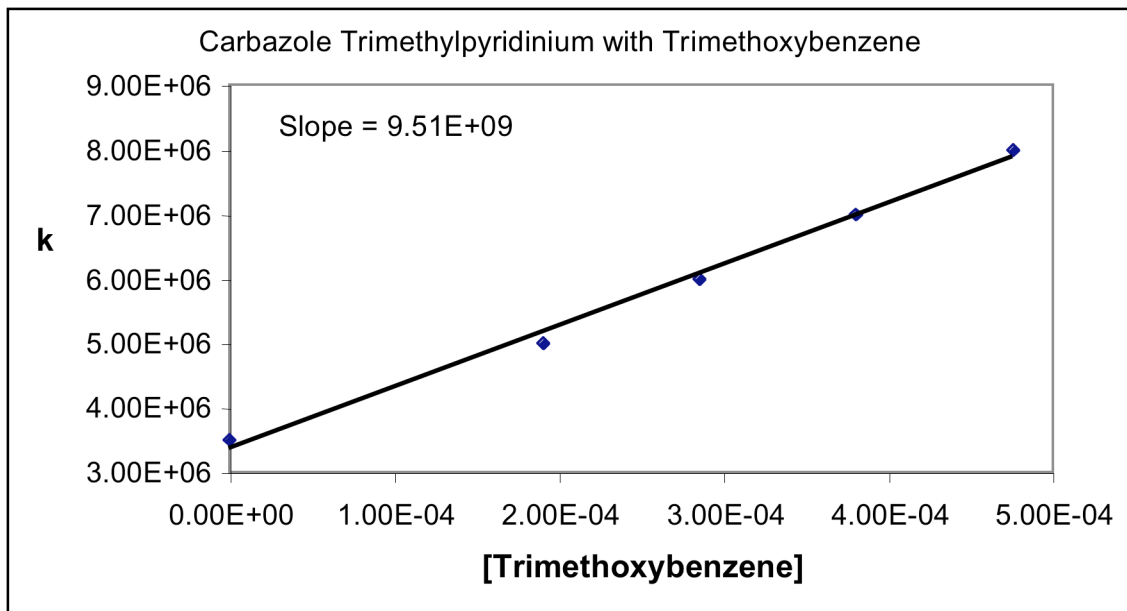


**Figure 7. 10.** Determination of trapping rate constant for trimethoxybenzene of the carbazoylyl nitrenium ion.

Product analysis was performed using a GC-MS equipped with an SPB-5 column (30 m, 0.25 mm). Yields were determined by GC area percent corrected for the GC response factors. Response factors were determined from the slope of the line plotting the concentration of the material versus the GC peak area percent.

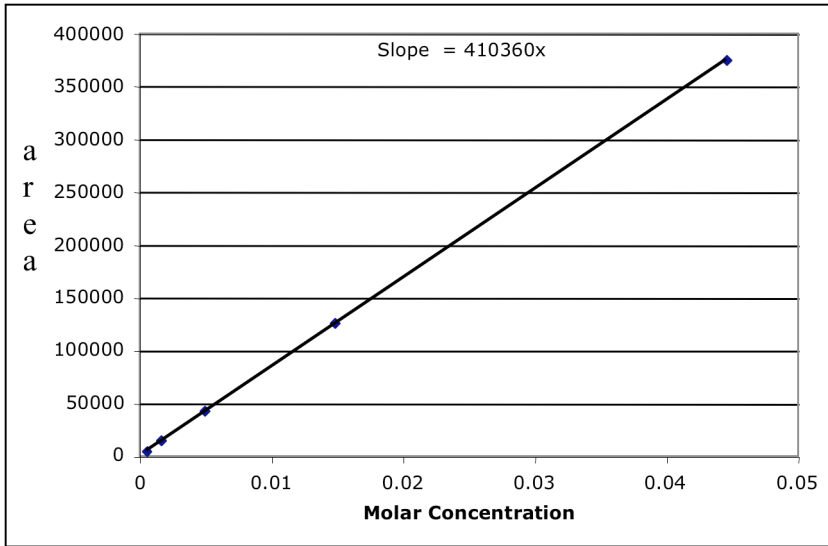
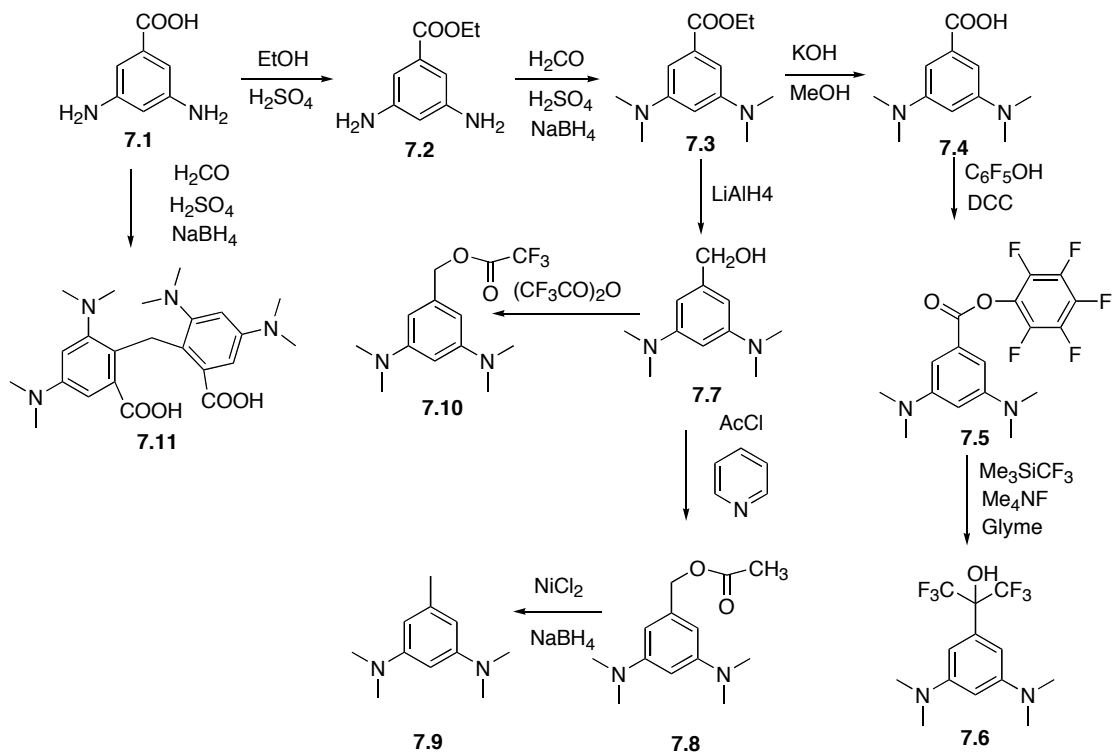


**Figure 7. 11.** GC response factor for 3,5-bis(dimethylamino)benzyl alcohol.

#### 8.4. Synthesis of photoprecursors.



**3,5-diaminobenzoic acid ethyl ester (7.2).** 10.01 g of 3,5-diaminobenzoic acid (7.1, Aldrich, 65.85 mmol) was added to 250 mL of absolute ethanol in a 500 mL RBF. 60 mL of concentrated sulfuric acid was then added slowly and the solution was refluxed for 3 days. Excess ethanol was removed by rotary evaporation, and 400 mL of H<sub>2</sub>O was then added. The solution was made basic with saturated Na<sub>2</sub>CO<sub>3</sub> and extracted three times with 100 mL of ethyl acetate. The organic layers were combined, dried with MgSO<sub>4</sub>, and condensed *in vacuo* to yield the ester **7.2** as a yellow oil (10.8 g, 95%), which was used in the next step without further purification. <sup>1</sup>H NMR (400 MHz, DMSO): δ 6.4 (d, 2.0 Hz, 2H), 6.0 (t, 2.0 Hz, 1H), 5.1 (s, 4H), 4.2 (q, 7.0 Hz, 2H), 1.2 (t, 7.0 Hz, 3H). Spectra match authentic sample (see Chen, et al. *Chem. Eur. J.* **2001**, 7 (3) 686-699).

**3,5-bis(dimethylamino)benzoic acid ethyl ester (7.3).** Formalin (15 mL 37%) and 24 mL 3M H<sub>2</sub>SO<sub>4</sub> were combined in a 250 mL flask and placed in an ice bath. Over the course of an hour, a suspension containing 1.15 g (6.39 mmol) of the ester **7.2**, 50 mL THF, and 7.90 g of NaBH<sub>4</sub> (208 mmol) was added, never letting the reaction temperature exceed 20°C. Another 100 mL THF was then added and the solution was allowed to stir for an additional 30 min. The reaction was then made basic with aqueous NaOH, diluted with 150 mL of H<sub>2</sub>O, and then extracted 3 times with ether. The ether was dried with MgSO<sub>4</sub>, and then evaporated to yield an orange solid, which was purified by flash chromatography with 50:50 hexane/ethyl acetate eluant followed by recrystallization in EtOH to give 0.90 g of the methylated ester **7.3** as a white solid (61%). <sup>1</sup>H NMR (400 MHz, CD<sub>3</sub>CN): δ 6.74 (d, 2.4 Hz, 2H), 6.24 (t, 2.4 Hz, 1H), 4.27 (q, 7.2 Hz, 2H), 2.9 (s, 12H), 1.13 (t, 7.2 Hz, 3H). <sup>13</sup>C NMR (100 MHz, CD<sub>3</sub>CN): δ 167.7, 152.1, 131.8, 102.8, 101.6, 61.2, 41.1, 15.1. MS (EI). 236.17 (M<sup>+</sup>).

**3,5-Bis(dimethylamino)benzyl alcohol (7.7).** 0.70 g (2.8 mmol) of the methylated ester **7.3** was dissolved in 5 mL of anhydrous THF and added slowly to a suspension containing 0.17 g LiAlH<sub>4</sub> (4.5 mmol) and 5 mL THF in an icebath. After the reaction was stirred for 1 hr, the flask was removed from the icebath and allowed to stir at r.t. overnight. The reaction was quenched with 50 mL of wet THF and then with 5% H<sub>2</sub>SO<sub>4</sub> until bubbling ceased. The solution was made basic by addition of aqueous NaOH, then extracted twice with 100 mL portions of ether. The organic layers were combined, dried over MgSO<sub>4</sub>, and evaporated to yield a yellow oil, which was

purified by flash chromatography with ethyl acetate eluant to yield **7.7** as a clear oil (0.39 g, 68%).  $^1\text{H}$  NMR (400 MHz,  $\text{CD}_3\text{CN}$ ):  $\delta$  6.14 (d, 2.0 Hz, 2H), 5.99 (t, 2.0 Hz, 1H), 4.43 (s, 2H), 3.05 (s, 1H), 2.85 (s, 12H).  $^{13}\text{C}$  NMR (100 MHz,  $\text{CD}_3\text{CN}$ ):  $\delta$  152.4, 143.6, 101.3, 97.0, 65.3, 40.5. MS(EI): 194 (M+).

**3,5-bis(dimethylamino)benzyl trifluoroacetate 7.10.** 0.97 g (5.0 mmol) of the benzyl alcohol (**7.7**) was dissolved in 10 mL of dry ether and stirred at  $-78^\circ\text{C}$  for 15 min. Then, 0.7 mL of trifluoroacetic anhydride was added dropwise and the solution was stirred 20 min. The reaction was warmed to r.t. and stirred an additional 10 min, then filtered to obtain 1.20 g (3.0 mmol) of the trifluoroacetate **7.10** as its pure TFA salt (60%). The salt, which was stable for weeks at  $0^\circ\text{C}$ , was freebased with sat. bicarbonate to the unstable conjugate base when needed.  $^1\text{H}$  NMR (400 MHz,  $\text{CD}_3\text{CN}$ ):  $\delta$  6.17 (d, 2.0 Hz, 2H), 6.05 (t, 2.0 Hz, 1H), 5.24 (s, 2H), 2.90 (s, 12H).  $^{13}\text{C}$  NMR (100 MHz,  $\text{CD}_3\text{CN}$ ): 152.5, 135.2, 101.3, 97.9, 71.7, 65.7, 40.3. MS(EI): 290 (M+)

**3,5-bis(Dimethylamino)benzylacetate 7.8.** 0.36 g (1.9 mmol) of the benzyl alcohol **7.7** was dissolved in 5 mL of DCM and 0.25 mL triethylamine. To this was added dropwise a solution containing 0.20 mL acetyl chloride in 5 mL dichloromethane. After addition was complete, the reaction was allowed to stir for 15 min. It was then placed in a separatory funnel and washed with water and saturated  $\text{NaHCO}_3$ . The organic layers were separated, dried with  $\text{MgSO}_4$ , and evaporated to obtain the ester as a yellow oil. The crude was then purified by flash chromatography (80:20

hexane/ethyl acetate) to yield 0.41 g of **7.8** (94%) as a colorless oil. <sup>1</sup>H NMR (400 MHz, CD<sub>3</sub>CN): δ 6.12 (d, 2.4 Hz, 2H), 6.01 (t, 2.4 Hz, 1H), 4.93 (s, 2H), 2.88 (s, 12H). <sup>13</sup>C NMR (100 MHz, CD<sub>3</sub>CN): 21.7, 41.1, 67.6, 97.6, 102.6, 137.8, 152.3, 171.2. HRMS 236.1529 (calc. 236.1525).

**3,5-bis(Dimethylamino)toluene 7.9.** The toluene **7.9** was synthesized from the benzyl acetate **7.8** using the NiCl<sub>2</sub>/NaBH<sub>4</sub> reduction as described by He et al. (He, Y., Pan, X., Zhao, H., Wang, S. *Synthetic Communications*. **1989**, 19 (17), 3051-3054). <sup>1</sup>H NMR (400 MHz, CD<sub>3</sub>CN): δ 6.03 (d, 2.0 Hz, 2H), 5.94 (t, 2.0 Hz, 1H), 2.9 (s, 12H), 2.24 (s, 3H). <sup>13</sup>C NMR (100 MHz, CD<sub>3</sub>CN): 152.43, 139.17, 103.37, 95.58, 40.50, 21.83. MS(EI): 178 (M<sup>+</sup>).

**Diacid homodimer 7.11.** Exhaustive methylation of **7.1** using the procedure as employed to synthesize **7.3** yielded an unexpected diacid homodimer **7.11** (52%). <sup>1</sup>H NMR (400 MHz, CD<sub>3</sub>CN): 7.0 (d, 2.8 Hz, 2H), 6.9 (d, 2.8 Hz, 2H), 4.6 (s, 2H), 3.0 (s, 6H), 2.7 (s, br, 6H). <sup>13</sup>C NMR (100 MHz, CD<sub>3</sub>CN): 175.8, 151.1, 145.9, 142.0, 115.8, 112.8, 105.9, 46.0, 39.3, 25.7. HRMS: 429.2979 (calc. 429.2457).

**3,5-bis(Dimethylamino)benzoic acid 7.4.** 1.00 g of ester **7.3** was suspended in 3 mL MeOH in a 25 mL RBF. 0.80 g KOH (3 eq) was added and the reaction stirred at 40° C 50 min. 10 mL H<sub>2</sub>O was added and the reaction was extracted with 15 mL ether. The aqueous layer was acidified with 3M H<sub>2</sub>SO<sub>4</sub> until pH 3-4 and cooled at which time the highly pure (GC, NMR) acid crashed out of solution (0.86 g, 98%). <sup>1</sup>H NMR

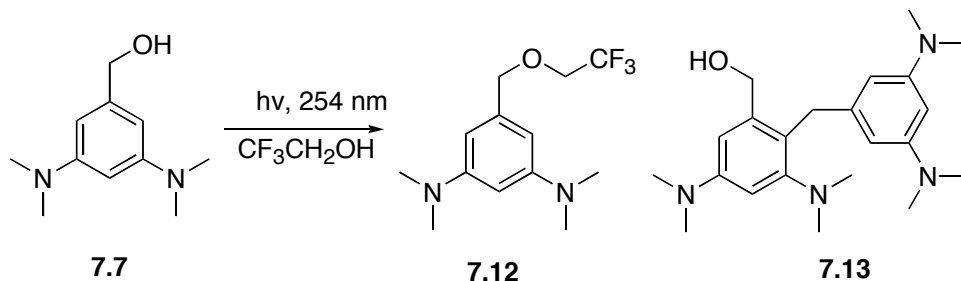


(400 MHz, CD<sub>3</sub>CN): 6.7 (d, 2.4 Hz, 2H), 6.3 (t, 2.4 Hz, 1H), 2.9 (s, 12H). <sup>13</sup>C NMR (100 MHz, CD<sub>3</sub>CN): 168.4, 152.2, 131.3, 103.1, 101.5, 40.3

**3,5-bis(Dimethylamino)benzoic acid pentafluorophenyl ester 7.5.** 0.22 g (1.05 mmol) of acid **7.4**, 0.21 g pentafluorophenol (1.15 mmol), and 3 mL distilled CH<sub>2</sub>Cl<sub>2</sub> were combined in a 3-neck RBF on a Schlenk line and stirred under nitrogen 5 min. Then 0.24 g of DCC was added and the reaction stirred an additional 3 h at room temperature under N<sub>2</sub>. The urea precipitate was filtered off, and the filtrate was pumped down *en vacuo*. The orange solid was recrystallized from ether and then hexanes to yield a fluffy straw-colored solid of **7.5** (0.19 g after recrystallization, 49%). <sup>1</sup>H NMR (400 MHz, CD<sub>3</sub>CN): 6.9 (d, 2.4 Hz, 2H), 6.3 (t, 2.4 Hz, 1H), 3.0 (s, 12H). <sup>13</sup>C (100 MHz, CD<sub>3</sub>CN): 164.3, 152.4, 127.9, 103.3, 102.5, 40.2. <sup>19</sup>F NMR (376 MHz, CD<sub>3</sub>CN): -154.9, -160.5, -164.6. HRMS 375.1137 (calc: 375.1132).

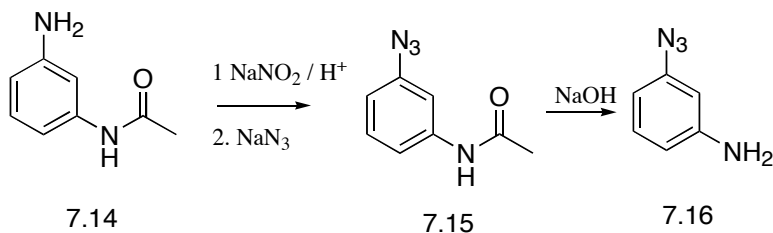
**2-(3,5-bis(Dimethylamino))-1,1,1,3,3,3-hexafluoro-2-propanol 7.6.** 0.32 g of ester **7.5** was added with a stirbar to a 50 mL 3-necked flask attached to an N<sub>2</sub> Schlenk line. 0.32 g Me<sub>4</sub>NF (anhydrous) and 2 mL anhydrous glyme were added and the reaction stirred at -50° C (CH<sub>3</sub>CN, dry ice) for 10 min. Then 0.6 mL of trimethylsilyl trifluoromethane was added and the reaction stirred 1 min before replacing with a -30° C bath (CCl<sub>4</sub>, dry ice). This was stirred under N<sub>2</sub> for three days, allowing the solution to warm to room temperature. The glyme was evaporated and to this was added 10 mL 1.5M H<sub>2</sub>SO<sub>4</sub>. The liquid was decanted leaving a gummy red residue. To the acidic filtrate was added sat NaHCO<sub>3</sub> solution, and a white solid

precipitated. This was dried, weighed (0.14 g, 50%), and found to be pure **7.6** by NMR.  $^1\text{H}$  NMR (400 MHz,  $\text{CD}_3\text{CN}$ ): 6.4 (d, 2.0 Hz, 2H), 6.2 (t, 2.0 Hz, 1H), 5.6 (s, br, 1H), 2.9 (s, 12H).  $^{19}\text{F}$  (376 MHz,  $\text{CD}_3\text{CN}$ ): -75.5.  $^{13}\text{C}$  (100 MHz,  $\text{CD}_3\text{CN}$ ): 152.2, 131.7, 125.0, 122.2, 100.2, 98.7. HRMS 331.12455 (calc. 333.12451).



**Isolation of TFE adduct and Friedel-Crafts heterodimer.** 0.080 g 3,5-bis(dimethylamino)benzyl alcohol was dissolved in 5.0 mL of distilled TFE and photolyzed on a Rayonet photoreactor with 254 nm bulbs for 8 h. The photolysate was purified by flash chromatography (80:20 hexanes/ethyl acetate). The first fraction yielded the TFE adduct **7.12**. The second fraction yielded the Friedel-Crafts heterodimer **7.13**. **TFE Adduct, 7.12.**  $^1\text{H}$  NMR (400 MHz,  $\text{CD}_3\text{CN}$ ):  $\delta$  6.16 (d, 2.4 Hz, 2H), 6.06 (t, 2.4 Hz, 1H), 4.56 (s, 2H), 3.93 (q, 8.8 Hz, 2H), 2.90 (s, 12H).  $^{13}\text{C}$  NMR (100 MHz,  $\text{CD}_3\text{CN}$ ): 152.47, 138.36, 126.44, 102.21, 97.48, 75.12, 67.00 (q,  $J = 33.3$  Hz), 40.47. MS(EI): 276 ( $\text{M}^+$ ). **Friedel-Crafts hetero-dimer 7.13.**  $^1\text{H}$  NMR (400 MHz,  $\text{CD}_3\text{CN}$ ):  $\delta$  6.50 (d, 2.0 Hz, 1H), 6.37 (d, 2.0 Hz, 1H), 6.12 (d, 2.0 Hz, 2H), 5.97 (d, 2.0 Hz, 1H), 4.38 (s, 2H), 4.25 (s, 1H), 4.01 (s, 2H), 2.90 (s, 18H, overlapping singlets), 2.78 (s, 6H).  $^{13}\text{C}$  NMR (100 MHz,  $\text{CD}_3\text{CN}$ ): 153.65, 152.44,

150.03, 143.63, 143.19, 122.30, 110.14, 102.95, 101.29, 97.00, 65.28, 64.19, 45.50, 40.48, 40.28, 22.82. HREI+: 371.2800 (calc. 371.2811)

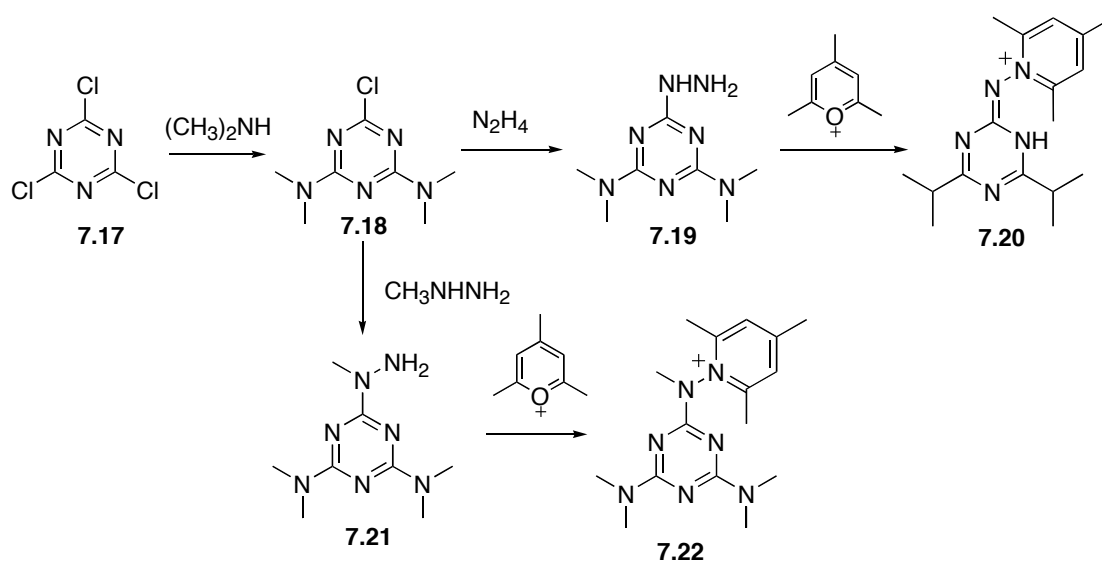


A shorter and more convenient procedure than the one reported (Smith, et al. *J. Am. Chem. Soc.* **1961**, 84, 485-489) was chosen to synthesize 3-aminophenylazide.

**3-azido acetanilide 7.15.** 3-amino acetanilide **7.14** (5.00 g, 33.3 mmol, Aldrich) was dissolved in 5 mL of H<sub>2</sub>O and 15 mL of conc. H<sub>2</sub>SO<sub>4</sub>, and stirred on an icebath 10 min. Sodium nitrite (2.30 g, 33.3 mmol) was added slowly over 10 min, and the reaction was allowed to stir for an additional 25 min. The solution was neutralized with a saturated NaHCO<sub>3</sub> solution. Then, sodium azide (2.17 g, 33.4 mmol) was added, and the reaction was stirred an additional 30 min. A red solid precipitated. This was filtered and washed with copious amounts of water to yield 3-azido acetanilide **7.15** (5.45 g, 93%). After drying, the product was found to be sufficiently pure by NMR and TLC to be used in the next synthetic step without further purification. <sup>1</sup>H NMR (Acetone): 2.06 (s, 3H); 6.78 (td, 6Hz, 2.4Hz, 1H); 7.35 (m, 2H); 7.62 (s, 1H); 9.32(s,1H). <sup>13</sup>C NMR (DMSO): 24.9, 109.9, 114.4, 116.3, 130.8, 140.5, 141.7, 169.5 *FAB MS (abundance)*: 176.8 (100, M<sup>+</sup>), 151.3 (22), 118.4 (30), 106.6 (31), 84.6 (29) 43.1 (13)

**3-azidoaniline 7.16.** The 3-azidoacetanilide **7.15** (2.50 g, 14.2 mmol) was dissolved in a minimal amount of methanol. This was added slowly to a solution containing sodium hydroxide (35 g) dissolved in 150 mL of water. The reaction was attached to a reflux condenser and stirred for 40 h at 40°C. The reaction was then stopped, extracted twice with chloroform, dried with MgSO<sub>4</sub>, and then condensed to dryness *in vacuo*. The product was purified by flash chromatography with 1:2 MeOH/CHCl<sub>3</sub>, with the first band collected. This gave pure **7.16** as a red oil (1.65 g, 92%). <sup>1</sup>H NMR (DMSO): δ 5.31 (s, 2H); δ6.16 (dd, 1.6Hz, 7.2Hz); δ6.26 (t, 2Hz, 1H); δ6.34 (dd, 2Hz, 9.6Hz, 1H); δ6.98 (t, 8 Hz, 1H). <sup>13</sup>C NMR (DMSO): 104.5, 107.3, 111.6, 130.8, 140.6, 155.4 *EI MS (abundance)*: 134 (25, M<sup>+</sup>), 105 (19), 84 (100), 79 (23), 66 (98). *IR*: 2110 cm<sup>-1</sup> (S)

**1-(4,6-Bis-dimethylamino-[1,3,5]triazin-2-ylamino)-2,4,6-trimethyl-pyridinium tetrafluoroborate**



Procedure for converting cyanuric chloride **7.17** into bis(dimethylamino) cyanuric chloride **7.18** has been reported previously. (See Simmonds and Stevens. *J. Chem. Soc. Perk. Trans. I.* **1982**, 1821-1825).

**Bis(dimethylamino)cyanuric chloride 7.18.** Cyanuric chloride **7.17** (27.00 g, 148 mmol, Aldrich) was dissolved in 200 mL acetone, and stirred on an icebath. To this solution was added 70 mL of 40% dimethylamine in water over 15 min. The reaction was stirred an additional 1.5 h at room temperature. The acetone was then evaporated, and the resulting mixture of white precipitate and water was filtered. The solid was washed with water, and recrystallized in *i*PrOH/H<sub>2</sub>O, to yield the pure 3,5-bis(dimethylamino)-triazinyl chloride **7.18** as a white solid (26.2 g, 89%; mp 49-52°C). <sup>1</sup>H NMR (400 MHz, CD<sub>3</sub>CN): 3.08(d, 12Hz, 6H). <sup>13</sup>C NMR (100 MHz, DMSO): 168.5, 165.9, 36.4, 36.5 FAB MS: 203 (40), 202 (100, M+), 200(35).

**Bis(dimethylamino)cyanuric hydrazine 7.19.** Into 170 mL of EtOH, was dissolved bis(dimethylamino)triazinyl chloride **7.18** (12.50 g, 62 mmol). To this was added hydrazine hydrate (10.86 g, 217 mmol), and refluxed 4 h. The ethanol was evaporated, and the resulting precipitated solid was filtered and collected to yield **7.19** as a solid (6.8g, 56%) pure enough to proceed to the next step without further purification. <sup>1</sup>H NMR (400 MHz, DMSO): 3.03 (s, 12H). <sup>13</sup>C NMR (100 MHz, DMSO): 36.4, 36.5, 165.9, 168.2, 168.5 *EI MS (abundance)*: 198 (15), 197 (100, M+), 182 (47), 168 (13), 138 (14), 96 (20), 71 (35).

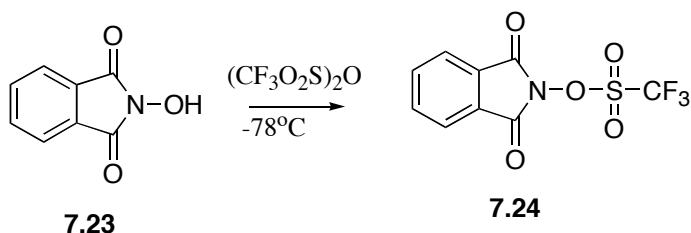
**Bis(dimethylamino)cyanuric trimethylpyridinium tetrafluoroborate 7.20.**

The hydrazine **7.19** (0.51 g, 2.5 mmol) was suspended in 50 mL of EtOH. To this suspension was added freshly-prepared trimethyl pyrylium salt **7.20** (1.2 g, 5.7 mmol). The solution turned red. The reaction was stirred for 2 days at room temperature. The precipitated solid was filtered and recrystallized in 95% EtOH to yield **7.20** (0.23 g, 23%) as sallow yellow crystals (m.p. 190-192). <sup>1</sup>H NMR (400 MHz, CD<sub>3</sub>CN): 2.64(s, 3H); 2.79(s, 6H); 3.17(s broad, 12H); 7.68(s, 2H), 9.5 (m, 2H). <sup>13</sup>C NMR (100 MHz, DMSO): 9.1, 19.7, 26.0, 31.6, 36.6, 123.7, 127.9, 155.2, 159.0 FAB MS (abundance): 303 (15, M+), 302 (70, M+), 238 (100), 123 (40).

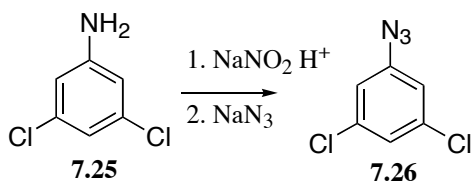
**Bis(dimethylamino)cyanuric-N-methyl hydrazine 7.21.** 8.00 grams of the bis(dimethylamino)cyanuric chloride **7.18** was added to 80 ml of EtOH . 8 g of solid NaHCO<sub>3</sub> was then added followed by 10.0 mL of methyl hydrazine. This suspension was refluxed for 2 h, and then evaporated to dryness. The residual solid was extracted with ether, dried with MgSO<sub>4</sub>, and then evaporated to give 3.80 g pure hydrazine **7.21**, which was used in the next step without further purification. <sup>1</sup>H NMR (400 MHz, CD<sub>3</sub>CN). 4.46 (s, 2H), 3.17 (s, 3H), 3.05 (s, 12H). <sup>13</sup>C (100 MHz, CD<sub>3</sub>CN): 167.2, 166.1, 35.4, 27.1. EIMS 211.1540 (calc 211.1545).

**Bis(dimethylamino)cyanuric-N-methyl-2,4,6-trimethylpyridinium tetrafluoroborate 7.22.** 10.00 g N-methylhydrazine **7.21** and 0.90 g freshly-prepared trimethylpyrylium tetrafluoroborate were added to 10 mL of ethanol and

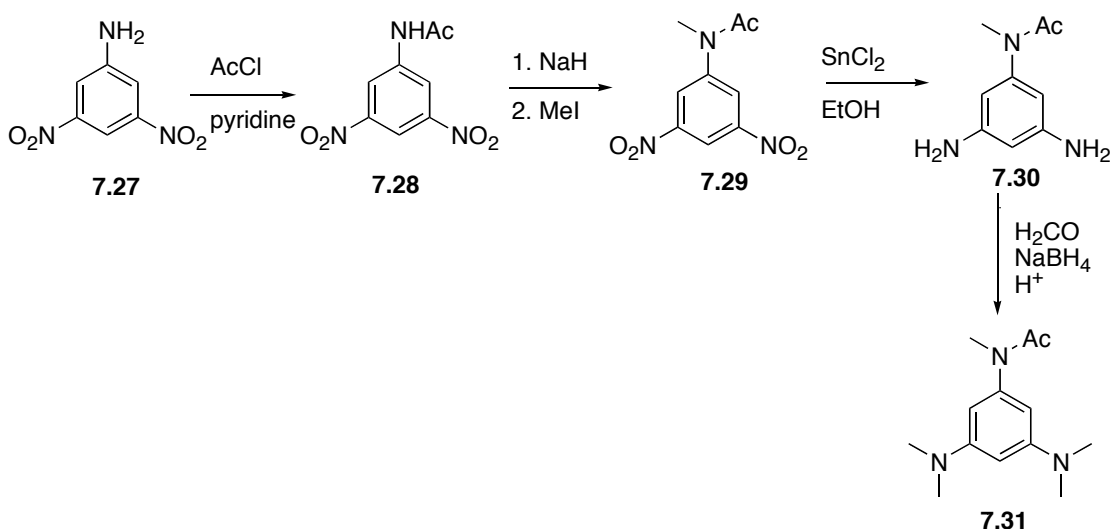
stirred at 50°C for 1 h. The EtOH was removed by rotary evaporation, and then the solid was washed with ether and filtered to give 0.12 g of the pyridinium salt **7.22** as a pale yellow solid. <sup>1</sup>H NMR (acetone): 7.95 (s, 2H), 3.75 (s, 3H), 3.19 (s, 3H), 3.14 (s, 3H), 3.03 (s, 3H), 2.70 (s, 6H) 2.67 (s, 6H). <sup>13</sup>C (acetone): 166.0, 165.6, 163.8, 161.4, 158.4, 128.5, 35.7, 35.5, 35.3, 21.6, 18.7. HRMS: 316.2261 (calc. 316.2250).



**N-Triflic Phthalamide 7.24.** Triflic anhydride (5.00 g) and N-hydroxy phthalamide **7.23** (2.41 g) were added to 75 mL of dichloromethane and stirred for 15 min at  $-78^\circ\text{C}$  (dry ice-acetone mixture). Then, 2,6-lutidine (1.90 g, 2.06 mL) was added, and the reaction was allowed to warm slowly to room temperature. The color changed from a peach color, to pinkish. The reaction was allowed to stand at room temperature for 15 min. The reaction mixture was then washed with water, 10% HCl, and brine, and the water layers discarded. The organic layer was condensed to dryness *in vacuo*, and recrystallized in EtOH to yield **7.24** as white crystals (3.45 g, 79%; mp 104-105°C). <sup>1</sup>H NMR (400 MHz, CD<sub>3</sub>CN): 8.03 (m, 2H); 8.06 (m, 2H) <sup>13</sup>C NMR (100 MHz, DMSO): 125.7, 129.8, 137.8, 160.8, 165.0 FAB MS: 296 (M<sup>+</sup>), 256, 213, 177, 119, 103, 85, 47, 23; HREI MS: observed 295.9849 (calculated: 295.9841)



**3,5-dichlorophenylazide.** 3,5-dichloroaniline **7.25** (2.0 g, Aldrich) was dissolved in 8 mL of trifluoroacetic acid and 5 mL of acetic acid, and stirred on an icebath. Then, sodium nitrite (0.47 g), dissolved in a minimal proportion of water, was added slowly, followed by 0.2 mL of conc.  $\text{H}_2\text{SO}_4$ . Then, sodium azide (0.44 g), dissolved in a minimal amount of water, was added dropwise. The reaction was allowed to stir for 2 h, and the precipitate from the reaction was filtered and recrystallized from methanol to yield **7.26** as yellow crystals (0.71g, 58%; mp 30-32°C).  $^1\text{H}$  NMR (400 MHz,  $\text{CD}_3\text{CN}$ ): 7.07(d, 2Hz, 2H); 7.25(t, 2Hz, 1H).  $^{13}\text{C}$  NMR (DMSO): 119.2, 125.4, 135.9, 143.5 MS (EI): 189 (40, M+2), 187 (60, M+), 163 (70), 159 (85), 124 (100), 97 (43), 88 (25)



**3,5-dinitroacetanilide 7.28.** 5.00 g of dinitroaniline **7.27** was dissolved in 25 mL dry THF. Then, 2.4 mL pyridine was added and the reaction stirred on an icebath 10 min. Then, 3.5 mL acetyl chloride was added slowly and the reaction stirred 20 min. The

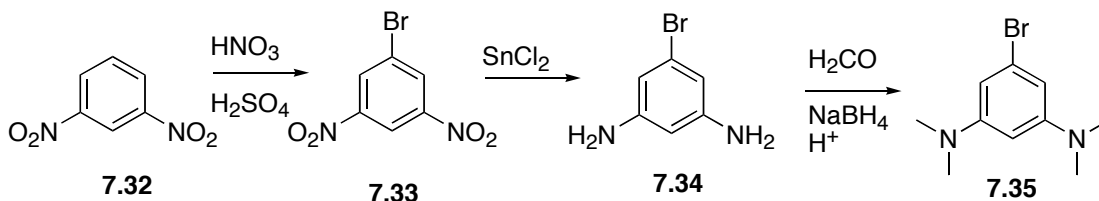


reaction was then dumped onto water and the product filtered (5.45 g, 89%), which was used in the next step without further purification.  $^1\text{H}$  NMR ( $\text{CD}_3\text{CN}$ ) 9.0 (s, 1H), 8.8 (d, 2.0 Hz, 2H), 8.6 (t, 2.0 Hz, 1H), 2.1 (s, 3H).  $^{13}\text{C}$  NMR (100 MHz,  $\text{CD}_3\text{CN}$ ): 170.1, 149.2, 141.6, 118.9, 113.0, 23.9. EIMS 225 (M+).

**N-methyl-3,5-dinitroacetanilide 7.29.** 4.00 g of the dinitroacetanilide **7.28** was dissolved in 100 mL dry THF. Then 4.50 g of NaH (cleaned by washing with pentane) was added, and stirred for 1 h at r.t. Then, 13 mL of MeI was added and the solution stirred a further 1 h.  $\text{H}_2\text{O}$  was slowly added to quench unreacted NaH and the solution was then made acidic with dilute  $\text{H}_2\text{SO}_4$ . It was then extracted 3x with EtOAc and the organic layer dried under vacuum to yield 2.61 g of product **7.29** that was used in the next step without further purification.  $^1\text{H}$  NMR ( $\text{CD}_3\text{CN}$ ): 8.8 (s, 1H), 8.5 (s, 2H), 3.3 (s, 3H), 2.2 (s, 3H).  $^{13}\text{C}$  (100 MHz,  $\text{CD}_3\text{CN}$ ): 195.1, 149.1, 111.1, 105.0, 29.9, 22.5. EIMS 239 (M+)

**N-methyl-3,5-diaminoacetanilide 7.30.** 2.00 g of the N-methylacetanilide **7.29** was added to 100 mL of abs. EtOH. 16.00 g  $\text{SnCl}_2$  dihydrate was then added and the reaction stirred at  $75^\circ\text{C}$  for 45 min. The reaction was dumped onto water, neutralized with  $\text{NaHCO}_3$ , and then extracted with EtOAc. The organic layer was condensed to dryness to yield 0.85 g **7.30**, which was used in the next step without further purification.  $^1\text{H}$  NMR ( $\text{CD}_3\text{CN}$ ): 5.9 (s, 1H), 5.8 (s, 2H), 4.1 (s, 4H), 3.1 (s, 3H), 1.8 (s, 3H).  $^{13}\text{C}$  NMR (100 MHz,  $\text{CD}_3\text{CN}$ ): 169.9, 150.2, 147.0, 103.0, 99.5, 30.1, 20.6. EIMS 179 (M+)

**N-Methyl-3,5-bis(dimethylamino)acetanilide 7.31.** 0.85 g of the diamine **7.30** was added to 40 mL THF and 5.80 g NaBH<sub>4</sub>. This suspension was added over the course of an hour to a stirred solution of 11 mL 37% formalin and 18 mL 3M H<sub>2</sub>SO<sub>4</sub> stirred on an icebath. Care was taken to ensure the reaction temperature never exceeded 20° C. The reaction was stirred an additional 30 min once addition was complete. The reaction was then neutralized with aqueous NaHCO<sub>3</sub>, and extracted 3 x with EtOAc. The organic layers were separated and dried with MgSO<sub>4</sub>, and condensed en vacuo. The resulting black oil was recrystallized in acetone to give a pure tan solid (0.44 g, 40%). <sup>1</sup>H NMR (CD<sub>3</sub>CN): 6.0 (s, 2H), 5.9 (s, 1H), 3.3 (s, 3H), 2.8 (s, 12H), 1.8 (s, 3H). <sup>13</sup>C NMR (100 MHz, CD<sub>3</sub>CN): 170.0, 152.9, 146.8, 100.8, 96.0, 40.2, 36.5, 21.7. EIMS 235 (M<sup>+</sup>)

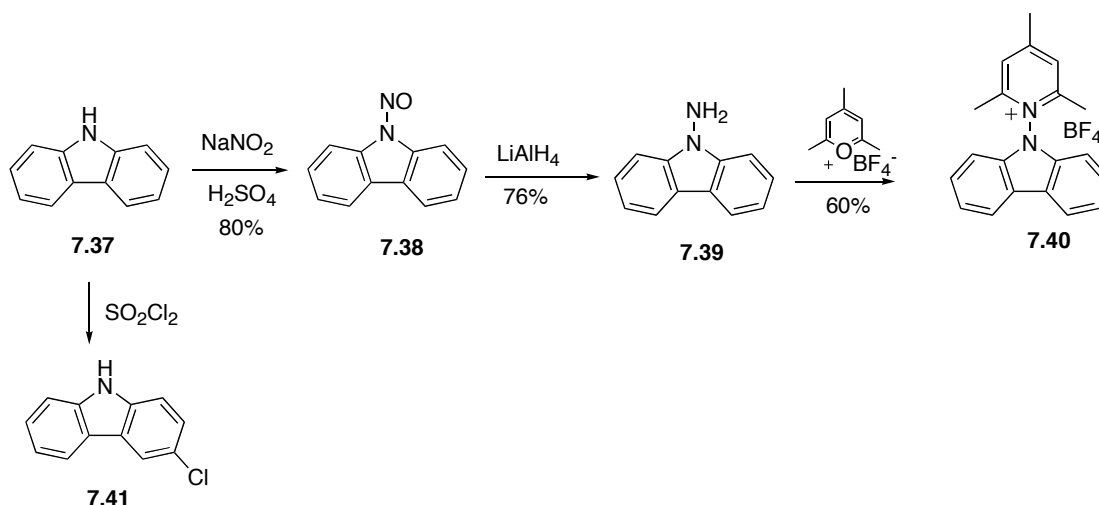


**1-Bromo-3,5-dinitrobenzene 7.33.** 15.00 g of 1,3-dinitrobenzene **7.32** was dissolved in 150 mL of conc. H<sub>2</sub>SO<sub>4</sub> and 5 mL conc. HNO<sub>3</sub>. To this solution was added 11.0 mL of Br<sub>2</sub> slowly through a dropping funnel and the solution was refluxed 5 days. The reaction was poured onto cold water and the yellow precipitate was filtered and dried to yield 21.70 g of the brominated product (99%). The compound was deemed sufficiently pure by <sup>1</sup>H NMR and was continued to the next step without

further purification.  $^1\text{H}$  NMR ( $\text{CD}_3\text{CN}$ ): 8.87 (t, 2.0 Hz, 1H) 8.74 (d, 2.0 Hz, 2H).  
 $^{13}\text{C}$  NMR: 149.4, 123.6, 123.5, 118.3. FABMS: 247 (M+).

**5-bromo-1,3-phenylenediamine 7.34.** To a solution containing 1.00 g of the dinitrobenzene **7.33** (4.1 mmol) and 100 mL of abs. EtOH was added 7.30 g  $\text{SnCl}_2$  dihydrate. The solution was stirred at  $70^\circ\text{C}$  under nitrogen for 40 min. It was then poured onto cold water, extracted twice with EtOAc, and the organic layer washed with brine and condensed to dryness to give 0.43 g of **7.34** (57%).  $^1\text{H}$  NMR ( $\text{CD}_3\text{CN}$ ): 6.1 (d, 1.6 Hz, 2H), 5.9 (t, 1.6 Hz, 1H), 4.1 (s, 4H).  $^{13}\text{C}$  NMR ( $\text{CD}_3\text{CN}$ ). 150.7, 123.2, 107.0, 99.2. EIMS: 187 (M+).

**5-bromo- (N,N,N',N'-tetramethyl)-1,3-phenylenediamine.** 1.50 g of the phenylene diamine (8.2 mmol) **7.34** was added to a suspension of 11 g  $\text{NaBH}_4$  in 75 mL THF. This was added slowly to a solution of formalin (22.5 mL, 37% in water), and 36 mL  $\text{H}_2\text{SO}_4$  (3M) on an icebath. When addition was complete the reaction was stirred a further hour, then added to 150 mL water, extracted with ether, and the organic layer evaporated to dryness. This gave 1.42 g (72%) of the product as an oil, which was found to be pure by NMR.  $^1\text{H}$  NMR ( $\text{CD}_3\text{CN}$ ): 6.2 (d, 2.4 Hz, 2H), 5.9 (t, 2.4 Hz, H), 2.9 (s, 12H).  $^{13}\text{C}$  (100 MHz,  $\text{CD}_3\text{CN}$ ): 153.1, 124.0, 104.6, 95.7, 40.1. EIMS: 243 (M+).



The synthesis of 7.37-7.41 was performed by Dr. Harry H. Gibson who visited us on sabbatical from Austin College.

**9-Nitrosocarbazole 7.38.** The 9-nitrosocarbazole was synthesized using a modification of Kyziol's procedure. (Kyziol, J., Tarnawski, J. *Revue Roumaine de Chimie*. **1980**, 25(5), 721-727). A 500-ml reaction flask was fitted with a magnetic stirrer, a reflux condenser and an addition funnel. Then 10.0 g (0.06 moles) of carbazole **7.37**, 120 ml of ethyl ether and 30 ml of 50% sulfuric acid were added. A solution of 8.28 g (0.12 moles) of sodium nitrite in 30 ml water was then added dropwise to the vigorously stirred suspension. After the addition, stirring was continued for 15 minutes, when most of the solid dissolved. The organic layer was separated, with any suspended solid being put into the discarded water layer, dried over anhydrous sodium sulfate and concentrated to a volume of about 25 ml. A solid quickly formed in the flask. 25 ml of ether was added, and the mixture warmed up so that all solid redissolved. The solution was then cooled to -20 degrees overnight and the golden-yellow needles of 9-nitrosocarbazole **7.38** were filtered, rinsed with about

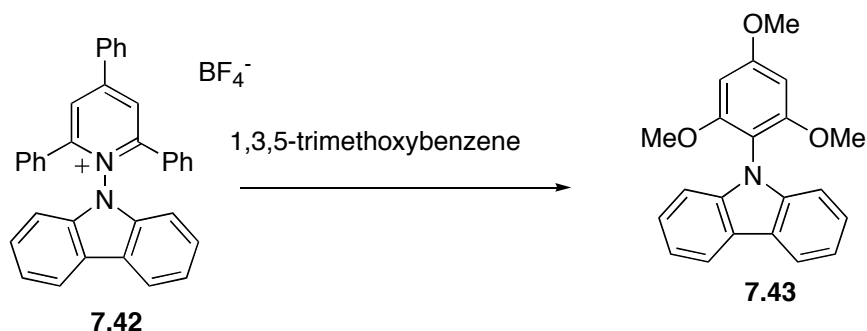
15-20 ml cold ether and dried *in vacuo*. The filtrate was put in a freezer for 1 h, with more crystals appearing. They were filtered and rinsed with ether. To remove the greenish discoloration within the solid, all the material was dissolved in ~75 ml of ether, washed with ~ 5% Na<sub>2</sub>CO<sub>3</sub>, then with water, dried with Na<sub>2</sub>SO<sub>4</sub>, and cooled. After collection of crystals, the ether layer was concentrated two or three times eventually down to 25 ml, producing pale-yellow crystals at every stage; mp 80-82 (lit. mp 81-82). <sup>1</sup>H NMR (300 MHz, CDCl<sub>3</sub>) δ 7.4-7.6 (m, 4 H), 7.9-8.0 (m, 2 H), 8.6 (m, 1 H).

**9-Aminocarbazole (7.39).** The 9-nitrosocarbazole **7.38** was reduced with LiAlH<sub>4</sub> to the N-amino compound **7.39** using the procedure of Kyziol (76% yield) (Kyziol, J., Tarnawski, J. *Revue Roumaine de Chimie*. **1980**, 25(5), 721-727). <sup>1</sup>H NMR (300 MHz, CD<sub>3</sub>CN) δ 5.0 (s, 2 H), 7.2 (t, 2 H), 7.5 (t, 2 H), 7.6<sup>183</sup> (d, 2 H), 8.1 (d, 2 H).<sup>183</sup>

**1-(9H-carbazol-9-yl)-2,4,6-trimethylpyridinium tetrafluoroborate (7.40).** 9-aminocarbazole **7.39** (0.365 g, 2 mmol) was dissolved in 20 ml of 100% ethanol and then 0.380 g (1.8 mmol) of freshly prepared 2,4,6-trimethylpyrilium tetrafluoroborate was added in small portions to the solution. The solution immediately turned bright yellow. Stirring was continued at room temperature for 15 minutes. The mixture was then heated to reflux for 30 minutes and the homogeneous mixture put into a refrigerator overnight. Pale yellow crystals formed. The crystals were isolated, washed with cold ethanol, and dried under vacuum. Based on the limiting amount of pyrilium, a 60% isolated yield (0.41 g; 1.1 mmol) of pale yellow crystals of **7.40** was

obtained: mp 141-143 °C; IR (solid) 1635 (m), 1483 (m), 1438 (m), 1090 (vs, br), 761 (s)  $\text{cm}^{-1}$ ;  $^1\text{H NMR}$  (300 MHz,  $\text{CH}_3\text{CN}$ )  $\delta$  8.31 (d, 2 H), 7.92 (s, 2 H), 7.58 (t, 2 H), 7.50 (t, 2 H), 7.14 (d, 2 H), 2.73 (s, 3 H), 2.22 (s, 6H);  $^{13}\text{C NMR}$  ( $\text{CD}_3\text{CN}$ )  $\delta$  164.1, 158.7, 137.1, 130.1, 128.5, 123.8, 122.6, 122.1, 108.8, 22.1, 18.2; MS (FAB)  $m/z$  (relative intensity) 287 ( $[\text{M} - \text{BF}_4]^+$ , 100), 166 (75); HRMS (FAB) calcd for  $\text{C}_{20}\text{H}_{19}\text{N}_2$   $[\text{M} - \text{BF}_4]^+$  287.1548, found 287.1556.

**3-Chlorocarbazole 7.41.** 3-chlorocarbazole was prepared by a modification of synthesis of Lopatinskii (Lopatinskii, V.P., Zherebtsov, I.P. *Metody Polucheniya Khimicheskikh I Preparatov*. **1964**, 11, 102-104). Into a 100-ml rbf equipped with stir bar, a reflux condenser, and addition funnel, 6.4g (3.83 ml, 47 mmol)  $\text{SO}_2\text{Cl}_2$  was added dropwise to a heterogeneous mixture of 6.68 g. carbazole and 20 ml  $\text{ClCH}_2\text{CH}_2\text{Cl}$  at 30°, producing a frothy mixture that did not stir well. The mixture was boiled with vigorous stirring (magnetic) 1 hr. and cooled, with a solid forming. After adding ca. 20 ml of additional  $\text{ClCH}_2\text{CH}_2\text{Cl}$  and cooling the reaction mixture, the brownish yellow solid was filtered off and washed with 25-30 ml of cold  $\text{ClCH}_2\text{CH}_2\text{Cl}$ . The solid was dried under vacuum. 1.4 g of the material was recrystallized from ~ 20 ml EtOH. Multiple recrystallizations were necessary to free the 3-chlorocarbazole from unreacted carbazole; mp 194-197° (lit 201.5°).



**1-(carbazol-9-yl)-2,4,6-trimethoxybenzene (7.43).** A solution of 1-(carbazol-9-yl)-2,4,6-triphenylpyridinium tetrafluoroborate **7.42** (0.10 g, 0.18 mmol), 1,3,5-trimethoxybenzene (0.85 g, 5.0 mmol), and trifluoroacetic acid (0.30 mL, 0.46 g, 4.0 mmol) in 9 mL of acetonitrile in a heavy-walled tube was degassed (two freeze-thaw cycles), sealed, and thermally decomposed for 22 h at 160°C. The acetonitrile was removed, the mixture taken up in ethyl acetate and neutralized with a 10% NaHCO<sub>3</sub> wash. After evaporation of solvent the residue was applied to preparative TLC plates (silica gel, 20 X 20 cm, 1000 microns) and developed twice with 15% ethyl acetate/85% hexanes giving numerous distinct bands. Isolation of material from the band having R<sub>f</sub> = 0.4 provided colorless crystals of 1-(carbazol-9-yl)-2,4,6-trimethoxybenzene: mp 175-177°C; IR (thin film, NaCl, cm<sup>-1</sup>) 3053, 2934, 1590, 1454, 1144); <sup>1</sup>H NMR (300 MHz, CD<sub>3</sub>CN) δ 8.13 (d, 2 H), 7.36 (t, 2 H), 7.22 (t, 2 H), 6.96 (d, 2 H), 6.44 (s, 2 H), 3.92 (s, 3 H), 3.61 (s, 6 H); <sup>13</sup>C NMR (100 MHz, CDCl<sub>3</sub>) δ 161.6, 158.9, 141.9, 125.8, 123.4, 120.5, 119.4, 110.4, 107.8, 91.7, 56.4, 56.0. MS m/z (relative intensity) 333 (100), 275 (11), 204 (10), 109 (14); HRMS (FAB) 333.1373 (calc. 333.1365).

#### **Determination of decomposition of 7.40 in the absence of traps:**

A solution of **7.40** (0.010 M, 0.41 mmol dissolved in 40.0 mL CH<sub>3</sub>CN) was photolyzed for 3.5 h at 350 nm. There was 53.5% decomposition as measured by NMR in an identical solution in CD<sub>3</sub>CN (because of its charged nature, **7.40** is not observed by GC and therefore percent decomposition could not be determined by GC). A quantitative analysis of collidine and carbazole via GC analysis showed that

0.22 mmol of collidine was formed as well as 0.06 mmol of carbazole. (GC response factors were determined from the slope of the line made by plotting 5 concentrations of the material against the area of the peak seen on the GC). This provides essentially a 100% yield of collidine and a 27% yield of carbazole. From the NMR it is quite obvious that the salt of collidine (generated because of acidic conditions as reaction occurs) is a major product and that carbazole is dramatically slower in forming. The same is true when one inspects the GC/MS trace. The photolysis reaction mixture was worked up by careful evaporation of the 40 mL of acetonitrile, uptake of the reaction mixture into homogeneous ethyl acetate layer, followed by extraction with 10% bicarbonate and back-extraction of the water layer. The ethyl acetate layer was dried and evaporated to a volume of 10.0 ml for GC analysis. A small amount of a goeey and insoluble (in ethyl acetate) residue was also obtained, presumably poly(carbazole) oligomers.



## Bibliography

- (1) Rajca, A.; Shiraishi, K.; Vale, M.; Han, H.; Rajca, S. *J. Am. Chem. Soc.* **2005**, *127*, 9014-9020.
- (2) Rajca, A. *Chem. Rev.* **1993**, *94*, 871-893.
- (3) Allemand, P. M.; Khemani, K. C.; Koch, A.; Wudl, F.; Holczer, K.; Donovan, S.; Gruner, G.; Thompson, J. D. *Science* **1991**, *253*, 301-303.
- (4) Narymbetov, B.; Omerzu, A.; Kabanov, V. V.; Tokumoto, M.; Kobayashi, H.; Mihailovic, D. *Nature* **2000**, *407*, 883-885.
- (5) Anderson, K. K.; Dougherty, D. A. *Adv. Mater.* **1998**, *10*, 688-692.
- (6) Mataga, N. *Theor. Chim. Acta* **1968**, *10*, 372-376.
- (7) Rajca, A.; Rajca, S.; Wongsriratanakul, J. *J. Am. Chem. Soc.* **1999**, *121*, 6308-6309.
- (8) Tomioka, H. *Acc. Chem. Res.* **1997**, *30*, 315-321.
- (9) Arduengo, A. J. *Acc. Chem. Res.* **1999**, *32*, 913-921.
- (10) Fujita, I.; Teki, Y.; Takui, T.; Kinoshita, T.; Itoh, K. *J. Am. Chem. Soc.* **1990**, *112*, 4074-4075.
- (11) Gomberg, M. *J. Am. Chem. Soc.* **1900**, *22*, 757-771.
- (12) Hirai, K.; Tomioka, H. *J. Am. Chem. Soc.* **1999**, *121*, 10213-10214.
- (13) Hirao, Y.; Ino, H.; Ito, A.; Tanaka, K. *J. Phys. Chem. A* **2006**, *110*, 4866-4872.
- (14) Itoh, T.; Jonbo, Y.; Hirai, K.; Tomioka, H. *J. Org. Chem.* **2004**, *69*, 4238-4244.

- (15) Itoh, T.; Nakata, Y.; Hirai, K.; Tomioka, H. *J. Am. Chem. Soc.* **2006**, *128*, 957-967.
- (16) Iwamura, H. *Adv. Phys. Org. Chem.* **1990**, *26*, 179-253.
- (17) Borden, W. *Diradicals*; Wiley & Sons: New York, 1982.
- (18) Borden, W. T.; Gritsan, N. P.; Hadad, C. M.; Karney, W. L.; Kemnitz, C. R.; Platz, M. S. *Acc. Chem. Res.* **2000**, *33*, 765-771.
- (19) Rajca, A.; Shiraishi, K.; Vale, M.; Han, H.; Rajca, S. *J. Am. Chem. Soc.* **2005**, *127*, 9014-9020.
- (20) Marcoux, L. S.; Adams, R. N.; Feldberg, S. W. *J. Phys. Chem.* **1969**, *73*, 2611-2614.
- (21) Dowd, P. *J. Am. Chem. Soc.* **1966**, *88*, 2587-2589.
- (22) Gajewski, J. J.; Shih, C. N. *J. Am. Chem. Soc.* **1967**, *89*, 4532-4533.
- (23) Falvey, D. E. *J. Phys. Org. Chem.* **1999**, *12*, 589-596.
- (24) Abramovitch, R. A.; Davis, B. A. *Chem. Rev.* **1964**, *64*, 149-185.
- (25) Falvey, D. E. In *Reactive Intermediates*; Moss, R. A., Platz, M. S., Maitland Jones, J., Eds.; John Wiley & Sons: New York, 2004.
- (26) Gassman, P. G. *Acc. Chem. Res.* **1970**, *3*, 26-33.
- (27) Huis, T. J. V.; Leinenger, M. L.; Sherrill, C. D.; H.F. Schaefer, I. *J. Comput. Chem.* **1998**, *63*, 1107.
- (28) Gonzalez, C.; Restrepo-Cossio, A.; Marquez, M.; Wilberg, K.; Rosa, M. *J. Phys. Chem. A* **1998**, *102*, 2732-2738.
- (29) Gibson, S. T.; Greene, J. P.; Berkowitz, J. *J. Chem. Phys.* **1985**, *83*, 4319-4328.

- (30) Cramer, C.; Dulles, F.; Falvey, D. *J. Am. Chem. Soc.* **1994**, *116*.
- (31) Cramer, C.; Truhlar, D.; Falvey, D. *J. Am. Chem. Soc.* **1997**, *119*, 12338-12342.
- (32) *Nitrenes*; Interscience: New York, 1970.
- (33) Srivistava, S.; Falvey, D. E. *J. Am. Chem. Soc.* **1995**, *117*, 10186-10193.
- (34) Sander, W.; Bucher, G.; Wierlacher, S. *Chem. Rev.* **1993**, *93*, 1583-1621.
- (35) Wentrup, C. *Science* **2002**, *295*, 1846-1847.
- (36) Rajca, A.; Wongsriratanakul, J.; Rajca, S.; Cerny, R. *Angew. Chem. Int. Ed. Engl.* **1998**, *110*, 1284-1288.
- (37) Rajca, A.; Rajca, S.; Wongsriratanaku, J. *J. Am. Chem. Soc.* **1999**, *121*, 6308-6309.
- (38) Rajca, A.; Wongsriratanakul, J.; Rajca, S. *Science* **2001**, *294*, 1503-1505.
- (39) Hirai, K.; Kamiya, E.; Itoh, T.; Tomioka, H. *Org. Lett.* **2006**, *8*, 1847-1850.
- (40) McIlroy, S.; Cramer, C. J.; Falvey, D. E. *Org. Lett.* **2000**, *2*, 2451-2454.
- (41) Moran, R. J.; Falvey, D. E. *J. Am. Chem. Soc.* **1996**, *118*, 8965-8966.
- (42) Abramovitch, R. A.; Evertz, K.; Huttner, G.; Gibson, H. H.; Weems, H. G. *J. Chem. Soc., Chem. Comm.* **1988**, 325-327.
- (43) Abramovitch, R. A.; Ye, X. *J. Org. Chem.* **1999**, *64*, 5904-5912.

- (44) Abramovitch, R. A.; Ye, X.; Pennington, W. T.; Schimek, G.; Bogdal, D. *J. Org. Chem.* **2000**, *65*, 343-351.
- (45) Famulok, M.; Boche, G. *Angew. Chem. Int. Ed. Engl.* **1989**, *28*, 468-469.
- (46) Kabbadj, Y.; Huet, T. R.; Uy, D.; Oka, T. *J. Mol. Spectrosc.* **1996**, *175*, 277-288.
- (47) Kung, A. C.; McIlroy, S.; Falvey, D. E. *J. Org. Chem.* **2005**, *70*, 5283-5290.
- (48) McIlroy, S.; Falvey, D. E. *J. Am. Chem. Soc.* **2001**, *123*, 11329-11330.
- (49) Rodrigues, J. A. R.; Abramovitch, R. A.; Sousa, J. D. F. d.; G.C.Leiva *J. Org. Chem.* **2004**, *69*, 2920-2928.
- (50) Thomas, S. I.; Falvey, D. E. *J. Phys. Org. Chem.* **2006**, *19*, 291-294.
- (51) Wei, Y.; Jang, G.-W.; Chan, C.-C.; Hsueh, K. F.; Hariharan, R.; Patel, S. A.; Whitecar, C. K. *J. Phys. Chem.* **1990**, *94*, 7716-7721.
- (52) Miller, J. A. *Cancer Res.* **1970**, *30*, 1570-1579.
- (53) Wei, Y.; Tang, X.; Sun, Y. *J. Polym. Sci., Part A: Chem.* **1989**, *27*, 2385-2396.
- (54) Kraka, E.; Cremer, D.; Bucher, G.; Wandel, H.; Sander, W. *Chem. Phys. Lett.* **1997**, *268*, 313-317.
- (55) Cramer, C. J. *J. Am. Chem. Soc.* **1998**, *120*, 6261-6267.
- (56) Dunnin, T. H. *J. Chem. Phys.* **1989**, *90*, 1007.
- (57) Wang, T.; Krylov, A. I. *J. Chem. Phys.* **2005**, *123*, 104304.
- (58) Migirdicyan, E.; Baudet, J. *J. Am. Chem. Soc.* **1975**, *97*, 7400-7404.

- (59) Wright, B. B.; Platz, M. S. *J. Am. Chem. Soc.* **1983**, *105*, 628-630.
- (60) Wenthold, P.; Kim, J.; Lineberger, W. C. *J. Am. Chem. Soc.* **1997**, *119*, 1354-1359.
- (61) Lejeune, V.; Berthier, G.; Despres, A.; Migirdicyan, E. *J. Phys. Chem.* **1991**, *95*, 3895-3897.
- (62) Lejeune, V.; Despres, A.; Mirdicyan, E. *J. Phys. Chem.* **1984**, *88*, 2719-2722.
- (63) Gajewski, J.; Chang, M. J.; Stang, P. J.; Fisk, T. E. *J. Am. Chem. Soc.* **1980**, *102*, 2096-2097.
- (64) Baeyer, A. *Ann.* **1910**, *372*, 80-151.
- (65) Baeyer, A. *Ann.* **1907**, *354*, 152-204.
- (66) Olah, G.; Prakash, S. *Carbocation Chemistry*; Wiley-Interscience: Hoboken H.J., 2004.
- (67) Bollinger, J. M.; Comisarow, M.; Cupas, C.; Olah, G. *J. Am. Chem. Soc.* **1967**, *89*, 5687-5691.
- (68) Cupas, C.; Comisarow, M.; Olah, G. *J. Am. Chem. Soc.* **1966**, *88*, 361-362.
- (69) Hammett, L. *Chem. Rev.* **1935**, *17*, 125-136.
- (70) Williams, A. *Free Energy Relationships in Organic and Bio-Organic Chemistry*; Royal Soc. of Chem.: Cambridge, England, 2003.
- (71) Winter, A. H.; Falvey, D. E.; Cramer, C. J. *J. Am. Chem. Soc.* **2004**, *126*, 9661-9668.

- (72) Andersson, K.; Malmqvist, P. A.; Roos, B. O.; Sadlej, A. J.; Wolinski, K. *J. Phys. Chem.* **1990**, *94*, 5483-5488.
- (73) Cramer, C. J. *Essentials of Computational Chemistry: Theories and Models*; 2nd ed.; John Wiley & Sons: Chichester, 2004.
- (74) Andersson, K.; Malmqvist, P.; Roos, B. O. *J. Chem. Phys.* **1992**, *96*, 1218-1226.
- (75) Cramer, C. J.; Dulles, F. J.; Falvey, D. E. *J. Am. Chem. Soc.* **1994**, *116*, 9787-9788.
- (76) Cramer, C. J.; Truhlar, D. G.; Falvey, D. E. *J. Am. Chem. Soc.* **1997**, *119*, 12338-12342.
- (77) Geise, C. M.; Hadad, C. M. *J. Org. Chem.* **2000**, *65*, 8348-8356.
- (78) Trindle, C. *J. Org. Chem.* **2003**, *68*, 9669-9677.
- (79) Worthington, S. E.; Cramer, C. J. *J. Phys. Org. Chem.* **1997**, *10*, 755-767.
- (80) Cramer, C.; Dulles, F.; Storer, J.; Worthington, S. *Chem. Phys. Lett.* **1994**, *218*, 387-394.
- (81) Johnson, W. T. G.; Cramer, C. J. *Int. J. Quantum Chem.* **2001**, *85*, 492-508.
- (82) Cramer, C. J.; Smith, B. A. *J. Phys. Chem.* **1996**, *100*, 9664-9670.
- (83) Li, J.; Worthington, S. E.; Cramer, C. J. *J. Chem. Soc. Perkin Trans. 2* **1998**, 1045-1052.
- (84) Yamaguchi, K.; Jensen, F.; Dorigo, A.; Houk, K. *Chem. Phys. Lett.* **1988**, *149*, 537.

- (85) Lim, M.; Worthington, S. E.; Dulles, F. J.; Cramer, C. J. In *Chemical Applications of Density Functional Theory*; Laird, B. B., Ross, R. B., Ziegler, T., Eds.; American Chemical Society: Washington, DC., 1996; Vol. 629, p 402.
- (86) Isobe, H.; Takano, Y.; Kitagawa, Y.; Kawakami, T.; Yamanaka, S.; Yamaguchi, K.; Houk, K. *Mol. Phys.* **2002**, *100*, 717-727.
- (87) Noodleman, L.; Case, D. A. *Adv. Inorg. Chem.* **1992**, *38*, 423-470.
- (88) Perdew, J. P.; Wang, Y. *J. Phys. Chem. B.* **1986**, *33*, 8800-8802.
- (89) Perdew, J. P. In *Electronic Structure of Solids*; Ziesche, P., Eschrig, H., Eds.; Akademie Verlag: Berlin, 1991, p 11-20.
- (90) Adamo, C.; Barone, V. *J. Chem. Phys.* **1998**, *108*, 664-675.
- (91) Tao, J.; Perdew, J. P.; Staroverov, V. N.; Scuseria, G. E. *Phys. Rev. Lett.* **2003**, *91*, 146401.
- (92) Staroverov, V. N.; Scuseria, G. E.; Tao, J.; Perdew, J. P. *J. Phys. Chem.* **2003**, *119*, 12129.
- (93) Cramer, C. J.; Wloch, M.; Piecuch, P.; Puzzarini, C.; Gagliardi, L. *J. Phys. Chem. A.* **2006**, *110*, 1991-2004.
- (94) Saunders, M.; Berger, R.; Jaffe, A.; McBride, J. M.; O'Neill, J.; Breslow, R.; J.M. Hoffman, J. *J. Am. Chem. Soc.* **1973**, *95*, 3017-3018.
- (95) Milanesi, S.; Fagnoni, M.; Albin, A. *J. Org. Chem.* **2005**, *70*, 603-610.
- (96) Nicolaides, A.; Smith, D. M.; Jensen, F.; Radom, L. *J. Am. Chem. Soc.* **1997**, *119*, 8083-8088.

(97) The changes in the singlet-triplet gap for the aryloxenium and arylnitrenium ions upon substitution with pi donors can not be used as accurate quantitative measures of the perturbation in the  $\pi,\pi^*$  triplet state as the unsubstituted analogs typically have n,  $\pi^*$  triplet states lower in energy than the  $\pi,\pi^*$  triplet states.

(98) The triplet silylenium ions appear to be approximately  $sp^3$  hybridized, in contrast to the singlet states which appear to be approximately  $sp^2$  hybridized.

(99) Stang, P. J.; Rappoport, Z.; Hanack, M.; Subramanian, L. R. *Vinyl Cations*; Academic Press: New York, 1979.

(100) Rappoport, Z.; Stang, P. J. *Dicoordinate Carbocations*; Wiley: New York, 1997.

(101) Fagnoni, M.; Albini, A. *Acc. Chem. Res.* **2005**, *38*, 713-721.

(102) Zollinger, H. *Angew. Chem. Int. Ed. Engl.* **1978**, *17*, 141.

(103) Aschi, A.; Harvey, J. N. *J. Chem. Soc., Perkin Trans. 2* **1999**, 1059-1062.

(104) Winter, A. H.; Falvey, D. E.; Cramer, C. J.; Gherman, B. F. *J. Am. Chem. Soc.* **2007**, *129*, 10113-10119.

(105) Dill, J.; Schleyer, P. v. R.; Pople, J. *J. Am. Chem. Soc.* **1977**, *99*, 1-7.

(106) Dichiarante, V.; Fagnoni, M.; Mella, M.; Albini, A. *Chem. Eur. J.* **2006**, *12*, 3905-3915.

(107) Fagnoni, M.; Mella, M.; Albini, A. *Org. Lett.* **1999**, *1*, 1299-1301.

(108) Milanese, S.; Fagnoni, M.; Albini, A. *J. Org. Chem.* **2004**, *70*, 603-610.



- (109) Guizzardi, B.; Mella, M.; Fagnoni, M.; Albini, A. *J. Org. Chem.* **2001**, *66*, 6353-6363.
- (110) Guizzardi, B.; Mella, M.; Fagnoni, M.; Albini, A. *J. Org. Chem.* **2003**, *68*.
- (111) Hanack, M. *Pure & Appl. Chem.* **1984**, *56*, 1819-1830.
- (112) Hanack, M. *Acc. Chem. Res.* **1970**, *3*, 209-216.
- (113) Okuyama, T. *Acc. Chem. Res.* **2002**, *35*, 12-18.
- (114) McNeely, S. A.; Kropp, P. J. *J. Am. Chem. Soc.* **1976**, *98*, 4319-4320.
- (115) Kobayashi, S.; Hori, Y.; Hasako, T.; Koga, K.-i.; Yamataka, H. *J. Org. Chem.* **1996**, *61*, 5274-5279.
- (116) Kotani, M.; Kobayashi, S.; Chang, J.-A. *J. Phys. Org. Chem.* **2002**, *15*, 863-868.
- (117) Shinjiro, K.; Chang, J.; Yuji, H.; Masaaki, M. *Kiso Yuki Kagaku Rengo Toronkai Yokoshu* **2000**, *15*, 194-195.
- (118) Lee, M.; Kim, M. S. *J. Phys. Chem. A.* **2006**, *110*, 9377-9382.
- (119) Lee, M.; Kim, M. S. *J. Phys. Chem. A.* **2007**, *111*, 8409-8415.
- (120) Zhang, W.; Stone, J. A.; Brook, M. A.; McGibbon, G. A. *J. Am. Chem. Soc.* **1996**, *118*, 5764-5771.
- (121) Siehl, H.-U.; Mueller, T.; Gauss, J.; Buzek, P.; Schleyer, P. v. R. *J. Am. Chem. Soc.* **1994**, *116*, 6384-6387.
- (122) Siehl, H.-A.; Koch, E.-W. *J. Org. Chem.* **1984**, *49*, 575-576.
- (123) Siehl, H.-A.; Mayr, H. *J. Am. Chem. Soc.* **1982**, *104*, 909-910.
- (124) *Dicoordinated Carbocations*; John Wiley & Sons: Chichester, 1997.

- (125) Muller, T.; Juhasz, M.; Reed, C. A. *Angew. Chem. Int. Ed. Engl.* **2004**, *116*, 1569-1572.
- (126) Hanack, M. *Acc. Chem. Res.* **1976**, *9*, 364-371.
- (127) Leopold, D. G.; Murray, K. K.; Lineberger, W. C. *J. Chem. Phys.* **1984**, *81*, 1048-1050.
- (128) Murray, K. M.; Leopold, D. G.; Miller, T. M.; Lineberger, W. C. *J. Chem. Phys.* **1988**, *89*, 5442-5453.
- (129) Admasu, A.; Gudmundsdottir, D.; Platz, M. S. *J. Phys. Chem. A.* **1997**, *101*, 3832.
- (130) Liu, J.; Mandel, S.; Hadad, C. M.; Platz, M. S. *J. Org. Chem.* **2004**, *69*, 8583-8593.
- (131) Desikan, V.; Liu, Y.; Toscano, J. P.; Jenks, W. S. *J. Org. Chem.* **2007**, *72*, 6848-6859.
- (132) Wasylenko, W. A.; Kebede, N.; Showalter, B. M.; Matsunaga, N.; Miceli, A. P.; Liu, Y.; Ryzhkov, L. R.; Hadad, C. M.; Toscano, J. P. *J. Am. Chem. Soc.* **2006**, *128*, 13142-13150.
- (133) Psciuk, B. T.; Bederskii, V. A.; Schlegel, H. B. *Theoretica Chimica Acta* **2007**, *118*, 75-80.
- (134) Lindh, R.; Rice, J. E.; Lee, T. J. *J. Chem. Phys.* **1991**, *94*, 8008-8014.
- (135) For the substituted vinyl cations, however, we did not locate any minima for non-classical structures using DFT such as the one seen in the parent system.

- (136) However, given that DFT underestimates singlet stability by 3-6 kcal/mol, the ground state is probably the singlet.
- (137) Becke, A. D. *Phys. Rev. A* **1988**, *38*, 3098-3100.
- (138) Becke, A. D. *J. Chem. Phys.* **1993**, *98*, 5648-5652.
- (139) Lee, C.; Yang, W.; Parr, R. G. *Phys. Rev. B* **1988**, *37*, 785-789.
- (140) Frisch, M. J. T., G. W.; Schlegel, H. B.; Scuseria, G. E.; Robb, M. A.; Cheeseman, J. R.; J. A. Montgomery, J.; Vreven, T.; Kudin, K. N.; Burant, J. C.; Millam, J. M.; Iyengar, S. S.; Tomasi, J.; Barone, V.; Mennucci, B.; Cossi, M.; Scalmani, G.; Rega, N.; Petersson, G. A.; Nakatsuji, H.; Hada, M.; Ehara, M.; Toyota, K.; Fukuda, R.; Hasegawa, J.; Ishida, M.; Nakajima, T.; Honda, Y.; Kitao, O.; Nakai, H.; Klene, M.; Li, X.; Knox, J. E.; Hratchian, H. P.; Cross, J. B.; Adamo, C.; Jaramillo, J.; Gomperts, R.; Stratmann, R. E.; Yazyev, O.; Austin, A. J.; Cammi, R.; Pomelli, C.; Ochterski, J. W.; Ayala, P. Y.; Morokuma, K.; Voth, G. A.; Salvador, P.; Dannenberg, J. J.; Zakrzewski, V. G.; Dapprich, S.; Daniels, A. D.; Strain, M. C.; Farkas, O.; Malick, D. K.; Rabuck, A. D.; Raghavachari, K.; Foresman, J. B.; Ortiz, J. V.; Cui, Q.; Baboul, A. G.; Clifford, S.; Cioslowski, J.; Stefanov, B. B.; Liu, G.; Liashenko, A.; Piskorz, P.; Komaromi, I.; Martin, R. L.; Fox, D. J.; Keith, T.; Al-Laham, M. A.; Peng, C. Y.; Nanayakkara, A.; Challacombe, M.; Gill, P. M. W.; Johnson, B.; Chen, W.; Wong, M. W.; Gonzalez, C.; Pople, J. A. Gaussian03, Rev B.01. Pittsburgh, 2003.
- (141) Kennedy, S. A.; Novak, M.; Kolb, B. A. *J. Am. Chem. Soc.* **1997**, *119*, 7654-7664.

- (142) Famulok, M.; Bosold, F.; Boche, G. *Angew. Chem. Int. Ed. Engl.* **1989**, *28*, 337-338.
- (143) Waldrop, D. J.; Basak, A. *Org. Lett.* **2001**, *3*, 1053-1056.
- (144) Waldrop, D. J.; Zhang, W. *Org. Lett.* **2001**, *3*, 2353-2356.
- (145) Amyes, T. L.; Richard, J. P.; Novak, M. *J. Am. Chem. Soc.* **1992**, *114*, 8032-8041.
- (146) Allen, A. D.; Tidwell, T. T. *Chem. Rev.* **2001**, *101*, 1333-1348.
- (147) Breslow, R.; Chang, H. W.; Hill, R.; Wasserman, E. *J. Am. Chem. Soc.* **1967**, *89*, 1112-1119.
- (148) Allen, A. D.; Fujio, M.; Mohammed, N.; Tidwell, T. T.; Tsuji, Y. *J. Org. Chem.* **1997**, *62*, 246-252.
- (149) Herndon, W. C.; Mills, N. S. *J. Org. Chem.* **2005**, *70*, 8492-8496.
- (150) Jiao, H.; Schleyer, P. v. R.; Mo, Y.; McAllister, M. A.; Tidwell, T. T. *J. Am. Chem. Soc.* **1997**, *119*, 7075-7083.
- (151) Sparrapan, R.; Eberlin, M. N.; Augusti, R. *Rap. Comm. Mass. Spectrom.* **2005**, *19*, 1775-1778.
- (152) Bogdal, D. *Heterocycles* **2000**, *53*, 2679-2688.
- (153) Bogdal, D. *ARKIVOK* **2001**, *vi*, 109-115.
- (154) Vinolle, J.; Gornitzka, H.; Maron, L.; Schoeller, W. W.; Bourissou, D.; Bertrand, G. *J. Am. Chem. Soc.* **2007**, *129*, 978-985.
- (155) Winter, A. H.; Thomas, S. I.; Kung, A. C.; Falvey, D. E. *Org. Lett.* **2004**, *6*, 4671-4674.

(156) The spectrum of the carbazolyl radical, while qualitatively similar in appearance to the proposed spectrum of the singlet nitrenium ion, can be distinguished by its much longer lifetime in CH<sub>3</sub>CN and the more defined 570 nm peak of the radical relative to the 570 nm peak of the nitrenium ion. See Supporting Information for radical spectrum and LFP of 4a in the presence of DMB.

(157) Shida, T. *Electronic Absorption Spectra of Radical Ions*; Elsevier: Amsterdam, 1988.

(158) Carbazole has an oxidation potential of +1.35 V in CH<sub>3</sub>CN (SCE reference). See Nie, G.; Xu, J.; Zhang, S.; Han, X. *J. Appl. Electrochemistry* 2006, 36, 937-944.

(159) Based on photolysis performed using 350 nm bulbs. 254 nm photolysis gave a complex mixture of products including five carbazole-collidine isomers, carbazole, collidine, and two TMB adducts. Many of these products from 254 nm photolysis presumably arise from secondary photolysis, chemistry resulting from excitation of TMB, or reactions with accumulated photoproducts.

(160) This rate constant for chloride trapping is slightly larger than the estimated diffusion limit for CH<sub>3</sub>CN ( $1.8 \times 10^{10} \text{ M}^{-1} \text{ s}^{-1}$ ). This anomaly could be explained by errors arising from obtaining trapping rate constants for a transient with a lifetime just inside the detection limit of our laser. Alternatively, it has been shown that the Stokes-Einstein-Smoluchowski equation often underestimates  $k_{\text{diff}}$  by a factor of ~2 due to assumptions about the radii of the reacting species.

(161) Hawari, J. A.; Engel, P. S.; Griller, D. *Chemical Kinetics* **1985**, 17, 1215-1219.

- (162) Thomas, S. I.; Falvey, D. E. *J. Org. Chem.* **2006**, *72*, 4626-4634.
- (163) The largest absorption band for this type of sigma complex has been previously observed for addition of TMB to diarylnitrenium ions at ca. 315-345 nm in CH<sub>3</sub>CN. While we suspect that a more intense absorption band exists in this region of the spectrum than the peak observed at 400 nm, we were unable to confirm this due to our use of a 355 nm excitation beam that prevented observation below 360 nm. See McIlroy, S.; Falvey, D. E. *J. Am. Chem. Soc.* **2001**, *123*, 11329-11330.
- (164) Gritsan, N. P.; Platz, M. S. *Chem. Rev.* **2006**, *106*, 3844-3867.
- (165) Scheschkewitz, D.; Amii, H.; Gornitzka, H.; Schoeller, W. W.; Bourissou, D.; Bertrand, G. *Science* **2002**, *295*, 1880-1881.
- (166) Perrin, C. L.; Rodgers, B. L.; O'Connor, J. M. *J. Am. Chem. Soc.* **2007**, *ASAP*, ASAP.
- (167) Little, R. D.; Brown, L. M.; Masjedizadeh, M. R. *J. Am. Chem. Soc.* **1992**, *114*, 3071-3075.
- (168) Schleyer, P. *Chem. Rev.* **2001**, *101*, 1115-1117.
- (169) Gomes, J. A. N. F.; Mallion, R. B. *Chem. Rev.* **2001**, *101*, 1349-1383.
- (170) Mitchell, R. H. *Chem. Rev.* **2001**, *101*, 1301-1315.
- (171) Krygowski, T. M.; Cyranski, M. K. *Chem. Rev.* **2001**, *101*, 1385-1419.
- (172) Chen, Z.; Wannere, C. S.; Corminboeuf, C.; Puchta, R.; Schleyer, P. v. R. *Chem. Rev.* **2005**, *105*, 3842-3888.
- (173) Dauben, H. J.; Wilson, J. D.; Laity, J. L. *J. Am. Chem. Soc.* **1968**, *90*, 811-813.

- (174) Krygowski, T. M.; Cyranski, M. K. *Tetrahedron* **1999**, *55*, 11143-11148.
- (175) Katritzky, A.; Jug, K.; Oniciu, D. C. *Chem. Rev.* **2001**, *101*, 1421-1449.
- (176) Cioslowski, J. *J. Am. Chem. Soc.* **1989**, *111*, 8333-8336.
- (177) Stanger, A. *J. Org. Chem.* **2006**, *71*, 883-893.
- (178) Mills, N. S.; Llagostera, K. B.; Tirla, C.; Gordon, S. M.; Carpenetti, D. *J. Org. Chem.* **2006**, *71*, 7939-7946.
- (179) Schleyer, P. v. R.; Puhlhofer, F. *Org. Lett.* **2002**, *4*, 2873-2876.
- (180) Bally, T. *Angew. Chem. Int. Ed. Engl.* **2006**, *45*, 6616-6619.
- (181) Stevens, P. J.; Devlin, F. J.; Chabalowski, C. F.; Frisch, M. J. *J. Phys. Chem.* **1994**, *98*, 11632-11627.
- (182) Bonesi, S. M.; Erra-Balsells, R. *J. Het. Chem.* **1997**, *34*, 877-889.
- (183) Kyziol, J.; Tarnawski, J. *Revue Roumaine de Chimie* **1980**, *25*, 721-727.